UNIVERSITÀ
DI PAVIA

PhD IN BIOMEDICAL SCIENCES

DEPARTMENT OF MOLECULAR MEDICINE

UNIT OF BIOCHEMISTRY

MOLECULAR MECHANISMS OF SYSTEMIC AMYLOIDOSIS: *IN VITRO* AND *IN VIVO* MODELS

PhD Tutor: **Chiar.mo Prof. Vittorio Bellotti**

PhD dissertation of
Giulia Faravelli

a.a. 2018/2019

Resistere,

Resistere,

Resistere.

INDEX

Chapter 1: Introduction to amyloidosis

1.1. Amyloidosis

The term amyloid comes from the discovery of the German physician Rudolf Virchow when, in 1854, he was studying the corpora amylacea in the brain and he discovered that they stained pale blue on treatment with iodine. He therefore concluded that the substance underlying the evident macroscopic abnormality was cellulose and gave it the name amyloid, derived from the Latin *amylum* and the Greek *amylon*. Later, in 1859, Friedreich and Kekulè identified the presence of protein material in the deposits, thus initially identifying amyloid as a single protein and later as a class of proteins, that can undergo changes in their conformation leading to fibrils formation (Sipe and Cohen 2000). Nowadays, we can refer to the contemporary definition of *amyloidoses* as a generic term used to describe a wide range of human diseases characterized by the misfolding and extracellular accumulation, in the form of highly organised fibrillary aggregates, of various proteins (Gillmore and Hawkins 2013). Such aggregates “arise from the failure of a specific peptide or protein to adopt, or remain in, its native functional conformational state with subsequent reduction in the quantity of protein that is available to play its physiological role” (Chiti and Dobson 2006). Within the protein conformational diseases, amyloidoses represent the largest group of misfolding diseases where specific peptides or proteins convert from their soluble functional states into toxic and highly insoluble amyloid fibrils which can deposit in human tissues. These diseases, although known for more than 150 years, have only recently been increasingly recognized in the pathogenesis of many human diseases with enormous social and medical impact and which are indeed associated with the formation of extracellular plaques or intracellular inclusions of protein aggregates with amyloid-like features.

1.1.2. Type of amyloidosis

To date, 37 peptides or proteins have been found to form amyloid deposits in human pathologies (Table 1) (Chiti and Dobson 2017). Surprisingly, there are no evident similarities among those proteins in sequence, structure, or function. Some of the proteins involved in amyloid disease, form deposits in the central nervous system,

giving rise to neurodegenerative conditions, such as Alzheimer's (AD) and Parkinson's diseases, whereas other proteins aggregate in different tissues and are therefore associated to non-neuropathic diseases. In particular, among the latter, half of them form aggregates in a range of tissues, including the heart, spleen, liver, and kidney, and give rise to ***systemic*** amyloidosis. The remaining half aggregate in one of a variety of specific tissues, giving rise to a diverse range of conditions, named ***localized*** amyloidosis, including for example type II diabetes and atrial amyloidosis (Table 1). The four most common types of systemic diseases are related to light chain (AL), inflammation (AA), dialysis ($A\beta_2M$), and hereditary and old age (ATTR).

Peptide or protein name	Number of residues[a]	Structure[b]	Associated diseases	Type of disease[c]
Amyloid-β peptide (Aβ)	40 or 42[d]	Intrinsically disordered	Alzheimer disease Hereditary cerebral hemorrhage with amyloidosis	Neuropathic Sporadic[f]
α-Synuclein (αs)[e]	140	Intrinsically disordered	Parkinson disease Parkinson disease with dementia Dementia with Lewy bodies Multiple system atrophy	Neuropathic Sporadic[f]
Prion protein (PrP)	208	Intrinsically disordered (1–102) All-α, prion-like (103–208)	Creutzfeldt-Jakob disease Fatal insomnia Gerstmann-Sträussler-Scheinker disease Huntington disease–like 1 Spongiform encephalopathy with neuropsychiatric features New variant Creutzfeldt-Jakob disease Kuru Hereditary sensory and autonomic neuropathy	Neuropathic Sporadic Hereditary Infectious Iatrogenic
Microtubule-associated protein tau (τ)[e]	352–441[d]	Intrinsically disordered	Pick disease Progressive supranuclear palsy Corticobasal degeneration Frontotemporal dementia with parkinsonism linked to chr17 Argyrophilic grain disease Tangle predominant dementia Guam Parkinson dementia complex Frontotemporal lobar degeneration Chronic traumatic encephalopathy Ganglioglioma Meningioangiomatosis Subacute sclerosing panencephalitis Lead encephalopathy Tuberous sclerosis Hallervorden-Spatz disease Lipofuscinosis	Neuropathic Sporadic[f]
Huntingtin exon 1 (HttEx1)[e]	~103–187[d]	Intrinsically disordered	Huntington disease	Neuropathic Hereditary
ABri peptide	34	Intrinsically disordered	Familial British dementia	Systemic and neuropathic[g] Hereditary
ADan peptide	34	Intrinsically disordered	Familial Danish dementia	Neuropathic Hereditary
Fragments of immunoglobulin light chains[h]	~100[d]	All-β, Ig-like	Light-chain amyloidosis	Systemic Sporadic[f]

(*Continued*)

Peptide or protein name	Number of residues[a]	Structure[b]	Associated diseases	Type of disease[c]
Fragments of immunoglobulin heavy chains[h]	~190[d]	All-β, Ig-like	Heavy-chain amyloidosis (mainly renal)	Systemic Sporadic
Full or N-term fragments of serum amyloid A protein (SAA)	45–104[d]	All-α, SAA-like four-helix bundle	AA amyloidosis	Systemic Sporadic
Transthyretin (TTR)	127	All-β, prealbumin-like	Senile systemic amyloidosis Familial amyloidotic polyneuropathy Familial amyloid cardiomyopathy Leptomeningeal amyloidosis	Systemic[g] Sporadic and hereditary
β_2-microglobulin (β_2-m)	99	All-β, Ig-like	Dialysis-related amyloidosis Hereditary visceral amyloidosis	Systemic Iatrogenic[f]
N-term fragments of apolipoprotein A-I (ApoAI)	69–100[d]	Intrinsically disordered	ApoAI amyloidosis (many organs)	Systemic Hereditary
C-term extended apolipoprotein A-II (ApoAII)	98	Unknown	ApoAII amyloidosis (mainly renal)	Systemic Hereditary
N-term fragments of apolipoprotein A-IV (ApoAIV)	~70	Unknown	ApoAIV amyloidosis (many organs)	Systemic Sporadic
Apolipoprotein C-II (ApoCII)	79	All-α, unknown fold	ApoCII amyloidosis (mainly renal)	Systemic Hereditary
Apolipoprotein C-III (ApoCIII)	79	All-α, unknown fold	ApoCIII amyloidosis (mainly renal)	Systemic Hereditary
Fragments of gelsolin	53 or 71[d]	Intrinsically disordered	Familial amyloidosis, Finnish type	Systemic Hereditary
Lysozyme (LYS)	130	α + β, lysozyme fold	Lysozyme amyloidosis (mainly visceral)	Systemic Hereditary
Fragments of fibrinogen α-chain	45–81[d]	Unknown	Fibrinogen amyloidosis (mainly renal)	Systemic Hereditary
N-term truncated cystatin C	110	α + β, cystatin-like	Hereditary cerebral hemorrhage with amyloidosis, Icelandic type	Systemic Hereditary
Islet amyloid polypeptide (IAPP)	37	Intrinsically disordered	Type II diabetes Insulinoma	Localized Sporadic
Calcitonin	32	Intrinsically disordered	Medullary carcinoma of the thyroid	Localized Sporadic
Atrial natriuretic factor (ANF)	28	Intrinsically disordered	Atrial amyloidosis	Localized Sporadic
N-term fragments of prolactin (PRL)	34	Unknown	Pituitary prolactinoma	Localized Sporadic
Insulin	(30 + 21)[i]	All-α, insulin-like	Injection-localized amyloidosis	Localized Iatrogenic

(*Continued*)

Peptide or protein name	Number of residues[a]	Structure[b]	Associated diseases	Type of disease[c]
Medin[j]	50	Intrinsically disordered	Aortic medial amyloidosis	Localized Sporadic
Lactotransferrin (lactoferrin)	691	α + β, periplasmic binding protein–like II	Gelatinous drop-like corneal dystrophy	Localized Sporadic[f]
Odontogenic ameloblast-associated protein (ODAM)	110–118[d]	Unknown	Calcifying epithelial odontogenic tumors	Localized Sporadic
Pulmonary surfactant-associated protein C (SP-C)	35	All-α, transmembrane helical fragment	Pulmonary alveolar proteinosis	Localized Sporadic
Leukocyte cell-derived chemotaxin-2 (LECT-2)	133	All-β, barrel-sandwich hybrid	Renal amyloidosis	Systemic Sporadic
Galectin 7 (Gal-7)[e]	136	All-β, concanavalin A-like lectins	Lichen amyloidosis Macular amyloidosis	Localized Sporadic
Corneodesmosin (CDSN)	167, 182, 206[d]	Intrinsically disordered	Hypotrichosis simplex of the scalp	Localized Hereditary
C-term fragments of kerato-epithelin (βig-h3)	50–200[d]	Unknown	Lattice corneal dystrophy, type 1 Lattice corneal dystrophy, type 3A Lattice corneal dystrophy, Avellino type	Localized Hereditary
Semenogelin-1 (SGI)	439	Unknown	Seminal vesicle amyloidosis	Localized Sporadic
Proteins S100A8/A9	92/113	All-α, EF hand-like	Prostate cancer	Localized Sporadic
Enfuvirtide	36	Unknown	Injection-localized amyloidosis	Localized Iatrogenic

[a]Lengths of the processed forms depositing into the aggregates, not the precursor proteins.
[b]Structural class and fold of the native, processed protein or peptide prior to aggregation, according to the Structural Classification of Proteins database.
[c]Diseases are classified as (*a*) neuropathic, systemic, or localized (non-neuropathic) and (*b*) sporadic, hereditary, iatrogenic (following medical treatment), or infectious.
[d]Fragments of various lengths were reported for ex vivo fibrils.
[e]Intracellular proteins, unlike the others that are extracellular.
[f]Predominantly sporadic, although hereditary forms are documented.
[g]Involving both the central nervous system and other organs, thus systemic but also neuropathic.
[h]Also forming nonamyloid deposits in light-chain or heavy-chain deposition diseases.
[i]Lengths of the A and B chains linked by a disulfide bridge.
[j]Medin is the 245–294 fragment of human lactadherin.

Table 1. Peptides or proteins responsible of extracellular amyloid deposits or intracellular inclusions with amyloid-like features in human diseases (Chiti and Dobson 2017).

The basic mechanism in the pathogenesis of amyloidosis is abnormal folding of proteins or misfolded proteins. Under normal circumstances, these abnormal or misfolded proteins are degraded by the proteasome pathway intracellularly, and by the macrophages extracellularly. In amyloidosis, these control mechanisms fail or there may be mutations that favour misfolding, which further leads to accumulation and aggregation to form fibrils. Some amyloid diseases are ***familial*** forms, while others are ***acquired***. So, the pathogenesis can be broadly categorized into two mechanisms, as it is showed in Figure 1: normal proteins, produced in abnormal numbers or production of normal amounts of mutant proteins.

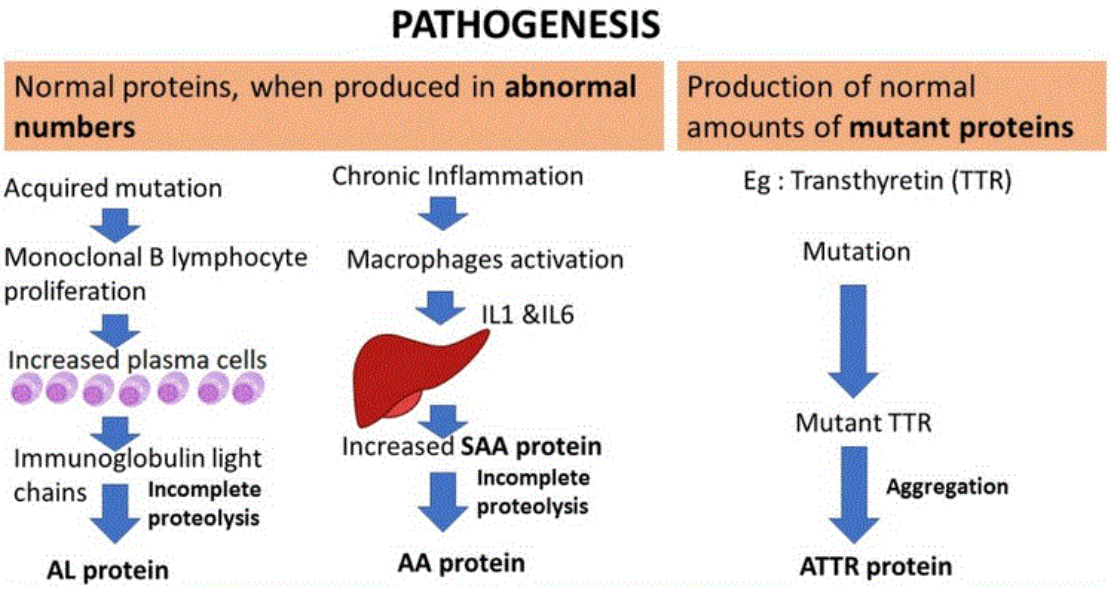

Figure 1. Pathogenesis of amyloid diseases. From Dr Vijay Shankar S, 2017, Diseases of Immune System, General Pathology.

Familial forms of amyloid-related diseases are generally associated to specific mutations within the gene encoding the peptide or protein that converts into amyloid deposits (Table 1) (Chiti and Dobson 2017). The pathogenicity of these mutations is linked with the increasing propensity of the protein to aggregate (Figure 2). There are, for example, more than 100 mutations linked to hereditary forms of transthyretin amyloidosis that are known to lead to destabilization of the native tetrameric form of the protein, resulting in an enhanced population of amyloidogenic monomers.

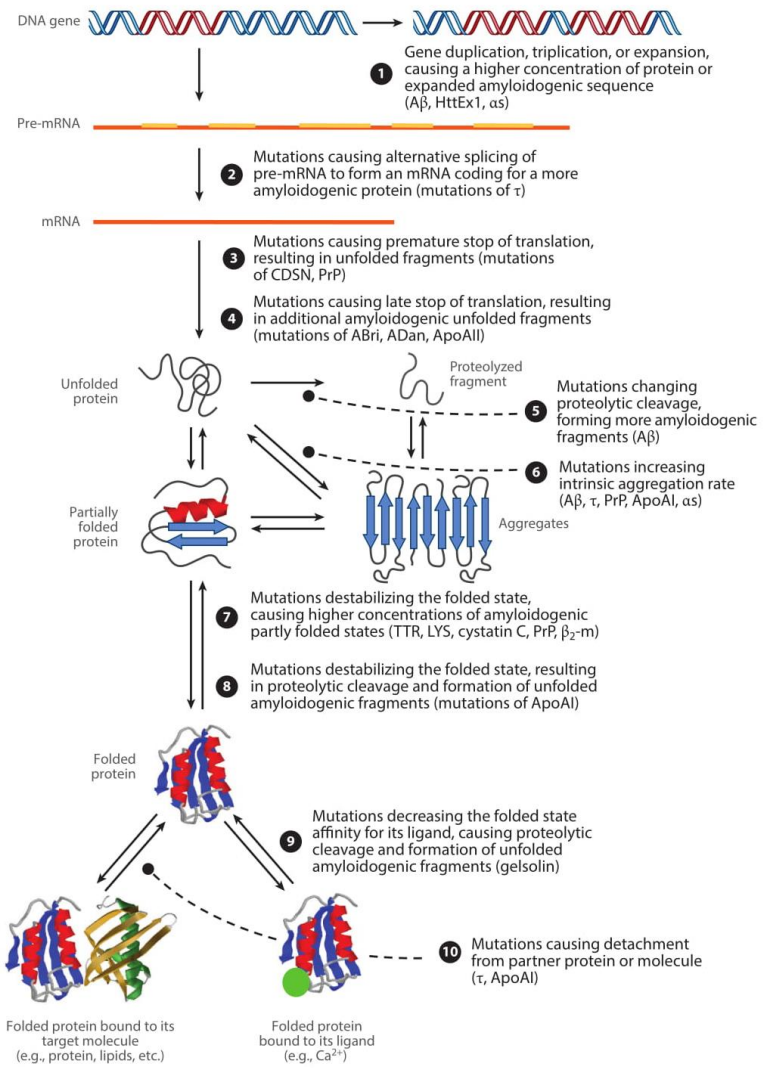

Figure 2. Schematic representation of the different mechanisms of action by which mutations associated with hereditary amyloid diseases can cause protein aggregation and its associated pathological states. Numbers **1 to 10** show a mechanism of action along with the names of the mutated peptides and proteins for which the mechanism is described in the literature (Chiti and Dobson 2017).

1.1.3. Composition of amyloid fibrils

Despite the heterogeneity of the various proteins involved in amyloid diseases, all of them produce morphologically, structurally, and tinctorially indistinguishable fibrils. Amyloid fibrils, whether extracted from patients or generated in the laboratory, are thread-like structures typically 7–13 nm in diameter, as observed by electro-microscopy (EM) or atomic force microscopy (AFM) techniques, and often microns in length (Chiti and Dobson 2017). They generally contain 2–8 protofilaments, each approximately 2–7 nm in diameter, which often twist around each other or associate laterally as flat ribbons 2–7 nm high and up to 30 nm wide. The fibrils possess a cross-β structure, in which β-strands are oriented perpendicularly to the fibril axis and are

assembled into β-sheets that run the length of the fibrils. This kind of structure has been detected with recent support from Fourier transform infrared spectroscopy, solid-state nuclear magnetic resonance (ssNMR), X-ray crystallography and scanning transmission electron microscopy (STEM) measurements (Figure 3).

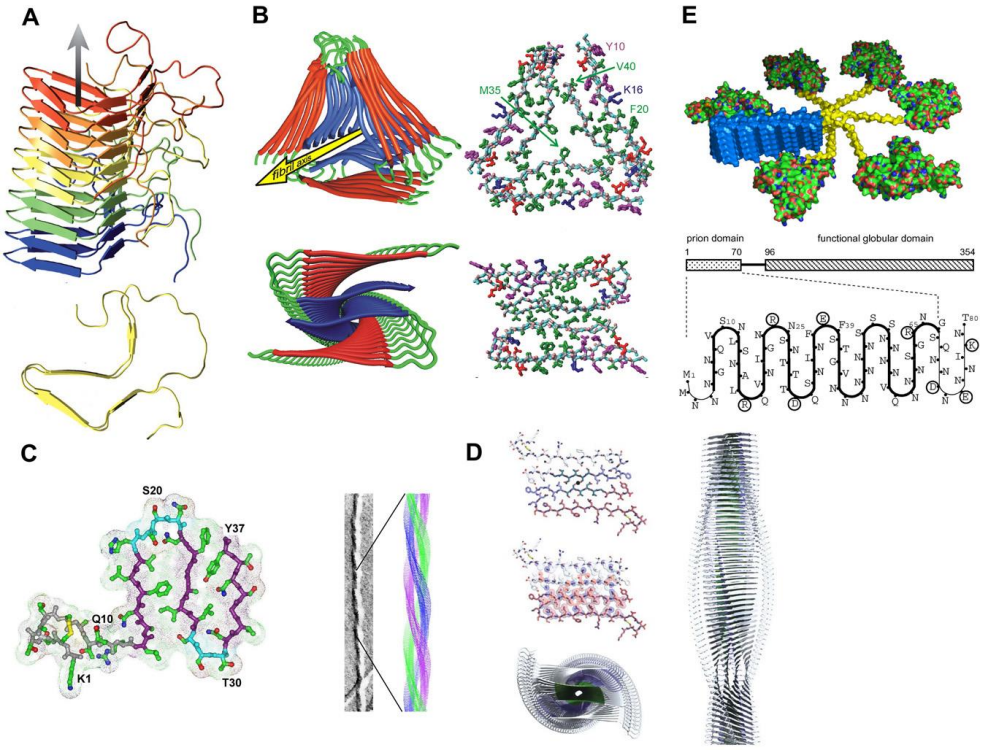

Figure 3. Molecular structure models of amyloid fibrils aided by packing constraints derived from STEM measurements. **a)** HET-s prion structure (Wasmer et al. 2008). **b)** Ab fibril structures (Paravastu et al. 2008). **c)** Amylin fibril structure (Kajava, Aebi and Steven 2005). **d)** Amylin fibril structure (Wiltzius et al. 2008); adapted with permission from The Protein Society. **e)** Ure2p (Kajava et al. 2004).

The existence of such ultrastructure of the fibril allows the regular intercalation and binding of dyes such as thioflavin-T (ThT), Congo red (CR), or their derivatives, conferring a diagnostic optical property to amyloid such as apple-green birefringence under polarized light microscopy (Figure 4d-f). Congo Red (CR) has been used as a diagnostic test for the presence of amyloid in tissue sections for several decades. It is likely that both the hydrophobic and the electrostatic components of the structure of CR are critical for its binding to proteins (Figure 4a-c). However, analysis of scientific data from recent studies shows that CR staining alone is not sufficient for confirmation

of the amyloid nature of protein aggregates *in vitro* or for diagnosis of amyloidosis in tissue sections (Yakupova et al. 2019). The following three features: a fibrillar morphology, cross-β structure, and characteristic tinctorial properties, are universally accepted as the hallmarks of amyloid structure, and any given protein aggregate needs to display all of them to be classified as such.

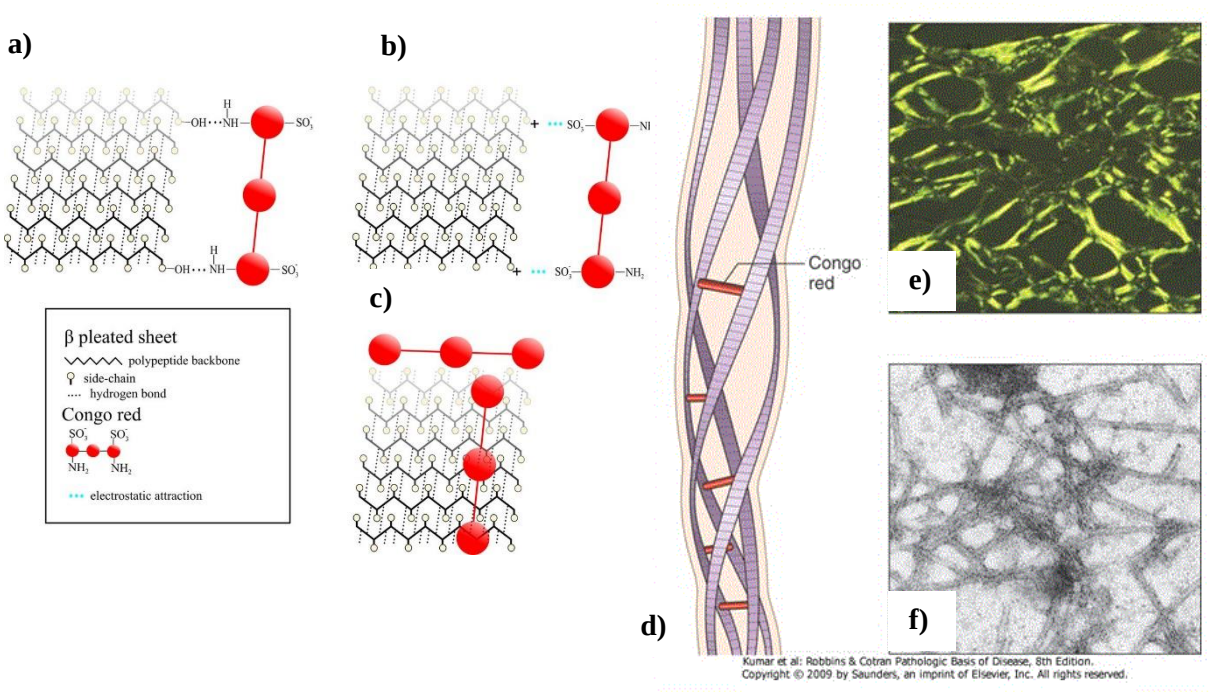

Figure 4. The main hypothetical models of the binding of Congo Red (CR) to amyloids. **a)** Dye binding mediated by hydrogen bonding between primary hydroxyl groups of the peptide chain (similar to the polysaccharide chain) and the amino groups of CR (PUCHTLER and SWEAT 1962). **b)** CR molecule could bind to positively charged amino acid residues along the peptide chains (Klunk, Pettegrew and Abraham 1989). **c)** Polar contacts drive CR binding (Reinke and Gestwicki 2011). Figure a,b,c were adapted from Yakupova et al. 2019. **d)** Cross-β-pleated sheet conformation of amyloid fibrils with CR binding. **e)** Polarized light and **f)** bright-field image of amyloid fibrils stained with CR. Adapted from Kumar et al. 2009.

In addition to fibrillar material, amyloid deposits contain a number of non-fibrillar components that interact with amyloid fibrils and are incorporated into the deposits in their native folded state. The influence of a number of the non-fibrillar components in amyloid-related diseases is well established; however, the mechanisms underlying these effects are poorly understood (MacRaild et al. 2004).

Among the various components, we can mention the presence of:

- ✓ Glycosaminoglycans (GAGs), as heparin and proteoglycans, which can be found strongly bound to the fibrils. GAGs seem to promote fibrils growth and stabilization, possibly due to the highly negatively charged sulphate groups (Kisilevsky 1992). Together with laminin, collagen-IV, and fibronectin, proteoglycans are part of the extracellular matrix and constitute the carbohydrate content of natural amyloid. These components facilitate the initial steps of fibrils nucleation by creating a scaffold for further fibril assembly.
- ✓ Amyloid P Component (SAP). It is a plasma glycoprotein synthetized by the liver, able to bind reversibly (Kd ~ 1 µmol/l) to all types of amyloid fibrils with a calcium-dependent mechanism, lacking from affinity towards the protein in their native state. SAP is an oligomeric protein, composed of 5 identical subunits of 23,500 Da, not-covalently bound to form a pentameric structure (Coker et al. 2000). SAP protects fibrils towards proteolysis and phagocytosis both *in vivo* and *in vitro* (Tennent, Lovat and Pepys 1995). In human and healthy plasma we can find about 100 mg of SAP (20-30 mg/l), while in patients affected by amyloidosis, the amount of SAP reaches up to 20 g. Therefore, it is possible to use ^{123}I-labelled SAP as an important tool for diagnostic for amyloid imaging (Gillmore, Hawkins and Pepys 1997).
- ✓ Collagen, that provides a scaffold for amyloid fibrils to attach on and expand in size.
- ✓ Apolipoprotein A-IV, which has currently been defined as a cause of renal amyloidosis following its deposition in the kidneys (Bois et al. 2017).
- ✓ Metal cations, such as Zn^{2+}, Fe^{3+}, and Cu^{2+}, probably released from metallo-proteins during inflammatory responses, are associated with amyloid plaques because of their ability to accelerate fibril formation.

1.1.4. Molecular mechanisms of amyloid formation

The hypothetical mechanism that leads toward the formation of amyloid fibrils has been widely studied and investigated by many researchers. In general, the process underlying the conversion of a normally soluble peptide or protein into an aggregated state in fibrils derives from important conformational changes of tertiary or quaternary structures or of the active site of the protein (Bellotti, Mangione and Stoppini 1999). The dynamic pathway that leads towards the formation of not native-like structures can proceed in parallel with the physiological process of protein folding or alternatively to that.

Moreover, it involves nucleation and growth steps (Knowles et al. 2009, Arosio, Knowles and Linse 2015). In the simplest type of nucleated polymerization mechanism, monomers that are completely or partially disordered can convert into nuclei through a thermodynamically unfavourable process that takes place early in the lag phase (Figure 5); fibrils then grow from these nuclei through the addition of monomers (Chiti and Dobson 2017). Such nuclei can be thought of as the smallest structures that are able to initiate fibril elongation, or the smallest species in which the rate of further monomer addition exceeds that of monomer release (Morris, Watzky and Finke 2009). Nuclei have even been suggested to be monomeric species that adopt a well-defined conformation able to aggregate rapidly (Figure 5).

The lag phase in amyloid fibril formation can be drastically shortened through the addition of preformed fibrils by using the “seeding” mechanism of fibrillogenesis (Harper and Lansbury 1997).

A significative role in the mechanism of the self-assembly process of amyloid fibrils is played by prefibrillar species (often termed oligomers), which are thought to represent the most pathogenic species in the diseases associated with amyloid fibril formation (Chiti and Dobson 2017). A representative class of oligomers that have been well characterized are the one related to $A\beta_{40}$/ $A\beta_{42}$ peptides (Choi et al. 2019, Chen and Mobley 2019). When aggregation is initiated by intrinsically disordered systems, the initial oligomers appear at first to adopt a disordered structure with more highly organized oligomers appearing later (Bleiholder et al. 2011).

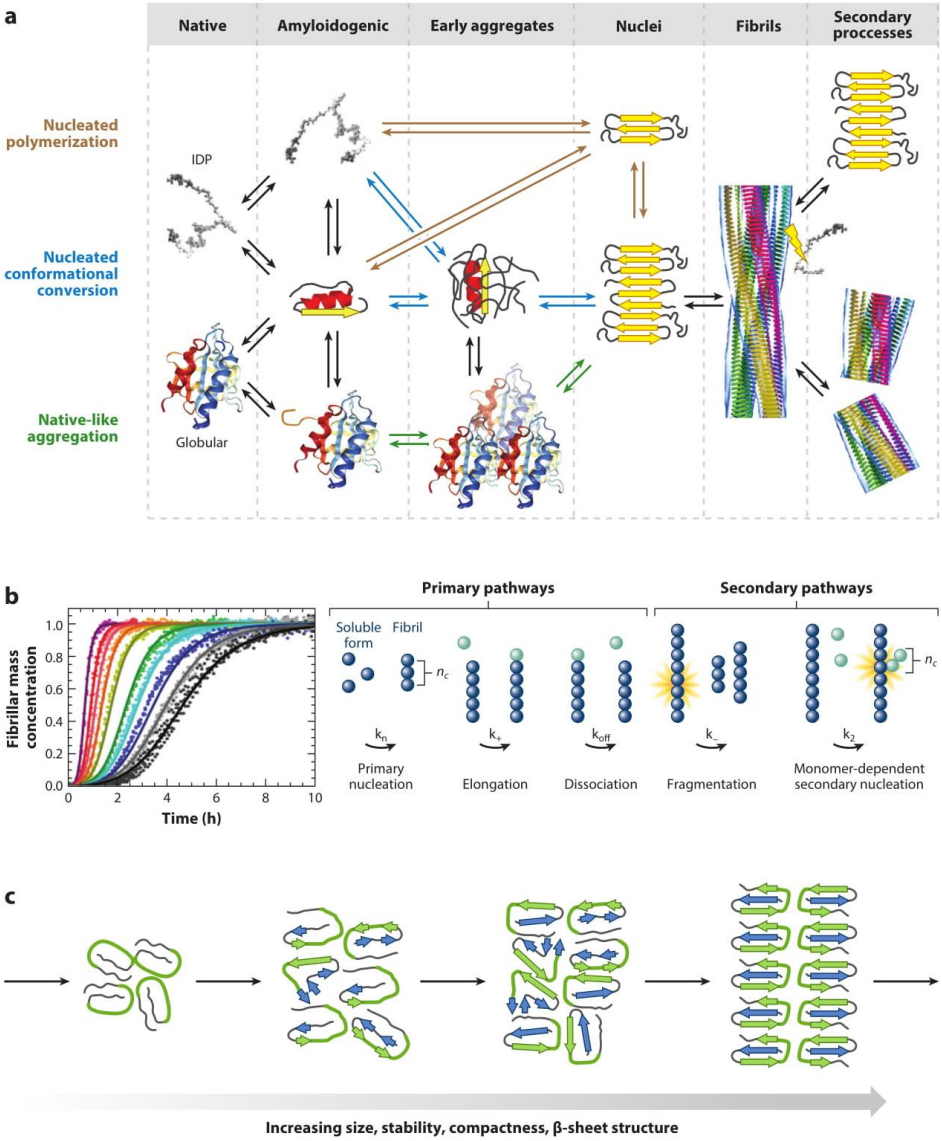

Figure 5. Mechanisms of amyloid fibril formation. **a)** Possible mechanisms of nucleus formation starting from a globular or intrinsically disordered protein (IDP). The vertical boxes refer to different stages of the amyloid fibril formation process, and different models of aggregation are shown horizontally, including nucleated polymerization (*brown arrows*), nucleated conformational conversion (*blue arrows*), and native-like aggregation (*green arrows*). The vertical box on the right refers to secondary processes, such as secondary nucleation (*top*) and fibril fragmentation (*bottom*). **b)** Time courses of aggregation of the amyloid-β peptide ($A\beta_{42}$) monitored with thioflavin-T fluorescence at different peptide concentrations and analyzed using a global fitting procedure (*left*) derived from a model that considers primary nucleation, elongation, dissociation, fragmentation, and secondary nucleation as key microscopic steps (*right*). **c)** Schematic representation of the structural

rearrangements occurring during oligomer formation. Amyloidogenic segments are colored in green. As aggregation proceeds (*left to right*) a set of structural rearrangements takes place; the bottom arrow shows the parameters that increase. Modified from Chiti and Dobson 2017.

Such early aggregates are typically small in size, do not bind amyloid-specific dyes, and do not exhibit a significant content of β-sheet structure and compactness. As aggregation proceeds, such oligomers undergo structural earrangements into species that are stabilized by β-sheet structure, that are generally antiparallel, and with weak binding to ThT and CR. Only later do species appear with a highly regular in-register parallel cross-β structure and fibrillar morphology (Chiti and Dobson 2017).

Since my PhD work has mainly been focused on the study of two amyloidogenic proteins: transthyretin and β_2-microglobulin, I reported the corresponding aggregation mechanisms of those protein in the following paragraphs 1.2 and 1.3 respectively.

1.2. Transthyretin and related amyloidosis

Wild-type transthyretin (WT TTR) is a human plasmatic protein of 55 kDa that was firstly discovered in 1942 in the cerebrospinal fluid (Kabat, Moore and Landow 1942). Wild type TTR was originally named “prealbumin” because it ran faster than albumin on electrophoresis gels in native conditions. Its current name derives from its role of transporter of thyroid hormone thyroxine (T4) and retinol-binding protein bound to retinol (ROBBINS, RALL and PETERMANN 1957). Transthyretin is mainly synthetized by the liver, by the choroid plexus and retinal pigment epithelium, and it is then secreted into the blood stream reaching a plasmatic concentration of 0.1-0.4 mg/ml (3.6 μM), and in the cerebrospinal fluid with a concentration of 0.017 mg/ml (0.36 μM), and in the eye. A minor site of synthesis are the β-cells of islets of Langerhans. Transthyretin has the shape of a non-glycosylated globular protein with the size of 70 Å x 55 Å x 50 Å; it is a stable tetramer, composed of four identical monomers (Figure 6). Each subunit has a primary sequence of 127 amino acids. A dimer is generated by the interaction between two monomers that is stabilized through hydrogen bonds. Two dimers, slightly rotated, originate the folded homo-tetramer, which is stabilized through hydrophobic interactions between the loops that connect the beta-sheets (Blake et al. 1978). The tetramer structure is characterized by the presence of a central channel inside which two identical binding sites for T4 and T3 hormones are located.

Over 100 mutations codify for protein variants of the wild-type TTR (http://amyloidosismutations.com/attr.html), causing familial amyloidosis, although they have a rare incidence (Dwulet and Benson 1987). Some of those mutations are not related to amyloid disease, such as P102R and T119M; some others on the contrary can influence the binding with thyroxine (G6S, A109T) (Sipe 1992).

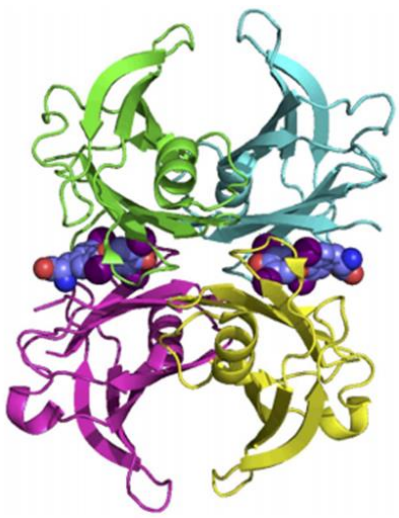

Figure 6. Crystallographic structure of human TTR (Richardson 2014).

TTR-related amyloidosis affects approximately 10,000 people worldwide (Benson and Kincaid 2007, Mangione et al. 2014), even if the incidence of the pathology was longer underestimated, because of poor diagnostic tools (Nencetti and Orlandini 2012).

Until now, four types of TTR-related amyloidosis have been reported (Table 2):
1. *Senile systemic amyloidosis* (SSA). Wild-type TTR is intrinsically amyloidogenic and tends to form microscopic and clinically silent amyloid deposits in the heart, in the lungs and in the blood vessels wall of the majority of elderly people (Westermark et al. 1990, Kolstoe et al. 2010).

2. *Familial amyloid cardiomyopathy* (FAC). Some mutations of TTR, such as V122I variant, have been associated with cardiac amyloidosis (Saraiva 1995). Around 4% of the African-American population carries this mutation, which is although also found in African and Afro-Caribbean ethnic groups.
The clinical phenotype is characterised by the presence of extensive amyloid deposits in the heart. A recent study highlighted a higher incidence of heart failure amongst the carriers of the mutation, although the mortality appeared comparable to that of non-carriers over long-term follow-up (Quarta, Falk and Solomon 2015).

3. *Familial amyloid polyneuropathy* (FAP) represents the most frequent form of inherited amyloidosis. It is a lethal autosomal dominant disorder in which amyloid deposits mostly in the peripheral nervous system (PNS). One of the most diffused mutations causing this disease is V30M TTR, where a valine at position 30 is replaced by a methionine. This mutation is commonly found in the Portuguese, Japanese and Swedish population (Saraiva et al. 1984, Tawara et al. 1983, Dwulet and Benson 1984, Westermark et al. 1990, Saraiva 1995).

4. *Central nervous system selective amyloidosis* (CNSA) which is another disease related to TTR mutations. It is a rare form of amyloidosis caused by the A25T TTR variant (Sekijima et al. 2003).

	Clinical Classification	Age of Appeareance	TTR Type	Geographical Area of Impact
WT TTR amyloidosis	Cardiomyopathy	>60	WT TTR	Worldwide (elderly population)
FAC	Cardiomyopathy	>65	V122I TTR	African-Americans, African, Afro-Caribbean
FAP	Peripheral neuropathy	30-80	V30M TTR	Europe (mainly Portugal and Sweden), Japan
FAP	Peripheral neuropathy and/or cardiomyopathy	>50	Non V30M	Worldwide
CNSA	CNS amyloidosis	<50	A25T, D18G TTR	Worldwide (rare)

Table 2. The most common TTR amyloidosis and age of onset (Nencetti and Orlandini 2012).

Among TTR variants, my work has been focused on S52P, V30M and V122I variants, which were already mentioned previously. The S52P TTR variant has been identified in an English family at the UCL Centre for Amyloidosis and Acute Phase Proteins at the Royal Free Hospital. This variant is associated with the most aggressive clinical phenotype so far described for familial TTR amyloidosis. It is indeed responsible for a severe form of autosomal-dominant hereditary systemic amyloidosis characterised by early onset (Mangione et al. 2014). The patients, who are heterozygous for the specific mutation, developed autonomic dysfunction and polyneuropathy in the third decade, followed by cardiomyopathy, euthyroid multinodular goiter and sicca syndrome.

The mechanism that underline TTR fibrillogenesis has been studied for many years. The first mechanism was proposed by Kelly and his group in 1992 and consist in the dissociation of TTR tetramer that leads to the release of the full-length monomer (Colon and Kelly 1992). In Kelly's method, the monomer misfolds and aggregates following exposure to denaturing conditions like acidic pH (Figure 7). Even though Kelly's mechanism has been accepted worldwide, some crucial issues remain opened. First,

by moving back to physiological conditions, the fibrils created using Kelly's method return soluble. This is extremely different from what observed with *ex vivo* fibrils that, once formed, do not revert to their soluble precursors. Furthermore, the amyloid-like material obtained *in vitro* after prolonged incubation at low pH is mostly amorphous and contains only a small proportion of amyloid-like fibrils when analysed by EM and AFM. Congo red staining also suggests low abundance of amyloid fibrils. Finally, the presence of TTR fragments in *ex vivo* amyloid deposits (Thylén et al. 1993, Ihse et al. 2013) cannot be explained by this mechanism where fibrils are only composed of full-length TTR.

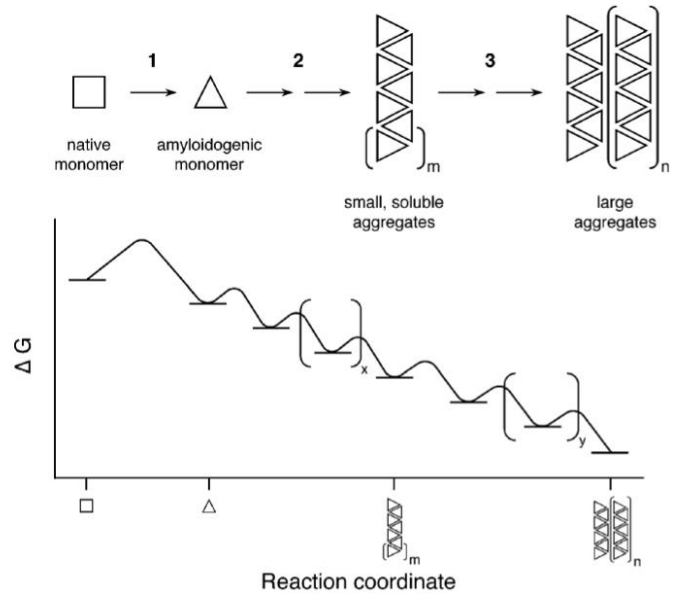

Figure 7. Model of Monomer-TTR Amyloidogenesis (Hurshman et al. 2004).

Recently, the group of Professor Bellotti have identified a previously unrecognised mechano-enzymatic mechanism in which shear stress and proteolysis play a key role towards the formation of amyloid fibrils (Marcoux et al. 2015). In presence of shear stress and in physiological conditions 49-127 fragment, generated after the proteolysis, is released from the tetramer and triggers rapid fibril formation. In this case, the fibrils formed has a similar morphology of the one found in *ex vivo* samples.

In particular, in the work of Marcoux and colleagues, biochemical analysis performed on *ex vivo* fibrils showed that the main components were the 49-127 TTR fragment originated only from the variant in combination with both variant and WT TTR full-length monomers. The specificity of the cleavage site suggested that the protease responsible for proteolysis *in vivo* could be a trypsin-like serine protease.

By exposing native S52P TTR to very low-dose trypsin, under physiological conditions, the same 49-127 fragment, observed in the *ex vivo* fibrils, was detected. By monitoring the aggregation, it was discovered that WT TTR and some amyloidogenic variants were actually susceptible to trypsin cleavage with the exception of the non-pathogenic T119M variant that it is known to be protect from aggregation of amyloidogenic isoform in the patients.

In each case, Congo red birefringence and electron microscopy analysis confirmed the presence of amyloid fibrils and SDS-page analysis confirmed the presence of the truncated fragment 49-127 (Figure 8). In the presence of trypsin alone, agitation alone or in the absence of trypsin, none of the proteins were cleaved and maintained their solubility .

Indeed trypsin, even though effective *in vitro* in priming TTR amyloidogenesis by selective proteolysis of the loop interconnecting strands C and D, is unlikely to represent the culprit protease responsible for proteolysis of TTR *in vivo*. In fact, it is uniquely synthesised by the liver and, once secreted, it is compartmented in the small bowel lumen. Considering that TTR is a circulating plasma protein, it is extremely likely that the enzyme associated with the formation of the amyloidogenic fragment is located in the extracellular matrix and/or in the plasma.

During my phD, I've been actively involved in the investigation of the putative protease active *in vivo*. In the work recenlty published by our research group (Mangione et al. 2018), we conducted a bioinformatics search for systemically active tryptic proteases with appropriate tissue distribution, using the MEROPS database (Rawlings, Barrett and Finn 2016), which is a manually annotated database with information on more than 4000 peptidases classified according to families and clans.

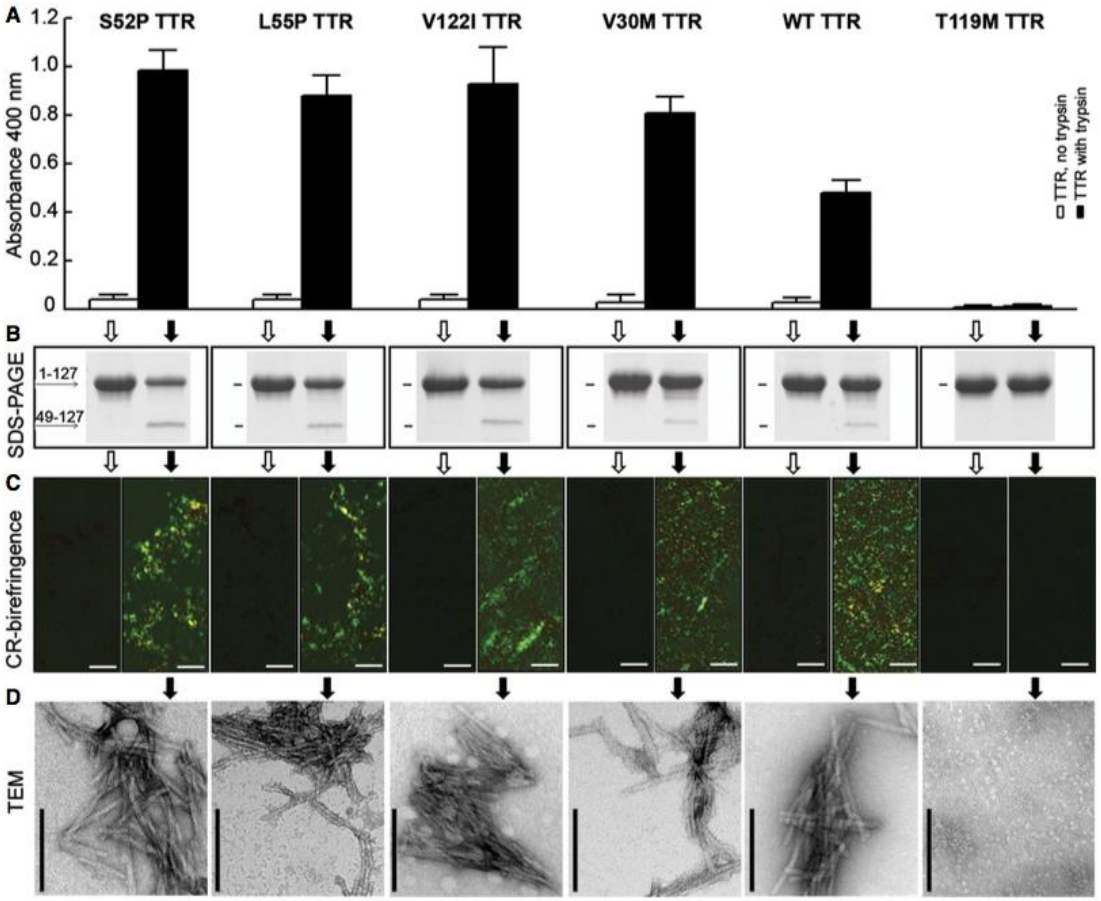

Figure 8. Effect of trypsin on the amyloidogenesis of S52P, L55P, V122I, V30M, WT, and T119M TTR variants. **a)** Aggregation was quantified as spectrophotometric turbidity at 400 nm of samples incubated in PBS pH 7.4 at 37°C for 72 h with magnetic bar agitation in the absence (open bars) or presence (solid bars) of trypsin at an enzyme:substrate ratio of 1:200. Each bar shows mean ± SD of three replicates. **b)** Selective proteolytic cleavage of TTR was monitored by SDS–PAGE under reducing conditions, stained with Coomassie Blue. **c)** Amyloid was identified by light microscopy of Congo red-stained specimens viewed under crossed polarized light (scale bar, 10 μM). **d)** Negatively stained transmission electron microscopy (TEM) (scale bar, 100 nm) of TTR samples treated with trypsin as described above (Marcoux et al. 2015).

From a pool of potential candidates, we were able to identify plasmin, on the basis of its structural similarity with trypsin, which selectively cleaves human TTR between residues 48 and 49 under physiological conditions *in vitro*. The effects of heparin and seeds were also confirmed in the presence of the newly identified enzyme.

Our findings, which are reported in Chapter 2.2., suggest that physiological fibrinolysis is likely to play a critical role in TTR amyloid formation *in vivo*.

Finally, in Chapter 2.3., I reported some results on the comparative analysis of structure and function structural of fibrils derived from different procedures of fibrillogenesis or extraction. In particular, in order to investigate the similarities between different type of fibrils, I measured their thermodynamic stabilities because this parameter is totally based on the structure and specific intermolecular interactions.

1.3. β_2-microglobulin and related amyloidosis

- **Dialysis-Related Amyloidosis**

β_2-microglobulin (β_2-m) is the extracellular non-covalently bound light chain of class I major histocompatibility complex (MHCI), a membrane bound protein assembly present on the membrane of all the cells and involved in immune recognition by T cells. It is a small, 99-residue, protein (11.8 kDa), presenting in nearly all nucleated cells and most biological fluids, including serum, urine, and synovial fluid. Its secondary structure consists of seven β-strands (A,B,C,D,E,F,G), which are organized into two β-sheets linked by a single disulfide bridge, presenting a classical β-sandwich typical of the immunoglobulin domain (Fig. 9) (Eichner and Radford 2011). The connecting loop between D and E strands (DE loop) has been proposed to be a critical region in the process of β_2-m aggregation (Eichner and Radford 2011). Indeed, this region makes contact with the MHCI heavy chain, but it has a great conformational variability in solution and different crystallographic structures.

In normal conditions, serum β_2-m, is filtrated through the renal glomeruli to the urine, then reabsorbed and degraded by the renal tubular epithelial cells. It can occur that serum β_2-m concentration increases in patients suffering from renal insufficiency and in haemodialysis patients reaching up to 30 to 50 times more than those in healthy subjects (Naiki et al. 2016).

Accumulation of amyloid fibrils from β_2-microglobulin was first recognized as a characteristic osteoarticular complication in long-term haemodialysis (HD) patients, and called “HD-related amyloidosis” (HRA). Indeed, in 1985, Fumitake Gejyo’s group (Gejyo et al. 1985) showed that the constituent of amyloid deposits of patients treated with chronic haemodialysis was the protein β_2-m (Figure 10).

Remarkably, β_2-m amyloid deposition is localized mainly in joints, bones and ligaments, causing destructive arthropathy, bone cysts and carpal tunnel syndrome. In patients heamodialyzed from a long time, β_2-m fibrils also deposits in general visceral tissues, like heart, gastrointestinal tract and lungs, and smaller deposits may be seen in medium-sized blood vessels.

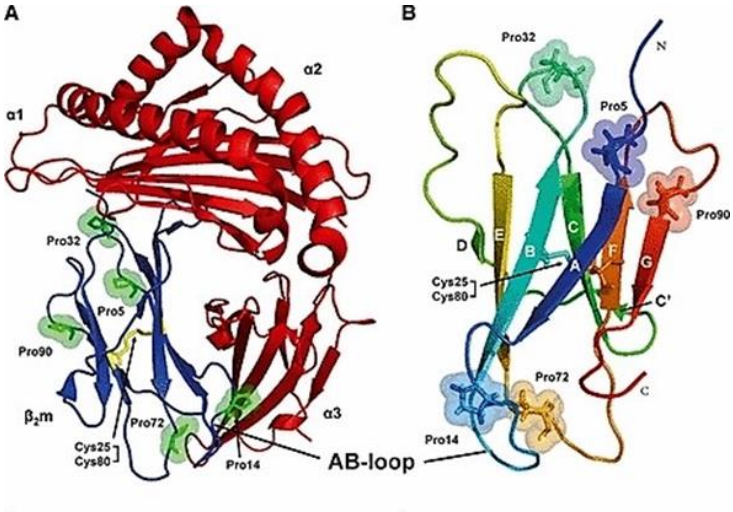

Figure 9. a) Representation of human MHC-I that shows the heavy (α1, α2, α3 in red) and the light chain (β_2-m in blue). Pro5, Pro14, Pro32, Pro72 e Pro90 residue (in green) and the disulfid bond among Cys25-Cys80 residue (in yellow) are highlighted. **b)** Representation of soluble native structure of β_2-m that shows A (6-11), B (21-28), C (36-41), D (50-51), E (64-70), F (79-83) e G (91-94) β-*strands*. From Eichner T *et al.*, 2011. PDB code: 3MYJ.

The presence of species in non-native conformation, derived from physiological dynamic conformational fluctuations of the native β_2-m, is likely to be required for trigger the aggregation process (Eichner and Radford 2011). Persistent high concentrations of β_2-m is a required but not sufficient condition to cross the energetic barrier necessary to obtain the first stable oligomeric species. Indeed other environmental factors are involved in triggering the aggregation process *in vivo*. These species have a high tendency to bind and interact with collagen, in particular type I collagen, which has been found in all natural fibril deposits and is important *in vitro* too to promote β_2-m fibrillogenesis in physiological-like conditions (Relini et al. 2006). In addition, other components of extracellular matrix present in osteo-articular tissues, like glycosaminoglycans, might facilitate amyloid formation. Moreover heparin, a drug of the family of glycosaminoglycans, commonly administered to dialyzed patients as anticoagulant, has been reported to stabilize β_2-m oligomers and strongly enhance the formation of β_2-m amyloid fibrils in the presence of type I collagen (Relini et al. 2008). Finally, many evidences suggest that proteolytic event in the first amyloid nuclei generates proteolysis species, which have a higher affinity for collagen and are thermodynamically more instable than WT β_2-m (Giorgetti et al. 2005). This isoform is

able to accelerate the exponential growth phase of the aggregation process. In particular, the proteomic analysis of natural β_2-m fibrils has shown that 30% of the total protein content in this deposits is constituted by the proteolysed form of β_2-m lacking the first six residues at the N-terminus, named ΔN6 β_2-m (Stoppini et al. 2000). ΔN6 has a higher thermodynamic instability than wild-type β_2-m and a strong tendency to aggregate, even at physiological pH (Esposito et al. 2000).

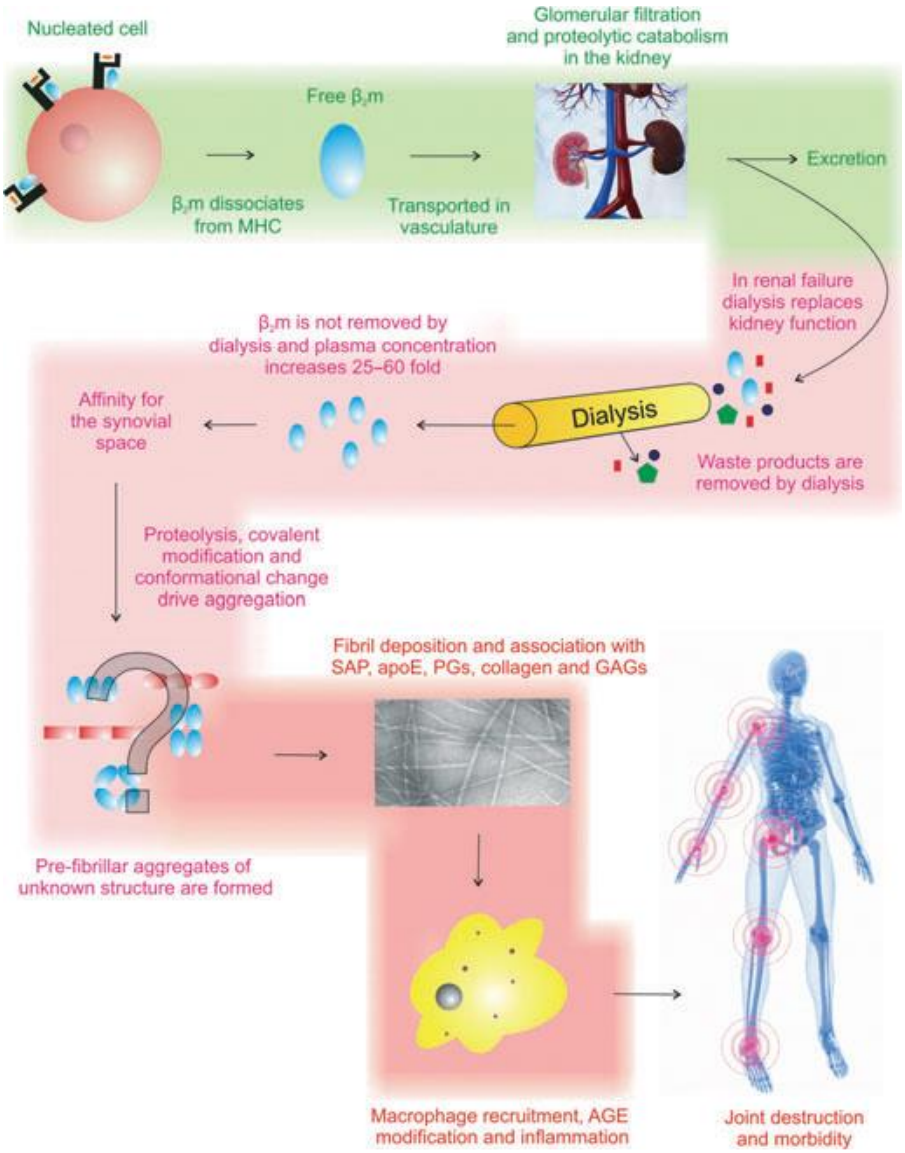

Figure 10. Schematic of the key processes which result in the pathological symptoms experienced in DRA (Eichner and Radford 2011).

- **D76N β_2-microglobulin-Related Amyloidosis**

In 2012, the group of Professor Bellotti and Dr. Valleix (Cochin Institute of Paris) discovered and described the first natural variant of β_2-m in a French family. This variant presents a single amino acid substitution in position 76 from the negative charged aspartate of wild-type protein to the uncharged asparagine (D76N β_2-m), caused from a single base substitution, 286G→A (GAT/AAT), in the *B2M* gene (Figure 11). Patients are heterozygous for this mutation and their main clinical symptoms are: slowly progressive bowel dysfunction, by alternation of diarrhoea and constipation, which leads over time to a strong weight loss (up to 20 kg in two years), persistent sicca syndrome and subsequent autonomic neuropathy. These manifestations are due to extensive visceral amyloid deposits composed only by the full-length D76N variant with a strong involvement especially of spleen and adrenal glands. No visceral amyloid deposits were found in the nervous system or in salivary glands (Valleix et al. 2012).
D76N β_2-m is responsible for a hereditary, systemic form of amyloidosis surprisingly completely different from DRA. Indeed, patients carrying the mutation have normal circulating concentrations of β_2-m (0.2 µM) and normal renal function. The late onset of the disease and the slowly progressive clinical course are consistent with the low plasma concentrations of β_2-m. Finally, in amyloid deposits no wild-type or ΔN6 β_2-m isoforms were observed.

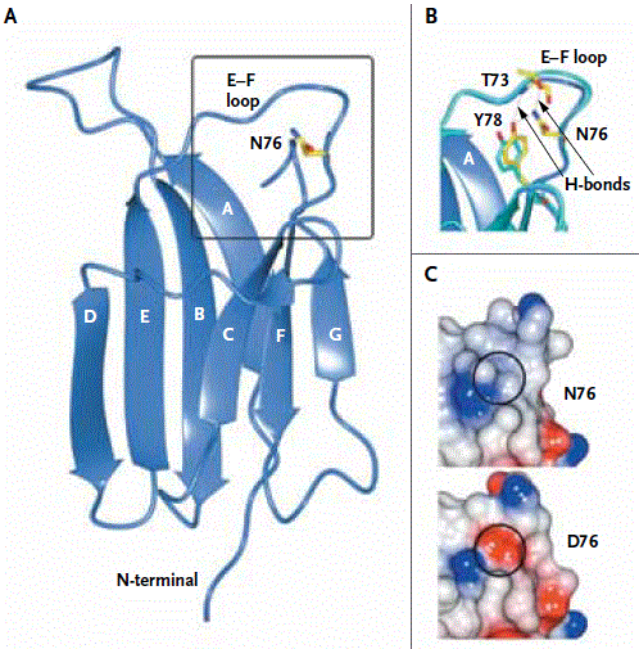

Figure 11. Crystal structure of D76N Variant β_2-microglobulin.**a)** Ribbon representation of the D76N variant. **b)** Close-up view of the E–F loop (residues 70 to 80) shown in Panel A, superimposed on the wild-type β_2-microglobulin structure (blue–green). Residues belonging to the D76N variant are yellow, and Tyr78 belonging to wild-type β_2-microglobulin is blue–green; hydrogen (H) bonds are shown as dashed lines. **c)** Surface electrostatic potential of the E–F loop region in the D76N variant (top) and in

wild-type β_2-microglobulin (bottom); circles indicate the mutated residue. Blue represents positively charged regions, and red negatively charged regions (Valleix et al. 2012).

The Asp76Asn β_2-microglobulin variant is thermodynamically unstable and remarkably fibrillogenic *in vitro* under physiological conditions. Indeed, the crystal structure of the D76N variant at 1.40 Å resolution provided clues to explain its reduced stability and its increased fibrillogenic potential (Figure 11). The amide group of Asn76 establishes a new hydrogen bond with Tyr78, which moves closer to residue 76 providing a hydrogen bond to the amide nitrogen of Thr73. In addition, the theoretical isoelectric point of the mutant shifts from 6.05 to 6.40 due to the loss of the negative charge of Asp76 (Valleix et al. 2012).

In particular, the globular native fold transition to the fibrillar state is primed by exposure to a hydrophobic-hydrophilic interface under physiological intensity shear flow (Figure 12, (Mangione et al. 2013).

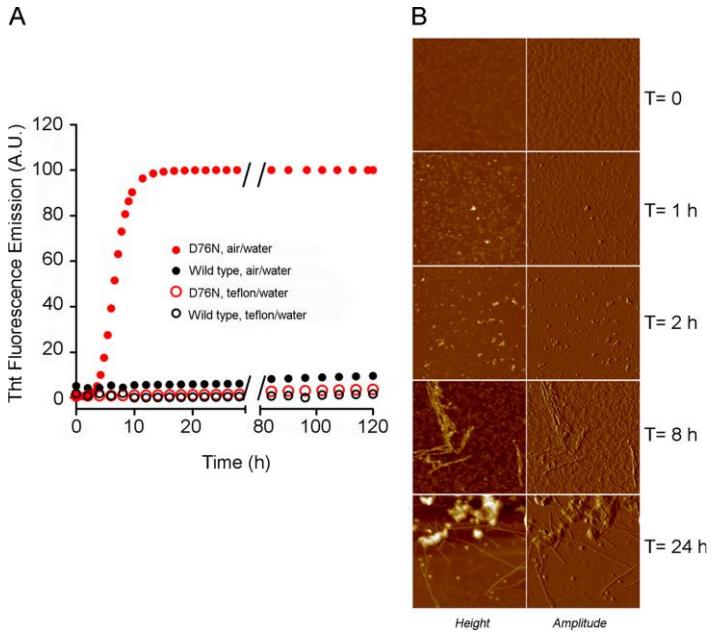

Figure 12. Fibrillogenesis of D76N and wild type β_2-m. **a)** The time course of aggregation of D76N β_2-m (*red*) and wild type (*black*) was monitored under stirring conditions by fluorescence emission of ThT (using 445 and 480 nm as excitation and emission wavelengths, respectively). Proteins were dissolved at 40 β_2-m in 25 mM sodium phosphate buffer, pH 7.4 at 37 °C. Aggregation experiments were monitored in the presence of air-water (*filled circles*) and Teflon-water interfaces (*empty circles*). **b)** Tapping mode AFM images of different stages of aggregation of D76N β_2-m carried out under stirring conditions and in the presence of an air-water interface. Oligomers formed after 1 h, prefibrillar aggregates coexisted with oligomers

after 2 h, filaments were observed after 8 h, and fibril clusters were observed after 24 h. Scan size, 1 β_2-m; Z range, 15 (times 0 and 24 h), 8 (times 1 and 2 h), and 3 nm (time 8 h). *a.u.*, arbitrary units (Mangione et al. 2013).

As you can see in Fig. 12, the formation of D76N β_2-m amyloid fibrils *in vitro* is enhanced by fluid agitation and exposure to a hydrophobic surface in physiological buffers. In contrast, fibrillogenesis of wild type β_2-m is extremely slow under physiological conditions, being minimal or absent after 100 hours of incubation (Mangione et al. 2013).

Within the extracellular space where amyloid is deposited in systemic amyloidosis, the interstitial fluid flows over the extensive surfaces of the fibrous network of elastin, collagen, and proteoglycans, the high hydrophobicity of which play a key role in promoting local unfolding of globular proteins. If a mutation reduces the stability of β_2-m (*i.e.* D76N mutation), the shear stress in the extracellular matrix of visceral organs such as liver, spleen, kidney, and heart is sufficient to unfold the unstable variant and prime a cascade of events as represented in Fig.13.

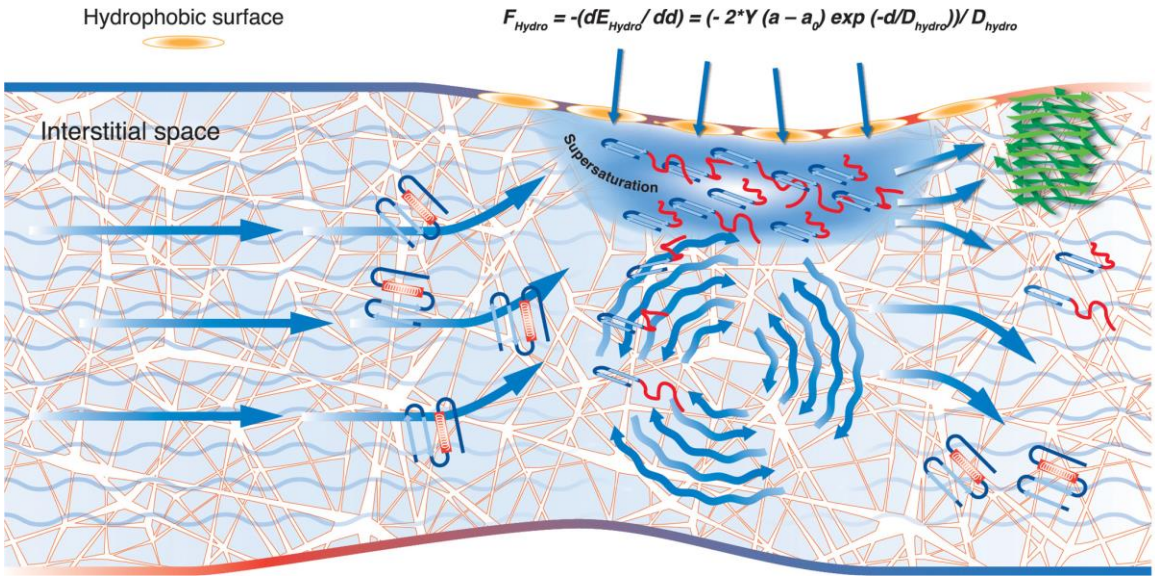

Figure 13. Schematic picture of the hypothetical events occurring in the interstitial space where globular soluble proteins undergo fibrillar conversion. Native globular proteins flow through a network of fibrous proteins (*i.e.* collagen and elastin) and GAGs. These matrix proteins expose hydrophobic patches with which the native globular proteins collide. At the interface between the hydrophobic surface and the aqueous fluid, proteins are exposed to

forces sufficient to perturb the folded state. The exposure of normally buried hydrophobic elements further facilitates the interaction with the hydrophobic matrix, local accumulation of partially folded globular conformers reaching a condition of supersaturation. Supersaturation is the precondition for protein aggregation and loss of solubility. Even minimal changes in the intensity of the shear flow can break the very labile soluble state of partially folded proteins when they reach the condition of supersaturation. If supersaturation is not reached, the simple unfolding of the proteins does not imply a fibrillar conversion and the protein can properly refold and escape from the aggregation (Stoppini and Bellotti 2015).

1.4. *Caenorhabditis elegans* as a model system for systemic amyloidosis

1.4.1. General biology and anatomy of *Caenorhabditis elegans*

In 1963, Sydney Brenner sent a letter to Max Perutz, the chairman of the Medical Research Council's Laboratory of Molecular Biology, proposing a nematode (round worm), *Caenorhabditis briggsae,* as a useful tool in order to solve the “classical problems of molecular biology” (Brenner 2002). Later, he moved his focus on the related nematode *Caenorhabditis elegans* (*C. elegans*) because the elegans strain grew better than the *briggsae* isolate in Brenner's laboratory (Félix 2008).

C. elegans is a free-living, transparent nematode that lives in temperate soil environments but it can be most easily be isolated from rotting vegetable matter, which contains an ample supply of their bacterial food source (Barrière and Félix 2014). In the laboratory it can be cultivated on agar plates and it needs *Escherichia coli (E. Coli)* bacteria as a food source (Cassada and Russell 1975).

Most of its population (99.5%) are self-fertile hermaphrodites, only 0.05% are male. *C. elegans* hermaphrodites are about 1 mm in length and 50 µm in diameter and essentially are females whose gonads temporarily produce sperm before they produce oocytes. Male individuals, on the contrary, have a single-lobe gonad with a tail specialized for the mating with hermaphrodites (Fig. 14a). The hermaphrodite individuals possess five autosomes and two sex XX chromosomes, the male ones have the XO karyotype (Reinke et al. 2004). Generally, males arise infrequently in the germ line (0.1%). The number of males can increase after mating (50%) or in adverse and stressful conditions such as high temperature, overcrowding or lack of food. This facilitates sexual reproduction, allowing genetic recombination, thereby increasing the probability that the progeny will adapt to the changed environmental conditions. The number of cells in *C. elegans* is always the same for each individuals and is about 959 somatic cells with 302 neurons for the hermaphrodite individuals and about 1031 cells with 381 neurons for the male ones (White J et al. 1988)

One attractive feature of *C. elegans* is that despite its simplicity, it has defined tissues. The animal is often described as a series of concentric tubes (Fig. 14). The outer layer of cells, the epidermis, encloses a pseudo-coelomic fluid-filled cavity housing the main organ systems. Just inside the epidermis are the bands of muscle, which control

movement of the organism, as well as the ventral and dorsal nerve cords that innervate the muscles. The muscles receive input from the neurons by sending muscle arms to motor neuron processes that run along the nerve cords or reside in the nerve ring. The obliquely striated body wall muscles are organized into strips in four quadrants, two dorsal and two ventral, along the whole length of the animal. Non-striated muscles are found in the pharynx and around the vulva, intestine and rectum.

The cells of the nervous system are arranged into ganglia in the head and tail. *C. elegans* neurons are mainly located in the head around the pharynx (Figure 14). In the body, a continuous row of neuronal cell bodies lies at the midline, adjacent to ventral hypodermis. In addition, there are two small posterior lateral ganglia on the sides as well as some scattered neurons along the lateral body. The processes from most neurons travel in either the ventral, or the dorsal nerve cord and project to the nerve ring in the head (Wormatlas).

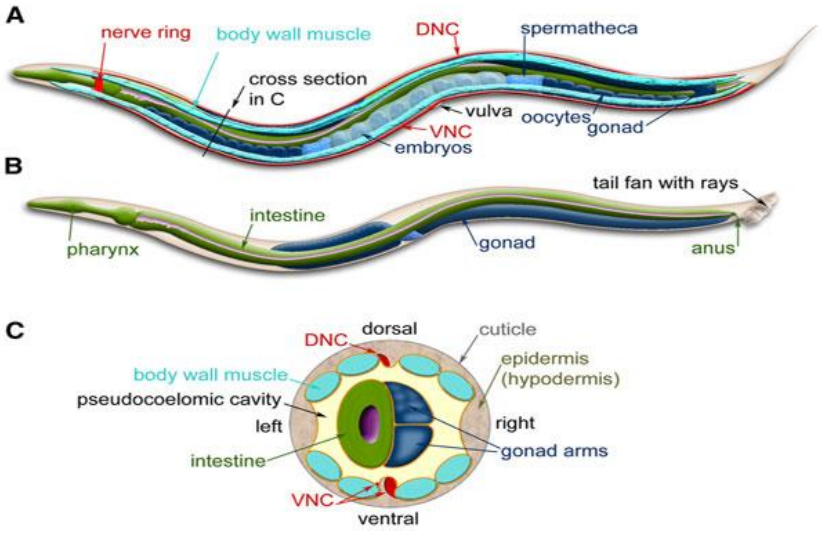

Figure 14. *C. elegans* anatomy. Major anatomical features of a hermaphrodite a) and male b) viewed laterally. **a)** The dorsal nerve cord (DNC) and ventral nerve cord (VNC) run along the entire length of the animal from the nerve ring. Two of the four quadrants of body wall muscles are shown. **b)** The nervous system and muscles are omitted in this view, more clearly revealing the pharynx and intestine. **c)** Cross-section through the anterior region of the *C. elegans* hermaphrodite (location marked with a black line in a) showing the four muscle quadrants surrounded by the epidermis and cuticle with the intestine and gonad housed within the pseudocoelomic cavity. Images modified from those found at www.wormatlas.org.

Within the pseudocoelom are:

- a digestive system. Food (bacteria) enters the anterior of the animals and passes through the pharynx, a two-lobed neuromuscular pump that grinds the food before it is passed on to the intestine for digestion (Figure14b, (You and Avery 2012). The pumping behaviour of the animals depends on the availability and the quality of the food; for example, animals pump more when hungry and less when full (Avery and Shtonda 2003). The C. *elegans* intestine is attached to the posterior pharynx and consists of 20 large, polyploid epithelial cells arranged in pairs that form a tube running the length of the animal.
- an excretory system which is involved in osmoregulation and in secretion of glycoproteins thought to make up a replenishable surface coat over the epicuticle. The excretory cell is the largest cell in the animal, with excretory canals running the length of the body that are connected to an excretory/secretory pore on the ventral side of the head.
- a reproductive system, which in hermaphrodites consists of functionally independent anterior and posterior arms. Each arm is reflexed with an ovary that is distal to the vulva, a more proximal oviduct, and a spermatheca connected to a common uterus centred around the vulva. The gonad forms an ovotestis that first produces haploid amoeboid sperm that are stored in the spermatheca and then produce much larger oocytes (Fig. 14A). The adult uterus contains fertilized eggs and embryos in the early stages of development. Vulval contractions, mediated by the hermaphrodite-specific neurons, are required for egg laying.

  The male gonad is a single reflexed organ extending anteriorly from its distal tip, then posteriorly to connect via the vas deferens to the cloaca near the anus (Fig. 14B). As with the hermaphrodite ovary, the germ-line nuclei are mitotic near the distal end. Meiotic cells in progressively later stages of spermatogenesis are distributed along the gonad to the seminal vesicle, in which spermatids are stored for release during copulation. Male-specific neurons, muscles, and hypodermal structures are required for mating with hermaphrodites (Riddle DL et al. 1997).

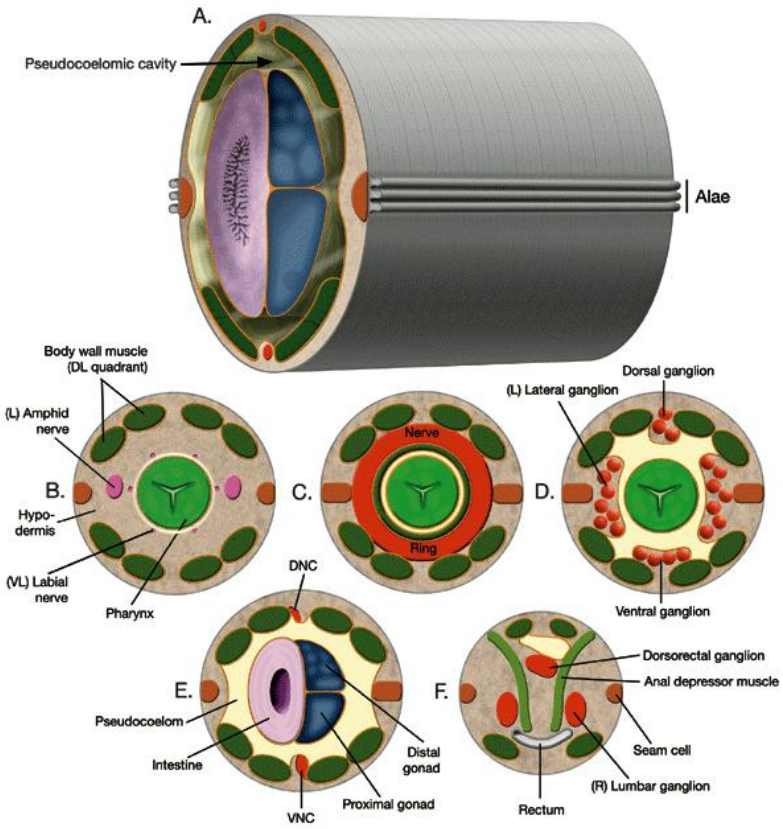

Figure 15. Nematode body plan with cross sections. **a)** Posterior body region: body wall (outer tube) is separated from the inner tube (alimentary system, gonad) by a pseudocoelom. Orange lines indicate basal laminae. **b)** Section through the middle of head. **c)** Section through posterior body. (DNC) Dorsal nerve cord; (VNC) ventral nerve cord. **d)** Section through posterior head. **e)** Section through posterior body. (DNC) Dorsal nerve cord; (VNC) ventral nerve cord. **f)** Section through tail, rectum area. From Wormatlas.

In addition, *C. elegans* has six cells in the pseudocoelomic cavity (Fig. 16), called coelomocytes, which act as scavengers in the body cavity (Grant and Sato 2006). These cells behave similarly to vertebrate macrophages, are highly active in endocytosis, and are thought to sort through and clear material in the pseudocoelomic cavity of the animal. *C. elegans*, like many other small animals, does not have a specialized respiratory or circulatory system. The nematode worm depends on diffusion of gases for supply of oxygen to its tissues. The outer tube is covered by the collagenous, extracellular cuticle, which is secreted by the underlying hypodermis (Riddle DL et al. 1997). At each of the four larval molts, a new cuticle of stage-specific composition is secreted, and the old cuticle is shed.

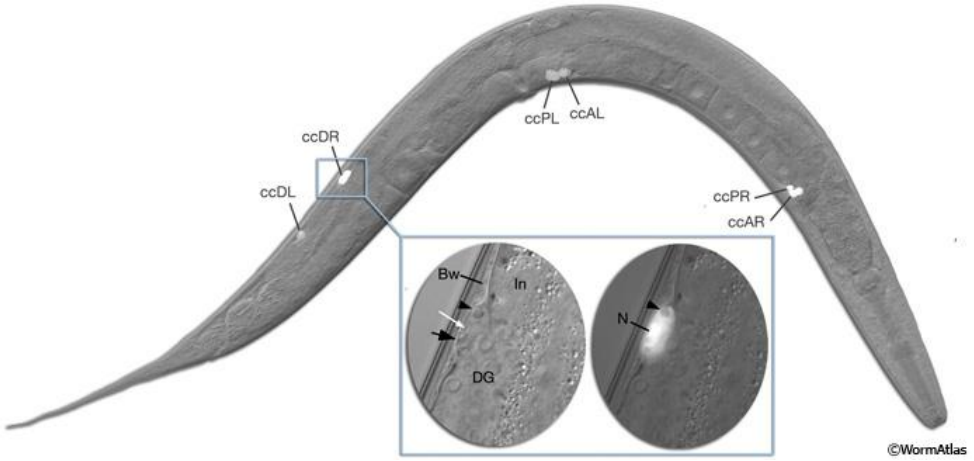

Figure 16. Coelomocytes in the adult hermaphrodite. Three pairs of coelomocytes reside in the pseudocoelomic cavity. Four of these cells are on the ventral side. Two of these (ccPR and ccAR) are situated close to the head, whereas the other two (ccPL and ccAL) are close to midbody, anterior to vulva. The remaining pair (ccDR and ccDL) is located dorsally in the posterior body. An epifluorescent image of a transgenic animal expressing the reporter gene *unc-122::GFP* in coelomocytes is overlayed on the DIC image of the whole animal, seen from the right side. (*Inset, left*) A magnified DIC image, right lateral view, of ccDR (*arrow*) between intestine (In), distal gonad (DG), and body wall (Bw). The nucleus contains a nucleolus (*white arrow*). *Arrowhead* points to a vesicle within the cell. (*Inset, right*) Magnified epifluorescent image of the same cell; the vesicle is seen as translucent. (N) Nucleus. From Wormatlas.

1.4.2. Life cycle and lifespan

The life cycle of *C. elegans*, similar to others nematodes, comprises an embryonic stage, four larval stages (L1-L4) and adulthood (Fig. 17). At the end of each larval stage, a new cuticle, of stage-specific composition, is synthesized and the old one is shed (Cassada and Russell 1975). During this period, pharyngeal pumping ceases and the animal enters a brief lethargus. The average development time and lifespan are strictly related to the temperature of incubation of worms. In general, *C. elegans* is able to grow and reproduce between 12-25°C; higher temperatures are considered stress conditions that can be tolerated for a short time. Embryogenesis takes approximately 16 h at 20°. A virtually impermeable eggshell is made after fertilization, allowing the

embryo to develop completely independent of the mother. However, embryos are usually retained within the hermaphrodite until about the 24-cell stage at which time they are laid (Corsi, Wightman and Chalfie 2015). The worms begin to eat and develop through the four larval stages. Approximately 16 hr after the L4 molt at 25°C (Figure 17a), adult hermaphrodites start producing progeny for a period of 2-3 days until they have utilized all of their self-produced sperm; additional progeny can be generated if the sperm-depleted hermaphrodite mates with a male. An individual hermaphrodite is capable of producing more than 300 progeny during its life. After the reproductive period, hermaphrodites can live several more weeks before dying of senescence. The total generation time from egg to adult worm is only of about 3 days and the lifespan of about 3 weeks (Cassada and Russell 1975).

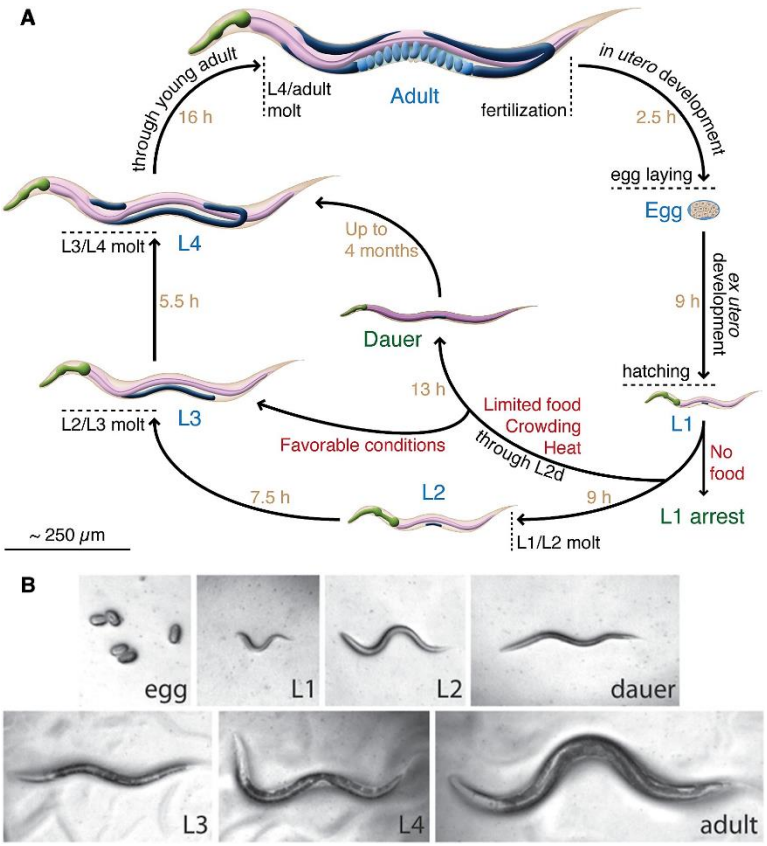

Figure 17. a) *C. elegans* life cycle at 25°C. Worms are drawn approximately to scale. **b).** Micrographs of laid eggs, larval stages and adults (Erkut C. 2014: C. elegans life cycle and developmental stages).

In stress conditions, such as lack of food, overcrowding and high temperature, the L1-L2 animals will enter an alternative life cycle and become "dauer larvae" (“dauer” in German means “lasting") until these unfavourable conditions improve. The dauer is capable of living for 3–6 months in a dormant state (Fielenbach and Antebi 2008). Its cuticle completely surrounds the worm and seals up the mouth preventing the animal from eating and thereby arresting development. The cuticle confers enhanced resistance to chemicals to the worm, providing with greater protection against environmental stresses and caustic agents. When the dauer larvae are transferred onto plates with bacteria, they lose their mouth plugs, molt, and continue their development as slightly different L4 larvae (Corsi et al. 2015).

1.4.3. Genome and Proteome

C. *elegans* was chosen as a model for biological research in the early 1960’s by Sidney Brenner (Brenner 1973) and it has been extensively studied with regard to its genetics and development. It was the first complete eukaryote to have its genome sequenced (*C. elegans* Sequencing Consortium, 1998) and in which cell lineage, which is invariant between animals, has been established. The sequence of all five autosomes and the single sex chromosome was first published on Science in 1998 (*C. elegans* Sequencing Consortium, 1998). Although the genome of this worm is substantially smaller than that of humans (it consists of about 100 million base pairs, *H.sapiens* genome is about 3,000 million base pairs), *C. elegans* has nearly as many genes (about 20,000 genes, while humans have 23.000 genes) (Hillier et al. 2005). Those genes (~15% of total) coding for proteins in *C. elegans* are organized in operons and this can perhaps explain in part why the genome of worms is 30-fold smaller than its human equivalent while having a similar number of genes. Indeed, in contrast to other eukaryotes, worms use operons in which a single promoter regulates upstream the transcription of a group of genes in a single filament of m-RNA in order to induce the co-expression of genes (in other eukaryotes each single gene have a promoter sequence). A second explanation could be that the *C. elegans* genome contains a smaller portion of non-coding DNA (DNA that does not code for proteins). Moreover,

despite the evolutionary distance of *C. elegans* from humans and its simplicity, a significant genetic overlap between the two organisms has been reported. Depending on the bioinformatics approach used, *C. elegans* homologues have been identified for 60–80% of human genes (Kaletta and Hengartner 2006).

The genome database of *C. elegans* is available worldwide, providing a working framework for researchers including those with interests in human genes. In order to diversify its proteome, *C. elegans* is able to perform both post-transcriptional modifications both post-translational modifications (Hulme and Whitesides 2011).

Recently, a repository of *C. elegans'* protein kinases, which form one of the largest protein families found in all species, catalysing the reversible phosphorylation of proteins and representing key therapeutic targets in drug development, has been created by UniProt Knowledgebase. The *C. elegans* kinome is composed of 438 kinases and almost half of them have been functionally characterized (Zaru et al. 2017).

Moreover, *C. elegans* has proven to be an exceedingly useful genetic model system for the study of how proteostasis works (Fig. 18). Namely, it has been used to study molecular chaperone function, identify genetic pathways that regulate aging, and even express intrinsically aggregation-prone disease-associated proteins as a means to perturb the protein folding environment and investigate how the *C. elegans* proteostasis machinery responds (Kikis, Gidalevitz and Morimoto 2010).

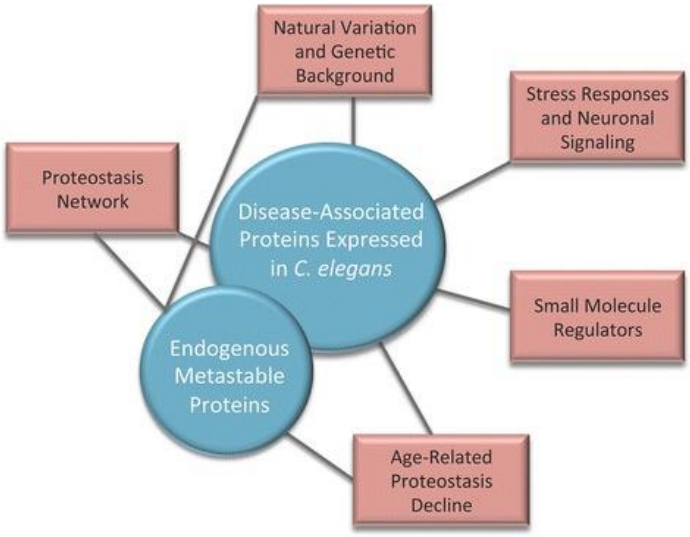

Figure 18. Using *C. elegans* models of protein folding to study the regulation of proteostasis. The figure shows how two different types of folding sensors, disease-associated aggregation-

prone proteins and metastable endogenous proteins (shown in *blue*), have been used to uncover the proteostasis network, reveal how natural variation and genetic background modulate the protein folding environment, reveal how proteostasis declines during aging, and identify small molecule regulators of proteostasis (shown in *red*). Black lines connect the two categories of folding sensors to the research areas in which each was employed as a tool (Kikis 2016).

1.4.4. Applying *C. elegans* to study human diseases

Many advantages in manipulating *C. elegans* allow its use as an animal model:

- It has small size and can be cultivated on agar plates in small incubators; it can be preserved in liquid nitrogen.
- Since the life-cycle (Fig. 17) and the lifespan is short, it is an appropriate model in order to observe quickly results of experiments (Kim, Kim and Park 2017) and it is suitable for the study of age-related diseases. The average worm gives rise to about 300 progeny; thus, one worm can produce about 100,000 offspring within a week.
- *C. elegans* show transparency, facilitating the study of cellular differentiation and other developmental processes in the intact organism. It is possible to observe each worm's cell through the light microscope in a non-invasive way and cellular events, such as mitosis or cytokinesis, can be followed in real-time. Furthermore, its transparency allows the use of fluorescence markers *in vivo* too.
- The anatomy is simple but some tissues are conserved in *C. elegans* such as the muscle, nervous, intestinal system.
- Despite the small number of neurons, the *C. elegans*' nervous system shows 118 types of neuronal cells making the worm extremely diversified. Moreover, it uses the most known neurotransmitters such as acetylcholine, GABA, glutamate, dopamine and serotonin that are implied in different human diseases. Indeed, those neurotransmitters have key functions for the motility, nutrition, mating, egg laying and for search for food behaviours that are phenotypic features easy to observe and quantify in order to study neuronal pathways.
- As already mentioned, the complete lineage of every cell in the *C. elegans* has been determined, which allows a fate map of this organism to be accurately

drawn at any stage of it's development, something that can't be found in any vertebrate.

- It’s possible to engineer worm models with some human disorders by microinjection of ectopic genes. Some *C. elegans* mutants have shown to mimic morphological and/or functional defects, which are encountered in some aspects of human disease (Culetto and Sattelle 2000).
- Without doubt, however, the greatest advantage of *C. elegans* is that gene function can be downregulated systematically by RNAi. Injection of double-stranded RNA or the feeding of bacteria carrying constructs making double-stranded RNA (Fig. 19) results in specific inhibition of the gene so targeted (Timmons, Court and Fire 2001). As well as revealing a model for genetic resistance to viral infection, this RNAi methodology has resulted in screens of every gene in the genome for a variety of different phenotypes, but especially for aging (Lee et al. 2003).

The nematode *C. elegans* has been proposed not only as a useful tool in order to mimic human diseases and for the investigation the pathological molecular mechanism (Culetto and Sattelle 2000), but also it has been proved to be suitable for the identification of new possible drug candidates and for the functional characterization of pharmacological targets (Kaletta and Hengartner 2006).

As already mentioned, since it is a small animal and it can proliferate quickly, it is a suitable model for the screening of small molecules with therapeutic activity.

At first glance, the nematode *C. elegans* may not be the most appropriate choice for investigating the efficacy of putative drugs. It is clear that the pathological conditions in worms are extremely different from the ones developed by humans. However, most of the diseases are caused by genetic, biochemical or physiological processes related to both endogenous factors (such as mutations) both exogenous (such as pathogens). Clinical manifestations of a pathology are specific for each species and can follow different modalities; on the contrary, the molecular processes that underlie the pathology are mostly preserved among different species. Indeed, as previously underlined, *C. elegans* shares with the mammals lots of molecular mechanisms and the preservation of those seems to be more significant with respect to the preservation of morphological features or symptoms (Carretero, Solis and Petrascheck 2017).

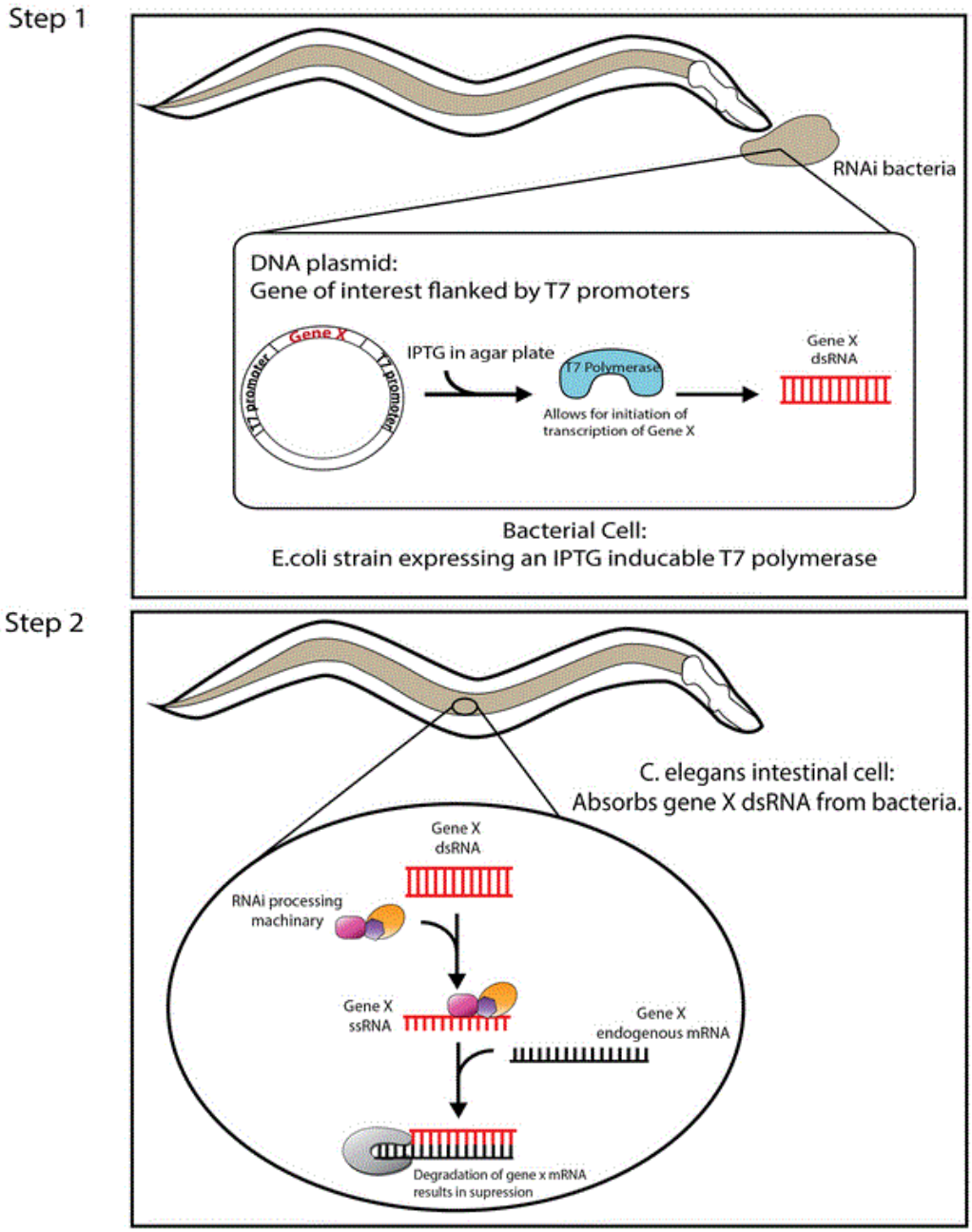

Figure 19. RNA interfering process in *C. elegans*. Credits to Sarah Tronnes.

Step 1. Transformation of the plasmid encoding dsRNA of interest into the (DE3) strain of *E. coli* bacteria that will express the double-stranded RNA. The bacteria also contains an IPTG inducible gene for T7 DNA polymerase, which transcribes the dsRNA in the plasmid. **Step 2.** After feeding the worms with the transformed HT115 (DE3) bacteria, dsRNA is taking up by *C. elegans* intestinal cells and processed into short interfering RNAs (siRNAs). RNAi can induce both post-transcriptional and transcriptional gene silencing.

C. elegans model cannot completely mimic the physio-pathology of a specific human disease; it is necessary to define the modalities and the potential restrictions of the model in order to validate it assuring the consistency between the animal model and the specific aspects of the human pathology (Kaletta and Hengartner 2006). Thanks to the advantage to exploit molecular similarities using orthologues genes, which cause different phenotypes in different species, it is possible to study pathological disease that do not exist in C. *elegans*. For example, Osteogenesis Imperfecta is caused by mutations in the gene of human collagen (COL1A1 and COL1A2). Despite the fact that *C. elegans* does not present bone tissue, a mutated form of collagen expressed by the worm is related to a particular phenotype, thus suggesting that the genetic defect can be studied also in the absence of the tissue affected by the pathology (Johnstone, Shafi and Barry 1992).

In the view of performing drug screening on *C. elegans*, a crucial factor to take into account is the bioavailability of drugs in worms. In fact, to reach their putative target, molecules should be able to pass the cuticle and the intestinal coating of nematodes, which represent a significant physical barrier for the majority of chemicals (Burns et al. 2010) (Fig. 20). A possible strategy for obtaining a selective permeability of the cuticle is to create transgenic nematode strains presenting an impaired cuticle (Gravato-Nobre et al. 2005). Once the drug reaches the target, it has to overcome the regulatory mechanisms of cells and tissues in order to determine a measurable pharmacological effect. Those conditions indicate that not all the molecules with *in vivo* activity are able to trigger an action in *C. elegans*. It is interesting noting that, since drugs can interact simultaneously with multiple objectives, it is possible to identify synergic or off-target effects by performing *in vivo* assays on *C. elegans* (Kaletta and Hengartner 2006).

It is therefore necessary to take into account that the use of *C. elegans* in order to evaluate the efficacy of putative drugs can have some limitations. A significant portion of the screened molecules could be not effective because they cannot reach the target.

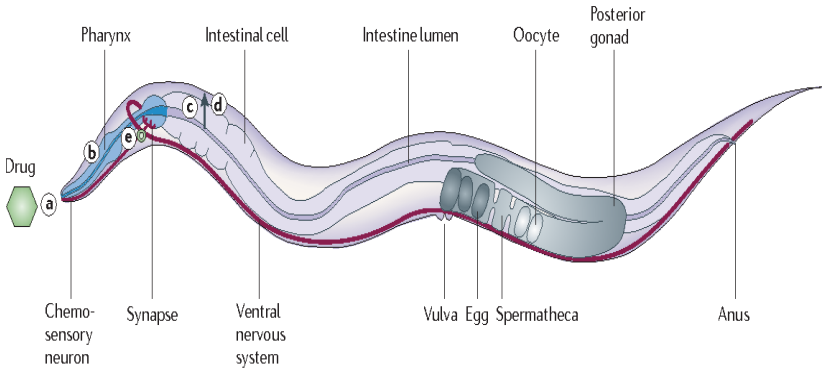

Figure 20: Drug entry route into *C. elegans*. The simplified body plan of a *C. elegans* adult hermaphrodite. Drugs have been reported to enter *C. elegans* via three distinct routes: ingestion; uptake through the skin; and uptake via exposed sensory neuronal endings. Uptake by ingestion is a relatively slow process that involves several distinct steps. **a)** Chemosensory neurons help to choose appropriate food sources. Compounds with unpleasant smell or taste might be avoided and not taken up effectively. **b)** The drug is taken up by aspiration through the pharynx. The activity of this feeding organ depends on satiety or food availability and is controlled by various neurotransmitter systems. **c)** Once the drug has entered the intestinal lumen, it has to be absorbed by intestinal cells. The apical side facing the lumen is covered by microvilli, increasing the absorption surface. Indeed, the intestinal cells express many transport proteins such as P-glycoproteins and peptide transporters. **d)** From the body cavity the drug is distributed rapidly throughout the body. **e)** The drug reaches its target. In this example, the drug binds to receptors at a synapse in the central nervous system, evoking a behavioural response such as reduced feeding activity (Kaletta *et al*., 2006).

1.4.5. Automated systems for *C. elegans* phenotyping

The recent developments in science, such as entire genome sequencing, DNA microarrays, miniaturization, informatics and robotics have drastically changed the approach of drug discovery. One of the technique that has been employed is High Throughput Screening (HTS) and consists in random screens of compounds to find hits showing an activity or an affinity on a selected target and/or in a model considered representative of a disease (Spring 2005). Two different approaches can be followed (Figure 21). The first one consist in performing *in vitro* experiments for the screening of molecules directed towards a specific target. The second one is based on the screening of molecules able to revert a pathological phenotype in a model able to mimic the disease. In this case, it's not necessary to identify the target before but the approach can be useful in order to understand better which are the molecular mechanisms of the disease. For that particular purpose, *C. elegans* has been shown to be a useful model. Despite the fact it is a simple organism, it can offer a level of complexity, which is higher than cell cultures, and it allows the study of pharmacological targets that could not be studied on isolated cells. Since it's quite easy to make transgenic *C. elegans* strains, it's possible to express human proteins (or mutated genes related to diseases) in the worms, the expression of the proteins may lead to a pathological phenotype in the nematode that doesn't need to be exact mapping the pathology. It's important to have something to measure: a larval growth or a motility defect (Carretero et al. 2017).

Because of the ease of manipulating C. *elegans* and the possibility of growing them in 96-well plates, we can use nematodes in high-throughput screening (HTS) (Ma et al. 2018).

Indeed, many molecules that have been shown to be effective in *in vitro* cell cultures, do not show any potency *in vivo* or they seems to be toxic (Giacomotto and Ségalat 2010). The use of *C. elegans* could prevent this kind of error.

The phenotypic characterization of C. *elegans* transgenic models consist in the performing of behavioural assays based on the evaluation of various parameters such as lethality, larval growth impairment, paralysis, abnormal morphology.

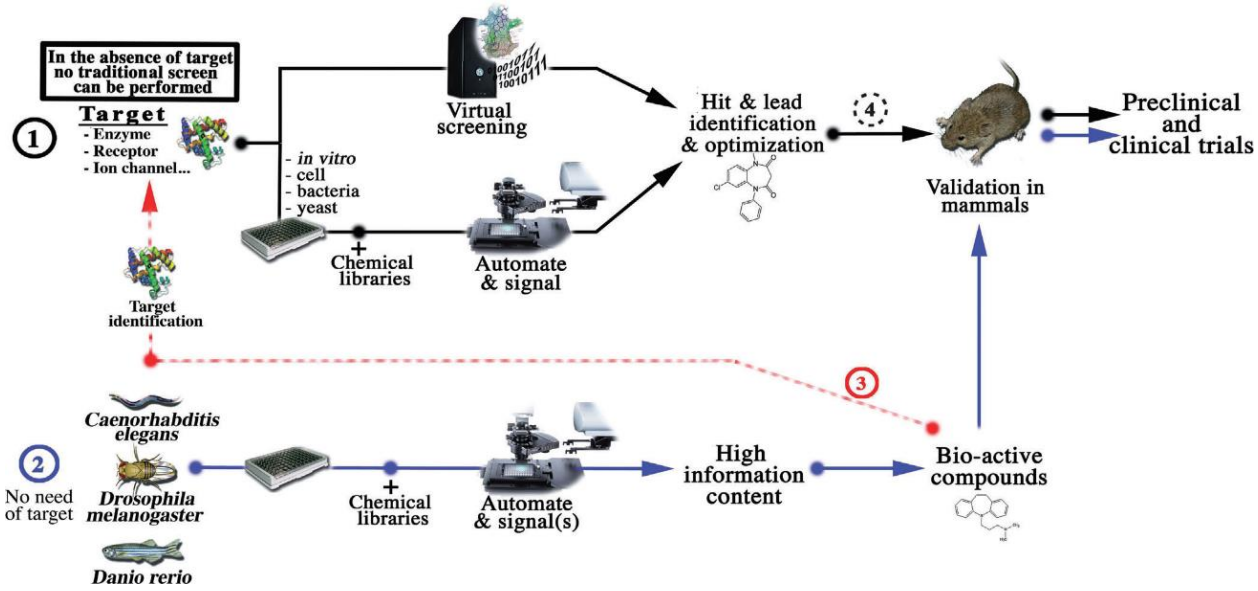

Figure 21. Whole-animal screening and drug discovery process. (1, black lines) show a schematic view of the different stages which came upon a drug discovery process based on traditional HTS. In the absence of target or in complex mechanism, screen can hardly set up. (2, blue line) An alternative may come from phenotypic chemical screens with small animal models like *C. elegans*, *D. melanogaster* and *D. rerio*. (3, red line) Identification of hits in these models may reveals new molecular mechanisms and targets. The target could be further used in traditional HTS. (4) *C. elegans*, *D. melanogaster* and *D. rerio* may also bridge the gap between traditional high-throughput screening and validation in mammalian models. HTS, High Throughput Screening (Giacomotto and Ségalat 2010).

The manual count of those parameters can be very time-consuming and error-prone leading to non-replicable results. In order to facilitate the phenotypic screening of C. *elegans* strains many automated assays have been developed in the recent years (Fig. 22).

C. elegans is an excellent candidate for whole organism-based high-throughput screening (HTS). It is possible to model complex human diseases that can not be easily reproduced *in vitro* or in unicellular models and drug efficacy and absorption, distribution, metabolism, excretion or toxicity (ADMET) characteristics can be simultaneously evaluated at the initial stages of the drug discovery pipeline (O'Reilly et al. 2014).

The first evaluation made by HTS was conducted in 2006 by Kwok and colleagues (Kwok et al. 2006); in this work, starting from 14100 small molecules, researchers have identified 308 compounds able to induce readable phenotypes in *C. elegans*. Although

this was the first example of a large-scale drug screen using *C. elegans*, the screen still relied on agar plates, and phenotypes were scored visually. In 2006, Lehner and colleagues developed an all-liquid workflow to facilitate HTS in *C. elegans* in a 96-well format (Lehner, Tischler and Fraser 2006).

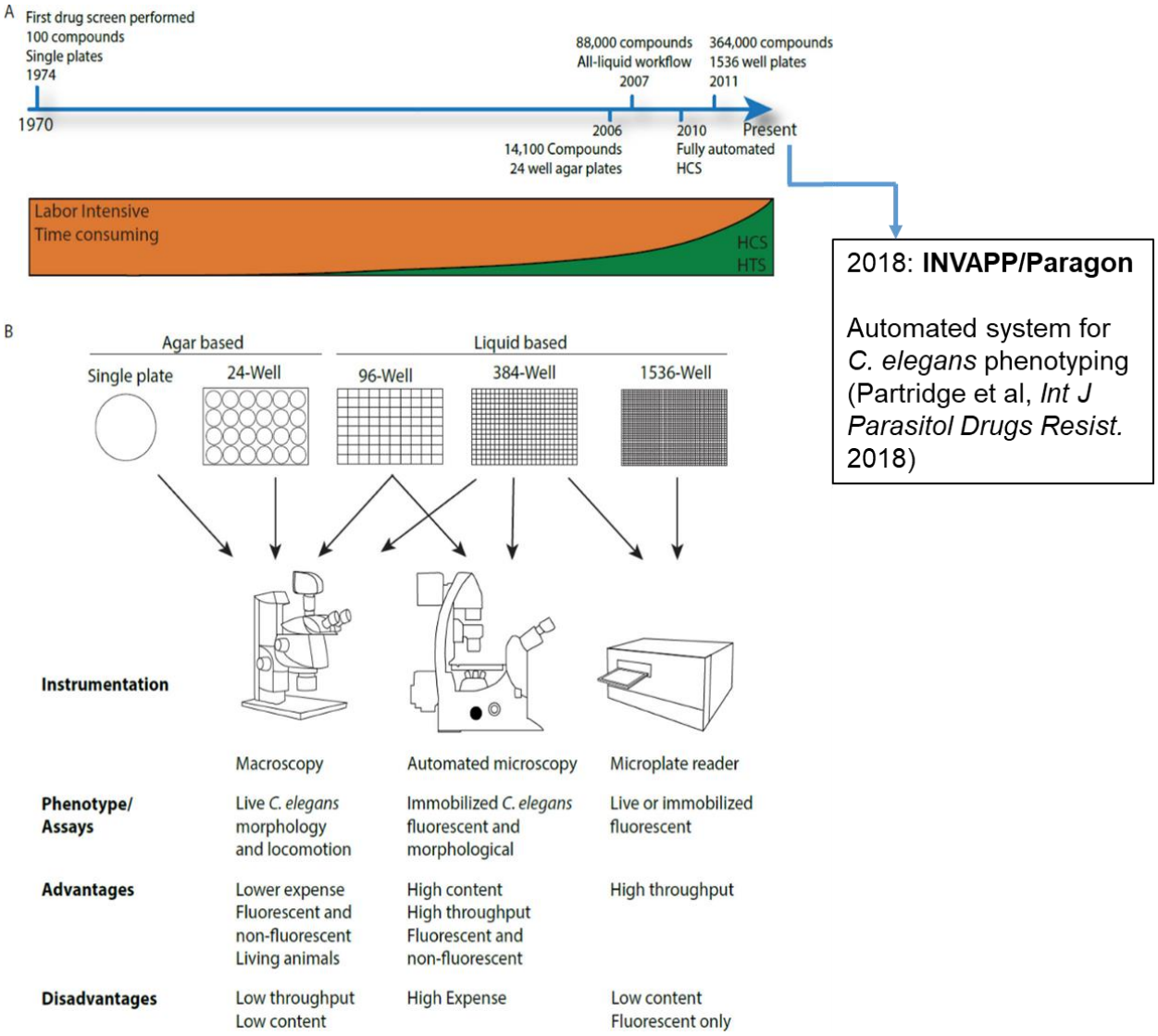

Figure 22. Historical timeline of *C. elegans*-based drug discovery. *C. elegans* was first used for drug testing in 1974 but not as a tool for HTS until recently. **a)** Timeline shows major milestones. In 2018, a new automated system, for *C. elegans* phenotyping, has been developed by Partridge and his collaborators (Partridge et al. 2018). **b)** Common instruments currently used for phenotypic assessment of *C. elegans* (O'Reilly et al. 2014).

In 2010, Gosai and his colleagues (Gosai et al. 2010) have developed an automated platform, which combines fluorescence microscopic analysis with an imaging

acquisition software for quantifying protein accumulation within the intestinal cells of *C. elegans,* expressing the mutant form of human α1-antitrypsin fused with GFP. With this system, a pilot screen of about 1,280 compounds was conducted and the researchers identified 33 hit compounds that significantly reduced the intracellular accumulation of misfolded protein aggregates.

Recently, a new system was developed by Mathew and his group, named "WormScan", (Mathew, Mathew and Ebert 2012) which employs a traditional flatbed scanner for imaging NGM plates where worms grow and study mortality, movement, fecundity and size of the nematodes. The method uses light stimulus from the scanner rather than physical stimulus to induce movement. With two sequential scans, using a specific algorithm able to find the differences between images, it is possible to quantify the induced phototactic response.

However, many others automated system for *C. elegans* phenotyping and drug screening have been developed and reported in literature in the recent years, a part from those already discussed.

During my PhD, thanks to the collaboration with UCL, I had the chance to employ and become familiar with the platform developed by Professor Sattelle's group, named INVAPP/Paragon system, for the characterization of worms' motility and growth (Partridge et al. 2018). The system will be described in details in the following paragraph and in the chapters 3 and 4.

- **INVAPP/Paragon automated system**

The group of Professor David Sattelle with whom we have a collaboration, has recently developed (Fig. 22) a high-throughput and automated system for screening libraries of small molecules for their effect on the motility and growth of diverse parasites. A schematic of the INVAPP hardware is shown in Figure 23. This system is composed by a high resolution camera (Andor Neo, resolution 2560x2160, with a line-scan lens (Pentax YF3528) that permits the acquisition of images of 96 well plates or agar plates where worms are cultured. The plates are positioned on a plate holder and they are illuminated from above by a led sorgent (Figure 23a). Several images of the plates are acquired at the maximum speed of acquisition of the camera (maximum frame rate 100 frames per second) using the μManager software of acquisition (https://micro-

manager.org/). The desirable movie frame length, duration of filming depends on the particular organism under study, and if worms are grown in liquid or in solid on agar plates. For my *C. elegans* experiments, I usually took 200 frames movies at different times of larval development of the worms. Then by using a set of MATLAB scripts, available at https://github.com/fpartridge/invappparagon, the videos are processed by counting the number of motile pixels. A pixel is identified as motile if its variance over time is higher than a fixed threshold (typically those greater than one standard deviation away from the mean variance, see Figure 23b). An example of this thresholding model is shown in Fig. 23c, which shows analysis of a 96-well plate containing adult, wild-type *C. elegans*. Dark pixels are those that have been determined to be motile. Once the motility threshold has been applied to the data, 'motile' pixels are assigned by well, by dividing the matrix evenly across the width and height of the image, with plateColumns and plateRows parameters used to specify the number of wells in the plate image. Finally, with this approach, it's possible to obtain a quantification of the motility which is express as the movement index parameter (Figure 23d). This parameter depends on how many worms are present in a well and on the size of the worms. We therefore have some information about the motility, growth of worms. As it is shown by Figure 23d, the quantified movement index increases as worms develop from L1 to adult stage.

Tens of thousands of compounds or conditions can therefore be readily screened per day.

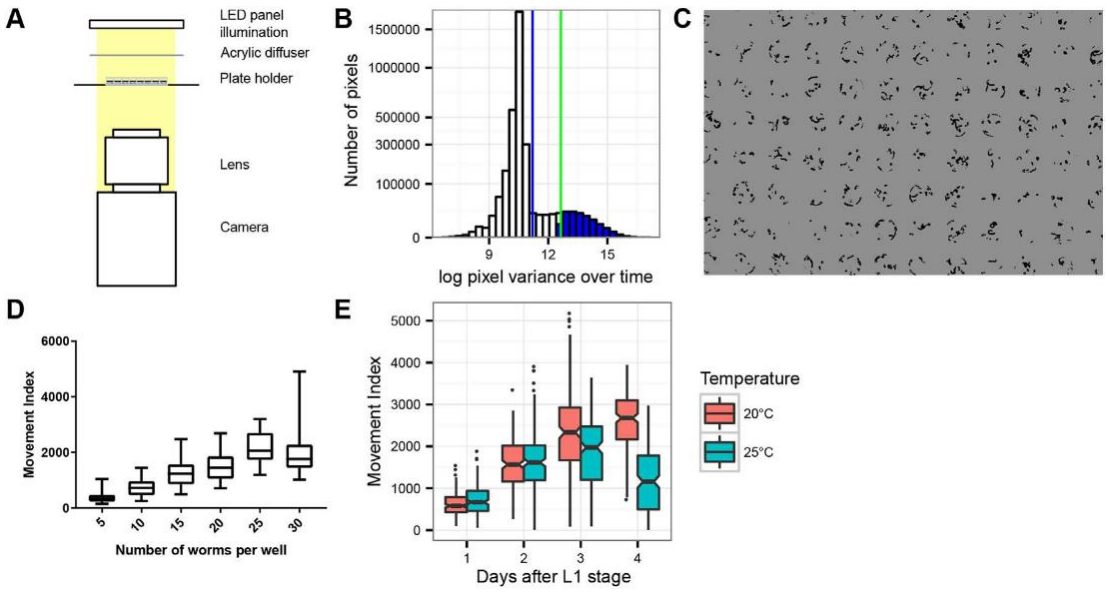

Figure 23. The INVAPP /Paragon movement index algorithm is a fully-automated high-throughput system able to determine motility and growth rate. **a)** Schematic of the INVAPP setup **b)** Principle of the algorithm: thresholding of moving pixels by statistical analysis of variance of each pixel through time. Histogram shows the distribution of pixel variance over time. Data was from obtained from a movie of all wells in a single 96-well plate containing wild-type *C. elegans*. The distribution is obtained by counting the number of pixels that fall into each bin of log pixel variance over time. Blue vertical line indicates mean pixel variance. The green vertical line indicates mean plus standard deviation of pixel variance; the blue shaded portion of the histogram indicates pixels that exceed this threshold so are deemed to be 'motile'. **c)** Image of 96-well plate containing *C. elegans* adults processed by the INVAPP/Paragon movement index system. Dark pixels are those categorized as moving by the algorithm. **d)** Increasing the number of *C. elegans* worms per well leads to increase in reported movement index. Boxplot bars indicate 95% confidence interval. Dataset contains 16 wells per group from a single 96-well plate. **e)** Movement index algorithm is able to quantify *C. elegans* growth in 96-well plates. Movement index increases with growth. Synchronised L1 population refed on day 0. Decrease in movement index in 25 °C group on Day 4 reflects completion of the *C. elegans* lifecycle and exhaustion of the bacterial food source. Boxplot notches indicate 95% confidence interval, n=192 wells of worms for each of the 20 °C and 25 °C groups. (Partridge et al. 2018)

During my PhD project, thanks to the collaboration with Professor David Sattelle, I had the chance to employ this new automated system of *C. elegans* phenotyping for carrying out experiments on the characterization of worm transgenic strain and appropriate controls. Using this system, I performed two kinds of experiments with

different outcomes (Fig. 24). The first one involved the measurement of motility of aged-synchronized transgenic worms that were grown at 20 or 25°C as appropriate for the *C. elegans* strain under test. Measurements were made in agar NGM or in liquid in 96-well plates (Figure 24a). In order to assess only the motility of adult worms, progeny were removed by constantly filtering adult worms with a 40 µM cell strainer (Falcon). A second approach was deployed when growth and progeny proliferation of nematodes needed to be evaluated (Figure 24b). In the latter case, the experiments were conducted on agar plates and only three worms at the L4 larval stage were introduced onto each plate. The aim of this experiment was to follow the growth development of progeny in order to detect possible larval impairment in transgenic strains expressing amyloidogenic proteins.

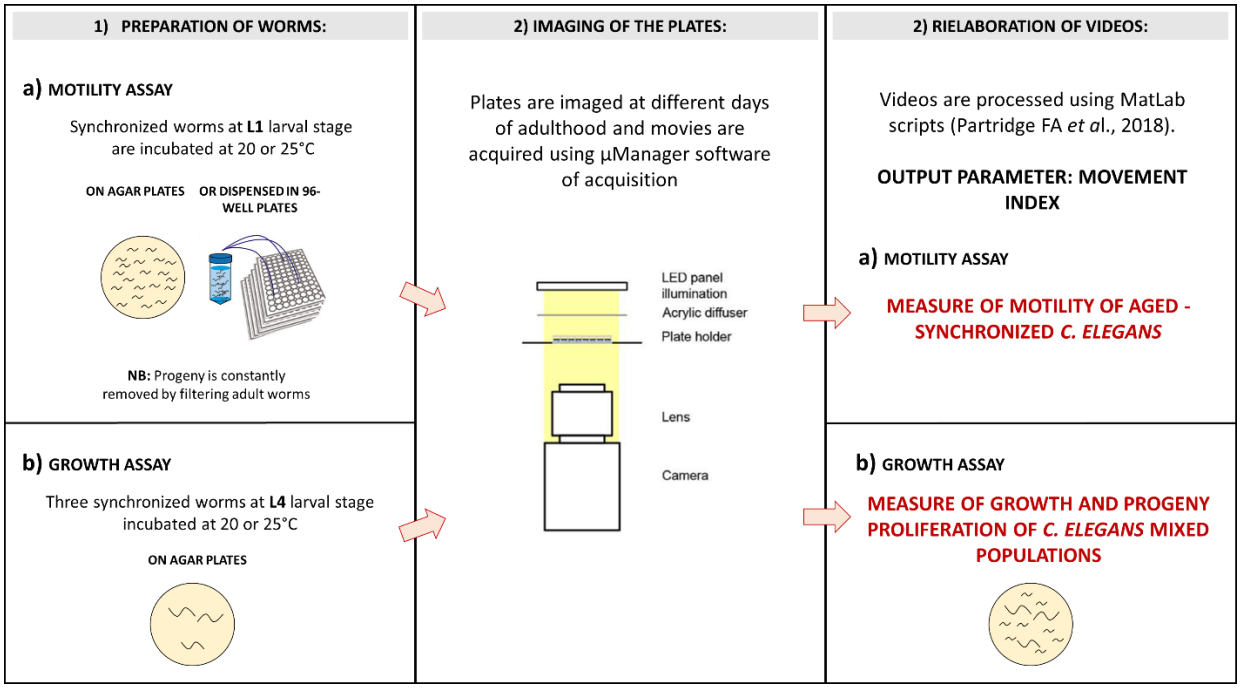

Figure 24. Scheme of the experiments conducted using the INVAPP/Paragon system for *C. elegans* automated phenotyping. **1)** *C. elegans* are grown on agar plates or in liquid in 96-well plates and incubated at 20-25°C. **2)** Subsequently plates are imaged as described in Partridge *et al*., 2018 and **3)** movies are analysed using MatLab scripts. The movement index parameter is calculated as reported giving information on motility **3a)** and growth dynamics of transgenic worms **3b)**.

1.5. Current animal models for systemic amyloidosis

The description of the molecular events that are involved in human diseases, including protein misfolding diseases, has not be completely clarified yet. However, the comprehension of these mechanisms is essential for planning possible prophylactic and therapeutic strategies. Therefore, the availability of a complex biological system, in which reproduce and recapitulate the pathological process of interest, has become extremely urgent.

Many efforts have been made in order to establish murine models for many of the systemic amyloidoses, but the pattern of amyloid deposition and toxicity does not mirror the human disease. The earliest model of systemic amyloidosis was then one proposed by McAdam and Sipe in 1976 (McAdam and Sipe 1976), which was widely used as the first *in vivo* demonstration of fibril seeding, in which, introduction of preformed fibrils from a sick animal into a healthy one, accelerated fibrillation. The inflammation inducible murine AA model presents amyloid deposition over time, but the inflammatory stimulus must be reintroduced to maintain amyloid deposits or they will be slowly cleared.

Similar attempts have been conducted in order to model ATTR amyloidosis in mice but those models have not been as successful as scientists would desire (Ibrahim et al. 2019). Despite recent success in the generation of mouse models with amyloid deposits in the nerves (Kan et al. 2018, Li et al. 2018), discrepancies in key physiologic and behavioural features of ATTR amyloidosis were seen (Ibrahim et al. 2019). Based on the development of those animal models, there have been several mechanism-driven therapeutic targets identified leading to the approval of Patisiran (Adams et al. 2018) and Tafamidis (Lamb and Deeks 2019) for the management of this disease. Finally, in 2018, Madhivanan and colleagues generated and characterized invertebrate models of the transthyretin amyloidoses that faithfully recapitulate cell-non-autonomous neuronal proteotoxicity by expressing human TTR in the *C. elegans* muscle (Madhivanan et al. 2018, Blancas-Mejía and Ramirez-Alvarado 2013).

Recently, Mishra and colleagues, (Mishra et al. 2019) have developed a transgenic zebrafish model in which a λ light-chain derived from a patient with AL amyloidosis is conditionally expressed in the liver under the control of the Gal4 upstream activation sequence enhancer system.

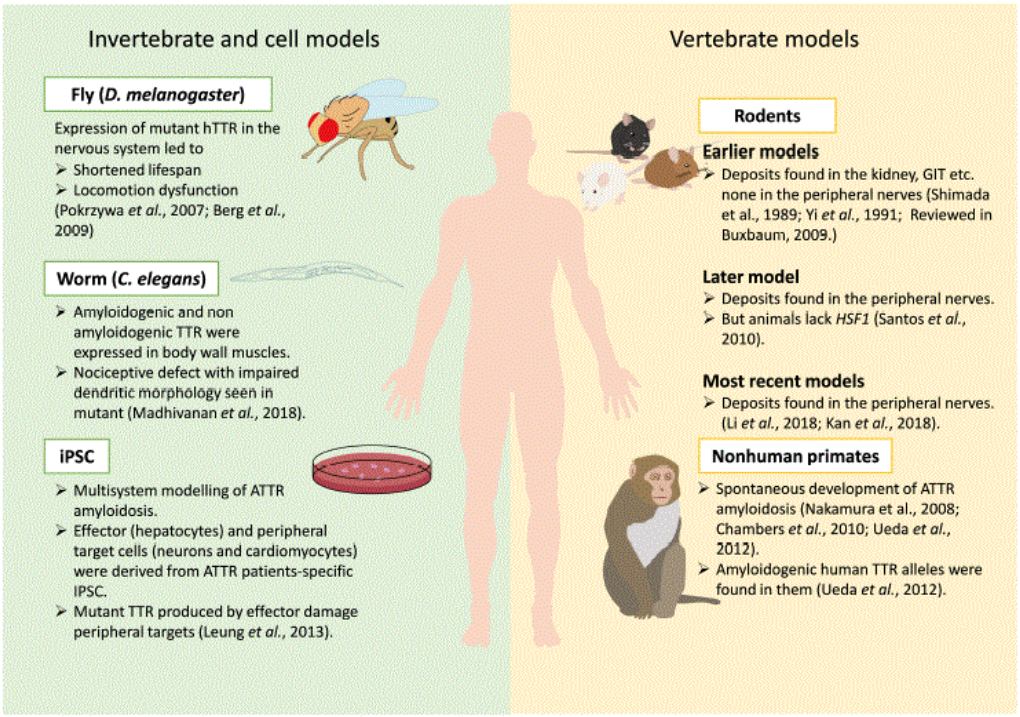

Figure 25. Current models available for studying ATTR amyloidosis. Various models for ATTR amyloidosis are depicted in this figure, including invertebrate, cell and vertebrate models. Key phenotypes and findings from these models are indicated with proper references (Ibrahim et al. 2019).

My research group, as I already mentioned before, has a long experience in studying *in vitro* β_2-microglobulin amyloidogenesis. For this pathology too, no efficient animal models are so far available.

Zhang and co-workers recently engineered a mouse model to express human wild type β_2-m but, despite its high plasma concentrations in mice, no β_2-m amyloid deposits were found, even after further injection of amyloid fibrils (Zhang et al. 2010). The group of Professor Bellotti have tried to generate transgenic mice expressing D76N variant, but unfortunately, they were unable to demonstrate the deposition of amyloid although we had evidence of a different tissue localization of wild type protein and the variant (unpublished).

In the absence of a suitable animal model of β_2-m related amyloidosis, my research group decided to explore the possibility of expressing the protein as a transgene in *C. elegans* and then exploring whether it was possible to reproduce some crucial events associated with its self-aggregation. In collaboration with Luisa Diomede, Professor Bellotti's group established the first *C. elegans* model expressing human β_2-

microglobulin and others two amyloidogenic isoforms (ΔN6 and P32G) in the muscle cells of the worms (Diomede et al. 2012). They showed that the expression of wild type full-length β_2-m, per se, affects the physiology of the worm and this is consistent with the intrinsic amyloid propensity and toxicity of normal β_2-m. However, the expression of the two more amyloidogenic species highly enhanced the damage to the biological cycle of the worms in this *C. elegans* model. The harm caused by β_2-m was detected in term of larval growth impairment, reduction in the lifespan and motility (Fig. 26a-c-d). Moreover, a statistically significant inverse correlation was observed between the concentration of β_2-m oligomers and larval growth (Fig.26b). Finally, an increased concentration of the reactive oxygen species was measured in all the *C. elegans* strains and, particularly in those expressing the P32G and ΔN6 β_2-m variants (Fig. 26e). Thus, it is perfectly consistent with the involvement of the mitochondrial function and efficiency in the mechanism of toxicity of the amyloid aggregates generated by several amyloidogenic peptides and proteins.

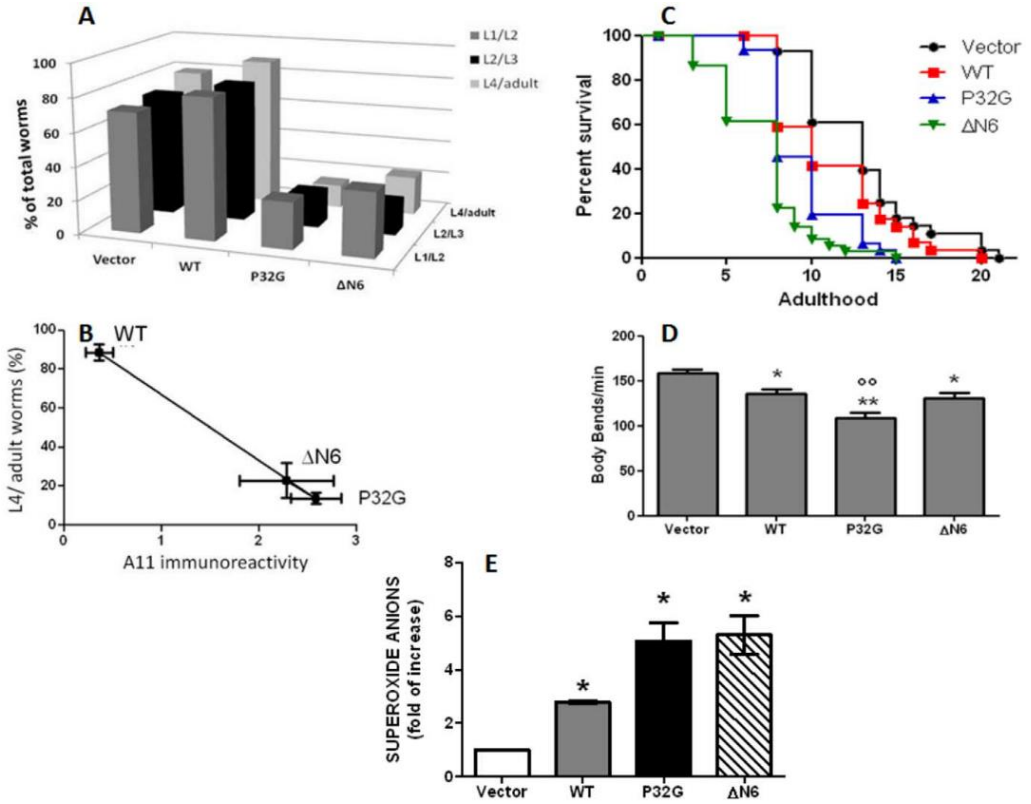

Figure 26. Behavioural phenotypes of transgenic *C. elegans* strains. **a)** Larval growth of control worms (Vector), wild type β_2-m expressing worms (WT) and nematodes expressing P32G or truncated form of β_2-m (DN6). One hundred synchronized eggs were placed into fresh

NMG plates and the number of L1/L2, L2/L3 and L4/adult worms were scored after 24, 48 and 72 hours, respectively. Data are expressed as percentage of total worms in the plate at each time point and are given as mean of three independent experiments (N = 300). **b)** Correlation between oligomers of β_2-m and reduction in growth rate of transgenic *C. elegans* strains. Percentage of adult worms of each transgenic strain, scored after egg synchronization, was correlated to the amount of A11-positive oligomeric assemblies detected by dot blotting. Data of both graphic axes represent mean of three independent experiments. **c)** Kaplan-Meier survival curves of transgenic hermaphrodite adult nematodes. Animals were placed in plates starting from L4, cultured at 20°C and transferred to fresh plates for each consecutive other days. Survival rate was scored every day and expressed as percent of survival. Plots are representative of three independent experiments (N = 30). **d)** Body bends in liquid of transgenic worms. At least three independent assays were performed (N = 100 animals for each group). Data are given as mean of number of body bends/min ± SE, *p,0.05 and **p,0.01 vs. the vector, °°p,0.01 vs. WT, according to one-way ANOVA. **e)** Superoxide anions production in control worms (Vector), wild type β_2-m expressing worms (WT) and in nematodes expressing P32G or truncated form of β_2-m (DN6). Age-synchronized worms were collected in PBS containing 1.6 ml of 1% Tween 20 and colorimetric NBT assay was carried out. Results show the fold increase in superoxide production calculated as NBT absorbance/mg of proteins (% NBT) compared to Vector; *p,0.05 vs. vehicle and °p,0.05 vs. WT, according to one-way ANOVA. Error bars indicate SD (Diomede et al. 2012).

After the discovery in 2012 of the first natural variant D76N β_2-m, my group tried to engineer *C. elegans* expressing this natural variant but because of its high amyloidogenic propensity and toxicity, the production of a transgenic strain constitutively expressing this isoform was not possible. For this reason, a temperature inducible system was used in order to allow protein expression only after up-shifting the temperature of incubation of worms from 16°C to 23-25°C, avoiding its toxicity in the embryonic stage (Faravelli and Raimondi et al. 2019, under revision by Scientific Reports). Furthermore, to achieve a correct extracellular localization of β_2-m in worms, we have replaced the human β_2-m signal peptide with the signal peptide of the endogenous *sel-1* protein (Grant and Greenwald 1997).

Thus, one of the main aims of my PhD work was to characterize this animal model to determine the extent to which it recapitulates some aspects of D76N β_2-m related amyloidosis. The work I undertook in characterising this strain is reported in the

manuscript submitted to Scientific Reports in Chapter 3. This represents the first animal model that recapitulates some aspects of D76N β_2-m amyloidosis, and also permits exploitation of the advantages offered by the *C. elegans* animal model.

1.6. Aim of the project

My PhD work has been focused on the investigation of the molecular mechanism underlying the conversion of two proteins, β_2-microglobulin and transthyretin, to pathogenic amyloid fibrils.

In order to understand the process that leads toward the aggregation and to investigate the toxicity of the different key actors of fibrillogenesis and deposition of amyloid fibrils, a comprehensive approach, which employs models of increased level of biological complexity, has been chosen.
Indeed, despite large investments in drug development, the overall success rate of drugs during clinical development remains low. One remarkable explanation is the existing gap between models used in preclinical research and and the complexity of the disease in patients.

The critical evaluation of the predictive validity of animal models is essential to address the clinical question. Reversely, clinical bedside findings that were not predicted by animal testing should be back translated and used to refine the *in vivo* models (Denayer T et al. 2014). Considering this situation, we can affirm that the process of modern medicine has the features of a ring in which patients are both at the starting point as well as at the end of the pathway. (Figure 27). Molecular caracterization of the disease for diagnostic purpose provide essential information for a personalized treatament and offer a wealth of precious biological information for reproducing *in vitro* the mechanism of the disease. The continuum between precision and transational medicine represents the major novelty of modern medicine and constitutes the major propelling strenght toward the discovery of new more effective therapies.

The medical and biological approach to amyloid diseases in the last decade is an excellent example of the coniugation between precision and translational medicine. This a very fascinating revoultion in medical science and in my PhD work I undertook my project on two pathogenic proteins, β_2-m and TTR inspired by the aim to make bridges between clinical and experimental medicine (Figure 28).

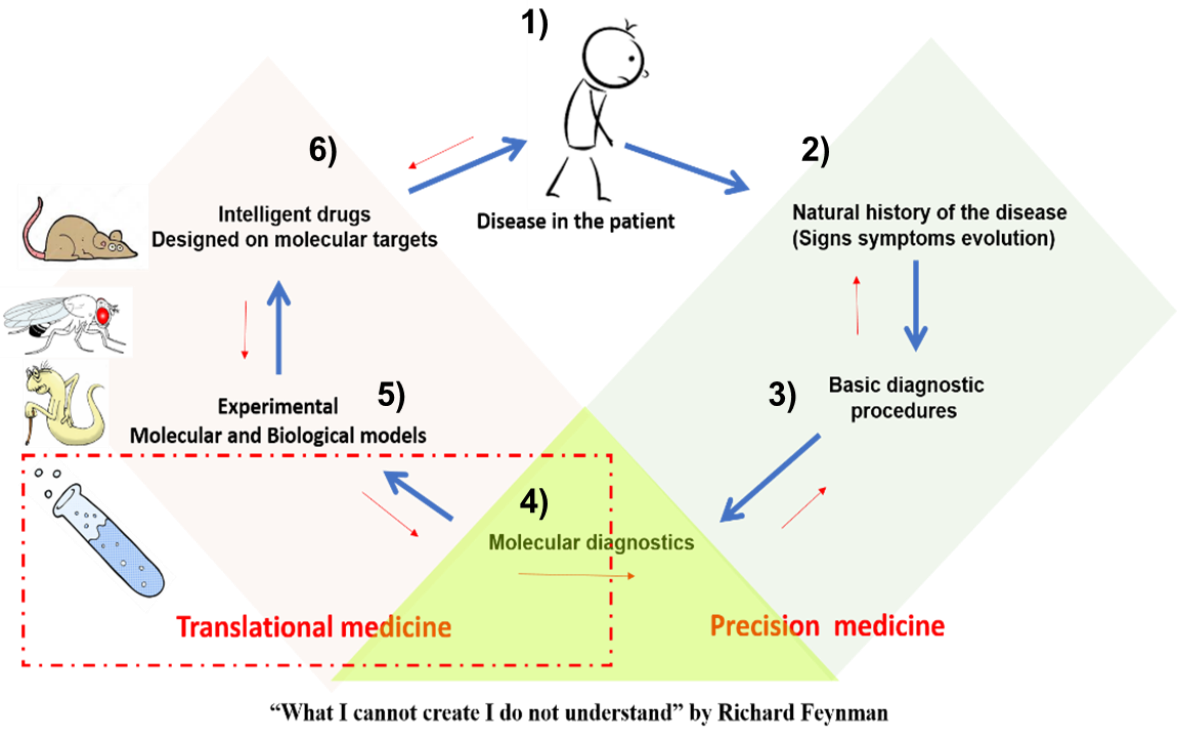

Figure 27. The schematic process of modern medicine (provided by Professor Vittorio Bellotti).

The first task of my PhD work has been focused on the *in vitro* study of the fibrillogenesis mechanisms of different TTR isoforms. In particular, as I reported in Chapter 2, taking into account the biocompatible mechano-enzymatic mechanism of aggregation proposed by our group (Marcoux et al. 2015), I investigate the ability of putative ligands to inhibit the mechanism of aggregation of TTR (see Chapter 2.1. (Verona et al. 2017). It's worth of note that in a recent work published in Journal of Biological Chemistry (Mangione et al. 2018), we reported the identification of the putative protease responsible for proteolytic cleavage *in vivo*. Finally I had the chance to study and characterize the stability of both *ex-vivo* and both *in vitro*-made transthyretin's fibrils (see Chapter 2.3).

The second part of my project consisted in the performing of *in vivo* experiments on a transgenic *C. elegans* strain espressing D76N β_2-m, that rappresent the mosts toxic β_2-m isoform responsible of a familiar amyloidosis (Valleix et al. 2012). Some of the data obtained from the characterization of this new animal model has been reported in Chapter 3.1. and in the paper submitted to *Scientific Reports* and actually under a second revision (Faravelli and Raimondi et al. 2019).

Some others experiments are still on-going and they are described in details in Chapter 3.2.

Finally, thanks to the skills acquired in *C. elegans* manipulation and thanks to the collaboration with Professor David Sattelle at UCL in London and Professor Ersilia De Lorenzi in Pavia, I have also had the opportunity to be actively involved in research projects investigating other amyloidogenic proteins such Aβeta peptide by using transgenic *C. elegans* strains.

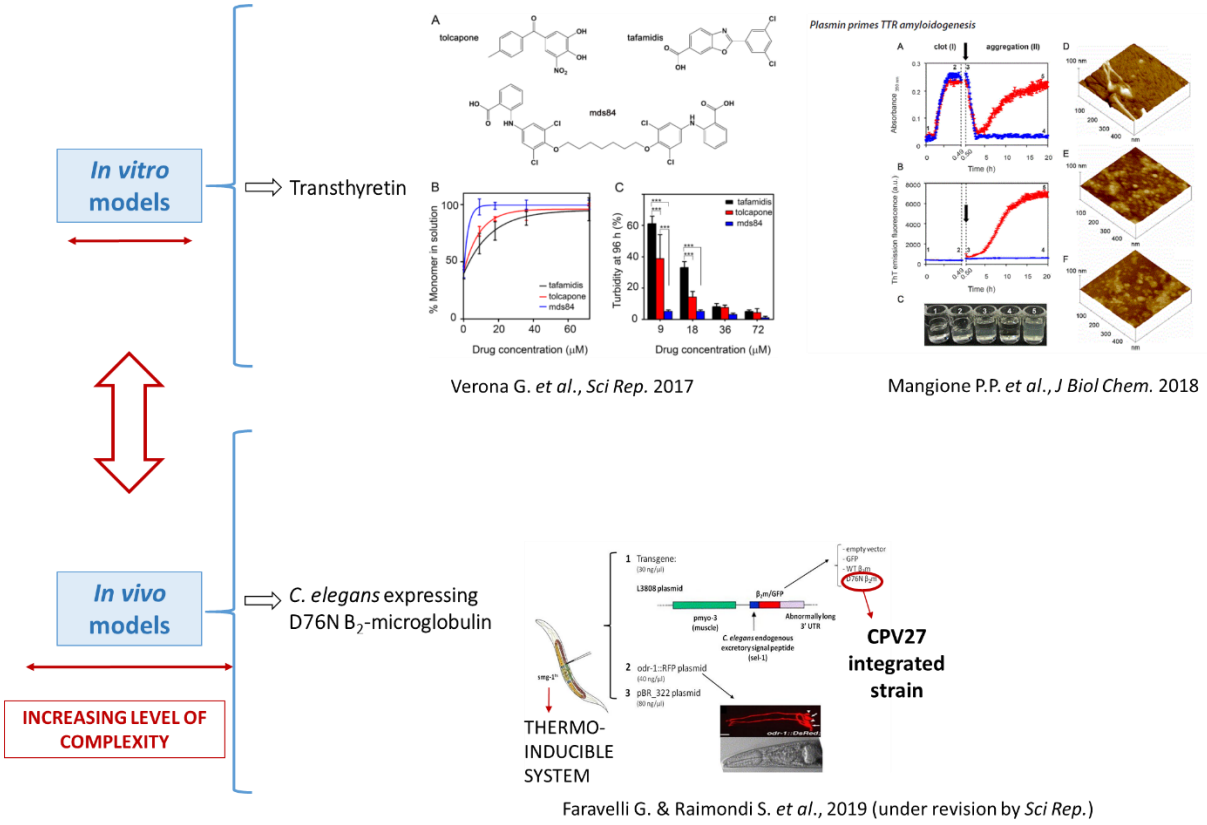

Figure 28. Fibrillogenesis carried out on two amyloidogenic proteins: transthyretin and β$_2$-microglobulin. In the upper part of the figure are reported the achievements obtained on TTR amyloidogenesis *in vitro*: a new biocompatible tool for drug discovery and the identification of culprit protease in mechano-enzymatic fibrillogenesis. In the lower part, the peculiar features of the new *C. elegans* model expressing the pathogenic β$_2$-microglobulin are summarized.

Chapter 2: *In vitro* studies of systemic amyloidosis

As already mentioned in Chapter 1, the first part of my PhD was focused on the investigation of protein aggregation *in vitro*. In particular, I've had the chance to contribute to two scientific papers.

In our first work, reported in paragraph 2.1, we investigated the inhibition of transthyretin amyloidogenic isoforms by small ligands (Verona et al. 2017). The study was based on the discovery of the previously unrecognised mechano-enzymatic mechanism in which shear stress and proteolysis play a key role towards the formation of amyloid fibrils (Marcoux et al. 2015). Indeed, in presence of shear stress and in physiological conditions 49-127 fragment, generated after the proteolysis, is released form the tetramer and triggers rapid fibril formation. This pathway of aggregation is efficiently inhibited only by ligands that occupy both binding sites in TTR. Among the monovalent ligands, Tolcapone, which is bound with similar high affinity in both TTR binding sites escaping the usual negative cooperativity, is the best candidate. However, mds84, a bivalent ligand of TTR 'superstabiliser' family (Kolstoe et al. 2010), is more potent than the monovalent ligands probably because of its additional interactions of its linker within the TTR central channel. In particular, my contribution in the work has regarded the experiments on the expression of recombinant V122I transthyretin variant and experiments on the fibrillogenesis of V122I TTR in the presence of ligands.

In our second paper, reported in paragraph 2.2, we showed our data on the identification of the putative protease responsible for proteolysis of transthyretin *in vivo* (Mangione et al. 2018). In a comprehensive bioinformatics search for systemically active proteases with tryptic specificity, plasmin was selected as the leading candidate. Indeed, plasmin selectively cleaves TTR *in vitro* between residues 48-49, releasing full length and truncated protomers that rapidly aggregate via nucleation and elongation into genuine amyloid fibrils. Nonetheless, those findings demonstrate that physiological fibrinolysis is likely to play a critical pathogenic role in TTR amyloid formation. Specifically, my work was focused on the experiments of expression and purification of recombinant TTR variants, proteolysis and fibrillogenesis of TTR variants and WT TTR in presence of plasmin or others proteases, preparation of amyloid seeds from

S52P TTR with plasmin and I've conducted experiments showing the effect of seeds on plasmin-mediated S52P TTR fibrillogenesis.

Finally, I have been actively involved in the comparatively analysis of the thermodynamic stability of natural and *in vitro* made TTR fibrils. The opportunity of using a method suitable for making fibrils presenting properties most similar to the natural ones is a major goal because the availability of natural source is very limited.

2.1. "Inhibition of the mechanoenzymatic amyloidogenesis of transthyretin: role of ligand affinity, binding cooperativity and occupancy of the inner channel".

Verona G. *et al*. *Sci rep* 2017.

www.nature.com/scientificreports

SCIENTIFIC REPORTS

OPEN

Received: 15 November 2016
Accepted: 21 February 2017
Published online: 15 March 2017

Inhibition of the mechano-enzymatic amyloidogenesis of transthyretin: role of ligand affinity, binding cooperativity and occupancy of the inner channel

Guglielmo Verona[1], P. Patrizia Mangione[1,2], Sara Raimondi[2], Sofia Giorgetti[2], Giulia Faravelli[2], Riccardo Porcari[1], Alessandra Corazza[1,3], Julian D. Gillmore[4], Philip N. Hawkins[4], Mark B. Pepys[1,4], Graham W. Taylor[1] & Vittorio Bellotti[1,2]

Dissociation of the native transthyretin (TTR) tetramer is widely accepted as the critical step in TTR amyloid fibrillogenesis. It is modelled by exposure of the protein to non-physiological low pH *in vitro* and is inhibited by small molecule compounds, such as the drug tafamidis. We have recently identified a new mechano-enzymatic pathway of TTR fibrillogenesis *in vitro*, catalysed by selective proteolytic cleavage, which produces a high yield of genuine amyloid fibrils. This pathway is efficiently inhibited only by ligands that occupy both binding sites in TTR. Tolcapone, which is bound with similar high affinity in both TTR binding sites without the usual negative cooperativity, is therefore of interest. Here we show that TTR fibrillogenesis by the mechano-enzymatic pathway is indeed more potently inhibited by tolcapone than by tafamidis but neither, even in large molar excess, completely prevents amyloid fibril formation. In contrast, mds84, the prototype of our previously reported bivalent ligand TTR 'superstabiliser' family, is notably more potent than the monovalent ligands and we show here that this apparently reflects the critical additional interactions of its linker within the TTR central channel. Our findings have major implications for therapeutic approaches in TTR amyloidosis.

The seminal observation that the native non-covalent TTR homotetramer dissociates at low pH into dimers and monomers that self-assemble into amyloid fibrils[1] is the basis for the current, widely accepted model for TTR amyloid formation. However low pH treatment of both wild type and amyloidogenic TTR variants produces mostly heterogeneous amorphous aggregates with a very low yield of authentic amyloid fibrils showing pathognomonic green birefringence in polarized light after Congo red staining, characteristic fibrillar electron microscopic appearance and the cross-β X-ray fibre diffraction signature. *Ex vivo* TTR amyloid deposits, especially in the heart, usually contain a substantial proportion of the *C*-terminal TTR fragment generated by proteolytic cleavage at Lys48-Thr49[2]. Following this observation we have identified and characterized a novel mechanism of TTR amyloid fibrillogenesis mediated by selective tryptic cleavage at residue 48. The highly amyloidogenic TTR *C*-terminal residue 49–127 polypeptide is released, catalysing amyloid fibril formation *in vitro*, and the whole process is strongly enhanced by biomechanical forces[3,4]. Abundant authentic amyloid fibrils are produced with pathognomonic features indistinguishable from natural *ex vivo* fibrils.

Compounds able to stabilize TTR, intended for use as drugs to treat and prevent systemic ATTR amyloidosis, have hitherto been identified exclusively by their capacity to inhibit TTR dissociation and aggregation induced by low pH *in vitro*. However, we have found that inhibition of the mechano-enzymatic pathway of TTR amyloid fibrillogenesis at physiological pH, ionic strength and temperature requires occupation of both thyroxine binding

[1]Wolfson Drug Discovery Unit, Centre for Amyloidosis and Acute Phase Proteins, University College London, London, NW3 2PF, UK. [2]Department of Molecular Medicine, Institute of Biochemistry, University of Pavia, Via Taramelli 3b, Pavia, 27100, Italy. [3]Department of Medical and Biological Sciences (DSMB), University of Udine, Piazzale Kolbe 4, 33100, Udine, Italy. [4]National Amyloidosis Centre, University College London, London, NW3 2PF, UK. Correspondence and requests for materials should be addressed to V.B. (email: v.bellotti@ucl.ac.uk)

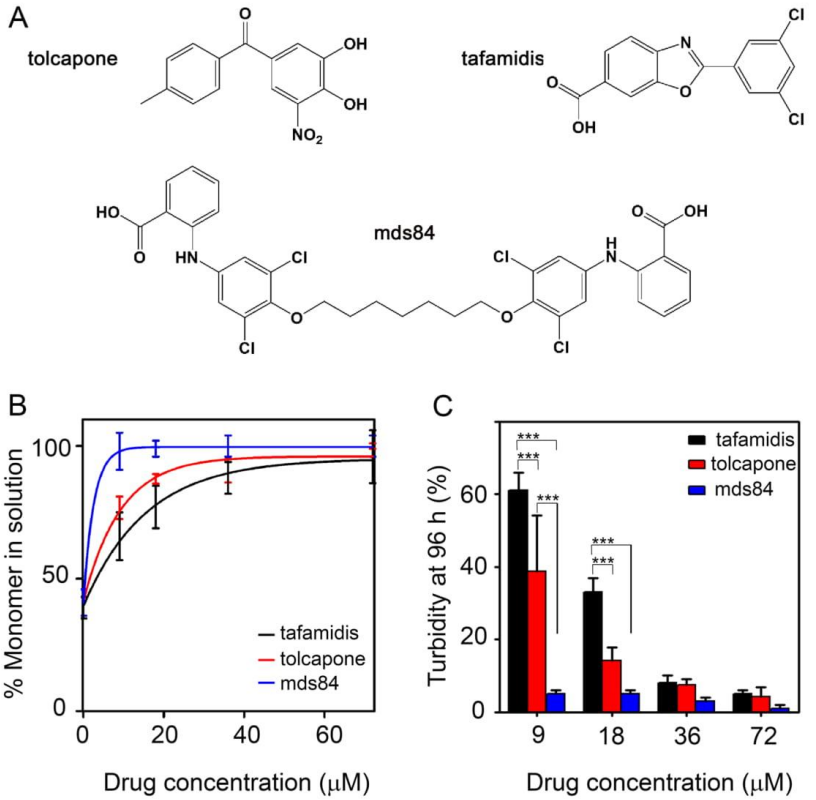

Figure 1. Comparative effect of tolcapone on proteolysis and fibrillogenesis of V122I TTR. (**A**) Chemical structures of tolcapone and tafamidis together with the TTR binding palindromic ligand, mds84. (**B**) Aggregation of 18 μM V122I TTR in the presence of 0, 9, 18, 36 and 72 μM of tolcapone, tafamidis and mds84 respectively in PBS pH 7.4 at 37 °C with fluid agitation was carried out after addition of trypsin at an enzyme:substrate ratio of 1:200. Selective proteolytic cleavage was monitored at 96 h by SDS-PAGE under reducing conditions (Supplementary Fig. S1). Intensities of the electrophoretic bands corresponding to the intact protomer in the whole mixture were normalized to 100% for the same band of the protein before addition of trypsin. The solid lines represent the nonlinear fit to the experimental mean (SD) of three replicates using GraphPad Prism v5. Two way ANOVA gave a P value < 0.001 for tafamidis vs mds84 at 9 and 18 μM; for tolcapone vs mds84 at 9 μM. (**C**) Aggregation of 18 μM V122I TTR was quantified as spectrophotometric turbidity at 400 nm normalized to 100% for aggregation of the protein in the absence of ligands. We know from previous work that TTR aggregation in this system is in the form of authentic amyloid fibrils[3,4]. All data shown represent mean (SD) of three independent experiments, and *** represents $P < 0.001$.

sites in each native TTR tetramer. This is most efficiently achieved by bivalent ligands, exemplified by the palindromic compound mds84[5], that is spontaneously bound simultaneously and pseudo-irreversibly in both sites. Sant'Anna and colleagues[6] have recently reported that tolcapone is a potent inhibitor of TTR dissociation and aggregation under denaturing conditions. They attribute its efficacy to occupation of both binding pockets with similar high affinity in contrast to the notable negative cooperativity observed with thyroxine itself and other monovalent ligands, including the TTR stabiliser drugs, tafamidis[7,8] and diflunisal[9], which are now in clinical use. This important observation prompted us to test the capacity of tolcapone to inhibit mechano-enzymatic amyloidogenesis of TTR using the V122I variant which is the most prevalent cause of hereditary cardiac amyloidosis[10].

Results and Discussion

We compared tolcapone with tafamidis[7,8] and the experimental bifunctional compound, mds84[5] (Fig. 1A). When stirred with V122I TTR at 37 °C in PBS in the presence and absence of trypsin for 96 h, all three ligands inhibited proteolytic cleavage of the protein in a dose-dependent manner (Fig. 1B and Supplementary Fig. 1). At molar

ratios of ligand:TTR tetramer higher than 2:1, the three compounds had similar efficacy with apparent almost complete inhibition of TTR cleavage. However at lower molar ratios, mds84 was the most potent inhibitor, followed by tolcapone and tafamidis.

Consistent with their inhibition of proteolytic TTR cleavage, the three compounds also inhibited fibril formation (Fig. 1C). At a ligand:TTR tetramer molar ratio of 0.5:1, mds84 and tolcapone reduced fibril formation by approximately 90% and 60% respectively, and tafamidis only by 40%. At molar equivalence, inhibition increased at 60% with tafamidis, ~80% with tolcapone and remained at ~90% with mds84. At twofold and greater molar excess of ligand, both monovalent ligands, tafamidis and tolcapone inhibited TTR fibrillogenesis by the same amount (~90%) as mds84.

Even when we compared the effect of the three compounds on the inhibition of TTR acidic-mediated aggregation[11], mds84 at equimolar concentration with TTR was the only ligand able to completely inhibit the process (Supplementary Information and Supplementary Fig. S2).

The inhibition of the mechano-enzymatic pathway of TTR amyloidogenesis, which we believe to be the most likely pathophysiological mechanism *in vivo*, depends on the occupation of both thyroxine binding sites. The superior potency of tolcapone among monovalent TTR ligands is consistent with its unique property of not inducing negative cooperativity[6].

The much more effective inhibition of proteolysis-mediated TTR fibrillogenesis by mds84 results from the simultaneous occupation of both thyroxine binding sites, and the internal channel between them, by this palindromic molecule[5]. It occurs rapidly and completely at equimolar concentrations of TTR and ligand. Binding of mds84 by native TTR is pseudo-irreversible under physiological conditions[5] and generates a stable complex. This in contrast to the reversible monovalent ligands for which a higher molar excess is required to saturate both binding sites *in vivo*. These limitations on efficacy against mechano-enzymatic mediated amyloidogenesis may explain the modest therapeutic benefit of monovalent ligands in the clinical studies reported so far[12].

To understand the superior inhibitory effect of bivalent ligands, we analysed the deposited X-ray structures of TTR complexed with monovalent ligands, tolcapone[6] and tafamidis[7], (Fig. 2) in comparison with bivalent ligands, mds84[5] and compounds 20 and 22 of Green *et al.*[13] (Supplementary Fig. S3). For a general description of the crystal structures we refer to a very exhaustive review by Palaninathan[14]. There is no PDB structure of the mds84-V122I TTR complex so the analysis is restricted to wild type TTR. This choice is justified by the almost perfect superposition of the wild type and V122I TTR structures in the absence of ligands (Supplementary Fig. S4A,B) with minor deviations when bound to tolcapone (Supplementary Fig. S4C,D). The average root mean square deviations (rmsd) for the TTR backbone residues are 0.45 and 0.9 Å for the two proteins in their free and bound form, respectively. Moreover, Val122 and Ile122 side chains point towards the external part of the pocket cavity and residue 122 is not present in the halogen binding pockets (HBPs; see Methods). Importantly, neither mono- nor bivalent molecules induce major rearrangements of the HBP residues with rmsd values calculated for the backbone atoms of HBP1, HBP2 and HBP3 ranging from 0.2 to 0.3 Å (Table 1). The superposition of the binding pockets of TTR with and without ligands is shown in Supplementary Fig. S5. Also there is no correlation between the number of ligand-protein hydrogen bonds, (Table 1) and inhibitory efficacy. A full list of hydrogen bonds between the ligand and the HBPs is reported in the Supplementary Information. However, in contrast with the monovalent ligands which interact only with the ligand pocket itself, the methylene linker of the bivalent compounds occupies the narrow TTR inner channel with an interaction surface increased by 48 $Å^2$, for mds84 compared with tolcapone. Binding of mds84[5], compound 20 and compound 22[13] by TTR creates, respectively, up to 9, 5 and 4 hydrophobic interactions, mainly with S117 Cβ and Leu110 Cδ2. These interactions make an estimated favourable energetic contribution of −4.6, −2.5 and −1.0 kcal/mol for the three ligands respectively. Occupancy of the central channel of TTR, estimated for mds84 to be around 80% of the void volume, may thus have a crucial role in preventing subunit sliding and also provide long distance stabilisation affecting the dynamics of CD loop, the selective cleavage of which potently primes amyloid fibrillogenesis. The pioneering study of Green *et al.*[13] identified the enhanced stabilisation of TTR by bivalent ligands with a central linker but their compounds did not interact with native TTR. They were bound only by renaturation of dissociated denatured TTR around the ligand.[13] In sharp contrast, both the mds84 prototype and its analogues are rapidly bound by the native TTR tetramer, traversing the inner channel to occupy it with the linker.[5] The unique total binding site in TTR, comprising the two halogen binding pockets and the inner channel, is entered by these ligands with a decreased entropic cost compared to all monovalent ligands[15]. The key factors responsible for the 'superstabiliser' property of mds84 and its analogues are thus likely to be the combination of entropic gain, increased hydrophobic contributions of the linker and a reduced void volume in the interface cavity.

The mechanism of binding of TTR by bivalent compounds cannot be fully clarified on the basis of the available crystallographic structures. These data reveal that the TTR inner cavity is very narrow and therefore apparently inaccessible to the bulky groups of the ligands. We hypothesize that the tetramer dynamics may be larger than expected and current studies in our laboratory using NMR might shed light on this important issue.

Finally, even at large molar excess of tafamidis or tolcapone that inhibited obvious *in vitro* aggregation, ultracentrifugation of the reaction mixture yielded a small amount of insoluble material which stained with Congo red to give typical green birefringence (Fig. 3A and Supplementary Fig. S6) and was fibrillar in the electron microscope (Fig. 3B). In the presence of mds84 such insoluble material was minimal but extensive searching by electron microscopy revealed some fibrils (Fig. 3B). Evidently, the mechano-enzymatic mechanism enables slow formation of some fibrils even when both binding sites are fully occupied in most TTR molecules. Effective targeting of all TTR molecules with stabilizer drugs is much more challenging *in vivo* than *in vitro* and it is therefore crucial to consider the significant pathogenic impact of even minimal amyloid fibril formation *in vivo*. There are potentially major implications, that should not be ignored, both for interpretation of current clinical studies in TTR amyloidosis and for the design of future therapeutic approaches such as the exploitation of non-natural peptides inhibitors of TTR aggregation[16] or antibodies recognizing cryptic epitope exposed only on the surface of aggregated TTR and not in the native tetrameric state[17].

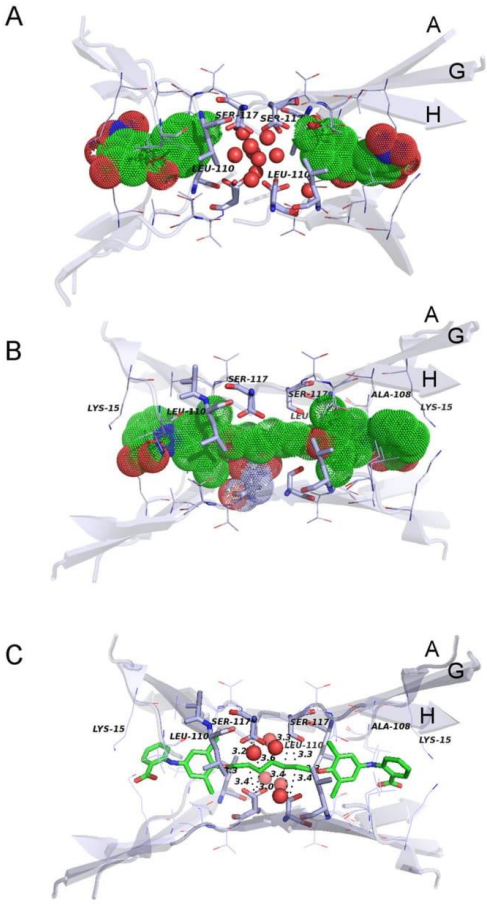

Figure 2. TTR binding sites in the presence of tolcapone and mds84. Wild type TTR binding sites occupied by tolcapone (**A**) and mds84 (**B**) with ligands shown as solvent accessible surfaces. For clarity, H_2O oxygens are shown as spheres with 50% of the van der Waals radius. (**C**) Wild type TTR-mds84 complex with highlighted distances of the principal hydrophobic contacts between the ligand methylene linker and TTR atoms.

Protein (PDB code)	*Rmsd (Å)	**Numbers of H bonds
WT TTR/tolcapone (4d7b)	0.247	3
WT TTR/tafamidis (3tct)	0.196	0
WT TTR/mds84 (3ipe)	0.173	2
WT TTR/compound 20 (2fbr)	0.298	6
WT TTR/compound 22 (2flm)	0.319	0

Table 1. Structural comparisons of TTR halogen binding pockets with and without ligands. *The root mean square deviation was calculated for the backbone atoms of all the three HBPs for the wild type TTR complexes compared to the same protein without ligand (PDB 1dvq). **The hydrogen bonds considered are those between the ligand and the HBPs atoms including crystallographic water molecules.

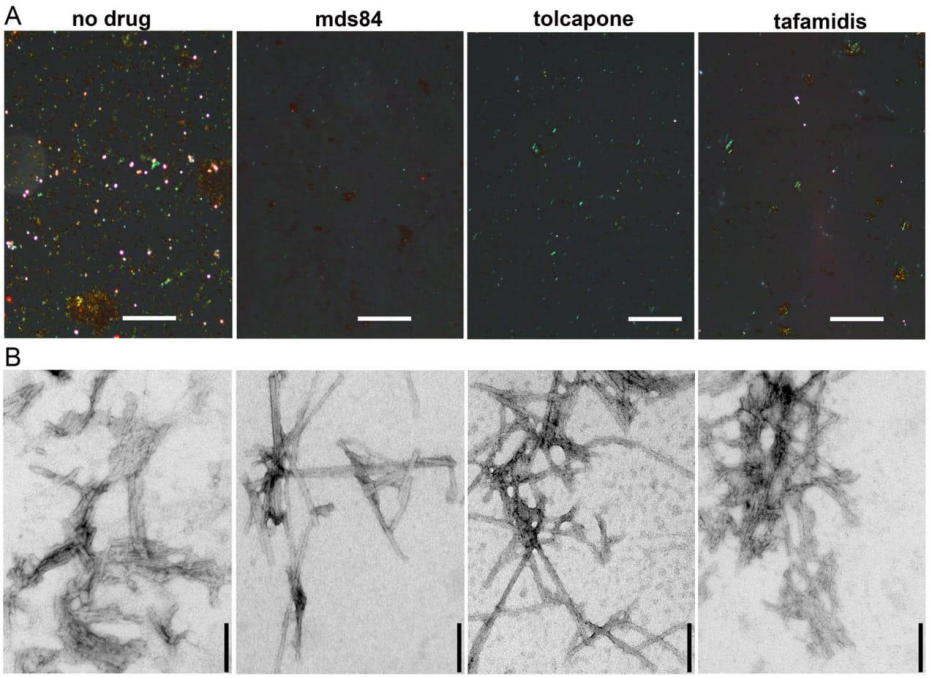

Figure 3. Residual amyloid aggregates in the presence of excess of ligands. (**A**) Congo-red stained specimens viewed under intense cross polarized light in the absence of any ligands and in the presence of fourfold molar excess of mds84, tolcapone and tafamidis (Supplementary Fig. S6). Some fragments of amyloid are present with maximally inhibitory ligand concentrations (Fig. 1), although least with mds84. Scale bar, 100 µM. (**B**) Typical fibrillar structures detected by exhaustive analysis of negatively stained electron microscopy images of the same TTR-ligand preparations. Scale bar, 100 nm.

Methods

Expression of recombinant TTR. V122I TTR was expressed using a pET3a vector containing the full-length cDNA for human V122I TTR in *E. coli* BL21 super competent cells. Expression colonies were grown to an optical density at 600 nm of 1.0 in Luria-Bertani broth containing 100 µg ml^{-1} ampicillin at 37 °C; protein synthesis was induced with 1 mM isopropyl-β-D-thiogalactoside at 18 °C overnight. The following day cells were harvested by centrifugation at 2,150 *g* for 30 min, the pellet was suspended in buffer containing 25 mM Tris-HCl, 2 mM EDTA, 0.1% Triton, pH 7.4 and sonicated at 12 µm amplitude for 10 cycles (1 min on/1 min off). The intracellular proteins were fractionated by 2 cycles of ammonium sulphate precipitation. TTR, which precipitated between 30 and 60% ammonium sulphate, was dissolved in 25 mM Tris-HCl, 0.1 M NaCl, pH 8.0 and fractionated on a Superdex 75 Hi Load 26/60 gel filtration column (GE Healthcare Life Science) equilibrated and eluted in the same buffer. TTR enriched fractions were dialyzed overnight against 25 mM Tris-HCl, pH 8.0, reduced with dithiothreitol and then applied to a Q-Sepharose anion exchange column equilibrated in 25 mM Tris-HCl pH 8.0 and eluted with a linear 0–1 M NaCl gradient in the same solvent. TTR enriched fractions were pooled, concentrated and further purified on the Superdex 75 Hi Load 26/60 column. Fractions containing TTR were dialyzed against water at 4 C for at least 3 days and then lyophilized. Purity was confirmed by SDS-PAGE and electrospray ionisation mass spectrometry.

Fibrillogenesis of V122I TTR in the presence of ligands. Fibrillogenesis experiments were performed in standard glass vials stirred at 1,500 r.p.m. (IKA magnetic stirrer) at 37 °C using 1 mg ml^{-1} of V122I TTR (18 µM tetramer) in PBS at pH 7.4 in the presence and in the absence (control) of 5 ng µl^{-1} of trypsin. Tolcapone, tafamidis and mds84 were dissolved individually at 10 mM in DMSO, followed by serial dilutions which, when added in appropriate volume to TTR, provided ligand:TTR tetramer molar ratios of 0.5:1, 1:1, 2:1 and 4:1 respectively. Turbidity at 400 nm was used to monitor fibril formation over time until it reached a plateau at 96 h. The thioflavin T assay[18] could not be used because tolcapone and mds84 interfere with the fluorescence measurement. At the end of the aggregation, susceptibility to trypsin was monitored using SDS-homogeneous 15% PAGE (GE Healthcare) under reducing conditions. Two-way Anova was performed using GraphPad Prism 5 for pairwise multiple comparison among tafamidis, tolcapone and mds84.

The pellet was harvested from each protein sample in the absence and in the presence of ligands by ultracentrifugation in a Beckman Optima TL ultracentrifuge at 135,000 *g*, 20 min. After resuspension of the pellet with a minimal volume of PBS, samples were stained with alkaline alcoholic Congo red and examined by high intensity cross polarized light microscopy[19]. Amyloid load was scored in the Congo red stained pellet of TTR in the presence of fourfold molar excess of each ligand (Supplementary Fig. S6). A blind quantification was carried out by an expert operator on six slides per each group of treatment using the following grading score: 0 (no spot detected), 1 (occasional spots), 2 (green birefringent spots clearly visible and corresponding to the stained material in the bright field), 3 (surface homogeneously covered by green birefringent material). The non-parametric Kruskall-Wallis test for mds84 vs tafamidis (or tolcapone) was applied using GraphPad Prism 5.

Samples were also examined by negative staining transmission electron microscopy. Briefly, a drop of each sample was allowed to dry on formvar coated copper EM grids for 2 min before blotting with filter paper to remove excess solvent and staining with 2% w/v uranyl acetate for 1 min. After further blotting and drying in air, transmission electron microscope (Jeol1200EX) images were obtained at 80 kV.

Structural analysis. X-ray structures of wild type TTR alone (PDP codes 1DVQ and 5CN3) and complexed with tolcapone, tafamidis, mds84, compound 20 and 22 (PDB codes 4D7B, 3TCT, 3IPE, 2FBR and 2FLM, respectively) were examined using VMD, SPDBV[20,21] and Pymol (PyMOL Molecular Graphics System, Version 1.8 Schrödinger, LLC). The energetic contribution of the linker to the binding was estimated by the SeeSAR programme (https://www.biosolveit.de/SeeSAR). The halogen binding pockets considered in the analysis are formed by Met13, Lys15, Leu17, Thr106, Ala108, Val121 (HBP1); Lys17, Ala108, Ala109, Leu110 (HBP2); Ala108, Ser117, Leu110, Thr119 (HBP3).

References

1. Colon, W. & Kelly, J. W. Partial denaturation of transthyretin is sufficient for amyloid fibril formation *in vitro*. *Biochemistry* **31**, 8654–8660 (1992).
2. Ihse, E. *et al.* Amyloid fibrils containing fragmented ATTR may be the standard fibril composition in ATTR amyloidosis. *Amyloid* **20**, 142–150, doi:10.3109/13506129.2013.797890 (2013).
3. Mangione, P. P. *et al.* Proteolytic cleavage of Ser52Pro variant transthyretin triggers its amyloid fibrillogenesis. *Proc. Natl. Acad. Sci. USA* **111**, 1539–1544, doi:10.1073/pnas.1317488111 (2014).
4. Marcoux, J. *et al.* A novel mechano-enzymatic cleavage mechanism underlies transthyretin amyloidogenesis. *EMBO Mol. Med.* **7**, 1337–1349, doi:10.15252/emmm.201505357 (2015).
5. Kolstoe, S. E. *et al.* Trapping of palindromic ligands within native transthyretin prevents amyloid formation. *Proc. Natl. Acad. Sci. USA* **107**, 20483–20488, doi:10.1073/pnas.1008255107 (2010).
6. Sant'Anna, R. *et al.* Repositioning tolcapone as a potent inhibitor of transthyretin amyloidogenesis and associated cellular toxicity. *Nat. Commun.* **7**, 10787, doi:10.1038/ncomms10787 (2016).
7. Bulawa, C. E. *et al.* Tafamidis, a potent and selective transthyretin kinetic stabilizer that inhibits the amyloid cascade. *Proc. Natl. Acad. Sci. USA* **109**, 9629–9634, doi:10.1073/pnas.1121005109 (2012).
8. Coelho, T. *et al.* Long-term effects of tafamidis for the treatment of transthyretin familial amyloid polyneuropathy. *J. Neurol.* **260**, 2802–2814, doi:10.1007/s00415-013-7051-7 (2013).
9. Berk, J. L. *et al.* Repurposing diflunisal for familial amyloid polyneuropathy: a randomized clinical trial. *J.A.M.A.* **310**, 2658–2667, doi:10.1001/jama.2013.283815 (2013).
10. Quarta, C. C. *et al.* The amyloidogenic V122I transthyretin variant in elderly black Americans. *N. Engl. J. Med.* **372**, 21–29, doi:10.1056/NEJMoa1404852 (2015).
11. Johnson, S. M. *et al.* Bisaryloxime ethers as potent inhibitors of transthyretin amyloid fibril formation. *J. Med. Chem.* **48**, 1576–1587, doi:10.1021/jm049274d (2005).
12. Plante-Bordeneuve, V. *et al.* Long-term treatment of transthyretin familial amyloid polyneuropathy with tafamidis: a clinical and neurophysiological study. *J. Neurol.*. doi:10.1007/s00415-016-8337-3 (2016).
13. Green, N. S., Palaninathan, S. K., Sacchettini, J. C. & Kelly, J. W. Synthesis and characterization of potent bivalent amyloidosis inhibitors that bind prior to transthyretin tetramerization. *J. Am. Chem. Soc.* **125**, 13404–13414, doi:10.1021/ja030294z (2003).
14. Palaninathan, S. K. Nearly 200 X-ray crystal structures of transthyretin: what do they tell us about this protein and the design of drugs for TTR amyloidoses? *Curr. Med. Chem.* **19**, 2324–2342 (2012).
15. Gilson, M. K. & Zhou, H. X. Calculation of protein-ligand binding affinities. *Annu. Rev. Biophys. Biomol. Struct.* **36**, 21–42, doi:10.1146/annurev.biophys.36.040306.132550 (2007).
16. Saelices, L. *et al.* Uncovering the Mechanism of Aggregation of Human Transthyretin. *J. Biol. Chem.* **290**, 28932–28943, doi:10.1074/jbc.M115.659912 (2015).
17. Hosoi, A. *et al.* Novel Antibody for the Treatment of Transthyretin Amyloidosis. *J. Biol. Chem.* **291**, 25096–25105, doi:10.1074/jbc.M116.738138 (2016).
18. Naiki, H., Higuchi, K., Hosokawa, M. & Takeda, T. Fluorometric determination of amyloid fibrils *in vitro* using the fluorescent dye, thioflavin T1. *Anal. Biochem.* **177**, 244–249 (1989).
19. Puchtler, H., Waldrop, F. S. & Meloan, S. N. A review of light, polarization and fluorescence microscopic methods for amyloid. *Appl. Pathol.* **3**, 5–17 (1985).
20. Guex, N. & Peitsch, M. C. SWISS-MODEL and the Swiss-PdbViewer: an environment for comparative protein modeling. *Electrophoresis* **18**, 2714–27123, doi:10.1002/elps.1150181505 (1997).
21. Humphrey, W., Dalke, A. & Schulten, K. VMD: visual molecular dynamics. *J. Mol. Graph.* **14**, 33–38, 27-28 (1996).

Acknowledgements

Supported by grants from the University College London Amyloidosis Research Fund, the U.K. Medical Research Council (MR/K000187/1), the Rosetrees Trust/Royal Free Charity PhD programme (M427), the Cariplo Foundation (Projects 2013–0964 and 2014–0700), the Telethon Foundation (Grant GG14127), the Italian Ministry of health (Ricerca Finalizzata RF-2013-02355259) and the Istituto Nazionale di Biostrutture e Biosistemi. Core support for the Centre for Amyloidosis and Acute Phase Proteins is provided by the UK National Institute for Health Research Biomedical Research Centre and Unit Funding Scheme. We thank Alejandra Carbajal and the Division of Medicine Electron Microscopy Unit, Royal Free Campus, University College London for imaging of amyloid fibrils *in vitro*.

Author Contributions

The study was conceived, designed and supervised by V.B. G.V., P.P.M., S.R., S.G., R.P. performed research. A.C., J.D.G., P.N.H., M.B.P., G.W.T. contributed to experimental design and discussion. All the authors analysed and interpreted the data. The paper was written by V.B., P.P.M., G.W.T. and M.B.P. and reviewed and approved by all co-authors.

Additional Information

Supplementary information accompanies this paper at doi:10.1038/s41598-017-00338-x

Competing Interests: The authors declare that they have no competing interests.

Publisher's note: Springer Nature remains neutral with regard to jurisdictional claims in published maps and institutional affiliations.

2.2. "Plasminogen activation triggers transthyretin amyloidogenesis *in vitro*".

Mangione PP. *et al*. *J Biol Chem* 2018.

JBC ARTICLE

⌘ *Author's Choice*

Plasminogen activation triggers transthyretin amyloidogenesis *in vitro*

Received for publication, May 15, 2018, and in revised form, July 6, 2018 Published, Papers in Press, July 17, 2018, DOI 10.1074/jbc.RA118.003990

P. Patrizia Mangione[‡§1], Guglielmo Verona[‡1], Alessandra Corazza[‡¶‖1], Julien Marcoux[**], Diana Canetti[‡], Sofia Giorgetti[§], Sara Raimondi[§], Monica Stoppini[§], Marilena Esposito[‡2], Annalisa Relini[‡‡], Claudio Canale[§§], Maurizia Valli[§], Loredana Marchese[§], Giulia Faravelli[§], Laura Obici[¶¶], Philip N. Hawkins[‖‖], Graham W. Taylor[‡], Julian D. Gillmore[‖‖], Mark B. Pepys[‡‖‖], and Vittorio Bellotti[‡§3]

From the [‡]Wolfson Drug Discovery Unit, Centre for Amyloidosis and Acute Phase Proteins, Division of Medicine, University College London, London NW3 2PF, United Kingdom, [§]Department of Molecular Medicine, Institute of Biochemistry, University of Pavia, 27100 Pavia, Italy, [¶]Department of Medicine (DAME), University of Udine, 33100 Udine, Italy, [‖]Istituto Nazionale Biostrutture e Biosistemi, 00136 Roma, Italy, [**]Institut de Pharmacologie et de Biologie Structurale, Université de Toulouse, CNRS, UPS, 31000 Toulouse, France, [‡‡]Department of Chemistry and Industrial Chemistry, University of Genoa, 16146 Genoa, Italy, [§§]Department of Physics, University of Genoa, 16146 Genoa, Italy, [¶¶]Amyloidosis Research and Treatment Center, Foundation IRCCS Policlinico San Matteo, 27100 Pavia, Italy, [‖‖]National Amyloidosis Centre, University College London and Royal Free Hospital, London NW3 2PF, United Kingdom

Edited by Paul E. Fraser

Systemic amyloidosis is a usually fatal disease caused by extracellular accumulation of abnormal protein fibers, amyloid fibrils, derived by misfolding and aggregation of soluble globular plasma protein precursors. Both WT and genetic variants of the normal plasma protein transthyretin (TTR) form amyloid, but neither the misfolding leading to fibrillogenesis nor the anatomical localization of TTR amyloid deposition are understood. We have previously shown that, under physiological conditions, trypsin cleaves human TTR in a mechano-enzymatic mechanism that generates abundant amyloid fibrils *in vitro*. In sharp contrast, the widely used *in vitro* model of denaturation and aggregation of TTR by prolonged exposure to pH 4.0 yields almost no clearly defined amyloid fibrils. However, the exclusive duodenal location of trypsin means that this enzyme cannot contribute to systemic extracellular TTR amyloid deposition *in vivo*. Here, we therefore conducted a bioinformatics search for systemically active tryptic proteases with appropriate tissue distribution, which unexpectedly identified plasmin as the leading candidate. We confirmed that plasmin, just as trypsin, selectively cleaves human TTR between residues 48 and 49 under physiological conditions *in vitro*. Truncated and full-length protomers are then released from the native homotetramer and rapidly aggregate into abundant fibrils indistinguishable from *ex vivo* TTR amyloid. Our findings suggest that physiological fibrinolysis is likely to play a critical role in TTR amyloid formation *in vivo*. Identification of this surprising intersection between two hitherto unrelated pathways opens new avenues for elucidating the mechanisms of TTR amyloidosis, for seeking susceptibility risk factors, and for therapeutic innovation.

The *in vivo* processes responsible for misfolding of native precursors, for formation of amyloid fibrils, and for the anatomical localization of amyloid deposition are not known either for transthyretin (TTR)[4] or for other types of systemic amyloidosis (1). The late onset of TTR amyloidosis, despite the abundance of circulating TTR from birth, is also mysterious.

In vitro studies suggest that TTR fibrillogenesis requires dissociation of the native tetramer, which is favored by the destabilizing mutations that are known to be amyloidogenic. Indeed the most aggressive, earlier onset forms of the disease are caused by highly destabilizing mutations whereas mutations that increase tetramer stability prevent amyloidosis (2). A single, selective, proteolytic cleavage in the loop interconnecting strands C and D dramatically destabilizes the native tetramer in the most unstable amyloidogenic S52P TTR (3) and the unusual Glu-51_Ser-52 duplicate variant (4) leading to abundant amyloid formation. In addition, mechanical forces, generated by a combination of physiological fluid flow and contact with hydrophobic surfaces, enhance susceptibility to this cleavage and thus uniquely promote formation of unequivocal amyloid

This work was supported by investment from the University College London Technology Fund and by the University College London Amyloidosis Research Fund, the United Kingdom Medical Research Council Grant MR/K000187/1, the Rosetrees Trust/Royal Free Charity PhD programme M427, the Cariplo Foundation Projects 2013 0964 and 2014 0700, the Italian Ministry of Health Ricerca Finalizzata RF 2013 02355259, the Italian Ministry of Research and University Dipartimenti di Eccellenza 2018-2022 grant to the Molecular Medicine Department (University of Pavia), and the Istituto Nazionale di Biostrutture e Biosistemi. Core support for the Wolfson Drug Discovery Unit is provided by the United Kingdom National Institute for Health Research Biomedical Research Centre and Unit Funding Scheme via the UCLH/UCL Biomedical Research Centre. The authors declare that they have no conflicts of interest with the contents of this article.

This article contains Figs. S1–S3.

[1] These authors contributed equally to this work.

[2] Present address: Dept. of Chemical Sciences, Federico II University, 80126 Naples, Italy.

[3] To whom correspondence should be addressed: Rowland Hill St., London NW3 2PF, United Kingdom. Tel.: 44 20 7433 2773; Fax: 44 20 7433 2803; E-mail: v.bellotti@ucl.ac.uk.

[4] The abbreviations used are: TTR, transthyretin; w/w, weight for weight; ThT, thioflavin T; tPA, tissue plasminogen activator; uPA, urokinase plasminogen activator; AFM, atomic force microscopy; buffer A, 20 mM Tris-HCl, pH 7.5 containing 150 mM NaCl and 5 mM $CaCl_2$.

fibrils, both by other amyloidogenic variants that are more stable than S52P and by WT TTR (5).

Trypsin, which we have previously used to trigger TTR amyloid fibril formation *in vitro*, is synthesized only by the exocrine pancreas and secreted exclusively into the small bowel lumen. It is therefore unlikely to be involved in pathogenesis of systemic TTR amyloidosis. However, we show here that plasmin, identified in our comprehensive bioinformatics search for pathophysiologically plausible candidate proteases, effectively replicates the role of trypsin in *in vitro* TTR amyloidogenesis. Furthermore, the normal, ubiquitous, continuous, physiological activation of plasminogen is fully consistent with a key role of plasmin in TTR amyloidogenesis.

Results

Search for candidate tryptic proteases in the MEROPS database

There were 344 peptidases in the MEROPS database (6) able to cleave substrates with tryptic specificity, that is C-terminal to lysine (position P1), and with relevantly wider tissue distribution than trypsin itself. Seventy-five of them were both human and extracellular according to the curated UniProt protein database, the majority being either serine chymotrypsin–like or metallopeptidase types (Table 1). Among the four enzymes with specificity higher than 30% for lysine at P1 (Table 2), trypsin was excluded because of its exocrine location. Tryptase alpha did not trigger TTR amyloid formation in our fibrillogenesis assay (3) and kallikrein-related peptidase 12 had very modest activity (Fig. S1). In contrast, plasmin not only fulfilled our search criteria but its active site is also strikingly similar to that of trypsin (Fig. 1).

Amyloidogenic cleavage of TTR by plasmin

Consistent with its known structure and proteolytic specificity, plasmin did indeed trigger TTR amyloid formation *in vitro*, although it was slightly less active than trypsin (Fig. 2). With S52P TTR in solution, stirred at physiological pH and ionic strength, and the same enzyme:TTR w/w ratio, the thioflavin T (ThT) signal increased more rapidly in the presence of trypsin than plasmin and reached a higher final value (Fig. 2*A*). Nevertheless, both samples contained abundant amyloid fibrils with the pathognomonic amyloid red-green birefringence after Congo Red staining when viewed in strong cross-polarized light, and showing typical fibrillar morphology in negative staining EM (Fig. 2, *B* and *C*). The crucial residue 49–127 fragment produced by the specific amyloidogenic cleavage was present after fibrillogenesis induced by plasmin but was slightly less abundant than with trypsin (Fig. 2, *D* and *E*), consistent with the longer lag phase and lower yield of fibrils (Fig. 2*A*). However, as in our previous studies with trypsin, TTR amyloid fibrillogenesis mediated by plasmin in the mechano-enzymatic process was accelerated by seeding with preformed TTR amyloid fibrils, which eliminated the lag phase and produced a

Table 1

Bioinformatics search for trypsin like protease(s)

Summary of the human extracellular proteases identified in the MEROPS database with lysine in position P1 of the substrate.

Clan	Family	Type	Number
A	A01	Asp_pepsin_like	3
C	C01	Cys_papain_like	1
MA	M01	Aminopeptidase_like	2
MA	M10	Metallopeptidase	14
MA	M12	Astacin_like	7
MA–MC	M13–M43	Neprilysin_like; carboxypeptidase	7
PA	S01	Ser_chymotrypsin_like	38
SB	S08	Ser_subtilisin_like	2
SR	S60	Ser_lactoferrin	1
Total			75

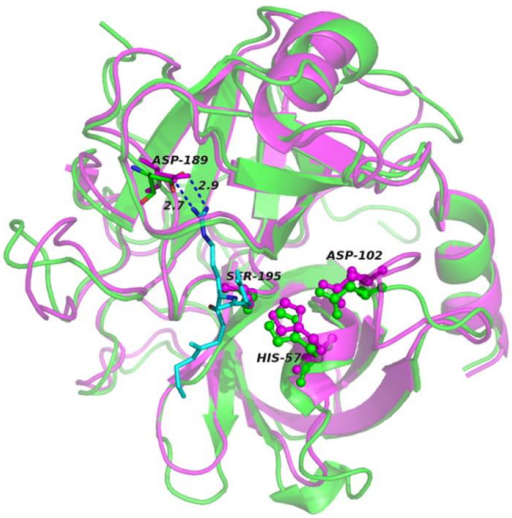

Figure 1. Structural and functional similarities between trypsin and plasmin in complex with the peptide P3-P3′ corresponding to sequence 46–51 of TTR. The backbones of trypsin (*magenta*; PDB ID:3D65) and plasmin (*green*; PDB ID: 3UIR) are overlaid; the catalytic triad, in *ball and stick*, with the Asp residue, in *sticks*, that lead to the correct orientation of the Lys-substrate (Lys-48 in TTR) are specifically highlighted. The numbering refers to trypsin residues. The P3-P3′ peptide backbone of textilinin-1 in the complex with plasmin is shown in *cyan*. The side chain of Lys in position P1 is also represented in *sticks* with the distances from Asp-189. For clarity the corresponding peptide complexed to trypsin is not shown.

Table 2

Secreted peptidases with specificity for lysine in position P1 higher than 30%

Plasmin and tryptase have structural similarities with trypsin; the structure of kallikrein-related peptidase 12 is not known.

Enzymes	Specificity for Lys at P1 (%)	Primary localization
S01.151: trypsin 1	60	Intestinal tract
S01.143: tryptase alpha	56	Lung, stomach, spleen, heart, and skin
S01.020: kallikrein-related peptidase 12	55	Salivary glands, stomach, uterus, trachea, prostate, thymus, lung, colon, brain, breast, and thyroid
S01.233: plasmin	45	Plasma and many other extracellular fluids

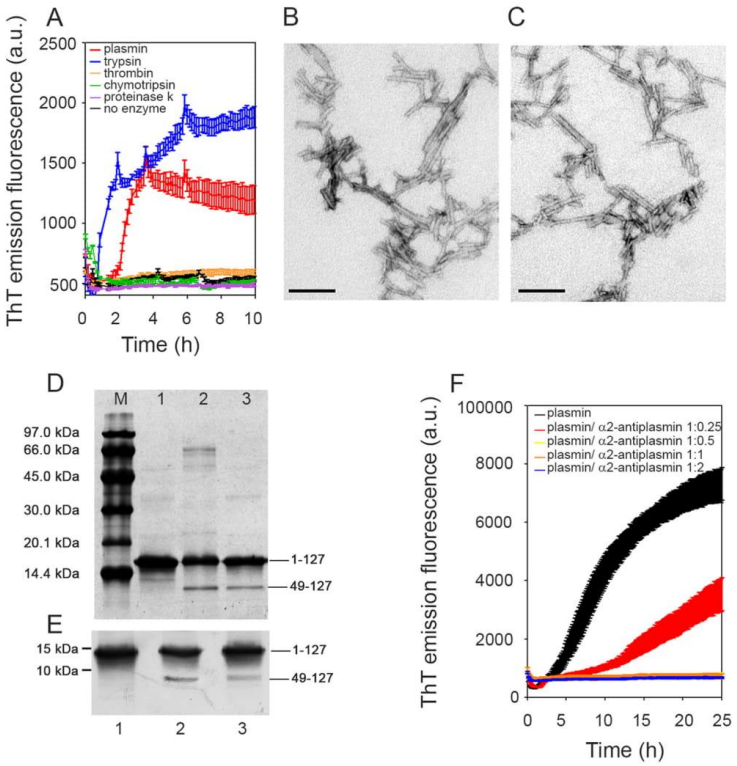

Figure 2. Plasmin-mediated amyloid fibrillogenesis of S52P TTR. *A*, increase in ThT emission fluorescence for S52P TTR incubated in the presence of plasmin compared with trypsin. No amyloid-specific ThT signal was seen after incubation of S52P TTR with thrombin, chymotrypsin, or proteinase K. *B* and *C*, negatively stained transmission electron micrographs of S52P TTR amyloid fibrils formed in the presence of trypsin (*B*) or plasmin (*C*). *Scale bar*, 100 nm. *D*, 15% SDS-PAGE under reducing conditions. *M*, marker proteins (14.4, 20.1, 30.0, 45.0, 66.0, and 97.0 kDa); *lane 1*, S52P TTR at time 0; *lane 2*, S52P TTR fibrils formed in the presence of trypsin; and *lane 3*, S52P TTR fibrils formed in the presence of plasmin. *E*, immunoblot analysis of samples separated in 15% SDS-PAGE (see *lanes 1*, *2*, and *3* in *D*). Position of marker proteins at 15 and 10 kDa are indicated. *F*, inhibition by α2-antiplasmin of fibril formation by S52P TTR mediated by 20 ng/μl plasmin. The data were normalized to the ThT signal plateau in the samples without α2-antiplasmin. Mean ± S.D. of three replicates is shown. *a.u.*, arbitrary units.

higher final yield (Fig. S2). Plasmin-induced fibrillogenesis was inhibited by α2-antiplasmin, the natural inhibitor of the enzyme (Fig. 2*F*).

The critical importance of protease specificity for TTR amyloid formation was exemplified by the failure of three different, potent, proteolytic enzymes, thrombin, chymotrypsin, and proteinase K, to trigger any amyloidogenesis (Fig. 2*A*). On the other hand, all the amyloidogenic TTR variants tested so far, as well as WT TTR, were cleaved by plasmin in our *in vitro* mechanoenzymatic system. They all formed unequivocal amyloid fibrils, although the yields were lower with V30M, L55P, and V122I TTR than with S52P and were lowest with WT TTR (Fig. 3). Crucially, the known, superstable, T119M TTR variant was not cleaved at all (Fig. 3). These observations are fully consistent with the usually earlier onset and more aggressive phenotypes in carriers of amyloidogenic TTR mutations, compared with the late onset of WT TTR amyloidosis, and with the protection against TTR amyloidosis in carriers of amyloidogenic TTR gene mutations afforded by co-inheritance of the gene for the T119M variant.

In contrast to the susceptibility of native TTR to cleavage by plasmin, which was greatly enhanced by mechanical forces, preformed TTR amyloid fibrils were completely resistant to degradation by plasmin (Fig. S3). This differs from Aβ-amyloid fibrils that are digested by plasmin, which has been suggested to be a putative protective mechanism against amyloid formation in Alzheimer's disease (7).

From fibrin to fibril formation

To study the amyloidogenicity of plasmin in a more physiological environment, we created a model fibrin clot on which fibrinolysis was initiated in the presence of either the highly amyloidogenic unstable S52P TTR variant or the superstable nonamyloidogenic T119M variant. Polymerization and depolymerization were monitored by nonspecific light scattering at 350 nm (Fig. 4*A*) and by the specific spectrofluorimetric signal of ThT binding to amyloid fibrils (Fig. 4*B*).

In phase I, fibrinogen was converted into fibrin by addition of thrombin, monitored by the rapid increase in turbidity. Once the clot was formed, tissue plasminogen activator (tPA), plas-

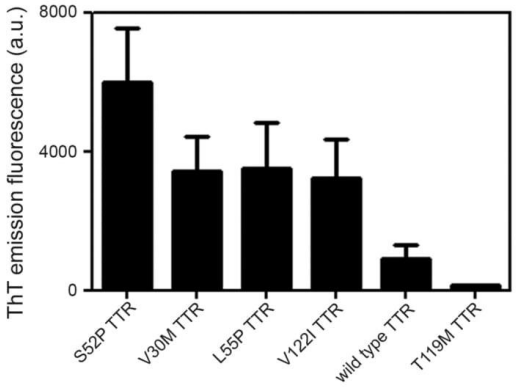

Figure 3. Plasmin-mediated fibrillogenesis. Relative ThT emission fluorescence intensities of TTR samples at 1 mg/ml after 25 h incubation with shaking in the presence of plasmin at an enzyme:substrate ratio of 1:50. Mean ± S.D. of three replicates is shown.

minogen, and TTR were gently layered on the clot surface, at the time point shown (*arrow*) in Fig. 4, *A* and *B*, producing physiological fibrinolysis of the clot as indicated by the rapid decline in turbidity in phase II. When S52P TTR was present, the initial fall in light scattering was swiftly followed by a sharp rise that correlated with the appearance and increase in the ThT amyloid fibril signal (Fig. 4*B*). In the presence of T119M TTR, which is not susceptible to cleavage by plasmin and does not form amyloid fibrils (5) (Fig. 3), there was no secondary rise in turbidity and no ThT signal (Fig. 4, *A*–*C*).

Atomic force microscopy analysis of the reactants at the end of the experiment with the stable T119M or the pathogenic S52P variant TTR (that is *4* and *5* in Fig. 4, *A*–*C*) showed remarkably different structures, consistent with the spectrometry results. S52P TTR produced morphologically typical mature amyloid fibrils, 4–7 nm in height (Fig. 4*D*) emerging from a thick layer of short fibrils. No fibrillar material was seen either with T119M TTR (Fig. 4*E*) or in the absence of any added TTR (Fig. 4*F*). Only single globular structures and short beaded chains were observed.

Discussion

The spectrum of systemic TTR amyloidosis comprises the many very rare hereditary forms caused by different mutations (8), the cardiac amyloidosis caused by the V122I variant in individuals of African origin (9) and cardiac amyloidosis, mostly in elderly men, caused by WT TTR (10). Recent advances in imaging have shown that the latter is substantially more prevalent than previously recognized (11). There are no licensed treatments that arrest disease progression and TTR amyloidosis is thus an important unmet medical need. Current trials of TTR gene expression knockdown by experimental siRNA (12) and antisense oligonucleotide (ASO) drugs (13) have shown promising results. However, elucidation of the mechanism underlying the *in vivo* transition of native, soluble, globular, tetrameric TTR into insoluble, polymeric, amyloid fibrils is crucial for understanding the natural history of the disease and for design of other effective therapies.

The influential original model of TTR denaturation and aggregation at low pH (14) demonstrated that tetramer disassembly is crucial, and that analogues of thyroxine, the natural ligand of TTR, can inhibit this process (15). The observations led to design, development, and clinical testing of tafamidis (16) and diflunisal (17), compounds that stabilize TTR against acid denaturation, for use as inhibitors of TTR amyloidogenesis, mimicking the trans-suppressive effect of the TTR-stabilizing T119M variant (2). Despite the capacity of tafamidis to increase the stability of TTR in plasma through the occupancy of just one of the two binding sites (18), its clinical use does not halt disease progression in a substantial proportion of patients (19). The limited clinical efficacy probably reflects the fact that the low pH model does not represent the actual pathophysiological mechanism of TTR amyloid fibrillogenesis. Indeed there is no relevant *in vivo* location in which TTR could be exposed to the acid conditions used *in vitro*.

We have recently demonstrated that specific proteolytic cleavage of the residue 48–49 bond in the flexible loop connecting strands C and D, in just a single TTR protomer within the native tetrameric TTR assembly, causes rapid dissociation into cleaved and uncleaved protomers. Under physiological conditions *in vitro*, these then swiftly form abundant TTR fibrils, which are indistinguishable from *ex vivo* TTR amyloid fibrils (3, 5). The whole process occurs in the presence of physiological scale mechanical forces provided by stirring and by exposure to hydrophobic surfaces. Discovery of the critical role of proteolysis explains the almost universal presence of the TTR residue 49–127 fragment in *ex vivo* TTR amyloid fibrils (20). Other features consistent with the mechano-enzymatic mechanism operating *in vivo* include the presence of a lag-phase preceding fibrillogenesis, and acceleration of fibril formation when preformed fibril seeds are present. We have also shown that binding of small ligands by the intact TTR tetramer significantly reduces its susceptibility to cleavage and aggregation. However, maximum inhibition is only achieved by ligands that simultaneously occupy both the two binding sites and the central channel between them in the core of the TTR molecule (21).

A crucial question about the mechano-enzymatic mechanism has hitherto been the identity of the tryptic protease responsible for TTR amyloidosis *in vivo*. The present demonstration of the efficacy of plasmin *in vitro* highlights it as an extremely plausible candidate. Other potent proteolytic enzymes were completely inactive in triggering TTR amyloid formation *in vitro*. Kallikrein-related peptidase 12, which has only very transient activity *in vivo*, did produce a small ThT signal of amyloid formation with S52P TTR, the most unstable and amyloidogenic TTR variant, but there was a long lag phase and very modest yield. Plasmin mediates the essential specific cleavage in TTR much more potently and, with classical kinetic phases of nucleation and elongation, it generates abundant fibrils that are identical to *ex vivo* TTR amyloid fibrils. The relative lower activity of plasmin compared with trypsin cannot be easily explained. The remarkable self-digestion of plasmin, once activated, may reduce its activity and therefore delay the formation of the first fibrillar nuclei thus contributing to a reduced yield of fibrils. A complete

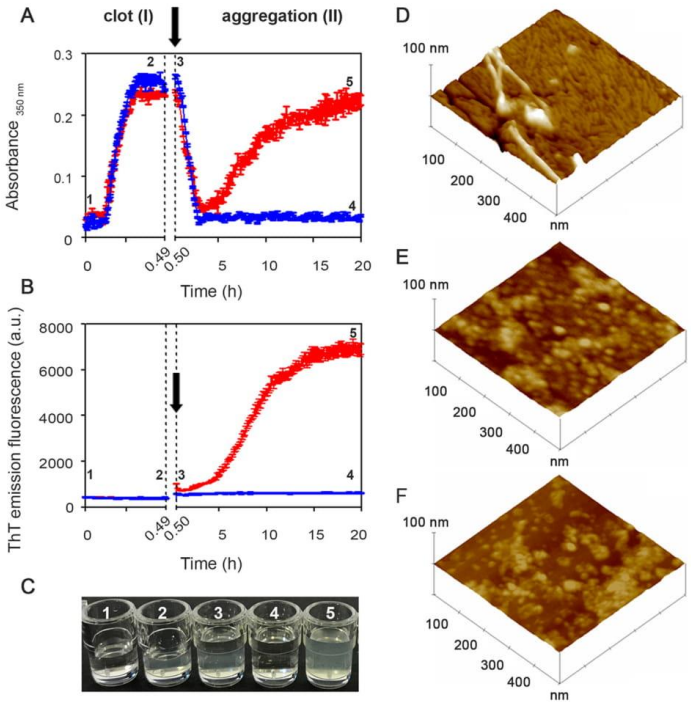

Figure 4. From fibrin to fibrils. *A* and *B*, spectrophotometric absorbance/light scattering at 350 nm (*A*) and amyloid-specific ThT emission fluorescence (*B*) during clotting of fibrinogen to fibrin (phase I) followed by fibrinolysis in the presence of S52P TTR (*red*) or of the highly stable T119M TTR variant (*blue*) (phase II). Following fibrinolysis, increase in turbidity and ThT were observed in the presence of S52P TTR whereas neither of these signals increased when T119M TTR was present instead. *Arrows* indicate addition of tPA, plasminogen, and TTR. The results shown are the mean ± S.D. of three independent experiments. *C*, wells containing a solution of fibrinogen in the presence of 1) thrombin and 2) fibrin clot; 3) a solution of tPA, plasminogen, and TTR layered over the clot surface; 4) fibrinolysis with no further aggregation in the presence of T119M TTR; 5) fibrinolysis in the presence of S52P TTR showing the turbidity of amyloid fibril formation. *D–F*, surface plots of topographic tapping mode AFM images showing (*D*) the presence of fibrillar structures in the sample containing clot, tPA, plasminogen, and S52P TTR; (*E* and *F*) the presence of globular structures in samples containing clot, tPA, and plasminogen (*E*) in the presence of T119M TTR or (*F*) in the absence of any TTR isoform.

characterization of the kinetics of all processes together with the determination of the TTR–plasmin structure should clarify the differences that we have observed. The several amyloidogenic TTR variants tested so far and the WT protein are all cleaved by plasmin, with varying efficiency replicating the findings with trypsin, whereas the stable, nonpathogenic, protective T119M variant is resistant. Furthermore, plasmin is ubiquitously and continuously activated *in vivo* to provide for essential fibrinolysis on the vascular wall and also in the extracellular matrix, precisely where TTR amyloid is deposited.

The possible *in vivo* scenario of plasmin-mediated TTR fibrillogenesis is summarized in Fig. 5. Plasminogen can be activated by tPA within the clot and also by urokinase plasminogen activator (uPA) in the extracellular matrix. Sufficient proteolysis of the TTR tetramer by plasmin may then provide the critical concentration of both truncated and full-length TTR protomers required for nucleation of fibrils. Once nucleation has occurred, the elongation of fibrils can progress at lower concentrations of monomers provided by either of the plasminogen activating pathways. Plasmin activity is finely regulated by activators, including tPA and uPA, and inhibitors, including α2-plasmin inhibitor and plasminogen activator inhibitor. The conditions for critical TTR cleavage, sufficient to initiate amyloidogenesis, may thus only arise rarely but there is certainly scope for variation in this complex system. For example, physiological fibrinolysis is notably affected by the intensity of normal physical activity (22). All these features of plasmin, combined with the importance of mechanical forces, are consistent with the prevalence of TTR amyloid deposition in the heart and carpal tunnel, both of which are notable sites of continuous repetitive vigorous movement. The pathogenetic significance of plasmin also opens a broad and completely novel perspective for investigation of factors that may determine individual susceptibility and the natural history of the familial and acquired forms of TTR amyloidosis, including the initiation, progression, and tissue distribution of amyloid deposition. In addition, the wholly unexpected and surprising confluence of the fibrinolysis pathway, the physiological remodeling of the extracellular matrix regulated by urokinase (23), and the pathogenesis of TTR amyloidosis are of considerable fundamental interest.

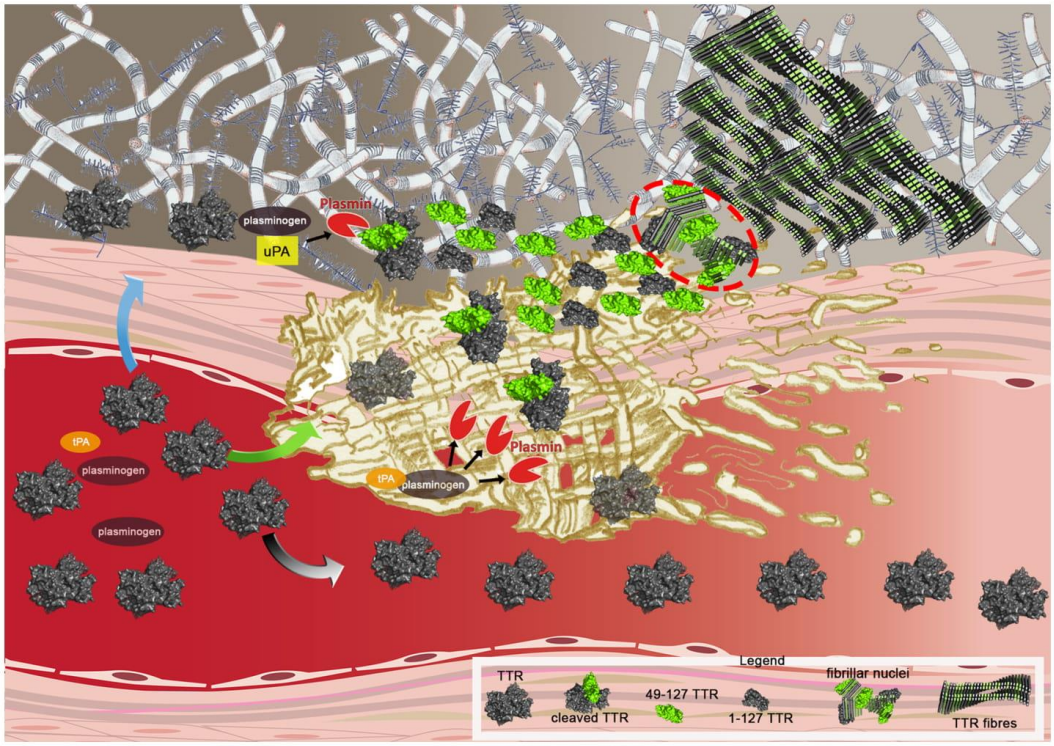

Figure 5. From fibrin to fibrils. Shown is a cartoon of the putative flow of events leading to TTR amyloid fibril formation caused by plasmin cleavage within the physiological scenario of fibrin formation and plasminogen activation. Circulating TTR can diffuse toward the extracellular compartment (*blue arrow*), be entrapped in the fibrin clot (*green arrow*), or escape from it (*gray arrow*). In the presence of activated plasminogen both in the presence of uPA (extracellular compartment) and tPA (within the clot), tetrameric TTR may be cleaved and then rapidly dissociate into a mixture of the truncated residue 49–127 fragment (*green*) and full-length protomers (*gray subunit*). The released subunits may generate the fibrillar nuclei (*highlighted within the red circle*) that then aggregate into amyloid fibrils, which accumulate in the extracellular space. The *legend* at the bottom of the figure identifies all the TTR species.

Experimental procedures

Reagents

Recombinant TTR variants were expressed and purified as described previously (21). Human fibrinogen was isolated from citrate-heparin–treated human plasma by affinity chromatography on recombinant clamping factor 221–559 fragment (24) and was absorbed with lysine-Sepharose 4B and gelatin-Sepharose 4B to remove traces of plasminogen and fibronectin, respectively. Enzymes purchased from Sigma-Aldrich were plasmin (P1867), proteinase K (P2308), chymotrypsin (C2160000), tPA (T0831), plasminogen (SRP6518), thrombin (T7572), and tryptase (T7063). Trypsin was purchased from Promega (V5280) and recombinant human kallikrein 12 from Biotechne (3095-S.E.). All the enzymes used were able to cleave the C-terminal end of Lys in the D-Val-Leu-Lys 4-nitroanilide dihydrochloride peptide (Sigma-Aldrich, V0882) following the manufacturer's instructions. All other reagents including α2-antiplasmin (SRP6313) were purchased from Sigma-Aldrich unless otherwise stated.

MEROPS database search

MEROPS (https://www.ebi.ac.uk/merops/) is a manually annotated database with information on more than 4000 peptidases classified according to families and clans. The residues of the proteolytic substrate are designated Pn—P4-P3-P2-P1-‖-P1′-P2′-P3′-P4′—Pm′ with ‖ indicating the scissile bond. Substrate specificity was based on the frequency of Lys at position P1.

Proteolysis and fibrillogenesis of S52P TTR

Recombinant S52P TTR, 100 μl volumes at 0.5 mg/ml in 20 mM Tris-HCl containing 150 mM NaCl, 5 mM $CaCl_2$, pH 7.4, containing 10 μM ThT (25) was incubated at 37 °C in Costar 96-well black plates in the presence of a protease at an enzyme: substrate ratio of 1:50. Plasmin, trypsin, thrombin, proteinase K, chymotrypsin, tryptase alpha, and kallikrein 12 were tested. The plate was sealed with clear sealing film and subjected to 900 rpm double-orbital shaking. Bottom fluorescence was recorded at 500-s intervals (BMG LABTECH, FLUOstar Omega). Homogenous 15% SDS-PAGE (GE Healthcare) under reducing

conditions was used to analyze protein composition before and after fibril formation. After electrophoretic separation, samples treated and untreated with trypsin or plasmin were blotted onto an activated PVDF membrane. Western blotting was developed with polyclonal sheep anti-human TTR (6 μg/ml, The Binding Site, United Kingdom/code AU066X) and polyclonal rabbit anti-sheep peroxidase conjugate (1.3 μg/ml, Dako, Denmark/code P0163) as primary and secondary antibodies, respectively. Peroxidase activity was visualized using a precipitating substrate containing 3,3′-diaminobenzidine and urea hydrogen peroxide (Sigma*FAST* DAB tablets, Sigma-Aldrich).

Effect of α2-antiplasmin on TTR fibril formation

Recombinant S52P TTR in 200 μl volumes at 1 mg/ml in 20 mM Tris-HCl at pH 7.5, containing 150 mM NaCl, 5 mM $CaCl_2$, 10 μM ThT, was incubated at 37 °C in sealed Costar 24-well black-wall plates, together with 20 ng/μl of plasmin while subjected to 900 rpm double-orbital shaking in the presence of 0.09, 0.18, 0.36, and 0.72 μM α2-antiplasmin and in its absence. Based on an average molecular mass of 55 kDa for plasmin, the selected inhibitor concentrations corresponded to molar ratios to plasmin of 0.25:1, 0.5:1, 1:1, and 2:1, respectively. ThT fluorescence emission was monitored using a BMG LABTECH FLUOstar Omega plate reader. Data were normalized to the ThT signal plateau reached in the samples without the plasmin inhibitor. All experiments were conducted in triplicate.

Fibrillogenesis of TTR variants and WT TTR

Recombinant S52P, V30M, L55P, V122I, WT and T119M TTR in 500 μl volumes at 1 mg/ml in 20 mM Tris-HCl containing 150 mM NaCl, 5 mM $CaCl_2$, 10 μM ThT, pH 7.5 were incubated at 37 °C in sealed Costar 24-well black-wall plates, together with 20 ng/μl of plasmin while subjected to 900 rpm double-orbital shaking. ThT fluorescence emission was monitored until it reached a plateau. All experiments were conducted in triplicate.

Preparation of amyloid seeds from S52P TTR with plasmin

S52P TTR at 1 mg/ml in 20 mM Tris-HCl, 150 mM NaCl, 5 mM $CaCl_2$, 10 μM ThT, pH 7.5 was incubated at 37 °C with plasmin at an enzyme:substrate ratio of 1:50 w/w in volume of 200 μl in a 96-well black-wall plate. The plate was sealed with clear sealing film, subjected to 900 rpm double-orbital shaking and bottom fluorescence was recorded (BMG LABTECH FLUOstar Omega). Aliquots of the final ThT positive material were stained with alkaline alcoholic Congo Red and viewed under high intensity cross-polarized light (26). Samples were also examined by EM (Joel1200EX) after negative staining with 2% uranyl acetate (3). After further blotting and drying in air, images were obtained at 80 kV.

Effect of seeds on plasmin-mediated S52P TTR fibrillogenesis

S52P TTR at 1 mg/ml in 20 mM Tris-HCl, 150 mM NaCl, 5 mM $CaCl_2$, 10 μM ThT, pH 7.5 was incubated at 37 °C with plasmin at an enzyme:substrate ratio of 1:50 w/w in a volume of 200 μl in a 96-well black-wall plate. S52P TTR fibrils, prepared as described above, were added at the outset at 0.1 mg/ml to three replicate wells; triplicate control well received addition of buffer alone. The plate was sealed with clear sealing film, subjected to 900 rpm double-orbital shaking, and bottom fluorescence was recorded at 500-s intervals (BMG LABTECH FLUOstar Omega). Data were normalized to the highest value of ThT signal after subtraction of the fluorescence intensity attributable to the added seeds alone.

Effect of plasmin on TTR amyloid fibrils

The concentration of S52P amyloid fibrils, produced as described above, was measured by bicinchoninic acid protein assay (Pierce). Fibrils at 0.1 mg/ml in 20 mM Tris-HCl, 150 mM NaCl, 5 mM $CaCl_2$, 10 μM ThT, pH 7.5 in 200 μl aliquots per well were incubated at 37 °C in sealed Costar 96-well black-wall plates in the presence or absence of plasmin at an enzyme:substrate ratio of 1:50 w/w, with agitation as above. Bottom ThT fluorescence was monitored at 500-s intervals as before in three replicate test and control wells.

Fibrinolysis and/or fibril formation

The two-stage procedure comprised clot formation in phase I followed by fibrinolysis and potential amyloid fibrillogenesis in phase II. The experiments were conducted in Costar 96-well black plates at 37 °C using a multimode plate reader (BMG LABTECH FLUOstar Omega) to monitor either changes in turbidity at 350 nm or ThT emission fluorescence. Fibrin polymerization was initiated by adding thrombin (0.5 NIH units/ml) to 1 μM human fibrinogen in 20 mM Tris-HCl, pH 7.5 containing 150 mM NaCl and 5 mM $CaCl_2$ (buffer A) in a total volume of 100 μl per well. Clot formation was monitored by recording the turbidity at 350 nm at 20-s intervals. After turbidity had reached a stable level (usually within 30 min), 100 μl of a solution containing tPA, plasminogen, and TTR in buffer A were gently layered on top of the fibrin clot to a final concentration of 0.027 μM, 1 μM, and 18 μM, respectively. The microtiter plate was then sealed with clear sealing film, subjected to 900 rpm double-orbital shaking and absorbance at 350 nm was measured at 500-s intervals at 37 °C. Blank subtraction and a correction based on the volume per well and the microplate dimensions were used to normalize all absorption values to 1-cm path length. ThT at 10 μM was present throughout. Bottom fluorescence was recorded at 20-s intervals for 30 min in stage I; after addition of tPA, plasminogen, and TTR in stage II, the ThT signal was monitored at 500-s intervals for 20 h. Pellets harvested at the end of stage II by centrifugation at 10,600 × *g* for 20 min were further analyzed by negative staining EM, light microscopy after alkaline alcoholic Congo Red staining as described above (26), and atomic force microscopy (AFM).

Atomic force microscopy

Pellets harvested at the end of phase II were resuspended in water and 100-fold diluted; 10 μl aliquots of the diluted samples were deposited on freshly cleaved mica and dried under mild vacuum. Samples in which no pellet was present were diluted and deposited as described above, but after drying they were rinsed with water to remove excess salts. Tapping mode AFM images were acquired in air using a multimode scanning probe microscope equipped with an "E" scanning head (maximum

scan size, 10 μm) and driven by a Nanoscope V controller (Digital Instruments, Bruker). Single-beam uncoated silicon cantilevers (type OMCL-AC160TS, Olympus and TESPA_V2, Bruker) were used. The drive frequency was between 260 and 310 kHz; the scan rate was 0.25– 0.5 Hz.

Author contributions—P. P. M., G. V., and A. C. data curation; P. P. M., G. V., A. C., J. M., D. C., S. G., S. R., M. S., M. E., A. R., C. C., M. V., L. M., G. F., L. O., G. W. T., and V. B. investigation; P. P. M., G. V., A. C., J. M., D. C., S. G., S. R., M. E., A. R., C. C., L. M., and G. F. methodology; P. P. M. and V. B. writing-original draft; G. V., A. C., J. M., D. C., M. V., P. N. H., G. W. T., J. D. G., and M. B. P. formal analysis; G. V. validation; A. C., M. S., L. O., P. N. H., J. D. G., M. B. P., and V. B. conceptualization; G. W. T. and M. B. P. writing-review and editing; M. B. P. and V. B. funding acquisition; V. B. supervision.

Acknowledgments—We thank Dr. Giampiero Pietrocola (Department of Molecular Medicine, University of Pavia) for providing human fibrinogen.

References

1. Pepys, M. B. (2009) A molecular correlate of clinicopathology in transthyretin amyloidosis. *J. Pathol.* **217,** 1–3 CrossRef Medline
2. Hammarström, P., Schneider, F., and Kelly, J. W. (2001) Trans-suppression of misfolding in an amyloid disease. *Science* **293,** 2459–2462 CrossRef Medline
3. Mangione, P. P., Porcari, R., Gillmore, J. D., Pucci, P., Monti, M., Porcari, M., Giorgetti, S., Marchese, L., Raimondi, S., Serpell, L. C., Chen, W., Relini, A., Marcoux, J., Clatworthy, I. R., Taylor, G. W., *et al.* (2014) Proteolytic cleavage of Ser52Pro variant transthyretin triggers its amyloid fibrillogenesis. *Proc. Natl. Acad. Sci. U.S.A.* **111,** 1539–1544 CrossRef Medline
4. Klimtchuk, E. S., Prokaeva, T., Frame, N. M., Abdullahi, H. A., Spencer, B., Dasari, S., Cui, H., Berk, J. L., Kurtin, P. J., Connors, L. H., and Gursky, O. (2018) Unusual duplication mutation in a surface loop of human transthyretin leads to an aggressive drug-resistant amyloid disease. *Proc. Natl. Acad. Sci. U.S.A.* **115,** E6428–E6436 CrossRef Medline
5. Marcoux, J., Mangione, P. P., Porcari, R., Degiacomi, M. T., Verona, G., Taylor, G. W., Giorgetti, S., Raimondi, S., Sanglier-Cianferani, S., Benesch, J. L., Cecconi, C., Naqvi, M. M., Gillmore, J. D., Hawkins, P. N., Stoppini, M., Robinson, C. V., Pepys, M. B., and Bellotti, V. (2015) A novel mechano-enzymatic cleavage mechanism underlies transthyretin amyloidogenesis. *EMBO Mol. Med.* **7,** 1337–1349 CrossRef Medline
6. Rawlings, N. D., Barrett, A. J., and Finn, R. (2016) Twenty years of the MEROPS database of proteolytic enzymes, their substrates and inhibitors. *Nucleic Acids Res.* **44,** D343–D350 CrossRef Medline
7. Tucker, H. M., Kihiko, M., Caldwell, J. N., Wright, S., Kawarabayashi, T., Price, D., Walker, D., Scheff, S., McGillis, J. P., Rydel, R. E., and Estus, S. (2000) The plasmin system is induced by and degrades amyloid-beta aggregates. *J. Neurosci.* **20,** 3937–3946 CrossRef Medline
8. Benson, M. D. (2003) The hereditary amyloidoses. *Best Pract. Res. Clin. Rheumatol.* **17,** 909–927 CrossRef Medline
9. Jacobson, D. R., Pastore, R. D., Yaghoubian, R., Kane, I., Gallo, G., Buck, F. S., and Buxbaum, J. N. (1997) Variant-sequence transthyretin (isoleucine 122) in late-onset cardiac amyloidosis in black Americans. *N. Engl. J. Med.* **336,** 466–473 CrossRef Medline
10. Ruberg, F. L., and Berk, J. L. (2012) Transthyretin (TTR) cardiac amyloidosis. *Circulation* **126,** 1286–1300 CrossRef Medline
11. Gillmore, J. D., Maurer, M. S., Falk, R. H., Merlini, G., Damy, T., Dispenzieri, A., Wechalekar, A. D., Berk, J. L., Quarta, C. C., Grogan, M., Lachmann, H. J., Bokhari, S., Castano, A., Dorbala, S., Johnson, G. B., *et al.* (2016) Nonbiopsy diagnosis of cardiac transthyretin amyloidosis. *Circulation* **133,** 2404–2412 CrossRef Medline
12. Adams, D., Suhr, O. B., Dyck, P. J., Litchy, W. J., Leahy, R. G., Chen, J., Gollob, J., and Coelho, T. (2017) Trial design and rationale for APOLLO, a Phase 3, placebo-controlled study of patisiran in patients with hereditary ATTR amyloidosis with polyneuropathy. *BMC Neurol.* **17,** 181 CrossRef Medline
13. Benson, M. D., Waddington Cruz, M., Wang, A., Polydefkis, M., Plante-Bordeneuve, V., Berk, J., Barroso, F., Adams, D., Dyck, P., Brannagan, T., Whelan, C., Merlini, G., Scheinberg, M., Drachman, B., Heitner, S., *et al.* (2017) Safety and efficacy of inotersen in patients with hereditary transthyretin amyloidosis with polyneuropathy (hATTR-PN). *Orphanet J. Rare Dis.* **12,** Suppl. 1, 165
14. Colon, W., and Kelly, J. W. (1992) Partial denaturation of transthyretin is sufficient for amyloid fibril formation in vitro. *Biochemistry* **31,** 8654–8660 CrossRef Medline
15. Miroy, G. J., Lai, Z., Lashuel, H. A., Peterson, S. A., Strang, C., and Kelly, J. W. (1996) Inhibiting transthyretin amyloid fibril formation via protein stabilization. *Proc. Natl. Acad. Sci. U.S.A.* **93,** 15051–15056 CrossRef Medline
16. Coelho, T., Maia, L. F., Martins da Silva, A., Waddington Cruz, M., Planté-Bordeneuve, V., Lozeron, P., Suhr, O. B., Campistol, J. M., Conceição, I. M., Schmidt, H. H., Trigo, P., Kelly, J. W., Labaudinière, R., Chan, J., Packman, J., Wilson, A., and Grogan, D.R. (2012) Tafamidis for transthyretin familial amyloid polyneuropathy: A randomized, controlled trial. *Neurology* **79,** 785–792 CrossRef Medline
17. Berk, J. L., Suhr, O. B., Obici, L., Sekijima, Y., Zeldenrust, S. R., Yamashita, T., Heneghan, M. A., Gorevic, P. D., Litchy, W. J., Wiesman, J. F., Nordh, E., Corato, M., Lozza, A., Cortese, A., Robinson-Papp, J., *et al.* (2013) Repurposing diflunisal for familial amyloid polyneuropathy: A randomized clinical trial. *JAMA* **310,** 2658–2667 CrossRef Medline
18. Bulawa, C. E., Connelly, S., Devit, M., Wang, L., Weigel, C., Fleming, J. A., Packman, J., Powers, E. T., Wiseman, R. L., Foss, T. R., Wilson, I. A., Kelly, J. W., and Labaudinière, R. (2012) Tafamidis, a potent and selective transthyretin kinetic stabilizer that inhibits the amyloid cascade. *Proc. Natl. Acad. Sci. U.S.A.* **109,** 9629–9634 CrossRef Medline
19. Planté-Bordeneuve, V., Gorram, F., Salhi, H., Nordine, T., Ayache, S. S., Le Corvoisier, P., Azoulay, D., Feray, C., Damy, T., and Lefaucheur, J. P. (2017) Long-term treatment of transthyretin familial amyloid polyneuropathy with tafamidis: A clinical and neurophysiological study. *J. Neurol.* **264,** 268–276 CrossRef Medline
20. Ihse, E., Rapezzi, C., Merlini, G., Benson, M. D., Ando, Y., Suhr, O. B., Ikeda, S., Lavatelli, F., Obici, L., Quarta, C. C., Leone, O., Jono, H., Ueda, M., Lorenzini, M., Liepnieks, J., *et al.* (2013) Amyloid fibrils containing fragmented ATTR may be the standard fibril composition in ATTR amyloidosis. *Amyloid* **20,** 142–150 CrossRef Medline
21. Verona, G., Mangione, P. P., Raimondi, S., Giorgetti, S., Faravelli, G., Porcari, R., Corazza, A., Gillmore, J. D., Hawkins, P. N., Pepys, M. B., Taylor, G. W., and Bellotti, V. (2017) Inhibition of the mechano-enzymatic amyloidogenesis of transthyretin: Role of ligand affinity, binding cooperativity and occupancy of the inner channel. *Sci. Rep.* **7,** 182 CrossRef Medline
22. Weiss, C., Seitel, G., and Bärtsch, P. (1998) Coagulation and fibrinolysis after moderate and very heavy exercise in healthy male subjects. *Med. Sci. Sports Exerc.* **30,** 246–251 Medline
23. Smith, H. W., and Marshall, C. J. (2010) Regulation of cell signalling by uPAR. *Nat. Rev. Mol. Cell Biol.* **11,** 23–36 CrossRef Medline
24. Liu, C. Z., Cheng, H. J., and Chang, L. Y. (2008) A new feasible method for fibrinogen purification based on the affinity of *Staphylococcus aureus* clumping factor A to fibrinogen. *Protein Expr. Purif.* **61,** 31–35 CrossRef Medline
25. Naiki, H., Higuchi, K., Hosokawa, M., and Takeda, T. (1989) Fluorometric determination of amyloid fibrils *in vitro* using the fluorescent dye, thioflavin T1. *Anal. Biochem.* **177,** 244–249 CrossRef Medline
26. Puchtler, H., Waldrop, F. S., and Meloan, S. N. (1985) A review of light, polarization and fluorescence microscopic methods for amyloid. *Appl. Pathol.* **3,** 5–17 Medline

2.3. Stability of transthyretin fibrils

As already reported before, the knowledge on the pathogenesis of transthyretin related amyloidosis is extensively based of the method of *in vitro* fibrillogenesis at low pH in which the protein aggregation is primed by the tetramer disassembly (Colon and Kelly 1992). More recently, as described in Chapter 2.1 and 2.2, we have generated a new method of fibrillogenesis in which a crucial role is played by the joined actions of the biomechanical forces and specific proteolytic enzymes (Mangione et al. 2018, Marcoux et al. 2015).

Therefore, we can consider the mechano-enzymatic method as the most suitable model for making TTR fibrils in physiological conditions and then for testing the effect of putative new interactors of TTR amyloid aggregation.

In this context, one of the goal was to investigate the similarities between *in vitro* fibrils and *ex vivo* counterpart. I have therefore comparatively analysed natural and *in vitro*-made fibrils by measuring their thermodynamic stabilities that are related to the structure and specific intermolecular interactions. The experiments were carried out on the V122I TTR variant, which is responsible for familial amyloid cardiomyopathy. This variant causes a rapid progression of the disease providing accelerated amyloid deposition, possibly due to the decreased stability of the protein (Dungu et al. 2012).

Our results showed that V122I TTR fibrils formed through the mechano-enzymatic methods (Marcoux et al. 2015, Mangione et al. 2018) are highly similar to the natural counterpart.

2.3.1. Materials and methods

- **Preparation of recombinant V122I TTR**

Site direct mutagenesis of peTM11 plasmid encoding hexahistidine-tagged wild type TTR BL21 was carried out using the QuickChange kit (Stratagene) and the primer CC ACC ACG GCT GTC ATC ACC AAT CCC AAG G containing the underlined codon for isoleucine at position 122. Transformed star (DE3) cells (Thermo Fisher Scientific) were then plated onto Luria broth (LB)-agar media containing 30 µg/ml kanamycin for overnight incubation at 37°C. A single colony was isolated and cultured overnight at 37°C in 2.5 ml LB medium containing 30 µg/ml kanamycin under shaking conditions (LB/kan). This preparation was inoculated into 250 ml LB/kan for an initial growth at 37°C. When the culture reached OD_{600}= 0.5, the temperature was reduced to 30°C. Protein expression was induced at OD_{600}=0.6 by adding isopropil-β-D-1-thiogalattopyranoside (IPTG, 1 mM final concentration) for overnight incubation. The cells were harvested by centrifugation, suspended in lysis buffer containing 20 mM Tris-HCl pH 8, 250 mM NaCl, 3 mM imidazole and finally sonicated at 4°C. The supernatant was clarified after 30 min centrifugation at 11,300 *g* and loaded onto a HisTrap FF crude nickel affinity chromatography column (GE Healthcare) equilibrated in lysis buffer. After extensive washing with 20 mM Tris-HCl, 10 mM imidazole, containing stepwise increasing concentrations of NaCl, 250 mM, 500 mM and 1 M, the column was eluted with 20 mM Tris-HCl, 250 mM NaCl, 250 mM imidazole, pH 8.0. His-tagged TEV protease (Sigma-Aldrich) was added at 1% w/w to selectively cleave the hexaHis-tag, which was then removed by affinity chromatography, together with the enzyme. Fractions containing TTR were pooled and subjected to size exclusion chromatography using a Superdex 75 Hi Load 26/60 column (GE Healthcare) equilibrated and eluted with 25 mM Tris-HCl, 100 mM NaCl, pH 8.0. Fractions containing TTR were dialyzed against water at 4°C for at least 3 days and then lyophilized. Purity and molecular weight were determined by SDS-PAGE analysis and mass spectrometry respectively.

- **Extraction of natural fibrils**

Amyloid fibrils were isolated from the heart of a patient with cardiac amyloidosis associated with the V122I TTR variant. The study was carried out in accordance with

the Declaration of Helsinki and the written consent of the patient. Fibrils were isolated from the cardiac tissue (~100 mg) by water extraction in the presence of 1.5 mM PMSF after repeated homogenization in the presence of 10 mM Tris-HCl containing 140 mM NaCl, 10 mM EDTA, 0.1 % (wt/vol) NaN_3, 1.5 mM PMSF, pH 8.0 and 30 min centrifugation at 60000 *g*. The yield in fibrils was monitored by microscopic analysis of the extracted material stained with Congo red. Quantification of total protein on water extraction fractions was performed by BCA assay (Pierce).

- **Preparation of *in vitro* fibrils**

Two sets of TTR fibrils were prepared *in vitro* following two methods: low pH procedure (Colon and Kelly 1992); mechano-enzymatic method (Marcoux et al. 2015); (Verona et al. 2017). Acidic-mediated protein aggregation was initiated by the addition of stock solution of recombinant tetrameric V122I TTR (0.4 mg/ml in PBS pH 7) to an equivalent volume of 200 mM sodium acetate, 0.1 %wt/vol NaN_3 pH 4.4 and incubation at 37°C was carried out in glass vials for seven days. The fibrils were separated from the supernatant by centrifugation at 20817 *g* for 20 minutes. The quantity of fibrils corresponded to the difference between the starting amount of soluble V122I TTR and the un-aggregated material that was still present when the aggregation process reached its conclusion.

Proteolysis-mediated fibrillogenesis of V122I TTR was carried out in glass vials (air/interface of 1.5 cm^2) stirred at 1,500 rpm (IKA magnetic stirrer) and 37°C for 96 h using 1 mg/ml TTR in PBS pH 7.4 in the presence of trypsin (5 ng/µl). The aggregated material was quantified as previously described for fibrils formed at low pH.

- **Microscopic analysis**

Both natural and synthetic fibrils were evaluated. The pathognomonic amyloid apple-green birefringence in both *in vitro* and *ex vivo* fibrils were evaluated under high intensity cross-polarized light after alkaline alcoholic Congo red staining.

Samples were also examined by negative staining transmission electron microscopy. Briefly, a drop of each sample was allowed to dry onto a formvar/carbon coated copper grid 8 min before blotting with filter paper to remove excess solvent and staining with 2% w/v uranyl acetate for 30 s. After further washing, blotting and drying in air, transmission electron microscope (Jeol JEM-1010) images were obtained at 80 kV.

- **Stability of native TTR**

Samples containing tetrameric V122I TTR (0.1 mg/ml) were incubated at increasing concentrations of guanidine thiocyanate (Gdn-SCN) in 50 mMphosphate, 1 mM EDTA, 1 mM DTT, pH 7.0, at 25 °C for 24h. Tryptophan fluorescence spectra were recorded between 310 and 410 nm with excitation at 295 nm using a 1 cm light path cell in a Perkin-Elmer LS55 spectrofluorimeter. All spectra were blank-subtracted. The fluorescence ratio between 355 (unfolded) and 335 nm (folded) was plotted as a function of Gdn-SCN (Hammarstrom 2001) to generate denaturation curves for further analysis.

- **Stability of TTR fibrils**

V122I TTR fibrils (1.5 mg/ml) were resuspended in sodium phosphate 50 mM, EDTA 1 mM, DTT 1mM buffer pH7 at increasing concentrations of Gdn-SCN (from 0 to 6M). Samples were mixed by vortexing before incubation at room temperature for 96 h in order to allow the samples to reach equilibrium. To separate non-aggregated fraction from aggregated protein, samples were centrifuged for 20 minutes at 20817 *g*.

The presence of persistent fibrillar material in the insoluble fraction after the incubation with denaturing agent was assessed with Thioflavin T (ThT) assay. The pellets were resuspended in 100 µl PBS containing ThT 10 µM and fluorescence emission was monitored at 485 nm, following excitation at 445 nm in a CLARIOstar microplate reader (BMG Labtech). Denaturation curves were generated by plotting ThT emission fluorescence values as a function of Gdn-SCN for further analysis.

- **Thermodynamic stability parameters for native TTR and fibrils**

Gdn-SCN denaturation curves were analysed according to a two-state unfolding model to describe the two type of transitions observed: native tetramer→unfolded monomer for the V122I TTR precursor; fibrillar →unfolded monomer for *ex vivo* and *in vitro* TTR fibrils. Experimental data were fit according the equation of Santoro-Bolen (Biochemistry 1988) to yield the Gibbs free energy $\Delta G^{0}_{(H2O)}$ of unfolding in the absence of denaturant and the Gdn-SCN midpoint concentration.

Experimental data were normalized to the apparent unfolded fraction using $F_{app} = (y - y_N)/(y_U - y_N)$, where y is the experimental value observed at a given denaturant concentration, and y_N and y_U are the values of the native (or fibrillar) and unfolded

protein, respectively, extrapolated from the pre- and post-transition base lines defined by the nonlinear least square fitting procedure used above (Bolen and Santoro 1988).

2.3.2. Results

- **Amyloid fibrils preparation**

The comparative analysis of thermal stability was performed on *ex vivo* fibrils and on two different types of *in vitro* made fibrils. The aggregation of the recombinant transthyretin variant Val122-Ile was carried out *in vitro* through two different methods: the low pH procedure according to Colon and Kelly (Colon and Kelly 1992) and the mechano-enzymatic method proposed in the work by Marcoux and colleagues (Marcoux et al. 2015). The extraction of natural fibrils from the heart of a patient carrying the mutation Val122-Ile was performed according to the classical water extraction procedure invented by Pras and co-workers. (Pras et al. 1968).

The samples were first characterized by microscopic analysis after Congo red staining and by electronic microscopy (EM). Figure 29 reports the microscopic images of the *in vitro* and *ex vivo* material suggesting that through the mechano-enzymatic method, the resulting aggregate presents a quite complete fibrillar structure similar to natural fibrils and it is classically birefringent after the Congo Red staining. On the contrary, the aggregation obtained at low pH contains very few fibrillar structures based on a dense background of amorphous aggregate.

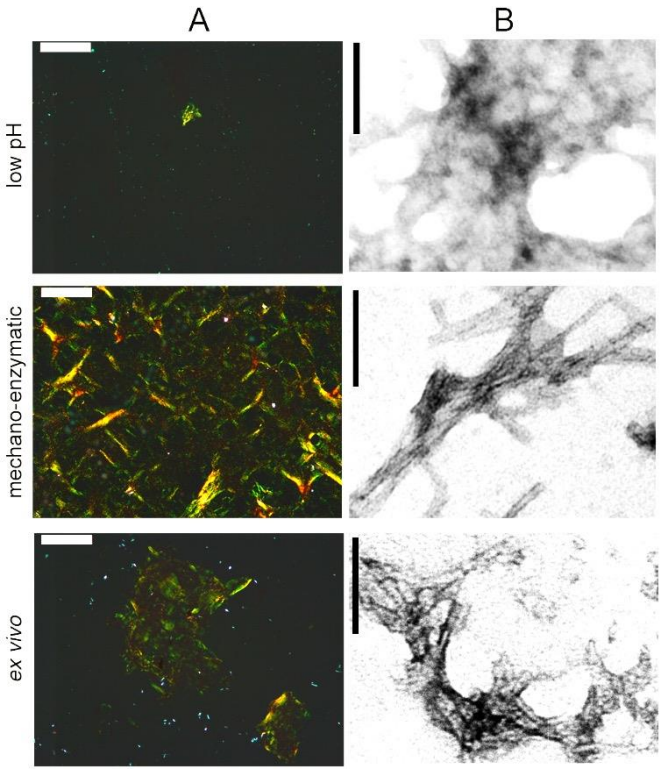

Figure 29. Microscopic analysis of *in vitro* and *ex vivo* TTR fibrils. **a)** Amyloid was identified by light microscopy of Congo red-stained specimens viewed under crossed polarized light (scale bar, 100 µM). **b)** Negatively stained transmission electron microscopy (TEM) (scale bar, 100 nm) of TTR in vitro fibrils prepared at low pH or with the mechano-enzymatic mechanism and *ex vivo* material.

The yield of transition from the native structure to the insoluble aggregate is much higher at low pH than through the proteolytic cleavage. Almost all the native TTR precipitates as insoluble material when it is incubated at low pH, whereas only 20% of TTR is converted into fibrils through the mechano-enzymatic mechanism.

- **Fibrils stability**

Before carrying out the stability characterization of TTR fibrils, thermodynamic stability of the native form of V122I TTR variant was evaluated in the presence of the chaotropic agent guanidine-thiocyanate (Gnd-SCN). Emission spectra were obtained by exciting the samples at 295 nm and recording tryptophan fluorescence in the range between 310 and 440 nm. By measuring, for each experimental point, the ratio between measured tryptophan emission fluorescence at 335 nm, representing the maximum folded protein, and at 355 nm, representing the maximum unfolded protein, the values were normalised and analysed with the Santoro and Bolen equation. The apparent fractions of unfolded protein were obtained and the midpoint denaturant concentration, Cm, was then extrapolated from the curves (Fig 30 A, table 3). The Gibbs free energy $\Delta G^{0}_{(H2O)}$ of denaturation was reported too in table 3. The Gibs energy of unfolding of native V122I TTR is similar to that measured by Quintas and co-workers (Quintas et al. 2001) for the variant Val30-Met.

The stability of three types of V122I TTR fibrils, obtained through different procedures and sources, was analysed by titrating at different concentrations of the chaotropic agent Gdn-SCN. The samples of fibrils (1.5 mg/ml) were incubated at different concentration of Gnd-SCN at room temperature for 96 hours. After the incubation, the supernatant was divided, by centrifugation, from the insoluble material, which was resistant to the treatment with the denaturant. The insoluble fraction, at each point of GdnSCN concentration, was resuspended in 10 µM ThT and fluorescence was measured at 485 nm, following excitation at 445 nm.

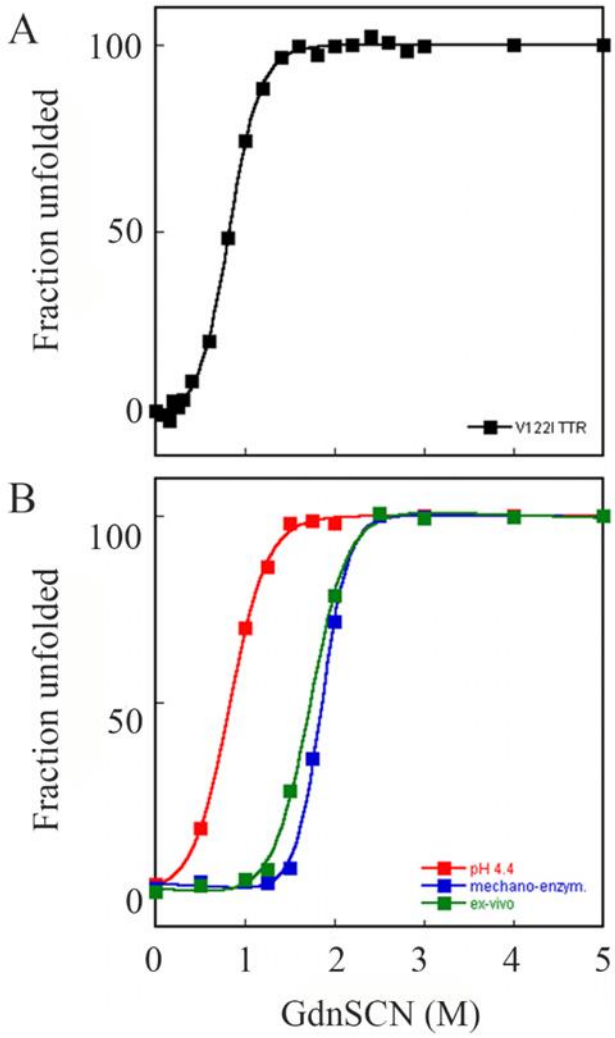

Figure. 30. Thermodynamic stability of V122I TTR precursor and fibrils. **a)** Denaturation profile for V122I TTR are derived from change in fluorescence (F355/F335) following 295 nm excitation. **b)** Denaturation of *in vitro* V122I TTR fibrils formed at low pH (red), mechano-enzymatic mechanism (blue) or *ex-vivo* ATTR V122I TTR fibrils (green) are based on ThT fluorescence assay of the residual pellet after denaturation and centrifugation. All experimental data in a) and b) were fitted to a two-state model transition and converted to the unfolded fraction as described in the Methods section. The solid lines represent the nonlinear fit to the experimental data from three independent experiments.

The disassembly of fibrils is parallel to the loss of the specific fluorescence of the thioflavin-fibrils complex. Gdn-SCN denaturation curves were analysed according to a two-state unfolding model according to the Santoro and Bolen equation and the effect of increasing concentration of Gdn-SCN on the fluorescence is reported in Figure 30B. Thermodynamic parameters for Gdn-SCN induced transition from fibrillary to unfolded monomer of V122I TTR were reported in table 3

The CM calculated for the disassembly of the TTR aggregate obtained at low pH is 0.84 ± 0.21 M, almost identical to the CM of unfolding determined for the native Ile-122 variant (Table 3).

On the contrary, the Cm of disassembly of fibrils prepared through the mechano-enzymatic mechanism is 1.8 M, similar to the CM of ex vivo fibrils and much higher than that measured for native TTR or the aggregated TTR obtained at low pH.

	$\Delta G^{0}_{(H2O)}$ (k cal mol^{-1})	C_m (M)
Precursor		
V122 I TTR	2.95 ± 0.38	0.84 ± 0.06
Fibrils		
low pH	2.81 ± 0.49	0.84 ± 0.21
mechano-enzymatic	7.80 ± 0.50	1.86 ± 0.04
ex vivo	6.83 ± 0.77	1.70 ± 0.22

Table 3. Thermodynamic parameters for Gdn-SCN induced unfolding of V122I TTR precursor and fibrils. The change in tryptophan fluorescence for V122I TTR or in ThT emission were analysed as previously described (Bolen and Santoro 1988). Values of free energy in the absence of denaturant [$\Delta G°_{(H2O)}$], and midpoint denaturant concentration (Cm) are shown as mean (SD) of three independent experiments.

From these data, we have obtained the Gibbs free energy $\Delta G^{0}_{(H2O)}$ of denaturation for fibrils and diagram of Figure 31 and table 3 summarize all the results. Figure 31, adapted from Hartl *et al* (Hartl, Bracher and Hayer-Hartl 2011) describes the scheme of the funnel-shaped free energy surface explored by proteins in the native and aggregate state achieved by the same proteins through different pathways: low pH, selective cleavage, and the *in vivo* still largely undetermined mechanism.

The data regarding the free energy of dissociation of TTR fibrils can be compared with a few other reports regarding other type of amyloid fibrils.

In two works carried out by my research group, it has previously determined the free energy of solubilisation of fibrils made *in vitro* on two amyloidogenic proteins: alfa synuclein and β_2-microglobulin. Regarding synuclein (Porcari et al. 2015), we have calculated a ΔG of -7.3 kcal/mol for wild type and -8.4 kcakl/mol for the pathogenic variant. Regarding β_2-m, in Natalello et al (Natalello et al. 2016) we have calculated a ΔG 0f -12 kcal/mol for fibril of D76N variant made *in vitro* in physiologic condition.

All these data confirm the low energy sink of amyloid fibrils, presenting a minimum largely lower that that achieved by globular proteins through intimate intramolecular bonds.

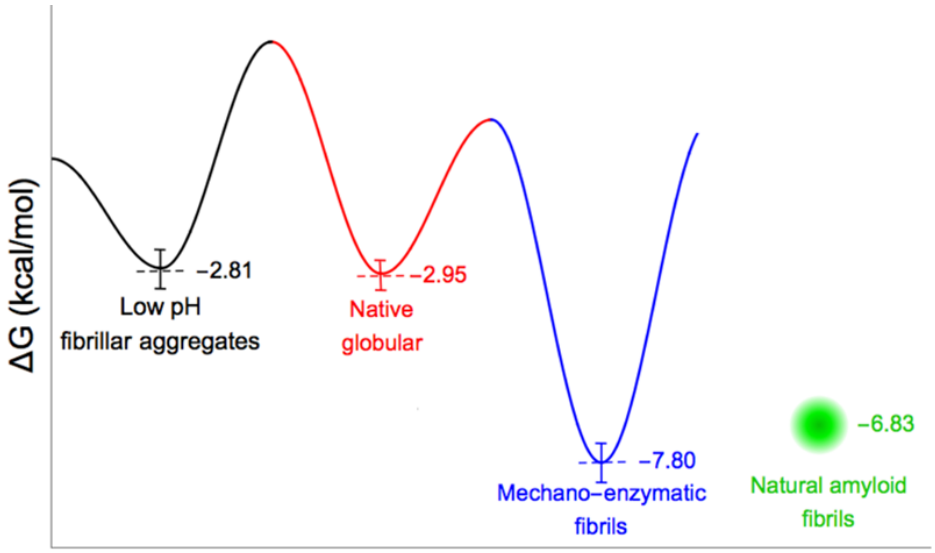

Figure 31. Schematic free energy landscape for V122I TTR variant on the pathways from the unfolded to the native state, or to the aggregate state, achieved by three different mechanisms: aggregation at low pH (black), mechano-enzymatic method (red) or natural fibrils extracted from patients (green).

Furthermore, the data we report illustrate the remarkable difference, in term of stability, observed on fibrils made through two different methods, suggesting that the fibrils formed through the mechano-enzymatic method are highly similar to the natural counterpart and then suitable to be used in drug discovery

Chapter 3: *C. elegans* as a model to study D76N β_2-microglobulin-Related Amyloidosis

The mechanism of toxicity of amyloid *in vivo* remains an unmet challenge and animal models may provide crucial clues on the identification of the protein species causing the tissue toxicity.

As I already mentioned in Chapter 1, *C. elegans* is a good experimental model that has been proposed and validated to investigate the molecular basis and the genetics of many human diseases. It may be a useful tool in order to understand the interaction among multiple biological systems in the amyloid related disease, allowing the study in the context of an intact, multi-organ and multi-cellular organism. In particular, a successful nematode model for examining the links among protein expression, toxicity and eventually aging has to meet some critical requirements. For example, it has to exhibit a protein-accumulation or aggregation-associated progressive phenotype that can be measured within the lifespan of the nematode.

With respect to the expression of β_2-m in *C. elegans*, the group of Professor Bellotti has previously described the phenotypes of transgenic *C. elegans* strains expressing β_2-microglobulin isoforms (P32G, WT and ΔN6 β_2-m) showing that transgenic worms displayed pathological features consistent with the intrinsic amyloidogenic propensity of the expressed protein (Diomede et al. 2012). However, the development of a transgenic *C. elegans* strain expressing D76N variant was very challenging, due to the high toxicity of the expressed protein at the embryonic stage. Therefore, a transgenic strain was prepared in which the expression of the β_2-m variant is under temperature-dependent control, deploying the well-characterized mRNA-surveillance system, of *C. elegans* (Mango 2001). With this system, worms express the amyloidogenic protein variant only when they are grown at higher temperatures, such as 23-25°C.

In my PhD project, I focused my attention on the characterization of the pathological phenotype of this new worm strain (named CPV27) in which the expression is switched-on commencing at the L1 larval stage, thereby offering a viable animal model for the D76N variant (Figure 32). The description of the generation of the strain and of its phenotype is reported in the following paragraph and the data were collected in a paper that is now under a second revision by Scientific Reports.

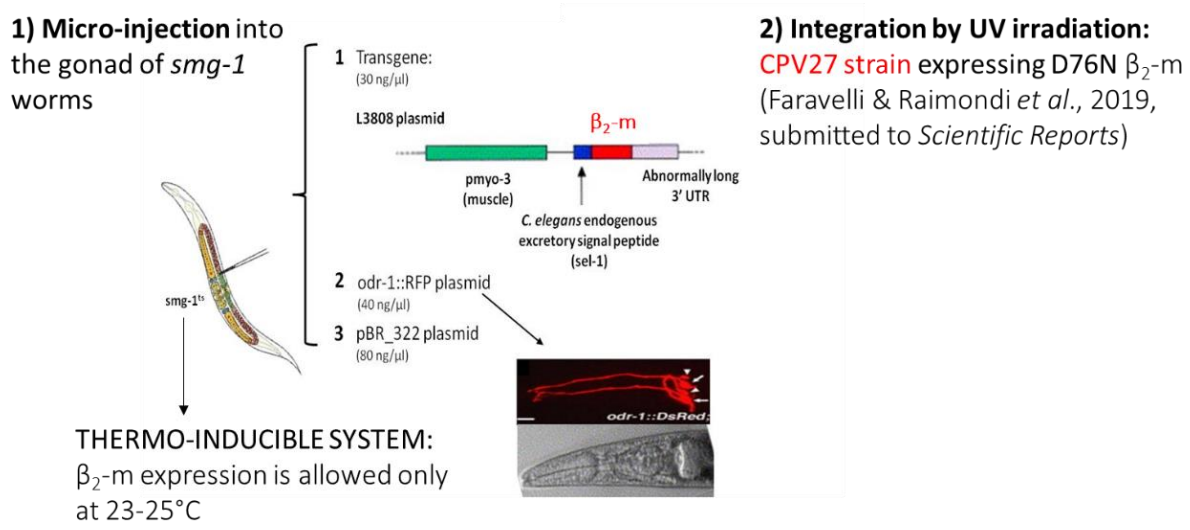

Figure 32. Construction of CPV27 *C. elegans* strain expressing D76N β_2-m. Phenotypic characterization of the strain is reported in the following paragraph.

Thanks to the automated system for *C. elegans* phenotyping developed by Partridge and his collaborators (Partridge et al. 2018), I was able to detect larval growth and motility defects in the CPV27 strain (Faravelli & Raimondi *et al*., 2019, under revision by *Scientific Reports*).

Lastly, in order to better examine the toxicity of protein expression in adult worms and to facilitate the drug screening experiments on a synchronized population of worms, we decided to establish a temperature-sensitive sterile strain expressing the D76N isoform. The data related to those experiments are reported in Chapter 3.2.

3.1. *C. elegans* expressing D76N β$_2$-microglobulin: a model for *in vivo* screening of drug candidates targeting amyloidosis.

(Under second revision by Scientific Reports)

Giulia Faravelli[1*+], Sara Raimondi[1+], Loredana Marchese[1], Frederick A. Partridge[2], Cristina Soria[1], P. Patrizia Mangione[1,3], Diana Canetti[3], Michele Perni[4], Francesco A. Aprile[4], Irene Zorzoli[1], Elia Di Schiavi[5], David A. Lomas[2], Vittorio Bellotti[1,3], David B. Sattelle[2] & Sofia Giorgetti[1*].

[1]Department of Molecular Medicine, Institute of Biochemistry, University of Pavia, 27100 Pavia, Italy.

[2]Centre for Respiratory Biology, UCL Respiratory, Division of Medicine, University College London, Gower Street, London, WC1E 6JF, United Kingdom.

[3]Wolfson Drug Discovery Unit, Centre for Amyloidosis and Acute Phase Proteins, University College London, London, UK.

[4]Centre for Misfolding Diseases, Department of Chemistry, University of Cambridge, Cambridge, CB2 1EW, UK.

[5]Institute of Biosciences and Bioresources (IBBR), CNR, 80131, Naples, Italy.

*giulia.faravelli01@universitadipavia.it, s.giorgetti@unipv.it

[+]these authors contributed equally to this work

ABSTRACT

The availability of a genetic model organism with which to study key molecular events underlying amyloidogenesis is crucial for elucidating the mechanism of the disease and the exploration of new therapeutic avenues. The natural human variant of β_2-microglobulin (D76N β_2-m) is associated with a fatal familial form of systemic amyloidosis. Hitherto, no animal model has been available for studying *in vivo* the pathogenicity of this protein. We have established a transgenic *C. elegans* line, expressing the human D76N β_2-m variant. Using the INVertebrate Automated Phenotyping Platform (INVAPP) and the algorithm Paragon, we were able to detect growth and motility impairment in D76N β_2-m expressing worms. We also demonstrated the specificity of the β_2-m variant in determining the pathological phenotype by rescuing the wild type phenotype when β_2-m expression was inhibited by RNA interference (RNAi). Using this model, we have confirmed the efficacy of doxycycline, an inhibitor of the aggregation of amyloidogenic proteins, in rescuing the phenotype. In future, this *C. elegans* model, in conjunction with the INVAPP/Paragon system, offers the prospect of high-throughput chemical screening in the search for new drug candidates.

Introduction

β_2-microglobulin is a protein composed of 99 amino acids with a characteristic β-sandwich immunoglobulin fold. It serves as the light chain of the class I major histocompatibility complex. Amyloid formation by wild-type β_2-m occurs as a severe complication of long-term dialysis for patients with end-stage kidney failure, as a result of the persistently high plasma concentration of β_2-m[1]. So far, only one genetic form of β_2-m related amyloidosis has been described and this is caused by the mutation Asp76Asn. The clinical and experimental work carried out on this variant has advanced our current understanding of amyloidogenesis of β_2-m and other globular proteins, including the role of biomechanical forces in protein misfolding[2] as well as the mechanism of β_2-m fibrillogenesis[1,3].

Whereas the mechanism of misfolding and aggregation *in vitro* has been extensively clarified, the mechanism of toxicity of amyloid in general and of β_2-m in particular remains an unmet challenge. Animal models offer important insights on the identification of the protein species causing the tissue toxicity. However, attempts to generate animal models for β_2-m associated diseases have stalled as, in spite of good levels of expression of β_2-m in transgenic mice expressing the wild type[4] protein or the pathogenic variant D76N, no pathological phenotype of β_2-m amyloidosis has been observed.

The nematode genetic model organism *Caenorhabditis elegans* (*C. elegans*) offer the prospect of studying the effects of the β_2-m variant *in vivo*. *C. elegans* models have already been successfully deployed to characterize important molecular aspects of other protein aggregation diseases such as Alzheimer's, Parkinson's and Huntington's diseases[5-9]. *C. elegans* has several advantages. It shares many characteristics with mammalian systems with respect to genetics, biochemical and physiological functions. It is small, transparent and a self-fertilizing hermaphrodite producing 300 identical progeny in 3 days; its life cycle is short (2-3 weeks) and it is easy and inexpensive to maintain in the laboratory[10]. Moreover, chemical and genetic screenings in *C. elegans* are becoming an established method to search for new therapeutic tools and to uncover and validate drug targets[11]. We have previously described the phenotypes of transgenic worm strains transiently expressing wild type β_2-microglobulin and some isoforms not related to the familial form of the disease[12]. As evidence of the reliability

of the *C. elegans* model, we observed that the severity of proteotoxicity *in vivo* correlated well with the protein's amyloidogenic propensity measured *in vitro*.

In this paper, we characterize a new transgenic *C. elegans* strain, named CPV27, expressing the D76N variant, in which the β_2-m gene is integrated into the *C. elegans* genome. The development of this new strain was challenging, due to the high toxicity of the expressed protein at the embryonic stage of development. We have therefore prepared a strain in which the expression of the disease- causing variant is under temperature-dependent control, using the well-characterized mRNA-surveillance system of *C. elegans*[12]. This new worm strain is the first robust animal model for studying *in vivo* the effects of the pathogenic variant of D76N β_2-m and represents a valuable new tool with which to explore further the disease mechanism and search for new drug candidates to combat β_2-m amyloidogenesis.

Results

Expression of the D76N β_2-m variant. We previously reported a *C. elegans* model of wild type β_2-m amyloidosis in which the protein was expressed in the body-wall muscles under the control of the promoter of the myosin gene *unc-54*[13]. However, our attempts to express the D76N β_2-m variant in *C. elegans* under the same promoter failed because the nematodes died before reaching the first larval stage, likely due to the high toxicity of the protein variant (data not shown). To bypass the lethal effect of such constitutive protein expression, we adopted the well-characterized *smg* inducible system[12]. In this protocol, at the permissive temperature of 16°C, the mRNA of the transgene is readily degraded, whereas an upshift to a non-permissive temperature that is still compatible with the normal growth of the worms (23-25°C) (Fig. 1a), inactivates the surveillance machinery allowing stabilization and translation of the transgene mRNA. The *smg* system enabled us to switch-on the expression of D76N β_2-m at the first larval stage (L1), thereby avoiding protein synthesis and its related toxic effects in the embryonic stage.

Transgenic *C. elegans* were engineered to express D76N β_2-m in body-wall muscles under the promoter of another myosin gene, *myo-3*. As the amyloid is an extracellular protein deposit, we sought to obtain protein secretion by replacing the previously used human β_2-m signal peptide[13] with the signal peptide of the endogenous *sel-1* protein[14]. We have used, as a co-injection marker, the p*odr-1::rfp* plasmid, which shows a strong pattern of red fluorescent protein (RFP) expression (RFP expressed in two head neurons, AWB and AWC). After engineering the D76N β_2-m expressing plasmid, microinjection into the gonad and integration of the transgene by UV irradiation, the exact genotype of D76N β_2-m expressing nematodes was confirmed by single worm PCR (Fig. 1b, lane 3,5) and DNA sequence analysis.

The strain obtained after integration *smg-1(cc546); pavIs1[pmyo-3::SPsel-1::hD76Nβ_2-m::Smg sensitive 3'UTR; podr-1::rfp]*, named CPV27, correctly expressed D76N β_2-m, as shown by western blot analysis (Fig. 1), when animals were grown at 25°C beginning at the L1 larval stage. Levels of protein increased from the first to the fifth day when nematodes were grown at 25°C (Fig. 1c). D76N β_2-m nematodes, maintained at 16°C and collected 24 h after the L4 stage, were also analyzed. The absence of expression of β_2-m at 16°C confirmed the efficiency and the specificity of

the thermo-inducible system, therefore the *smg-1(cc546)* ancestral strain (PD8120 strain) served as a negative control (Fig. 1c).

Aggregation state of the β_2-m variant. A search of amyloid deposits was carried out by microscopic analysis of worms stained with the amyloid probe NIAD-4 as previously described[15]. However, we did not detect amyloid material at any stage of development (data not shown). In spite of a lack of clearly visible amyloid deposits, the β_2-m variant in worms displayed a high propensity to form soluble self-assemblies as shown by both electrophoresis and size exclusion chromatography (Fig. 2). Worms were lysed and after centrifugation, both supernatant and pellet were first analysed by SDS-PAGE and β_2-m detected by immunoblotting. As clearly shown in Fig. 2a, almost all the β_2-m present is recovered in the supernatant and not in the pellet obtained from the worm lysate.

Chromatographic analysis carried out on the supernatant in physiological buffer reveals that β_2-m is eluted in a wide range of molecular weights; from the most abundant 11 kDa of the monomeric state (fractions 14-16, Fig. 2b-c) to heterogeneous oligomeric states up to and beyond 100 kDa (fractions 8-9, Fig. 2b-c). Such heterogeneous states of aggregation are not present when recombinant β_2-m was loaded at different concentrations (Fig. 2a) and this finding is confirmed when the soluble fraction of recombinant β_2-m is analysed by size exclusion chromatography (Fig. 2d-e). The *smg-1* mutant worms were analysed as well and used as negative controls in order to exclude any possible cross-reaction of the antibody (S2b).
Our hypothesis, which has been confirmed by the experiments on the characterization of CPV27 transgenic strain reported below, was that the expression and accumulation of monomeric and oligomeric species of D76N β_2-m variant correlate with a pathological phenotype in our *C. elegans* strain.

Effects of β_2-m expression on the *C. elegans* phenotype.

INVAPP/Paragon analysis of worms' growth and motility. To investigate the effect of expressing D76N β_2-m on nematode growth and motility, an automated analysis was carried out using the recently developed INVAPP/Paragon system[16]. Briefly, the automated platform is able to quantify growth and/or motility of nematodes, by acquiring images of nematode growth medium (NGM) plates containing worms and by thresholding pixel variance to determine motion. Quantified movement is recorded as

a movement index parameter, which increases with the number and size of worms per plate, reflecting a larger number of 'motile' pixels in the recording. After placing three L4 larvae per plate, we followed the growth and motility of their progeny. At day six at 25°C (Fig. 3a), both the *smg-1* controls and D76N β_2-m expressing worms were imaged with INVAPP/Paragon (Fig. 3b) and their movement index was measured (Fig. 3c). D76N β_2-m expressing worms showed slower growth and reduced overall motility than the *smg-1* control strain. Indeed, the movement index was 53% of the value observed for the *smg-1* control strain (Fig. 3c, **p<0.01, t-test). The INVAPP/Paragon platform shows that an abnormal behavioural phenotype is associated with the expression of the amyloidogenic protein.

To check whether the phenotype of the D76N β_2-m strain correlated with the expression of the D76N variant of β_2-microglobulin, we silenced the β_2-m gene by feeding worms with bacteria that produce dsRNA targeting the β_2-m transgene. Western blot analysis of worms treated with RNAi bacteria were compared with those fed with control bacteria (Fig 4a-b) showing that the D76N β_2-m protein was significantly reduced relative to the control (Fig. 4c). Most importantly, the reduction in the levels of β_2-m expression correlated with the near complete abrogation of the D76N β_2-m strain pathological phenotype (Fig. 4d, dark grey bar, n=3, ˚p<0.05 vs. not silenced D76N β_2-m expressing worms, t-test).

The index movement parameter recorded by the INVAPP/Paragon system, combines the contributions of different phenotypic features: motility, larval development and size of the progeny.

In order to further dissect the results obtained with INVAPP/Paragon, we have carried out a body bends assay, a lifespan measurement and a brood size assay.

Body bends assay. The results of body bends assay at 23°C are reported in Fig. 5a. At day 1 of adulthood, there is no difference between D76N and controls. A statistically significant reduction in the number of body bends per minute is observed from the fifth day (about 8% decrease; n=3, **p<0.01 at day 5 and *p<0.05 at day 6 when compared to corresponding *smg-1* controls, one-way ANOVA, N=40 animals for each group). The body bends assay shows that the phenotypic abnormality of D76N β_2-m expressing worms, quantified using the INVAPP/Paragon system, was only partially due to dysfunctions in coordination and motility. For this reason, other phenotypic assays were performed.

Lifespan. Measurement of lifespan was performed on synchronized nematodes upshifted to 23°C from the first larval stage. The D76N β_2-m strain showed a median survival of 8 days, while that of the *smg-1* control strain was 10 days (Fig. 5b). Apparently, the difference between the two strains is mostly attributable to the first part of the Kaplan-Meier graph, and after ten days of adulthood, the two plots become closely aligned. A Peto-Peto-Prentice test shows that these differences are significant (χ^2=5.52, p=0.019).

Brood size assay. Brood size assay of transgenic animals was then performed by counting the number of eggs laid from a single nematode during the first 48 h of adult life at 23°C (Fig. 5c, n=3 *p<0.05 vs *smg-1* control strain according to t-test). The D76N β_2-m-expressing animals showed a 17% reduction in brood size compared to the *smg-1* control strain (Figure 5c). In addition, the egg viability test was performed, by counting the number of unhatched eggs 24 h after their deposition (Fig. 5d, ***p <0.001 vs. the control strain, t-test). When compared to the control strain, egg viability was significantly reduced in the D76N β_2-m expressing strain: *smg-1* control nematodes had less than 10% unhatched progeny, while 35% of the eggs produced by D76N β_2-m-expressing worms did not hatch (Fig. 5d).

We therefore confirmed that the phenotypic impairment, shown by the movement index parameter, is attributable to a sum of various contributions: defect in the motility, reduction in the lifespan and fertility and larval development impairment of the D76N β_2-m expressing strain. No significant difference was detected in D76N β_2-m expressing adult worms in terms of dimensions in comparison to controls (S4).
Experiments performed on extrachromosomal strains expressing WT and D76N β_2-m confirmed the higher toxicity of the variant compared to the WT form (S5).

Phenotypic rescue by doxycycline. This novel transgenic *C. elegans* model was used to investigate the phenotypic rescuing capacity of doxycycline, a drug able to inhibit *in vitro* the fibrillogenesis of D76N β_2-m[17,18]. Nematodes treated with 100 µM doxycycline from L1 larval stage were analysed after 6 days at 25°C using the INVAPP/Paragon system, showing that the treatment increased the movement index by two-fold, compared to untreated controls (Fig. 6a, ***p<0.001 vs the untreated control according to one-way Anova). Thus confirming the efficacy of this drug in

reducing the cytotoxicity of amyloidogenic proteins also *in vivo*[13,17,19]. In order to analyze only the contribution of the drug on movements, we performed a body bends assay on adult worms that were grown in presence of 100 μM doxycycline. At day 5 of adulthood, we observed a recovery in the motility of D76N β_2-m worms treated with this drug compared to controls not treated, indicating that doxycycline also has an effect on movement (Fig. 6b, ***$p<0.001$ vs the untreated control, according to one-way ANOVA).

To understand the still elusive protective mechanism of doxycycline, we tested in our model the formation of oligomers in the presence of the drug. By using size exclusion chromatography followed by western blot analysis, we successfully observed a reduction of the oligomeric β_2-m species in nematodes treated with doxycycline (Fig. 6c, S6). As shown in Fig. 6c, the fraction of oligomers is considerably reduced in the D76N β_2-m worms treated with the drug (Fig. 6c, red bars).

Conclusions

The *smg*-system enables the inducible expression of D76N β_2-m, thereby circumventing its lethal toxicity in the very early stages of *C. elegans* development. The novel *C. elegans*' strain (CPV27) expressing this rare and pathogenic variant of β_2-m represents the first robust animal model for studying the pathogenic conformer of the β_2-m protein. Although amyloid deposits were not detected, we have shown that the β_2-m variant self-aggregates *in vivo* generating soluble, high molecular weight, oligomeric species that are responsible for an abnormal phenotype in our novel *C. elegans* strain.

We demonstrated the capacity of doxycycline to rescue the adverse phenotype resulting from D76N β_2-m, most likely by interfering with the formation of oligomeric conformers *in vivo*[12,17].

Our attempts to visualize and localize β_2-m using anti-β_2-m antibody tagged with a fluorescent dye were not completely successful (data not shown) but, in order to consider more deeply the pathogenesis of D76N β_2-m-induced pathological phenotype, it will be important to pursue immunofluorescence studies with improved antibodies.

In conclusion, the INVAPP/Paragon platform is a useful tool for studying the proteotoxicity of this β_2-m variant. In future, this platform, which tends itself to high-throughput chemical screening, may expedite the search for new drug candidates for the treatment of D76N β_2-microglobulin related amyloidosis, an unmet clinical need.

Methods

Construction of *C. elegans* strain and maintenance. Transgenic animals with thermo-inducible expression of β_2-m based on the well-characterized *smg* mRNA-surveillance system[12] were prepared modifying the pPD118.60 plasmid (L3808, a gift from Andrew Fire, Addgene plasmid #1598; http://n2t.net/addgene:1598; RRID:Addgene_1598), which was then injected in PD8120 *smg-1(cc546) C. elegans* strain, provided by the *Caenorhabditis* Genetics Center (CGC, University of Minnesota, USA). To modify plasmid pPD118.60, oligonucleotides containing compatible sticky ends and encoding the signal peptide of *C. elegans sel-1* (Forward oligo:5'GCCGCATGATTAAAACCTATCTGACACTGTTGCTACTAGCAACTCGGCCA CGTGTG 3'; Reverse oligo: 5'CTAGCACACGTGGCCGAGGTTGC TAGTAGCAACAGTGTCAGATAGGTTTTAATCATGC3') (Primm, Milan, Italy) were ligated between the unique *Not*I and *Nhe*I sites in the pPD118.60 plasmid. Amplified cDNA for human D76N β_2-m was inserted in the engineered plasmid containing *sel-1* signal peptide between the unique *Not*I and *Nhe*I restriction sites. DNA sequencing was carried out to confirm that the sub-cloned plasmid was correct. The plasmid obtained (PAV1) was therefore injected into *smg-1(cc546)* strain as part of a DNA mix containing 30 ng/µl of β_2-m construct PAV1 together with 40 ng/µl of plasmid p*odr-1::rfp* as co-injection marker (kind gift of C. Bargmann, Rockfeller University, New York, USA), and extrachromosomal transmitting lines were obtained. A strain expressing WT β_2-m was also similarly established, inserting amplified cDNA for human WT β_2-m in the engineered plasmid aforementioned (see S4 for the phenotypic characterization of the strain). Completely stable chromosomally integrated lines expressing D76N variant were subsequently derived after UV irradiation[20], and one clone named CPV27, was chosen for subsequent analysis. After irradiation, CPV27 strain was back-crossed with *smg-1* ancestral worms in order to remove background mutations arising from the irradiation process. Transgenic worms were thus engineered to express human D76N β_2-m under the temperature inducible control of the body-wall muscle-specific *myo-3* promoter.

The *smg-1* ancestral strain and D76N β_2-m strain were grown in Petri dishes on nematode growth medium (NGM) and fed with the OP50 strain of *Escherichia coli*[20]. Age synchronized worms were obtained by bleaching adult nematodes with alkaline solution (500 mM NaOH, 1.5% NaClO) and eggs were isolated and maintained at

16°C. When they reached the L1 larval stage, the expression of D76N β_2-m was induced by increasing temperature to 23 or 25°C.

Genotype characterization. *C. elegans* DNA was extracted using lysis buffer for DNA extraction (10 mM Tris-HCl pH 8.3, 50 mM KCl, 2.5 mM $MgCl_2$, 0.45% Tween20, 0.45% Triton X-100, 200 µg/ml proteinase K) and by incubation for 1 h at 60°C. To check the presence of the injected plasmid, single worm PCR was carried out using the following primers: L3808ForEst: 5'TGCTATG
AAAACGGCACAAA 3', L3808RevEst: 5' TTCTTCTTCACGTTCCTCACTG 3'. Expected molecular weight of PCR products was verified by DNA electrophoresis on 1.5% agarose gel. After purification of the PCR products with QIAquick PCR Purification Kit (Qiagen), DNA sequencing was performed (Eurofins Genomics Italy, Milano).

β_2-m expression. Worms were collected at the first or fifth day of adulthood, in M9 buffer (45 mM KH_2PO_4, 42 mM Na_2HPO_4, 85mM NaCl, 1mM $MgSO_4$ in water) and lysed by sonication in lysis buffer (25 mM Tris-HCl pH 7.5, 5 mM NaCl, 5 mM EDTA, 1mM DTT, protease inhibitor cocktail Roche Applied Science). For each lysate, equal amounts of total proteins, quantified with the Pierce BCA Protein Assay Kit (ThermoScientific), were loaded onto either a 4-20% Mini-PROTEAN TGX (Biorad) or 8-18% Excel SDS gel (GE Healthcare) for electrophoresis performed under reducing conditions. Proteins were transferred to Immobilon P membranes (Millipore) and blocked with 5% non-fat milk, in tris-buffered saline and Tween 20 (TBS-T), for one hour. Western blots were developed with 4.6 µg/ml rabbit polyclonal anti-human β_2-m antibody (A0072, Dako) O.N. at 4°C and 1.3 ng/ml anti-rabbit IgG peroxidase conjugate (A0545 Sigma) for 1 h RT, as primary and secondary antibody respectively. To normalize the content of total protein, western blot was developed with 0.185 µg/ml anti-glyceraldehyde 3-phosphate dehydrogenase antibody (anti-GAPDH selected as loading control, ab181602 Abcam) O.N. at 4°C, and 1.3 ng/ml secondary anti-rabbit IgG peroxidase conjugate (A0545 Sigma) antibody for 1h RT. Immuno-reactive bands were detected by ECL chemio-luminescence (Millipore), and quantified with Image Studio Lite (LI-COR Biosciences).

Self-assembly of D76N β_2-m in CPV27 *C. elegans* strain. A pellet containing transgenic *C. elegans* was resuspended in M9 and lysis buffer for further sonication. After centrifugation at 21,000 *g* for 10 min at 4°C, the soluble fraction was collected and diluted to 1 mg/ml with water. A single 500 µl sample containing 0.5 mg total protein was loaded into a Superdex 75 10/300 GL gel filtration column equilibrated and eluted with PBS pH 7.5 at a flow rate of 0.5 ml/min using an Akta Pure FPLC. Fractions of 1 ml were collected and analysed by 8-18% SDS-PAGE and immuno-blotted as above.

Larval growth and motility automated assay (INVAPP/Paragon system). Three synchronized nematodes, at their L4 larval stage, were picked onto NGM 6-well plate and incubated at 25°C. After six days at 25°C, plates were imaged using a fast high-resolution camera (Andor Neo, resolution 2560x2160, maximum frame rate 100 frames/s) with a line-scan lens (Pentax YF3528) as previously described[16]. Plates were placed in a holder built into the cabinet and imaged from below. Movies were captured using µManager and analyzed with a set of MATLAB scripts (https://github.com/fpartridge/invappparagon[16]). Briefly, this involved calculating the variance through time for each pixel. Pixels whose variance was above the threshold (typically those greater than one standard deviation away from the mean variance) were considered 'motile'. The 'motile' pixels were counted and a movement score generated for each well/plate.

Gene silencing by RNA interference (RNAi). The RNAi experiments were performed using a feeding procedure[21]. *C. elegans* were fed with HT115 (DE3) bacteria expressing dsRNA targeting β_2-m. Human β_2-m cDNA was inserted in the L4440 vector (kind gift of A.Fire, Stanford University, USA) between *Kpn*I and *Sac*I restriction sites to obtain plasmid PAV2. HT115 *E. coli* bacteria were transformed with PAV2 plasmid and then cultured onto LB plates with 100 µg/ml ampicillin and RNAi production was induced by the addition of 1 mM IPTG. Control HT115 bacteria were prepared after transformation with the empty L4440 vector. Synchronized nematodes at the L4 larval stage were cloned onto NMG plates seeded with RNAi bacteria or the control. Plates were imaged after 5 days at 25°C using the INVAPP/Paragon system and motility scored. Animals were also collected for western blot analysis.

Body bends assay. Body bends assays were performed using a stereomicroscope (M165 FC Leica) equipped with a digital camera (Leica DFC425C and SW Kit). Worms at day 1, 5 and 6 of adulthood incubated from L1 larval stage at 23°C in presence or absence of 100 µM of doxycycline were picked and transferred into a 96-well microtiter plate containing 100 µl of M9 buffer. The number of left-right movements in a minute was recorded. In order to remove the progeny, worms were transferred onto fresh NGM plates every day.

Life-span assay. Forty synchronized adult worms maintained at 16°C were upshifted to 23°C at the larval stage L1. Every day, they were transferred onto a freshly prepared NGM plate until the cessation of egg-laying to avoid the overlapping of generations. Viability was monitored until all worms were reported dead when they failed to display touch-evoked movement.

Brood size assay and embryonic lethality. Synchronized populations, were grown at 16°C until their first larval stage, and then upshifted to 23°C. Afterwards L4 transgenic hermaphrodites were individually cloned onto agar plates maintained at 23°C and subsequently transferred onto fresh plates at 8-to-16 hour intervals until the second day of adulthood. Then total number of eggs laid in 48 hours was scored and embryos were considered dead if they had not hatched after 24 h at 23°C. The brood size of each animal is the sum of non-hatched and hatched progeny. Embryonic lethality is the number of non-hatched embryos divided by the sum of non-hatched and hatched progeny.

Doxycycline treatment. Synchronized nematodes at L4 larval stage, incubated at 25°C from the L1 larval stage to allow protein expression, were placed into NGM agar plates seeded with HT115 E. *coli* resistant to tetracycline and in the presence of 0 or 100 µM of doxycycline. Plates were imaged six days later using the INVAPP/Paragon system and motility scored. Worms were also collected and lysed in order to perform size-exclusion chromatography and western blot analysis as reported before.

Statistical analysis. Data were analysed using independent Student's t-test or one-way ANOVA test with GraphPad Prism 6.0 software (CA, USA). A p value under 0.05 was considered statistically significant.

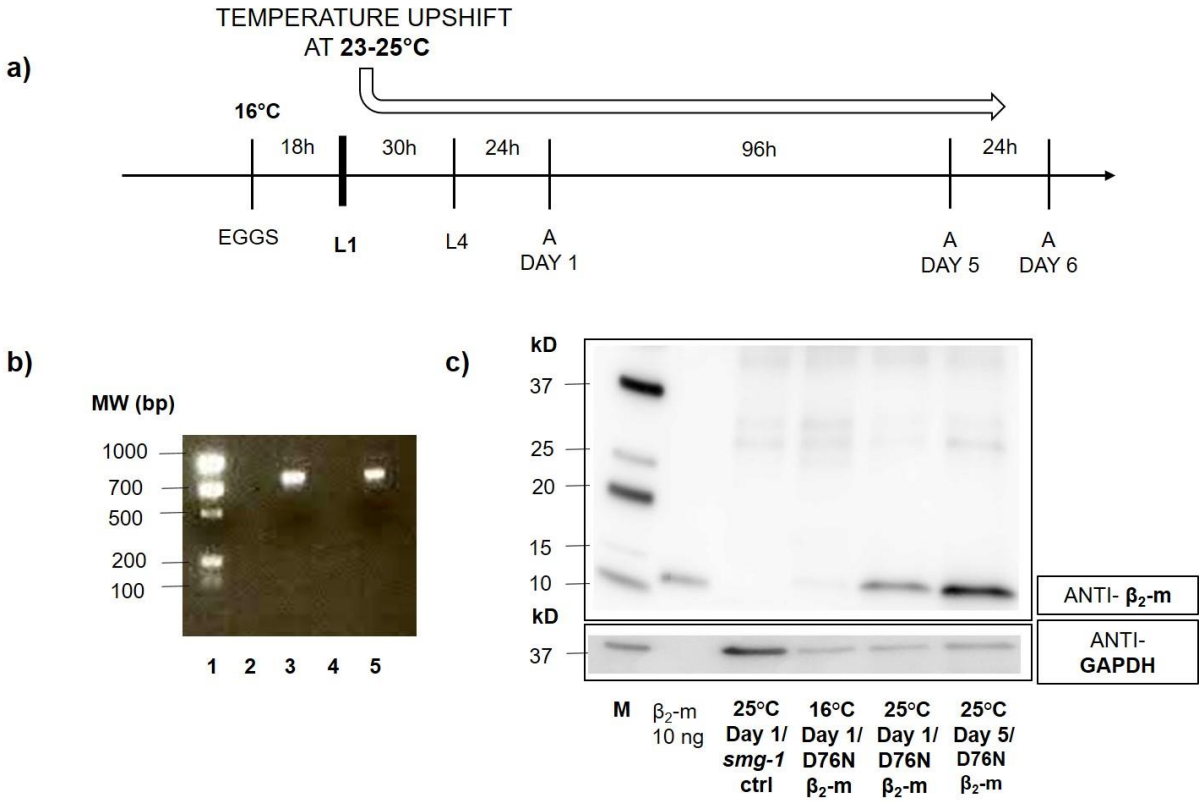

Figure 1. D76N β_2-m *C. elegans* strain genotype characterization and β_2-microglobulin expression. **(a)** Scheme of *C. elegans* manipulation highlighting the stage in which the β_2-m expression is activated by temperature switch. Eggs were maintained at 16°C and L1 larvae were up-shifted to 23-25°C in order to induce the expression of the protein. (**b)** PCR genotyping of adult transgenic nematodes. The expected size of PCR products (about 800 bp) was observed after DNA electrophoresis on 1.5% agarose gel (lane 1: EZ Load Precision, BioRad, lane 2,4: pcr products of DNA extracted from *smg-1* (cc546) ancestral strain, lane 3,5: pcr products of DNA extracted from D76N β_2-m worms. **(c)** Representative western blot of β_2-m expression. Equal amounts of protein (10 µg) were loaded for each sample from *smg-1* (- ctrl) or D76N β_2-m expressing nematodes and immunoblotted with polyclonal anti-human β_2-m antibody (Dako) and anti-GAPDH antibody used as loading control (M= Molecular weight standard: Precision Plus Western C, BioRad). Uncropped scans of immunoblots are shown in Supplementary Fig. S1.

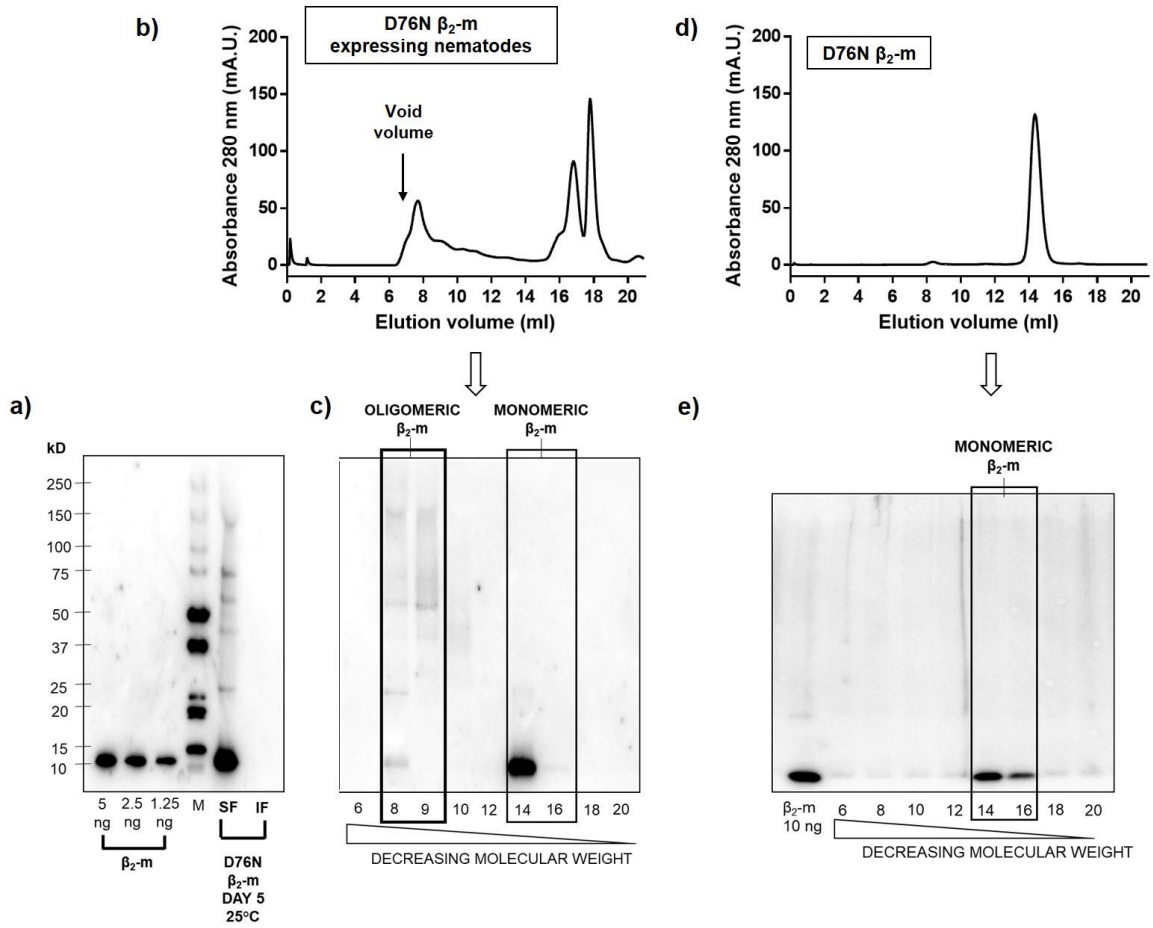

Figure 2. Self-assembly of β_2-m D76N in transgenic *C. elegans* strain. **(a)** Immunoblot analysis of soluble (SF) and insoluble fraction (IF) of worm lysates grown at 25°C resolved via 8-18% SDS PAGE and detected with anti-β_2-m antibody (DAKO). The insoluble fraction was washed twice in PBS buffer before loading onto gel. (M= Molecular weight standard: Precision Plus Western C, BioRad). **(b-d)** Size-excluded soluble proteins from β_2-m expressing nematodes and recombinant D76N β_2-m. Shown is the absorbance at 280 nm (Abs 280) of eluted material against elution volume. Fractions (1 ml) were collected. **(c-e)** Immunoblot analysis of size-excluded fractions (6-20) of β_2-m expressing worms' lysates and recombinant β_2-m resolved via 8-18% SDS PAGE and detected with anti-β_2-m antibody (DAKO). Uncropped scans of immunoblots are shown in Supplementary Fig. S2a.

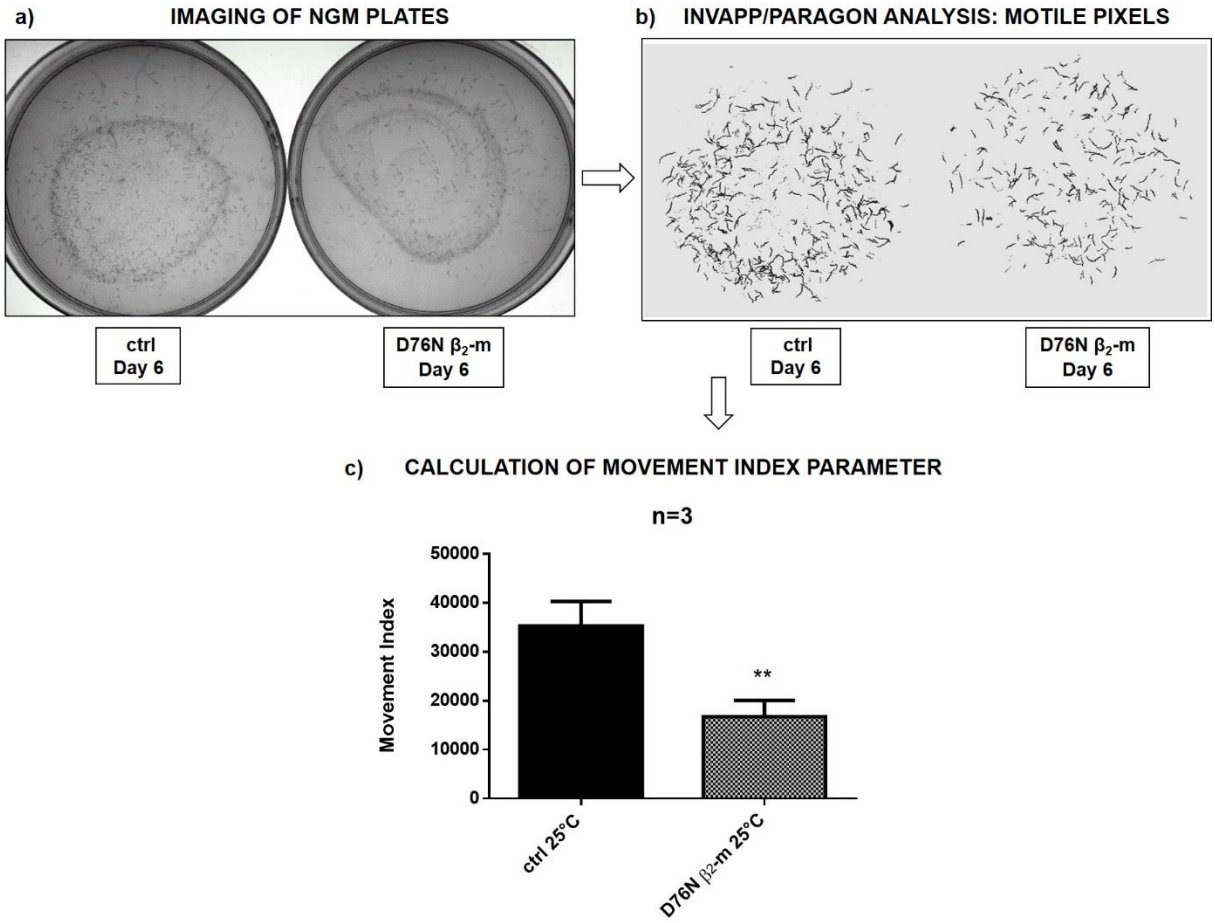

Figure 3. Movement index analysis using the INVAPP/Paragon system. 3 L4 worms/well were placed onto NGM 6-well plates, fed with OP50 *E. coli*, and maintained at 25°C for six days **(a)**. Worms were imaged using INVAPP Paragon software **(b).** Data are mean of movement index parameter ± SEM; which was obtained after processing the acquired images **(c)**. Three independent experiments were carried out and the results were plotted using GraphPad Prism (v6), **p<0.01 vs the control (s*mg-1*) according to t-test.

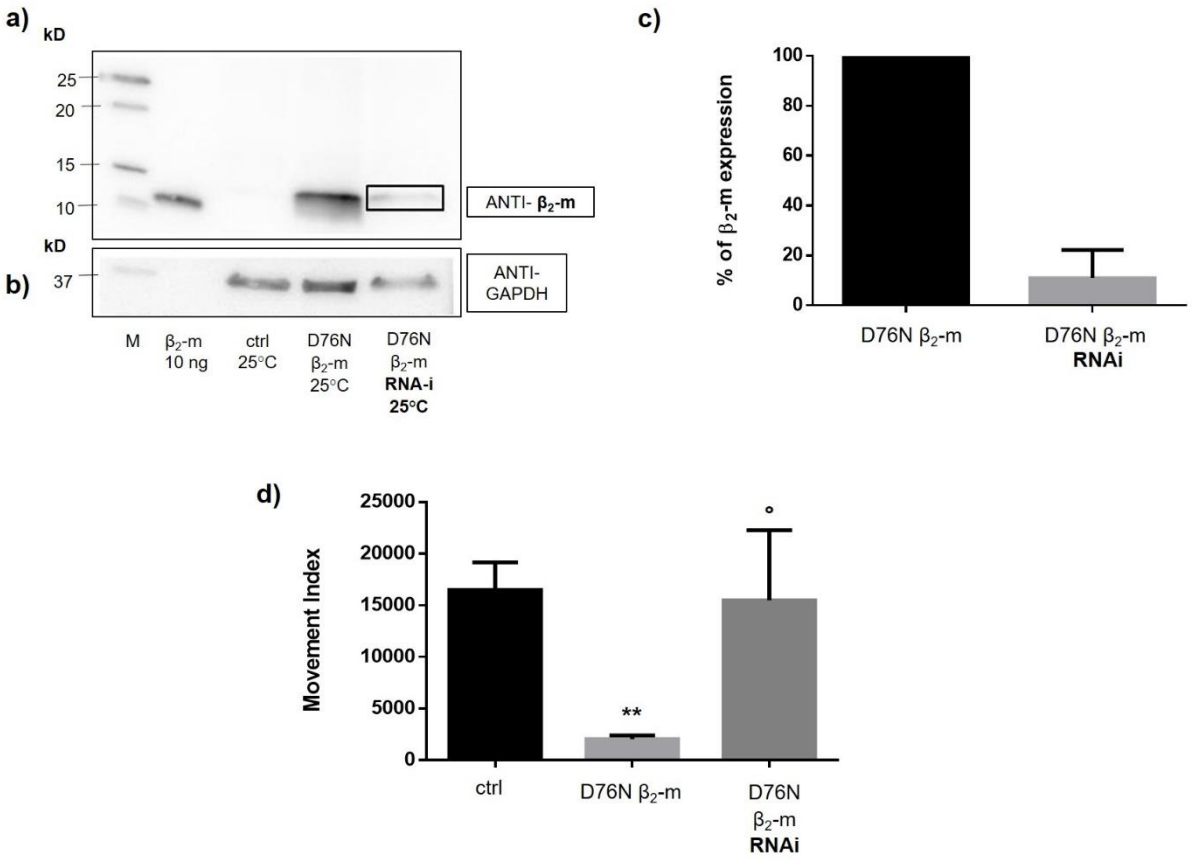

Figure 4. D76N β_2-m expression is prevented by RNA-interference (RNAi). Equal amounts of proteins (40 µg) were loaded on each lane and Immunoblotted with polyclonal anti-human β_2-m antibody (**a)** and with anti-GAPDH (**b**). Lanes: M = Precision Plus Western C (Bio Rad) molecular weight standard. s*mg-1* incubated at 25°C and collected at day 1 of adulthood. D76N β_2-m expressing nematodes incubated at 25°C and collected at day 1 of adulthood and fed with HT115 bacteria transformed, as reported before in the Methods section, with PAV2 plasmid for RNA-interfering (black box) or with control bacteria. Uncropped scans of immunoblots are shown in Supplementary Fig. S3. **(c)** Percentage of β_2-m expression is given as D76N β_2-m/GAPDH ratio of the WB band density of the RNAi strain relative to the control at their first day of adulthood. Density of the bands was determined by Image Studio Lite (LI-COR Biosciences). Three independent WB experiments were carried out and the results were plotted using GraphPad Prism (v6), p=0.0052 vs the control level of expression (black) according to one sample t-test. **(d)** Index movement analysis. Three L4 worms were placed into NGM plates, fed with HT115/L4440 or HT115 bacteria transformed with PAV2 for RNA interference. Plates were maintained at 25°C for 5 days. At this stage, the plates with adult worms and progenies were analysed by INVAPP Paragon software. Three independent experiments were carried out and the results were plotted using GraphPad Prism (v6). Data are mean of movement index parameter ± SEM; **p<0.01 vs ctrl worms and °p<0.05 vs the non-silenced D76N β_2-m expressing according to one-way Anova.

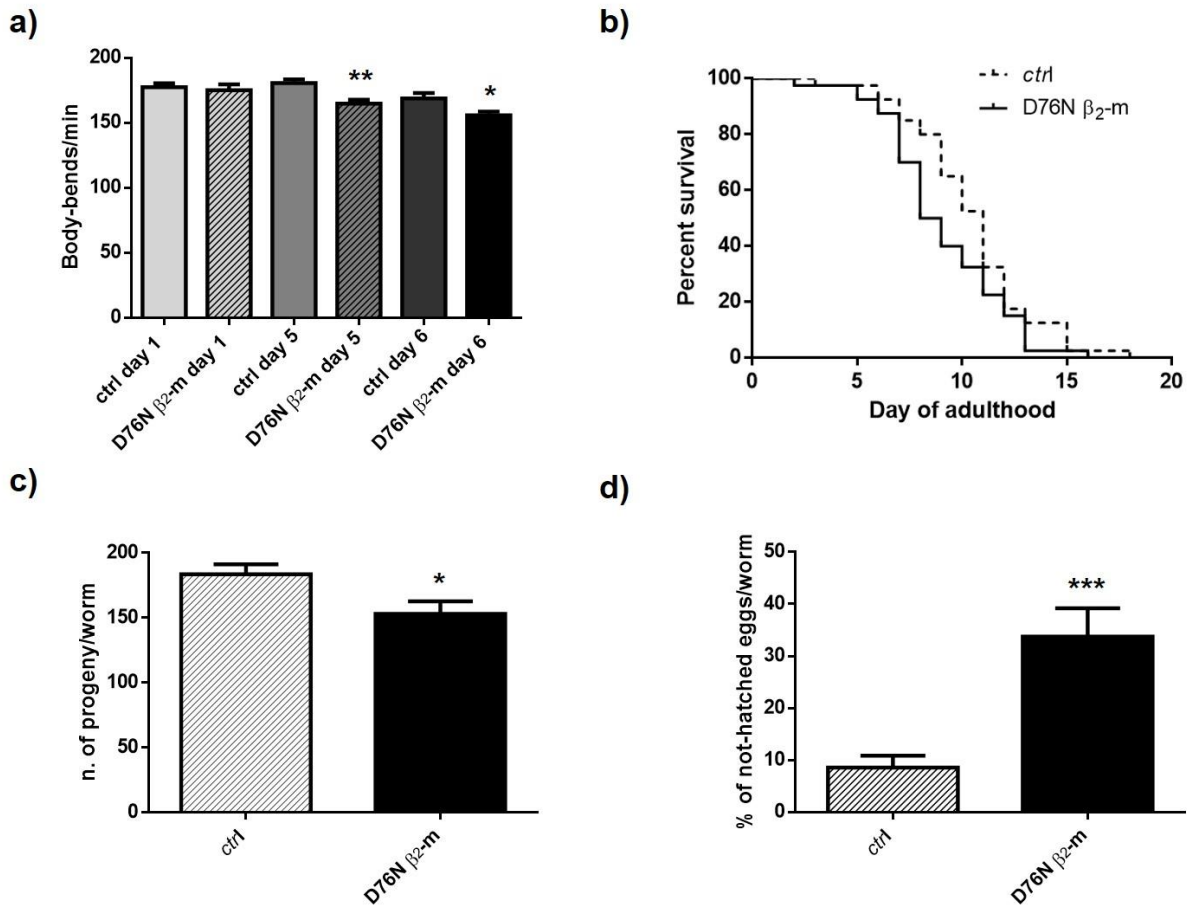

Figure 5. Characterization of the phenotype of D76N β_2-m strain by classic behavioral assays. **(a)** Egg-synchronized control worms (*smg-1*) and D76N β_2-m expressing worms were placed at 23°C into fresh NMG plates seeded with OP50 *E*. *coli*. At day 1, 5 and 6 of adulthood body bends were scored in liquid. At least three independent assays were performed. Data are mean of number of body bends/min ± SEM; **p<0.01 and *p<0.05 vs the control strain (*smg-1*), according to one-way ANOVA (N = 40 animals for each group). **(b)** Kaplan–Meier survival curves of control nematodes and D76N β_2-m strain. Data are expressed as mean of three independent experiments (N=40 animals for each group, χ^2=5.52, p=0.019 according to Peto-Peto-Prentice test). **(c)** Total eggs deposition for s*mg-1* and D76N β_2m strains maintained at 23°C. At least three independent assays were performed. Error bars represent the SEM, *p<0.05 vs. the control strain (*smg-1*) according to t-test. **(d)** Percentage of not-hatched eggs of *smg-1* and D76N β_2-m strains analyzed 24 h after deposition. At least three independent assays were performed. Error bars represent the SEM, ***p <0.001 vs. the control strain according to t-test.

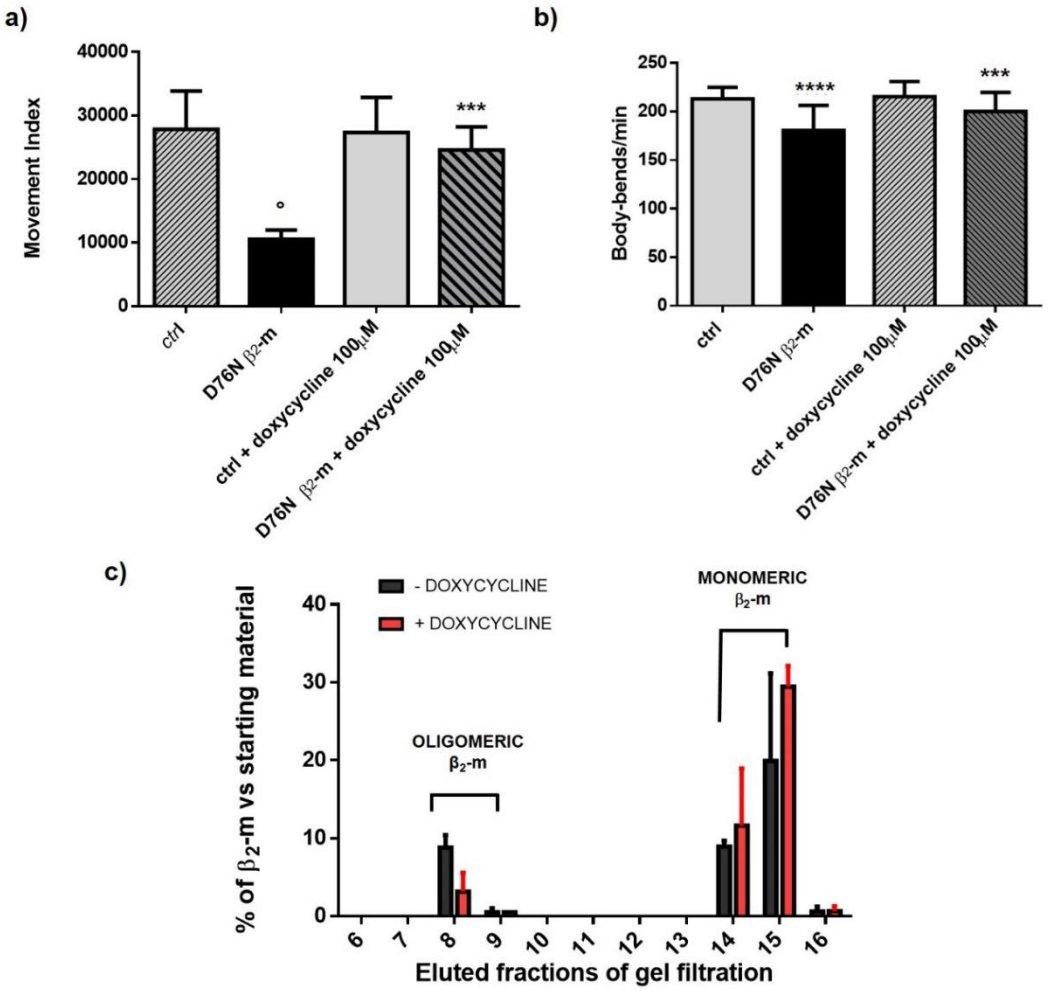

Figure 6. (a) Movement index analysis in presence and absence of doxycycline. Three L4 worms/well were placed onto NGM 6-well plates, fed with OP50 E. *coli*, and incubated at 25°C for six days in presence of 0 or 100 μM of doxycycline from the L4 larval stage. Then the plates with adult worms and progenies were analyzed by INVAPP Paragon software. Three independent experiments were carried out and the results were plotted using GraphPad Prism (v6), ***p<0.001 vs the untreated control (D76N β_2-m expressing nematodes) and ˚p<0.5 vs. the ctrl worms according to one-way Anova. **(b)** Egg-synchronized control worms (*smg-1*) and D76N β_2-m expressing worms were placed at 23°C into fresh NMG plates seeded with OP50 *E*. *coli*. At day 5 of adulthood body bends were scored in liquid. At least three independent assays were performed. Data are mean of number of body bends/min ± SEM; ***p<0.001 vs the untreated control (D76N β_2-m expressing nematodes) and ****p<0.0001 vs the ctrl worms, according to one-way ANOVA (N = 40 animals for each group). **(c)** Percentage of β_2-m in eluted fractions from gel filtration of D76N β_2-m expressing worms treated with 0 or 100 μM of doxycycline, is given as ratio of D76N β_2-m quantity of eluted fraction/soluble fraction starting material quantified from WB bands density related to the monomeric molecular weight (mean

± SEM, n = 2). Uncropped scans of immunoblots are shown in Supplementary Fig. S6. Density of the bands was determined by Image Studio Lite (LI-COR Biosciences).

References

1 Stoppini, M. & Bellotti, V. Systemic amyloidosis: lessons from beta2-microglobulin. *J Biol Chem* **290**, 9951-9958, doi:10.1074/jbc.R115.639799 (2015).

2 Marcoux, J. *et al.* A novel mechano-enzymatic cleavage mechanism underlies transthyretin amyloidogenesis. *EMBO Mol Med* **7**, 1337-1349, doi:10.15252/emmm.201505357 (2015).

3 Mangione, P. P. *et al.* Structure, folding dynamics, and amyloidogenesis of D76N beta2-microglobulin: roles of shear flow, hydrophobic surfaces, and alpha-crystallin. *J Biol Chem* **288**, 30917-30930, doi:10.1074/jbc.M113.498857 (2013).

4 Zhang, P. *et al.* Mouse model to study human A beta2M amyloidosis: generation of a transgenic mouse with excessive expression of human beta2-microglobulin. *Amyloid* **17**, 50-62, doi:10.3109/13506129.2010.483116 (2010).

5 Link, C. D. Expression of human beta-amyloid peptide in transgenic Caenorhabditis elegans. *Proc Natl Acad Sci U S A* **92**, 9368-9372, doi:10.1073/pnas.92.20.9368 (1995).

6 McColl, G. *et al.* Utility of an improved model of amyloid-beta (Abeta(1)(-)(4)(2)) toxicity in Caenorhabditis elegans for drug screening for Alzheimer's disease. *Mol Neurodegener* **7**, 57, doi:10.1186/1750-1326-7-57 (2012).

7 Madhivanan, K. *et al.* Cellular clearance of circulating transthyretin decreases cell-nonautonomous proteotoxicity in Caenorhabditis elegans. *Proc Natl Acad Sci U S A* **115**, E7710-e7719, doi:10.1073/pnas.1801117115 (2018).

8 van Ham, T. J. *et al.* C. elegans model identifies genetic modifiers of alpha-synuclein inclusion formation during aging. *PLoS Genet* **4**, e1000027, doi:10.1371/journal.pgen.1000027 (2008).

9 Morley, J. F., Brignull, H. R., Weyers, J. J. & Morimoto, R. I. The threshold for polyglutamine-expansion protein aggregation and cellular toxicity is dynamic and influenced by aging in Caenorhabditis elegans. *Proc Natl Acad Sci U S A* **99**, 10417-10422, doi:10.1073/pnas.152161099 (2002).

10 Carretero, M., Solis, G. M. & Petrascheck, M. C. elegans as Model for Drug Discovery. *Curr Top Med Chem* **17**, 2067-2076, doi:10.2174/1568026617666170131114401 (2017).

11 Kaletta, T. & Hengartner, M. O. Finding function in novel targets: C. elegans as a model organism. *Nat Rev Drug Discov* **5**, 387-398, doi:10.1038/nrd2031 (2006).

12 Mango, S. E. Stop making nonSense: the C. elegans smg genes. *Trends Genet* **17**, 646-653 (2001).

13 Diomede, L. *et al.* C. elegans expressing human beta2-microglobulin: a novel model for studying the relationship between the molecular assembly and the toxic phenotype. *PLoS One* **7**, e52314, doi:10.1371/journal.pone.0052314 (2012).

14 Grant, B. & Greenwald, I. Structure, function, and expression of SEL-1, a negative regulator of LIN-12 and GLP-1 in C. elegans. *Development* **124**, 637-644 (1997).

15 Aprile, F. A. *et al.* Selective targeting of primary and secondary nucleation pathways in Abeta42 aggregation using a rational antibody scanning method. *Sci Adv* **3**, e1700488, doi:10.1126/sciadv.1700488 (2017).

16 Partridge, F. A. *et al.* An automated high-throughput system for phenotypic screening of chemical libraries on C. elegans and parasitic nematodes. *Int J Parasitol Drugs Drug Resist* **8**, 8-21, doi:10.1016/j.ijpddr.2017.11.004 (2018).

17 Giorgetti, S. *et al.* Effect of tetracyclines on the dynamics of formation and destructuration of beta2-microglobulin amyloid fibrils. *J Biol Chem* **286**, 2121-2131, doi:10.1074/jbc.M110.178376 (2011).

18 Raimondi, S. *et al.* A specific nanobody prevents amyloidogenesis of D76N beta2-microglobulin in vitro and modifies its tissue distribution in vivo. *Sci Rep* **7**, 46711, doi:10.1038/srep46711 (2017).

19 Diomede, L. *et al.* Tetracycline and its analogues protect Caenorhabditis elegans from β amyloid-induced toxicity by targeting oligomers. *Neurobiol Dis* **40**, 424-431, doi:10.1016/j.nbd.2010.07.002 (2010).
20 Brenner, S. The genetics of behaviour. *Br Med Bull* **29**, 269-271, doi:10.1093/oxfordjournals.bmb.a071019 (1973).
21 Fire, A. *et al.* Potent and specific genetic interference by double-stranded RNA in Caenorhabditis elegans. *Nature* **391**, 806-811, doi:10.1038/35888 (1998).

Acknowledgements

Strains were provided by the CGC, which is funded by NIH Office of Research Infrastructure Programs (P40 OD010440). Supported by grants Cariplo Foundation (2014-0700), the Telethon Foundation (GG14127), the Italian Ministry of Health (Ricerca Finalizzata RF-2013-02355259), the Italian Ministry of Research and University Dipartimenti di Eccellenza 2018-2022 grant to the Molecular Medicine Department (University of Pavia), and the Istituto Nazionale di Biostrutture e Biosistemi. D.A.L. D.B.S. and F.A.P. acknowledge the support of The UK Medical Research Council Programme Grant MR/N024842/1. F.A.A. is supported by a Senior Research Fellowship award from the Alzheimer's Society UK (Grant Number 317, AS-SF-16-003). We are also indebted to the UCLH/NIHR Biomedical Research Centre for support. We thank Giuseppina Zampi for technical help, Marco Gnesi for statistical analysis of lifespan experiments.

Author contributions statement

D.B.S., F.A.P., V.B., D.A.L., P.P.M., F.A., E.D.S., and S.G., conceived the experiments, G.F., S.R., L.M., C.S., D.C., M.P., and I.Z., conducted the experiments and analyzed the results. All authors reviewed the manuscript.

Competing interests

The authors declare no competing interests.

SUPPLEMENTARY MATERIAL

C. elegans expressing D76N β_2-microglobulin: a model for *in vivo* screening of drug candidates targeting amyloidosis.

(Under second revision by Scientific Reports)

Giulia Faravelli[1*+], Sara Raimondi[1+], Loredana Marchese[1], Frederick A. Partridge[2], Cristina Soria[1], P. Patrizia Mangione[1,3], Diana Canetti[3], Michele Perni[4], Francesco A. Aprile[4], Irene Zorzoli[1], Elia Di Schiavi[5], David A. Lomas[2], Vittorio Bellotti[1,3], David B. Sattelle[2] & Sofia Giorgetti[1*].

[1]Department of Molecular Medicine, Institute of Biochemistry, University of Pavia, 27100 Pavia, Italy.

[2]Centre for Respiratory Biology, UCL Respiratory, Division of Medicine, University College London, Gower Street, London, WC1E 6JF, United Kingdom.

[3]Wolfson Drug Discovery Unit, Centre for Amyloidosis and Acute Phase Proteins, University College London, London, UK.

[4]Centre for Misfolding Diseases, Department of Chemistry, University of Cambridge, Cambridge, CB2 1EW, UK.

[5]Institute of Biosciences and Bioresources (IBBR), CNR, 80131, Naples, Italy.

*giulia.faravelli01@universitadipavia.it, s.giorgetti@unipv.it

[+]these authors contributed equally to this work

Faravelli and Raimondi *et al*. Supplementary Figure S1

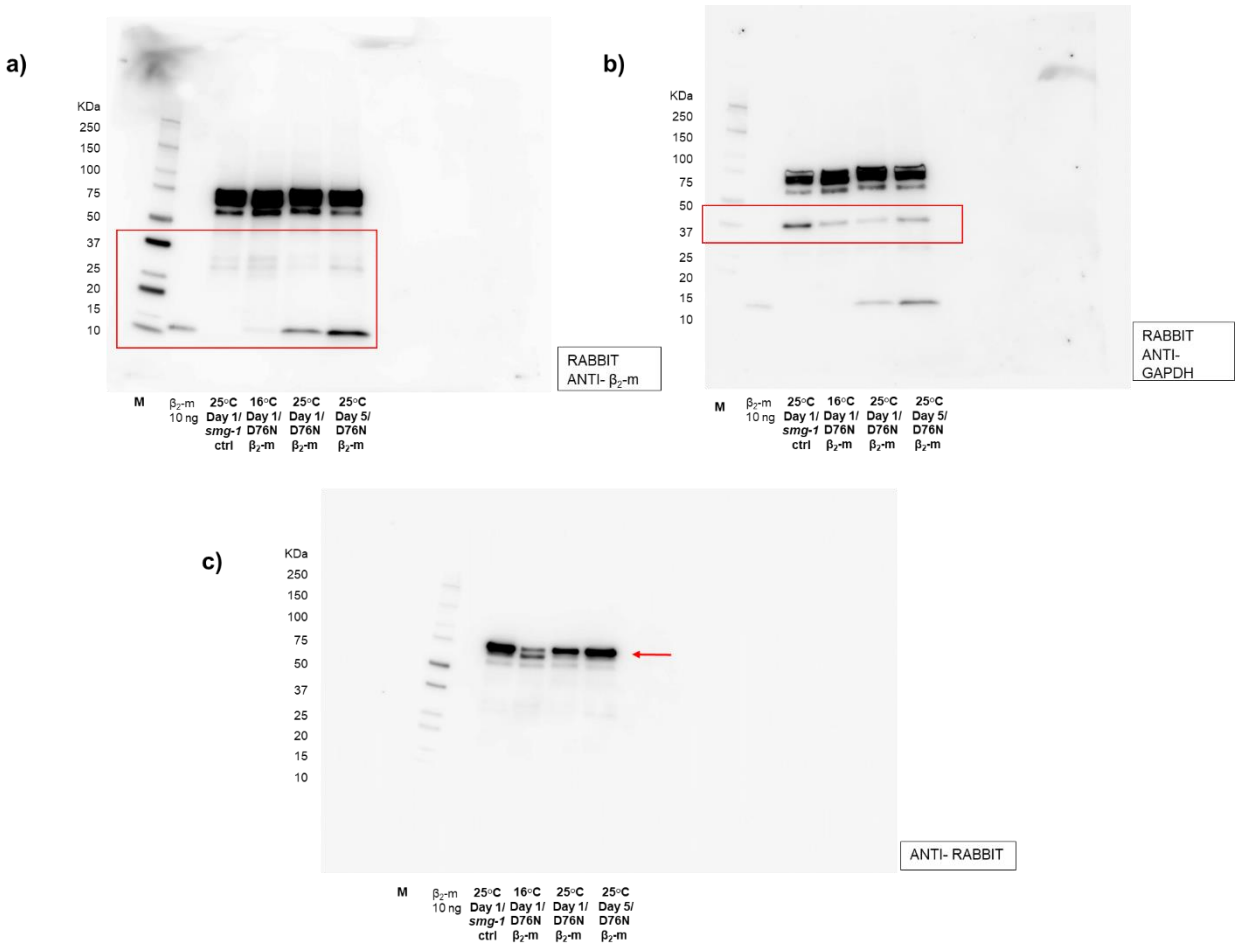

Supplementary Figure S1. **Western blots for detection of a) β2-m and b) GAPDH.** We probed the membrane with rabbit polyclonal anti-human β2-m antibody (A0072, Dako) **a)** and with both rabbit polyclonal anti-human β2-m antibody and anti-glyceraldehyde 3-phosphate dehydrogenase antibody (anti-GAPDH selected as loading control, ab181602 Abcam) as primary antibodies **b)** and anti-rabbit IgG peroxidase conjugate (A0545 Sigma) as secondary antibody. Portions (red squares) are used in Figure 1c. (M= Molecular weight standard: Precision Plus Western C, BioRad). **c)** Western blot analysis was carried out on the same samples and detected by using only the polyclonal swine anti-rabbit secondary antibody. This analysis shows that the aspecific band (red arrow) seen at 75 kD is attributable to the cross-linking of the secondary antibody.

Faravelli and Raimondi *et al*. Supplementary Figure S2

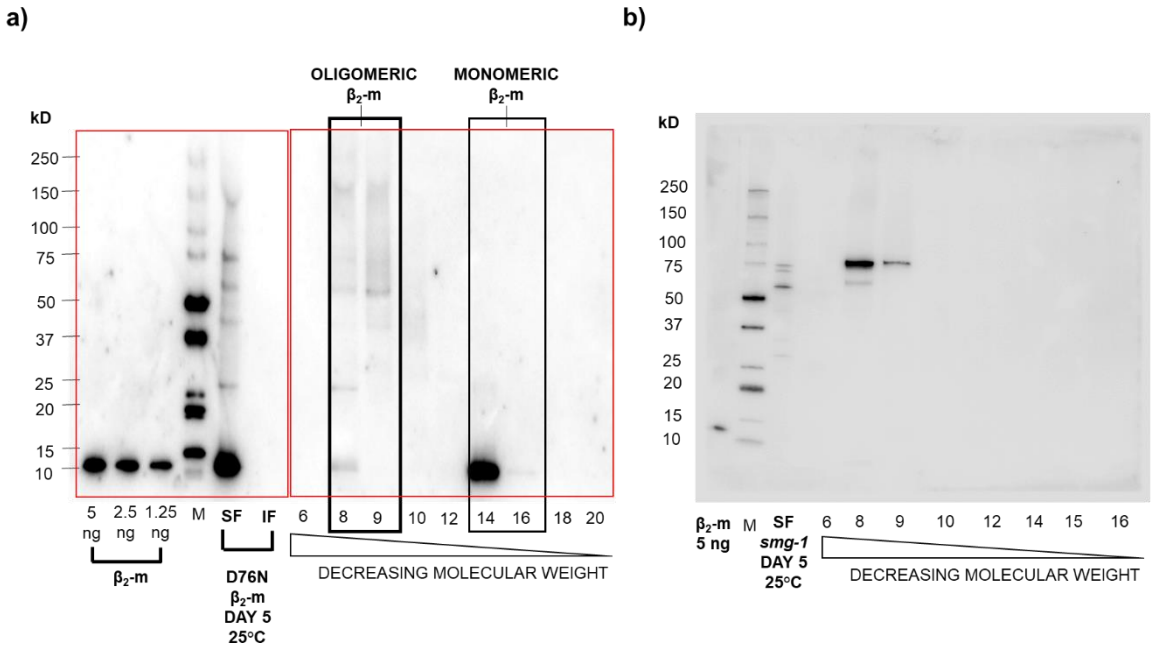

Supplementary Figure S2. **a) Western blot for detection of β_2-m.** Portions (red squares) are used in Figures 2a and 2c. (M= Molecular weight standard: Precision Plus Western C, BioRad). **b)** The soluble fraction of *smg-1* control worms was analysed by gel filtration and by western blot, as reported in the main text, as negative control.

Faravelli and Raimondi *et al*. Supplementary Figure S3

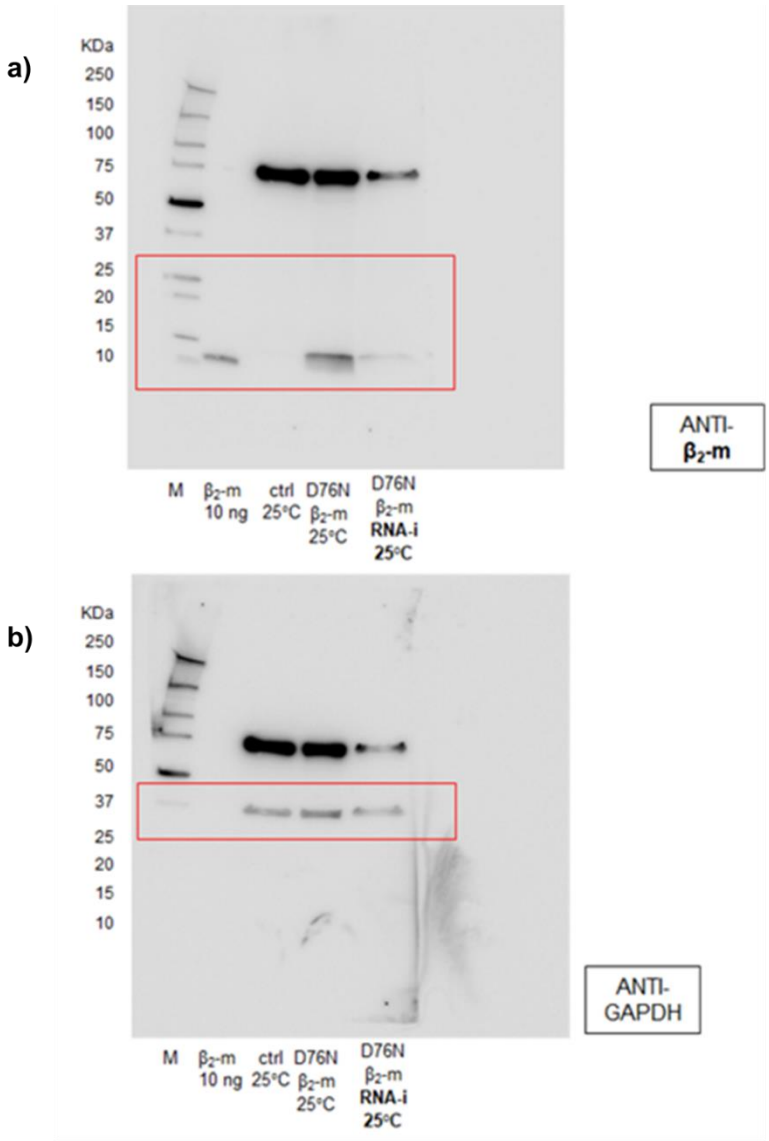

Supplementary Figure S3. **Western blots for detection of a) β2-m and b) GAPDH.** Portions (red squares) are used in Figures 4a and 4b. (M= Molecular weight standard: Precision Plus Western C, BioRad).

Faravelli and Raimondi *et al*. Supplementary Figure S4

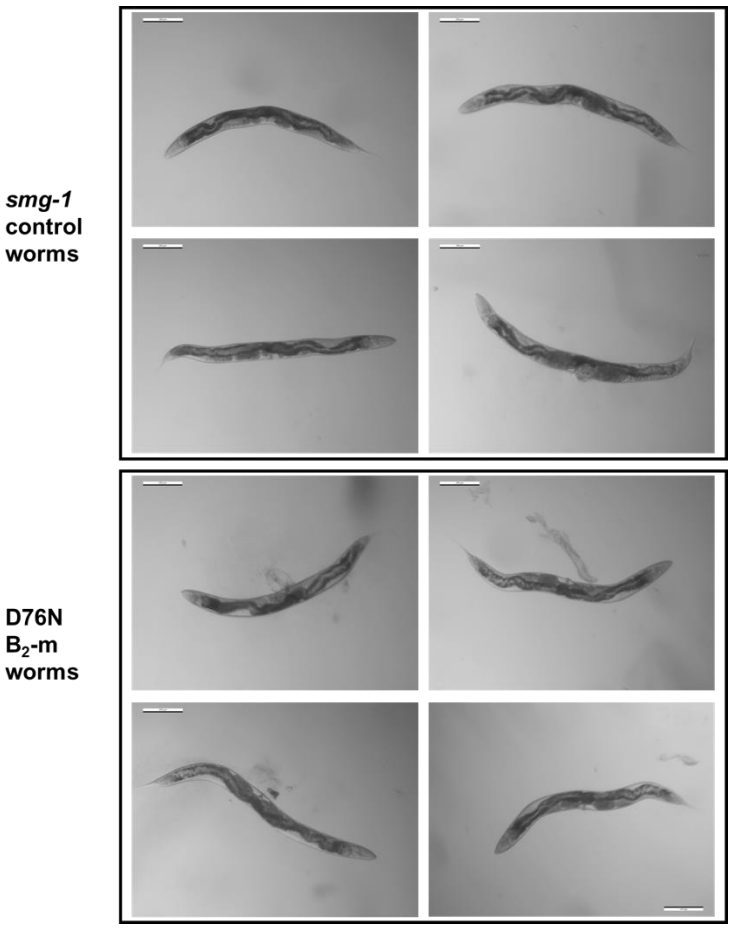

Supplementary Figure S4. Bright-field images of D76N β_2-m. 4 CPV27 worms (lower panel) and *smg-1* controls (upper panel) at day 4 of adulthood were incubated from the L1 larval stage at 23°C. Images were obtained with an inverted contrasting microscope (DM IL Leica Microsystems) and a CDD camera. Scale bars: 200 μM.

Faravelli and Raimondi *et al*. Supplementary Figure S5

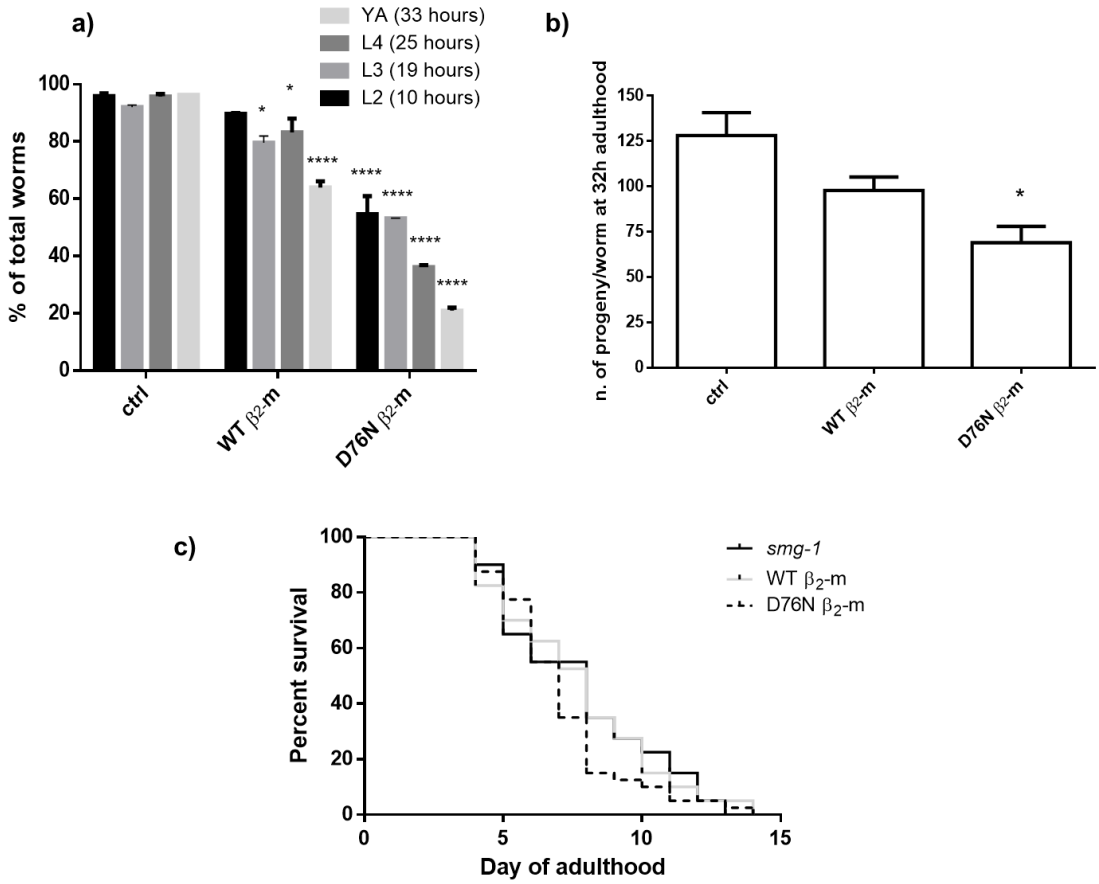

Supplementary Figure S5. Characterization of the phenotype of WT and D76N β_2-m expressing strain. a) Larval growth of control non-transgenic animals, WT and D76N β_2-m expressing strains exposed to 25°C from the first larval stage. All animals are mutated in *smg-1 (cc456)*. One hundred synchronized L1 nematodes were placed into fresh NMG plates seeded with OP50 as food and the number of L2, L3, L4 and young adult worms was scored after 10, 19, 25 and 33 hours, respectively. Data are expressed as percentage of total worms in the plate at each time point and are given as mean of two independent experiments (N = 200). Error bars represent the SD, *p<0.05 and ****p<0.0001 vs. the control strain (*smg-1*) according to one-way ANOVA. **b)** Total eggs deposition for non-transgenic animals, WT β_2-m and D76N β_2-m strains maintained at 23°C for 32 hours after the upshift of the temperature from L3 larval stage. N = 20 nematodes in each graph. Error bars represent the SD, *p<0.05 vs. the control strain (*smg-1*) according to one-way ANOVA. **c)** Kaplan–Meier survival curves

of control nematodes, WT and D76N β_2-m expressing strain at 25°C. Data are expressed as mean of two independent experiments (N=40 animals for each group). The median survival is about 8 days for control strain and WT β_2-m expressing worms, while is 7 days for worms expressing the D76N variant.

Faravelli and Raimondi *et al*. Supplementary Figure S6

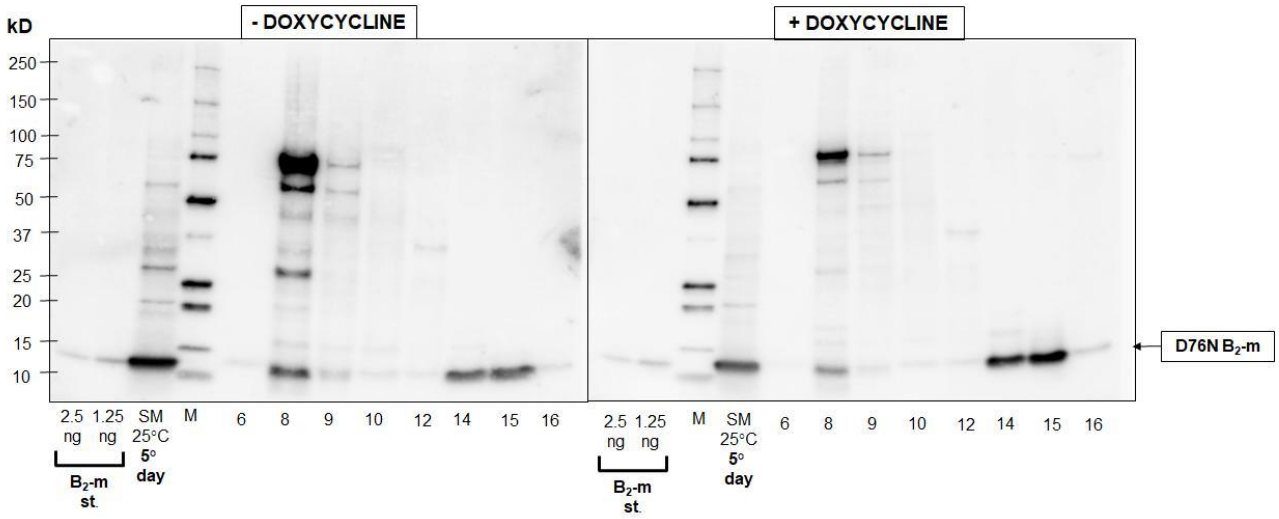

Supplementary Figure S6. Effect of doxycycline on D76N β2-m expression in CPV27 strain. Western blot analysis of gel filtration eluted fractions of CPV27 worms' lysates treated in the absence or in the presence 100 µM of doxycycline. Size-excluded fractions (6-16) were resolved via 8-18% SDS PAGE, blotted and detected with a polyclonal anti-β2-m antibody (DAKO) as described in the Methods section in the main text. (M= Molecular weight standard: Precision Plus Western C, BioRad).

3.2. Preparation of temperature-sensitive, sterile *C. elegans* transgenic strains

With the aim of studying the proteo-toxicity of synchronized adult *C. elegans* expressing human D76N β_2-m variant without the problem of having offspring growing on NGM plates, we decide to prepare worm mutants that are sterile at high temperatures such as 25°C.

The construction of *C. elegans* sterile strains was preferred to the use of the well-know Fluorodeoxyuridine (FUdR), an inhibitor of DNA synthesis which is able to prevent a synchronous population of *C. elegans* from reproducing (Mitchell et al. 1979). From our own experiments, we observed that FUdR could interact with β_2-m expression in our *C. elegans* strains by reducing the amount of the protein visible in the WB analysis. Indeed, those results are consistent with the report by Brunquell J. and collaborators, that treatment with FUdR reduces age-dependent polyglutamine aggregation in a Huntington's disease model and affects proteostasis (Brunquell, Bowers and Westerheide 2014).

In order to produce this sterile strain, it was necessary to introduce a mutation within the CPV27 strain (previously described in the paragraph 3.1). The variant NL2099: rrf-3(pk1426) II, kindly provided from Professor David Sattelle, was selected for crossing into the D76N β_2-m -expressing strain. This mutant variant possesses a 3015bp deletion within the gene *rrf-3* on chromosome II and results in enhanced RNAi as well as temperature-sensitive sterility (Simmer et al. 2002). Moreover, the NL2099 strain presents increased sensitivity to RNAi when compared to WT animals (from Plasterk Lab 11/05, CGC), therefore the crossing of our β_2-m worms with this strain, would be helpful for future genome-wide studies of gene function by RNAi screening. To allow selection of the crossed progenies, we used the RFP marker present in transgenic CPV27 worms. A *smg-1* (cc456) temperature-sensitive strain was also created in order to serve as a healthy control.

3.3.1. Methods

- ***C. elegans* grown and maintenance**

The *smg-1* (cc456) ancestral strain, D76N β_2-m strain (previously described and characterized in paragraph 3.1.) and NL2099 strain were grown in Petri dishes on nematode growth medium (NGM) and fed with the OP50 strain of *Escherichia coli* (Brenner et al. 1973). Age synchronized worms were obtained by bleaching adult nematodes with alkaline solution (500 mM NaOH, 1.5% NaClO) and eggs were isolated and maintained at 16°C. When they reached the L1 larval stage, the expression of D76N β_2-m was induced by increasing the temperature to 25°C.

- **Crossing NL2099 worms in CPV27 expressing D76N β_2-m**

NL2099: rrf-3(pk1426) II *C. elegans* carrying a homozygous rrf-3 deletion allele. (Deletion sequence: TGCACATATTctacagaatt ------- --------tacccgattaAATGGACAA TT) were used for the crossing.

1) Construction of D76N β_2-m temperature-sensitive, sterile strain. First, 10 L4 worms from CPV27 strain (PavIs1) were placed onto NGM plate (4X) seeded with OP50 E. *Coli* bacteria and incubated at 30°C for 6 h to allow the generation of male progeny. Then, males were selected at the L4 larval stage and picked to new NGM plates: 5 males (L4 or young adults) + 2 L4 from NL2099 strain (2X medium plates) were selected to allow the crossing (P0) as illustrated below. F1 progeny were selected for the presence of the RFP marker. Subsequently, F2 progeny were also selected for the presence of the RFP transgenic marker (50X individual plates were created). After checking that F2 worms laid some eggs, adults were collected individually and transferred in a PCR tube in 3 lysis buffer and frozen at -80°C for subsequent PCR analysis. F2s were screened for the deletion of the *rrf-3* gene.

P0: $\frac{CPV27}{CPV27};\frac{smg-1}{smg-1};\frac{+}{+}$ (males, red) x $\frac{+}{+};\frac{+}{+};\frac{rrf-3}{rrf-3}$ (hermaphrodites)

F1: $\frac{CPV27}{+};\frac{smg-1}{+};\frac{+}{rrf-3}$ pale red hermaphrodites

F2: desired phenotype = $\frac{CPV27}{CPV27};\frac{smg-1}{smg-1};\frac{rrf-3}{rrf-3}$

- **Single worm PCR**

In order to amplify DNA from *C. elegans* strains to determine genomic DNA sequence and thereby identify the presence of the *rrf-3* mutation, a PCR protocol which first involved lysis of a single worm was used (modified from Chin Sang lab protocol: http://post.queensu.ca/~chinsang/lab-protocols/single-worm-pcr.html). A single gravid adult worm was picked into a PCR tube containing 3 µl of PCR buffer (95 µl PCR reaction buffer, 5 µl 20 mg/ml (w/v) proteinase K). The tube was immediately frozen at -80°C overnight. The next day, the tube was heated (65°C, 60 min) to lyse the worm and release genomic DNA. The proteinase K was inactivated by heating the tube to 95°C for 15 min. The PCR was performed following the 50 µl reaction NEB protocol for OneTaq 2X Master Mix (https://international.neb.com/protocols/2012/09/06/protocol-for-onetaq-2x-master-mix-with-standard-buffer-m0482). Briefly, the following components were added to the tube containing the lysed worm: 1 µl of 10 mM both forward and reverse primers (0.2 µM final concentration), 25 µl One taq 2X Master Mix, 20 µl nuclease-free water. Mineral oil was added to the top of the reaction mixture before placing in a PCR thermocycler. The PCR conditions are shown in Table 4.

Step	Temperature/°C	Time
Initial Denaturation	94	30s
30 Cycles	94 45-68 68	15-30s 15-60s 1min/kb
Final Extension	68	5min
Hold	4-10	Indefinitely

Table 4. Cycling conditions for single worm PCR protocol.

2) Construction of *smg-1* (cc456) temperature-sensitive, sterile strain.

NL2066 males were selected at the L4 larval stage and picked to NGM plates: 5 males (L4 or young adults) + 2 L4 from the Pav32 strain generated after the crossing of CPV27 and NL2099 (2X medium plates) to allow the crossing (P0, see the scheme reported below). F1 progeny were selected for the pale red signal of the RFP marker

indicating crossed progeny. Subsequently, F2 progeny without the RFP signal were selected (50X individual plates were created). After checking that F2 worms laid some eggs, adults were individually collected in the bottom of a PCR tube in lysis buffer and frozen at -80°C. F2s were screened for the presence of the *smg-1* gene.

P0: $\frac{CPV27}{CPV27};\frac{smg-1}{smg-1};\frac{rrf-3}{rrf-3}$ (red, hermaphrodites) x $\frac{+}{+};\frac{+}{+};\frac{rrf-3}{rrf-3}$ (males)

F1: $\frac{CPV27}{+};\frac{smg-1}{+};\frac{rrf-3}{rrf-3}$ pale red

F2: all F2s are *rrf-3* homozygotes. 1/12 of non red F2s are $\frac{+}{+};\frac{smg-1}{smg-1};\frac{rrf-3}{rrf-3}$

Single worm PCR was conducted with the same protocol as before using the following primers:

Forward primer: TTCCTGAAATCGAAAGACCCAGC

Reverse primer: CATCCAGTGGAGAAGGTCATCA

F2	$\boldsymbol{\frac{smg-1,}{CPV27}}$	$\boldsymbol{\frac{+}{CPV27}}$	$\boldsymbol{\frac{smg-1}{+}}$	$\boldsymbol{\frac{+}{+}}$
$\boldsymbol{\frac{smg-1}{CPV27}}$	$\frac{smg-1}{smg-1};\frac{CPV27}{CPV27}$	$\frac{+}{smg-1};\frac{CPV27}{CPV27}$	$\frac{smg-1}{smg-1};\frac{+}{CPV27}$	$\frac{+}{smg-1};\frac{+}{CPV27}$
$\boldsymbol{\frac{+}{CPV27}}$	$\frac{smg-1+}{+};\frac{CPV27}{CPV27}$	$\frac{+}{+};\frac{CPV27}{CPV27}$	$\frac{smg-1}{+};\frac{+}{CPV27}$	$\frac{+}{+};\frac{+}{CPV27}$
$\boldsymbol{\frac{smg-1}{+}}$	$\frac{smg-1+}{smg-1};\frac{CPV27}{+}$	$\frac{+}{smg-1};\frac{CPV27}{+}$	$\frac{smg-1}{smg-1};\frac{+}{+}$	$\frac{+}{smg-1};\frac{+}{+}$
$\frac{+}{+}$	$\frac{smg-1+}{+};\frac{CPV27}{+}$	$\frac{+}{+};\frac{CPV27}{+}$	$\frac{smg-1}{+};\frac{+}{+}$	$\frac{+}{+};\frac{+}{+}$

Table 5. F2 genotype after crossing. All F2s are *rrf-3* homozygotes, therefore this character was omitted from the scheme. Cells highlighted in red in the table identify F2 worms with the RFP marker. Only 1/12 of F2s have the $\frac{+}{+};\frac{smg-1}{smg-1};\frac{rrf3}{rrf3}$ genotype (in yellow).

- **DNA gel electrophoresis**

PCR products were mixed with 3 µl of gel loading dye (6X) (NEB, Ipswich; Massachusetts), loaded into wells of agarose gels (2% agarose, 1X Tris-Acetate-EDTA

(TAE) buffer , 0.5% v/v ethidium bromide) in TAE buffer. A Quick-Load 1kb DNA ladder (NEB, Ipswich; Massachusetts) was included in the first lane (5 µl). The DNA gel was run at 65V for approximately 2 h before observation under UV. After purification of the PCR products with QIAquick PCR Purification Kit (Qiagen), DNA sequencing was performed (Eurofins Genomics Italy, Milano).

- **Western blot analysis**

Worms were collected in M9 buffer at the first or fifth day of adulthood, and lysed by sonication in lysis buffer. For each lysate, equal amounts of total proteins, quantified with the Pierce BCA Protein Assay Kit (ThermoScientific), were loaded onto a 4-20% Mini-PROTEAN TGX gel (Biorad) for electrophoresis performed under reducing conditions. Proteins were transferred to Immobilon P membranes (Millipore) and blocked with 5% non-fat milk, in tris-buffered saline and Tween 20 (TBS-T), for one hour. Western blots were developed as reported before in Chapter 3.1 (Faravelli & Raimondi *et al*., 2019, under revision by Scientific Reports).

- **Motility assay using INVAPP/Paragon system**

Twenty synchronized nematodes, at their L4 larval stage and grown at 25°C from L1, were picked onto NGM plates. At day 2 and 5 of adulthood at 25°C, plates were imaged using the INVAPP/Paragon system (Partridge et al. 2018) as reported before in Chapter 3.1 (Faravelli & Raimondi *et al*., 2019, under revision by Scientific Reports).

3.3.2. Results

- **Generation of the crossed sterile strains mutants**

CPV27 sterile strain: The F2 generation of the genetic crosses between males CPV27 worms and NL2099 hermaphrodites were placed at 25°C and observed for the red neuron marker. Thirteen candidate populations were then analysed by single worm PCR to detect the gene deletion using the following primers which flank a 991bp sequence of *rrf-3*: forward 5'-ATTTCTGCGATTGCGATTGG- 3'; reverse 5'-ACACTTCCGCGTGTGATTAG -3'. The lack of a PCR product at the 991bp position indicates that the gene has been deleted. Six of the F2 generation appeared to contain the *rrf-3* mutation (Figure 33, samples in red). Coupling this with the phenotypic evidence observed that when placing these strains at 25°C they produced little to no offspring (data not shown) confirmed that they contained the *rrf-3* deletion mutation and that they would be suitable to use.

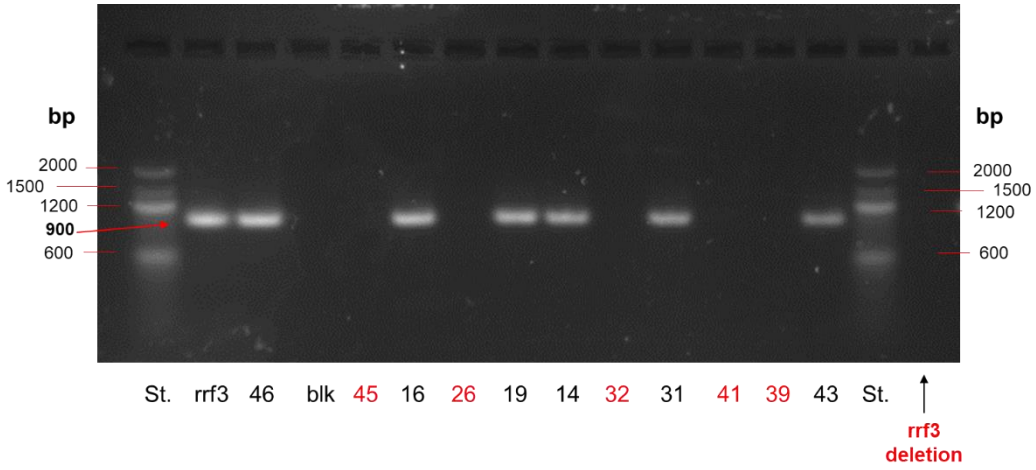

Figure 33. PCR genotyping of adult transgenic nematodes. The expected deletion of the *rrf-3* gene of PCR products (about 900 bp) was observed after DNA electrophoresis on 2% agarose gel in samples 45,26,32,41,39 which are highlighted in red in the figure. (St: EZ Load Precision, BioRad).

In order to control that the *smg-1* (cc456) mutation responsible of the thermo-inducible phenotype of CPV27 worms (see paragraph 3.1) was still present in the crossed strains, single worm PCR was performed in order to detect the *smg-1* gene and PCR products, after purification, were sequenced in order to visualize allele mutation. Two transgenic strains were selected for DNA sequencing. Only one of them was shown to

carry the mutation and it was termed Pav32; the other one, Pav45, did not carry the mutant allele, having the mRNA surveillance system functional also at higher degrees, did not express β_2-m at all (see WB analysis reported below).

Smg-1 sterile strain: To compare the phenotype of this new temperature-sensitive, sterile strain, a *smg-1* (cc456) sterile strain was prepared as well following the same procedure reported before. For this experiment, we chose to cross our new Pav32 sterile strain expressing the β_2-m variant with the already employed NL2099 strain. The F2 generation of the genetic crosses between males Pav32 worms and NL2099 hermaphrodites were placed at 25°C and observed for the absence of the red neurons marker. Eight candidate populations were then analysed by single worm PCR to detect the *smg-1* gene using the primers reported before, obtaining the expected 900 bp band on a 2% agarose gel. Six of the F2 generation appeared to contain the gene (Figure 34, samples: 3,4,5,6,7,8).

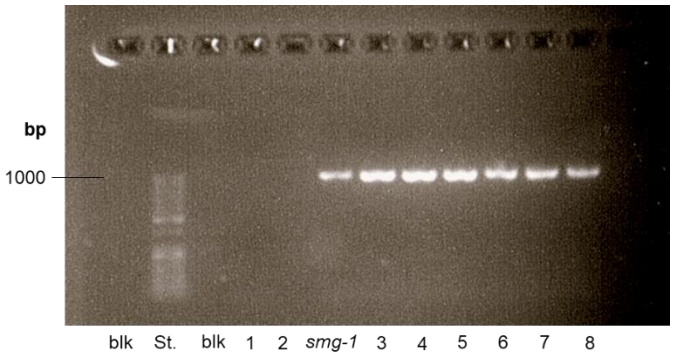

Figure 34. PCR genotyping of adult transgenic nematodes. The expected size of the *smg-1* gene of PCR products (about 900 bp) was observed after DNA electrophoresis on 2% agarose gel in samples 3,4,5,6,7,8. (St: EZ Load Precision, BioRad).

Subsequent DNA sequencing was performed (Eurofins, Milano) in order to select only mutants with the *smg-1* (cc456) mutation responsible of thermo-inducible phenotype in *C. elegans*. Only two strains (sample 3 and 4) were positive for the mutation and were named **SMG3** and **SMG4**.

Finally, in order to exclude the presence of β_2-m gene in the strains selected, a further single worm PCR was performed using the following primers: L3808ForEst: 5' TGCTATGAAAACGGCACAAA 3'; L3808RevEst: 5' TTCTTCTTCACGTTCCTCACTG

3'. We confirmed that the new crossed *C. elegans* lines do not carry β_2-m gene. As it is clearly shown in Figure 35, neither SMG3 neither SMG4 carry the β_2-m transgene.

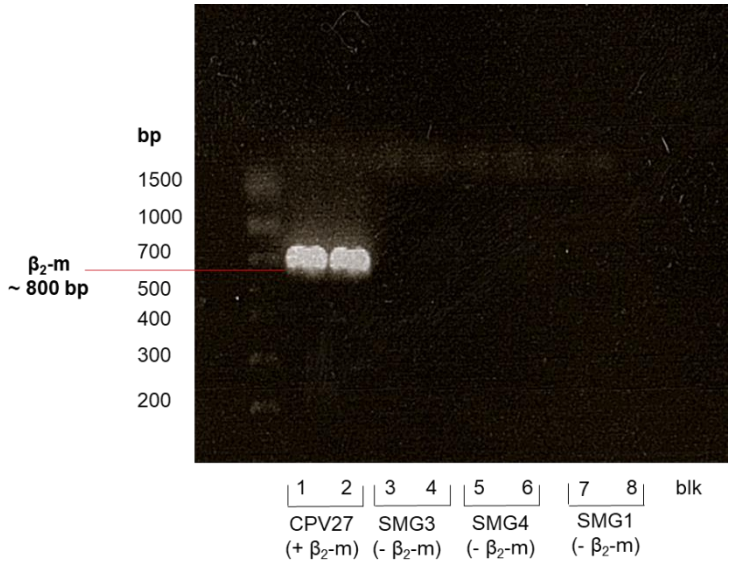

Figure 35. PCR genotyping of adult transgenic nematodes. No presence of β_2-m gene was observed in worms from the SMG3 (samples 3-4) or SMG4 (samples 5-6) strains. CPV27 and *smg-1* strain were used as a positive and negative control respectively. PCR products were observed after DNA electrophoresis on 2% agarose gel (St: EZ Load Precision, BioRad).

- **Characterization of the sterile strain phenotype**

The Pav32 strain obtained after crossing with NL2099, carrying the *rrf-3* deletion, correctly expressed D76N β_2-m when animals were grown at 25°C commencing from the L1 larval stage, as shown by western blot analysis (Fig. 36). Levels of protein increased from the first to the fifth day when nematodes were grown at 25°C (Fig. 36). The pattern of expression was similar to the one of D76N β_2-m nematodes from CPV27 strain, grown at 25°C. The absence of expression of β_2-m was observed for SMG3 and SMG4 nematodes. In addition, the Pav45 strain, which does not carry the *smg-1* mutation responsible of temperature sensitivity, was analyzed and the results confirmed the lack of the thermo-inducible system function. Therefore, Pav32 and SMG4 strains were selected as putative transgenic lines for further analysis focused on the study of β_2-m toxicity and drug screening.

First, motility assays were conducted in order to evaluate the phenotype of the new *C. elegans* strains generated after the crossing.

As previously reported in Chapter 1, by using the INVAPP/paragon system, it is possible to get a quantification of two different parameters depending on how the experiment is designed. Both motility and growth development can be monitored in *C. elegans*. In this particular case, by using a transgenic sterile strain and in absence of progeny, we were able to study the proteotoxic effect on motility.

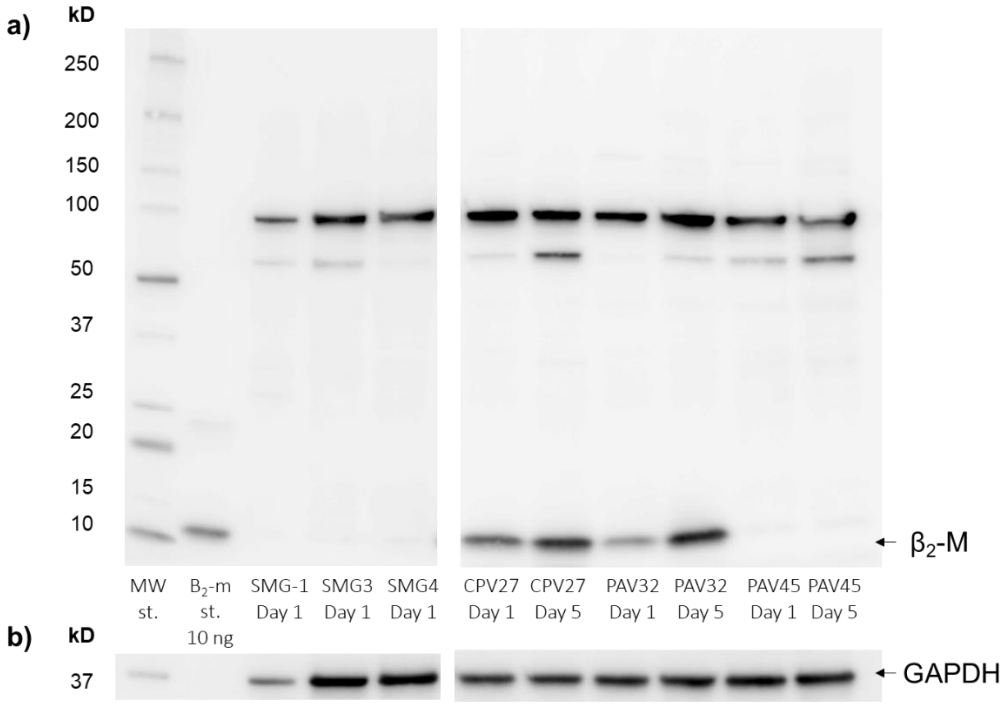

Figure 36. Pattern of expression of temperature-sensitive sterile *C. elegans* strains. **a)** Representative western blot of β_2-m expression. Equal amounts of protein (20 µg) were loaded for each sample and immunoblotted with polyclonal anti-human β_2-m antibody (Dako) and anti-GAPDH antibody used as loading control (M= Molecular weight standard: Precision Plus Western C, BioRad).

In figure 37, I report some preliminary results in which I measured the motility of Pav32 using the automated INVAPP/Paragon system (Partridge et al. 2018) in comparison with SMG4 strain which is used as a healthy control. Worms expressing the D76N β_2-m variant move less than the non-expressing controls (SMG4) (Fig. 37) showing a reduction in motility of 36.5% and 42% respectively compared to controls. The difference between the two strains became evident at day 5 of adulthood. Similar results were obtained with the body bends assay performed on the CPV27 strain (see Chapter 3.1. Faravelli & Raimondi *et al*., 2019, submitted to Scientific Reports).

Moreover, those findings overlap entirely with the ones obtained with the CPV27 strain (Faravelli & Raimondi *et al*., 2019, under revision by Scientific Reports, see the manuscript reported in Chapter 3.1). Therefore, we plan to make use of this new *C. elegans* model for future experiments, which offer the opportunity to study proteo-toxicity and drug efficacy on aged-synchronized worms avoiding problems related associated with progeny proliferation.

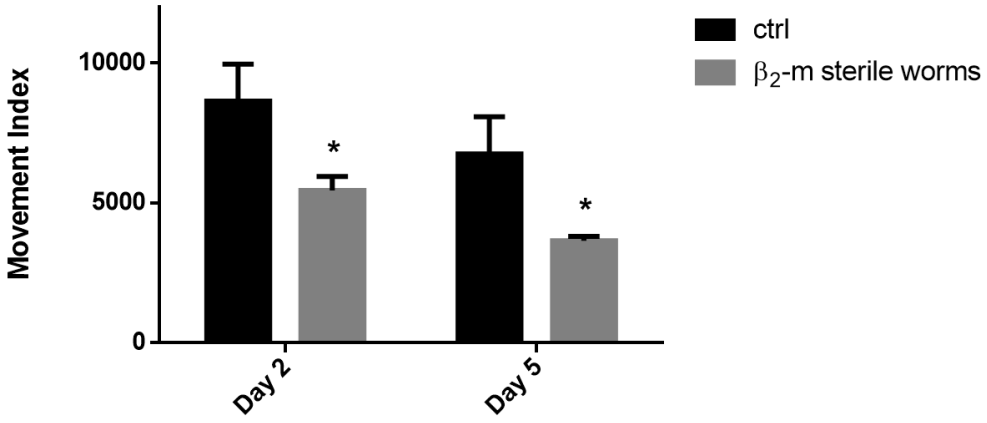

Figure 37. Motility assay using INVAPP/Paragon system. Twenty synchronized nematodes from SMG4 (ctrl) and Pav32 (β_2-m sterile worms), at their L1 larval stage, were picked onto NGM plates and incubated at 25°C. At day 2 and 5 of adulthood, plates were imaged and movies were analyzed with a set of MATLAB scripts as reported before. Data are mean of three independent experiments ± SD; *$p<0.05$ vs the control strain (*smg-1*), according to one-way ANOVA (N = 20 animals for each group).

Chapter 4: Drug screening approach for amyloid diseases using *C. elegans*

As previously said in Chapter 1, the nematode *C. elegans* can be a valuable tool in order to perform high-throughput screening and in the search for new drug candidates. In particular, the INVAPP/Paragon system has been applied for the identification of new molecules with potential therapeutic activity for Alzheimer's disease. The societal burden presented by Alzheimer's disease warrants both innovative and readily applied approaches to its underlying mechanism, which can be accelerate the search for novel therapeutic targets and strategies (Griffin, Caldwell and Caldwell 2017).

In 1992, John Hardy and Gerald Higgins formulated the "amyloid cascade hypothesis" in which they showed that the Aβ peptides that constitute amyloid plaques are among the causative agents of Alzheimer's pathology (Hardy and Higgins 1992). Amyloid plaques were considered the principal neurotoxic mediators in AD. However, recent studies pointed soluble oligomeric species of Aβ peptides, a class of peptides with different lengths which are produced from the metabolism of amyloid precursor protein (APP), as being the most toxic form in AD (Winblad et al. 2016, Hayden and Teplow 2013, Walsh and Selkoe 2007, Benilova, Karran and De Strooper 2012).

Transgenic *C. elegans* strains have been established in order to study the Abeta toxicity in Alzheimer's disease; some of them are reported in Table 6. The expression of recombinant Aβ circumvented APP processing in *C. elegans*. In doing so, expression of the Aβ cleavage product provides the utility of examining direct modifiers of Aβ toxicity, rather than modifiers of Aβ production as a result of APP processing. Initially, the use of the *unc-54* promoter to constitutively express a signal peptide: $A\beta_{1-42}$ minigene in nematodes, allowed to intracellular Aβ amyloid deposition in muscle cells and resulted in an age-dependant paralysis phenotype in the *C. elegans* CL2120 strain (Table 6) (Fay et al. 1998, Link et al. 2001). Later, McColl and his collaborators discovered that existing Aβ models predominantly express amino-truncated $A\beta_{3-42}$ and not the full-length peptide (McColl et al. 2009).

In addition to the formation of amyloid plaques, neurofibrillary tangles, composed of aberrantly phosphorylated protein tau that is normally responsible for stabilizing microtubule structures, are another pathological feature of AD. Since, the *C. elegans* orthologue, ptl-1, has a similar structure and function to mammalian tau, nematodes

represent a practical model for probing tau-induced pathologies and transgenic models have been established for this purpose (Griffin et al. 2017).

In this Chapter, I report the experiments conducted in order to assess the efficacy of different molecules in restoring the normal phenotype of transgenic worms expressing Aβ peptide.

Firstly, I tested some curcumin derivatives (paragraph 4.1) on the CL2120 *C. elegans* strain, on the basis that those polyphenols are able to prevent phenotypic toxicity in different *C. elegans* models of Alzheimer's disease (Alavez et al. 2011, McColl et al. 2012).

Secondly, I described the experiments conducted on the GMC101 strain, which express the full length $A\beta_{1\text{-}42}$ (McColl et al. 2012), following a library-screen approach. Indeed, no large-scale screen has been performed for drugs that modulate Aβ toxicity directly in *C. elegans* so far. Rather, drug candidates from screens in other Aβ models have been tested in *C. elegans*. Doing so, positive candidates could possibly appear negative in yeast or *in vitro* cell cultures, when they would otherwise incite behavioural changes in response to Aβ or tau, in a metazoan system (Griffin et al. 2017).

Target-oriented screening of large collections of chemically diverse molecules may be a useful approach toward the discovery of novel bioactive compounds exhibiting a specific effect on protein targets, such as inhibitors or for pharmacological chaperones (López et al. 2012). This kind of approach was followed by López and colleagues, which reported the discovery of chemically unrelated inhibitors of the *in vitro* aggregation of the $A\beta_{17\text{–}40}$ peptide by screening two commercial chemical libraries. The libraries were initially screened in a high throughput, fluorescence-based aggregation assay, followed by discrimination of false positives and confirmation of true positives by means of turbidimetry and electron-microscopy assays, respectively. Five structurally unrelated inhibitory compounds have been identified out of 11 250 assayed, which have been tested for *in vivo* activity against $A\beta_{1\text{–}42}$ aggregation using recently developed Podospora (Benkemoun et al. 2006) and yeast (Morell et al. 2011) models (López et al. 2012).

In collaboration with Professor David Sattelle, we therefore decided to follow a library-scale approach in order to find novel candidates able to revert the phenotypic defect of *C. elegans* transgenic strains expressing the Aβ peptides and with potential therapeutic activity against AD. In particular, our aim was to test a library of modulators

of protein-protein interaction since it has been reported that such molecules are likely to represent the next generation of highly innovative drugs that will reach the market over the next decade (Morelli, Bourgeas and Roche 2011).

Aβ models	genotype	strain name (ref)
chronic Aβ paralysis	*dvIs2* [pCL12(*unc-54*/human Aβ peptide 1−42 minigene) + pRF4]	CL2006[18]
Aβ in muscles	*dvIs14* [(pCL12) *unc-54*::Aβ 1−42 + (pCL26) *mtl-2*::GFP]	CL2120[33]
control for Aβ muscles	*dvIs15* [(pPD30.38) *unc-54* (vector) + (pCL26) *mtl-2*::GFP]	CL2122[33]
permissive pan-neuronal Aβ	*dvIs50* [pCL45 (*snb-1*::Aβ 1−42::3′ UTR(long) + *mtl-2*::GFP] I	CL2355[84]
acute Aβ paralysis	*dvIs27* [*myo-3p*::Aβ (1−42)::*let-851* 3′UTR) + *rol-6* (*su1006*)] X	CL4176[32]
Aβ(1−42) in muscles	*dvIs100* [*unc-54p*::Aβ-1−42::unc-54 3′-UTR + *mtl-2p*::GFP]	GMC101[22]
pan-neuronal Aβ(1−40)	*Ex*[pPD49.26 + P*aex-3*::Aβ(1−40); *ttx-3*::rfp p*lin-15*(+)]	MT309[38]
pan-neuronal Aβ(1−42)	*Is*[pTI11.1+P*unc-119*::Aβ(1−42); P*myo-2*::YFP]	(ref 42)
glutamatergic Aβ	[*baIn*l*32*; P*eat-4*::ssAβ 1−42, P*eat-4*::gfp, P*myo-2*::mCherry]	UA166[20]

Table 6. *C. elegans* strains modelling Alzheimer's disease. Highlighted in yellow: Abeta expressing strains used for experiments reported in this chapter; in green: the one used as control strain (Griffin et al. 2017).

4.1. Testing the efficacy of curcumin compounds on worms expressing Aβeta peptide

The aetiology of Alzheimer's disease is still incomplete but it has widely reported that Aβ aggregation plays a key role in the onset and progression of the disorder (Chiti and Dobson 2017). Therefore, agents able to block or reverse the amyloid process could be an effective approach for treating AD. A variety of anti-amyloid agents have been developed and according to the amyloid cascade hypothesis proposed by Hardy and Higgins in 1992 (Hardy and Higgins 1992), they target the process at different levels.
Many natural products (NPs) have been described as possible modulators of the amyloid process (Shao and Xiao 2013). Among them, Curcumin, which is the primary bioactive compound found in the rhizome of *Curcuma longa*, is one of the most extensively studied because of its pleiotropic properties. Indeed, a comprehensive up-to-date database, the Curcumin Resource Database (CRDB), has been created and collect relevant data and related information on curcumin and its analogues (Kumar et al. 2015). Based on the information of the CRDB, to date more than 10000 publications have been reported on curcumin and its analogues and a few less than one thousands of curcumin-based patents have been registered (Nelson et al. 2017).
However, Curcumin exhibits some important limitations as a potential drug because of poor bioavailability, poor absorption, distribution, metabolism and excretion (ADME) properties, as well as potential toxicological effects (Nelson et al. 2017). For these reasons, several structure–activity relationship (SAR) studies have been conducted and the curcumin pharmacophore was dissected by modifying the functional groups in the search of derivatives as putative binding partners of different aggregation states of Aβ peptides.
Recently, I had the occasion to collaborate with the group of Professor Ersilia De Lorenzi (University of Pavia) that, in association with Federica Betulli (University of Bologna), have identified two new curcumin analogues (Figure 38, 1-2), named Cur5 and Cur6, with demonstrated multipotent activity *in vitro* (Bisceglia et al. 2019).

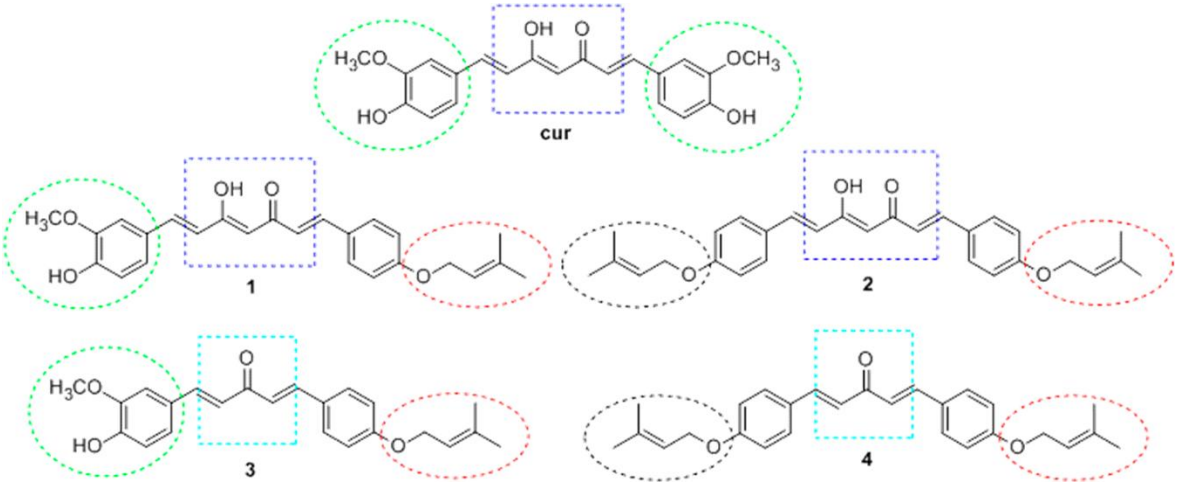

Figure 38. Design strategy toward the curcumin-based analogues 1−4. Structures of curcumin (cur), the newly synthesized curcuminoids (1, 2), and their monocarbonyl analogues (3, 4) (Bisceglia et al. 2019).

Those newly synthesized curcumin-based analogues present some structural modifications (Figure 38) and the choice of the functional group was mainly addressed to reduce curcumin neuronal toxicity, as well as to favour the crossing of the BBB by modulating the hydrophilic/lipophilic balance of the compounds. have demonstrated to stabilize small aggregates and consistently to hinder the formation of larger assemblies (Bisceglia et al. 2019). Curcumin-based analogues were tested *in vitro* on neuroblastoma (SH-SY5Y) and microglia cells showing anti-inflammatory and antioxidant properties.

Therefore, the aim of my study was to test those compounds for their protective activity *in vivo* in genetically engineered *C. elegans* expressing Aβ peptide. Compounds were first tested on the well-characterized CL2120 strain (Link et al. 2001) performing classical body bends assays in order to evaluate the motility of worms treated with this molecules.

Then, thanks to the collaboration with Professor David Sattelle (UCL, London), I had the occasion to test the efficacy of the curcumin-related compounds using the INVAPP/paragon system of phenotyping (Partridge et al. 2018) on the worm transgenic strain GMC101 expressing $A\beta_{1-42}$ (McColl et al. 2012).

4.1.1. Methods

- ***C. elegans* growth and maintenance**

The N2 wild-type, GMC101and CL2120 strains (previously described) were grown in Petri dishes on nematode growth medium (NGM) at 20°C and fed with the OP50 strain of *Escherichia coli* (Brenner et al. 1976). Age synchronized worms were obtained by bleaching adult nematodes with alkaline solution (500 mM NaOH, 1.5% NaClO) and eggs were isolated and maintained at 20°C. Later, L1 larvae were incubated at 20 or 25°C.

- **Body bends assay**

For the body bend assay, plates containing curcumin, Cur6 and Cur5 were prepared as follows: 150 µl of concentrated stock solutions of each compound were added to molten NGM at 50°C and then 4 ml were poured into each plate. The plates were placed in a laminar flow hood at room temperature for 30 min and then 50 µl of a suspension of *E. coli* OP50 was spotted to form a circular lawn on the centre of each plate. Body bends assay was performed at room temperature using a stereomicroscope (M165 FC Leica) equipped with a digital camera (Leica DFC425C and SW Kit). After 48 h exposure to 100 µM curcumin, Cur6 and Cur5, adults synchronized worms were picked and transferred into a 96-well microtiter plate containing 100 µl of M9 buffer. At this point, the number of left–right worms tail movements in 1 min was recorded. Three independent assays were performed (N=30 animals for each group). A subset of worms of the N2 strain was used as a negative control strain.

- **Motility assays using INVAPP/Paragon analysis**

C. elegans strains were maintained at 20 °C on nematode growth medium agar seeded with the E. *coli* strain OP50. To obtain worms for screening, a mixed-stage liquid culture was prepared by washing well-fed worms from one small NGM plate into a medium of 50 ml S-complete buffer with a pellet of approximately 2–3 g E. *coli* HB101. Cultures were agitated at 200 rpm, 18 °C approximately for five days, and then L1 larvae were filtered. For the screening assay, C. *elegans* were cultured in a 96-well plate format. Synchronised L1 were diluted to approximately 25-30 worms per 100 µl in S complete medium with around 1% w/v HB101 *E. coli*. Assay plates were prepared with 100 µl of L1 suspension and 1 µl of DMSO or compound in ethanol solution (EtOH) per well. Plates were incubated at 25 °C before imaging using the INVAPP/Paragon system at

first day of adulthood. Whole-plate 200 frame movies were recorded at 30 frames per second (7 s total).

4.1.2. Results

- **Body bends assay on CL2120 *C. elegans* strain**

CL2120 expressing $A\beta_{3-42}$ were treated with Cur, Cur6 and Cur5 at concentration of 100 µM and 50 µM. These concentrations have commonly been used in literature for this type of experiment (Alavez et al. 2011). To evaluate the effect of these compounds, the body bends assay is carried out *in vivo* on untreated worms and on worms exposed to compounds. N2 strain represents the negative control, since it does not express Aβ peptide, whereas mutated CL2120 is the positive control because it does not receive treatment. In Figure 39, the results of body bends analyses are reported. As expected, worms belonging to N2 group maintain normal movements, as more than 200 body bends/min are counted. On the contrary, in the mutated strain CL2120 the deposition of amyloid fibrils leads to a progressive paralysis and a reduction in the number of body bends per minute is observed. At both concentrations of 50 or 100 µM, all compounds tested determined a significant recovery in worm mobility (compared to non-treated *C. elegans* CL2120, Figure 39). In particular, Cur5 and cur6 shown a higher efficacy, especially at the concentration of 100 µM, in rescuing the $A\beta_{3-42}$ phenotype.

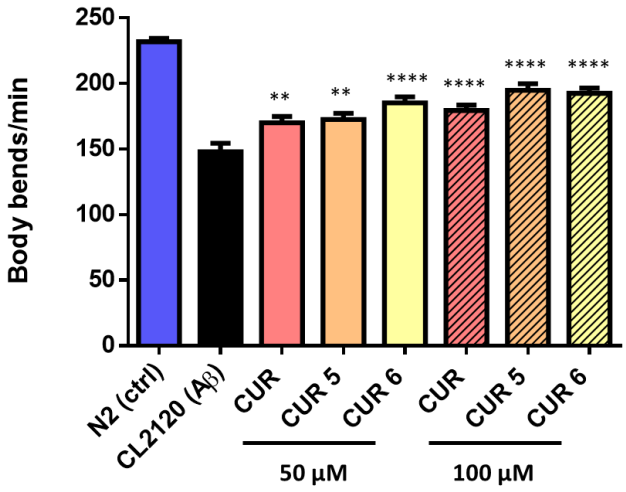

Figure 39. Effect of curcumin (CUR), Cur6 and Cur5 (100 µM and 50 µM) on behavioural phenotype of *C. elegans*. Body bends assay was performed in triplicate on adult worms after 48 h exposure to small molecules. Data are mean ±SD (N=30 animals for each group); ***p*<0.01 and *****p*<0.0001 versus not-treated CL2120 according to one-way ANOVA. N2 is the non mutated strain, CL2120 is the AD strain.

Based on this promising data, I tried to test the curcumin analogues by INVAPP paragon system by using the improved model of Alzheimer's disease strain expressing the full-length $A\beta_{1-42}$.

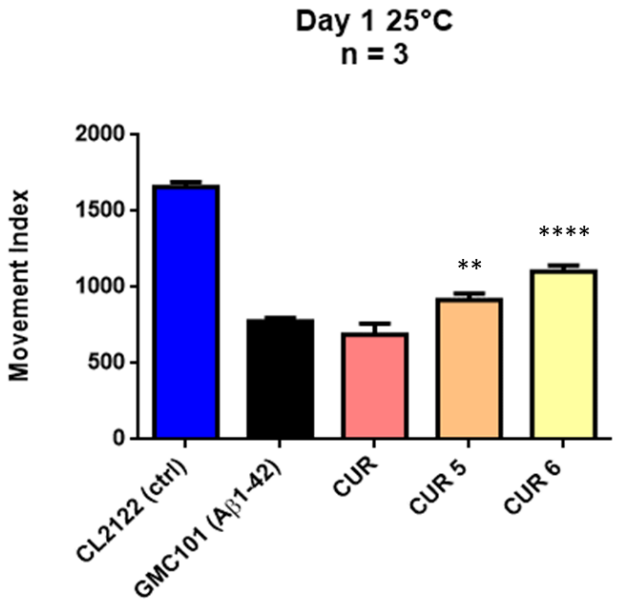

Figure 40. Curcumin analogues screening on GMC101 worms expressing $A\beta_{1-42}$ peptide. Worms were grown at 25°C in 96-well plates in the presence of EtOH or compounds at the concentration of 30 µM in 96-well plates. CL2122 worms, not expressing the amyloidogenic peptide, were used as healthy controls. Three independent assays were performed. ***p*<0.01 and *****p*<0.0001 versus not-treated GMC101 according to one-way ANOVA.

In this preliminary experiment as reported in Fig. 40, I showed the CUR5 and CUR6 efficacy in restoring the abnormal phenotype of transgenic *C. elegans* expressing Aβ peptide, tested at the concentration of 30 µM. On the contrary, in the tested conditions, curcumin has shown to have no effect.

Considering those data, I cannot exclude that the absence of effect of curcumin may be related to the known intrinsic toxicity if this compound (Nelson et al. 2017).

Furthers experiment will be performed and more concentrations will be tested in order to evaluate this effect.

4.2. Library-scale screening on *C. elegans* strains

In recent years, the number of small molecule disrupting protein-protein interactions (PPIs) has grown rapidly partly due to the improvement of *in silico* drug discovery methods. PPIs are now considered as the next generation of very promising therapeutic targets (Morelli et al. 2011). Following those considerations, a hand-curated database of protein-protein interactors' inhibitors (2P2I), has been created (Basse et al. 2016, Basse et al. 2013).

2P2I database (http://2p2idb.cnrs-mrs.fr/) is dedicated to the structure of protein-protein complexes with known small molecule inhibitors. They have selected from the PDB, 31 PPIs and 242 small molecule inhibitors found at the interface (Table 7). Interfaces in $2P2I_{DB}$ have been analysed in terms of geometrical parameters, atom and residue properties, buried accessible surface area and other biophysical parameters and compared to those of representative datasets of heterodimeric complexes.

Family	AB	K_d[a] (μM)	A	AL	Ligand[b]	MW[c]	Kd[d] (μM)	PSA/100 Å^2	BEI	SEI
Bcl/Bak	1BXL	0.34	1R2D	1YSI	1YSI	N3B	552	0.036[f]	1.37	13.48
					2O22	LIU	597	0.067[f]	1.58	12.01
					2YXJ	N3C[e]	813	0.001[f]	1.47	11.07
HDM2/p53	1YCR	0.6	1Z1M	1RV1	IMZ	686	0.14[g]	0.67	9.99	10.22
				1T4E	DIZ	581	0.08	0.67	12.21	10.59
				3JZK	YIN	536	1.23[g]	0.40	11.05	14.80
XDM2/p53	1YCQ	n/a	1Z1M	1TTV	IMY	567	0.16[g]	0.66	11.97	10.3
HDM4/p53	3DAB	0.21	3JZO	3LBJ	WW8	630	n/a	0.60	n/a	n/a
Xiap/Caspase 9	1NW9	75	1F9X	1TFQ	998	443	0.012	0.91	17.88	8.70
				1TFT	997	535	0.005	1.00	15.52	8.30
				2JK7	BI6	487	0.067[f]	0.91	14.73	7.88
				2OPY	CO9	439	30	1.55	10.28	2.92
				3CM2	X23	492	0.34[f]	1.31	13.15	4.94
				3G76	CZ3	969	0.23[g]	2.44	6.78	2.72
				3HL5	9JZ	507	34[f]	1.16	8.81	3.85
Xiap/Smac	1G73	n/a	2VSL	2JK7	BI6	487	0.067[f]	0.91	14.73	7.88
				2OPY	CO9	439	30	1.55	10.28	2.92
				3CM2	X23	492	0.34[f]	1.31	13.15	4.94
ZipA/FtsZ	1F47	21.6	1F46	1Y2F	WAI	424	12	0.52	11.61	9.46
				1Y2G	CL3	343	83	0.63	11.90	6.48
HPV E2/E1	1TUE	0.06	1QQH	1R6N	434	608	0.04	1.44	12.17	5.14
IL-2/IL-2R	1Z92	0.01	1M47	1M48	FRG	447	8.2	0.65	11.38	7.82
				1PW6	FRB	534	6[g]	0.77	9.78	6.78
				1PY2	FRH	663	0.06[g]	1.26	10.89	5.73
Integrase/LEDGFp75	2B4J	0.01	2ITG	3LPT	723	314	n/a	0.47	n/a	n/a
TNF-α/TNFRc1	1TNF	n/a	2E7A	2AZ5	307	548	22[g]	0.38	8.50	12.25
TNFR1A/TNFB	1TNR	n/a	1EXT	1FT4	703	457	0.27[g]	1.44	14.37	4.56

Table 7. Families of protein–protein and protein–ligand complexes in the freely available 2P2I database (http://2p2idb.cnrs-mrs.fr) and binding efficiency indices of the ligands. The PDB codes of the protein–protein complexes (AB), unbound proteins (A) or protein–inhibitors

complexes (AL) are given. At least one PPI inhibitor is indicated for each PPI target family. The ligand three-letter codes (as defined in the PDB files) of 24 representative small molecule inhibitors out of 39 in 2P2IDB are shown as well as binding constants. When possible, binding efficiency (BEI) and surface efficiency (SEI) indexes are calculated. Where a direct binding dissociation constant was not available, Ki or IC50 values were used instead. n/a: not available. a) Protein–protein dissociation constants, b) Ligand 3-Letter code as defined in the PDB chemical component dictionary, c) Ligand MW in g mol_1, d) Protein–ligand binding constants (kd, ki or IC50), e) Compound ABT-737, f) Ki, g IC50 (Morelli et al. 2011).

Dr. Graham Wynne (Oxford University), collaborator of Professor Sattelle, has designed a library of about 1000 molecules which are potential 2P2I starting from a small set of reference molecules that can be found on PPIs database (Figure 41).
During my stay at UCL, in Sattelle's lab, I had the chance to test this library *in vivo* on *C. elegans* transgenic strains.
Our idea was to screen the library in order to see if we can find any candidate able to interfere with the mechanisms of toxicity implicated in *C. elegans* models expressing amyloidogenic proteins. First, I decided to focus my attention on the well-characterized GMC101 strain (McColl et al. 2012) that expresses $A\beta_{1-42}$ peptide in the muscle cells of the worms and I tested the library by applying the INVAPP/Paragon automated system of phenotyping (Partridge et al. 2018) looking for phenotypic rescue of worms' motility.

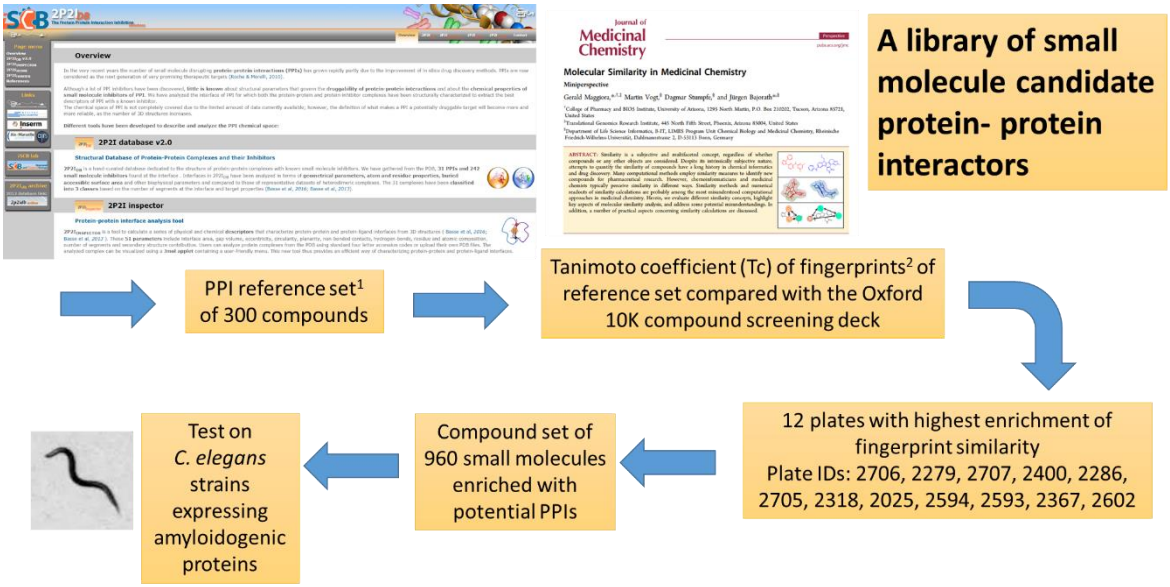

1. http://2p2idb.cnrs-mrs.fr/index.html
2. https://pubs.acs.org/doi/pdf/10.1021/jm401411z

Figure 41. Schematic representation of the procedure adopted by Dr. Graham Wynne for the rational design of 2P2I library.

4.2.1. Methods

- ***C. elegans motility and growth assays***

C. elegans strains were maintained at 20 °C on nematode growth medium agar seeded with the E. *coli* strain OP50. To obtain worms for screening, a mixed-stage liquid culture was prepared by washing well-fed worms from one small NGM plate into a medium of 50 ml S-complete buffer with a pellet of approximately 2–3 g E. *coli* HB101. Cultures were agitated at 200 rpm, 18 °C approximately for five days, and then L1 larvae were filtered. For the screening assay, C. *elegans* were cultured in a 96-well plate format. Synchronised L1 were diluted to approximately 25-30 worms per 100 µl in S complete medium with around 1% w/v HB101 *E. coli*. Assay plates were prepared with 100 µl of L1 suspension and 1 µl of DMSO or compound in DMSO solution per well. Final DMSO concentration was 1% v/v. Plates were incubated at 25 °C before imaging using the INVAPP/Paragon system 3-4 days later. Whole-plate 200 frame movies were recorded at 30 frames per second (7 s total). For the panel screen, we screened n= 4 wells for each concentration, with each replicate concentration on different plates.

- **Library of Protein-protein-interactors inhibitor's**

The library was provided from Oxford University as 10 mM solutions in DMSO in 96 well plates. It was then screened in the *C. elegans* growth assay as described (final concentration 100 µM, n=4, 1% v/v final DMSO).

4.2.2. Results

We applied the INVAPP/Paragon assay system to the identification of novel protein-protein interactor's inhibitors with potential for anti-aggregation activity. The library was provided from Dr. Graham Wynne as reported before. Recent successes in the Inhibition of Protein–Protein Interactions with small molecules have emerged from both academic and private research as a new way to modulate the activity of proteins and generate new drugs against this tremendous reservoir of potential targets (Morelli et al. 2011).

The library is composed of about 1000 molecules, which are 2P2I. We screened the library composed by 12 separate 96 well plate sets in a blinded fashion approach (see Figure 42 for plates IDs). We tested all the compounds on transgenic worms commencing from L1 larvae incubated at 25°C in order to enhance the age-dependent paralysis phenotype (McColl et al. 2012) by using the INVAPP/Paragon *C. elegans* motility assay. A plot showing the results of this screen is shown in Figure 42 (N=4). As it can be appreciated in the figure, the movement index for the strain expressing Aß peptide is reduced if compared to the controls. Each symbol in the graph represents a single compound tested at the concentration of 100 µM. From our screening, we were able to identify some molecules that are capable of increasing the movement index parameter for the Abeta worms reported in table 8.

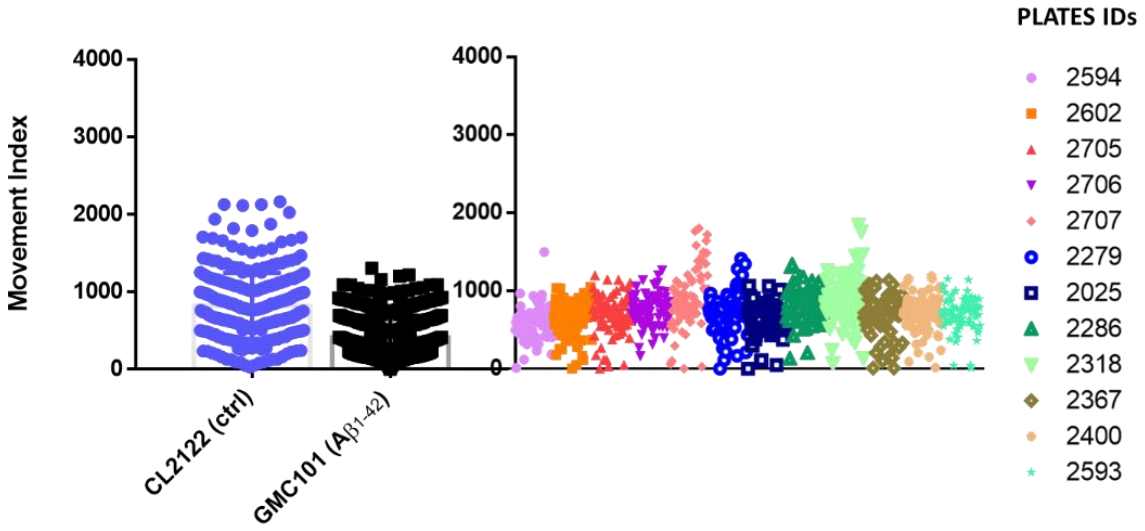

Figure 42. PPIs library screening on worms expressing Aβeta peptide. Worms were grown at 25°C in 96-well plates in the presence of DMSO or compounds at the of 100 µM. 12 plates

were screened containing in each well a compound from the 960 PPIs library. CL2122 worms, not expressing the amyloidogenic peptide, were used as healthy controls. Three independent assays were performed.

Plate ID	Wells showing movement index rescue
2318	C11, E10
2707	D8, F8, C11, D11, E11
2594	E9
2279	C10, C11, D9

Table 8. Wells showing motility rescue in the library screening. Each well correspond to a different compound from plates with ID codes: 2318, 2707, 2594, 2279.

To confirm identity of the hit molecules, we focused on the top 11 putative hit compounds (Table 8) in a secondary screen using the same INVAPP/Paragon *C. elegans* motility assay as before (Fig. 43).

Those data confirmed the preliminary results reported in figure 42. With this approach, I was able to select 11 molecules of interest whose structures cannot be disclosed for potential patentability. However, we can say that the molecules selected as putative HIT compounds present some structural similarities.
Further experiments are needed in order to characterize the dose-dependent activity of those compounds and to define their mechanism of action.

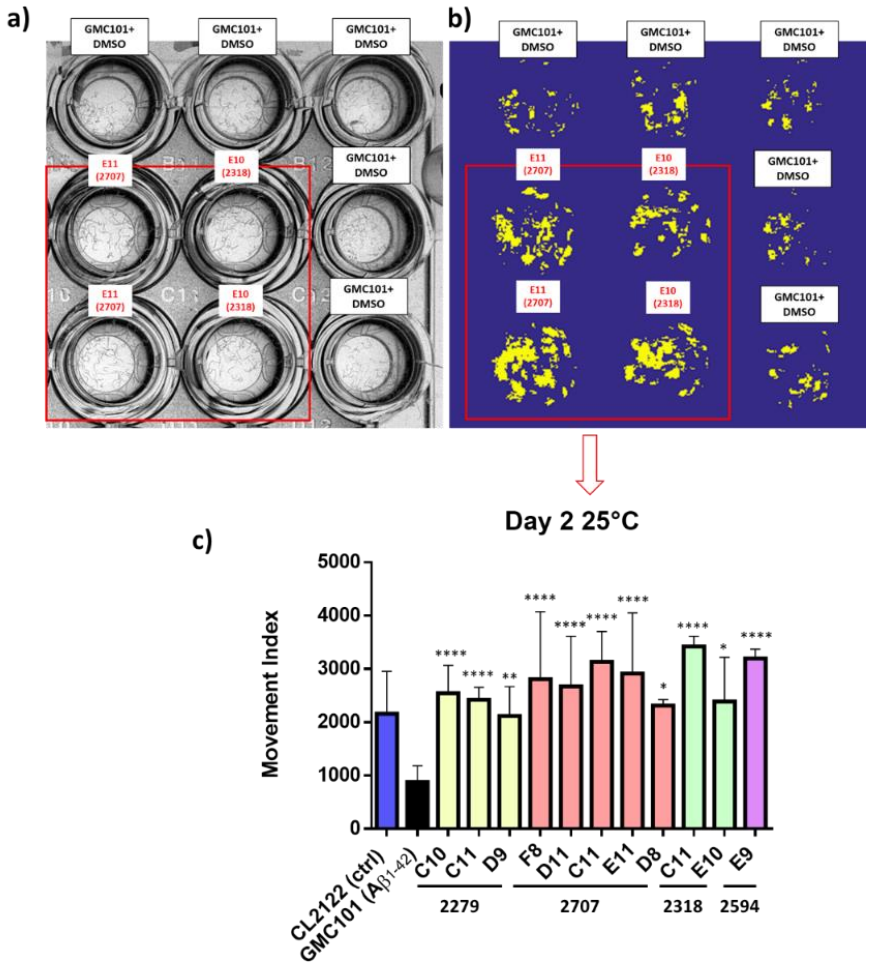

Figure 43. Motility assay using INVAPP/Paragon system. **a)** Image showing a portion of a 96-well plate used for the screening. Wells containing GMC101 worms treated with 100 µM compounds were highlighted in red. **b)** Diagnostic image in which motile pixels have been identified given by the INVAPP/Paragon system of the same portion of plate depicted in a). **c)** Movement index parameter for GMC101 worms treated with DMSO or with compounds. The CL2122 strain was used as control strain. *p<0.05, p<0.01 and ****p< 0.0001 vs DMSO treated GMC101 according to one-way Anova (GraphPad prism, v6).

Chapter 5: Discussion

Systemic amyloidosis is a fatal disease caused by misfolding of native globular proteins that then aggregate extracellularly as insoluble fibrils, damaging structure and function of affected organs. It is responsible for about one per thousand of all deaths in developed countries (Pepys 2006). Amyloidosis can occasionally be hereditary but it is largely an acquired, age-related condition and, as life expectancy increases, it has become increasingly important. Despite much progress in understanding amyloid fibrillogenesis *in vitro*, the formation of amyloid fibrils *in vivo* is poorly understood. Comprehensive elucidation of the processes operating under physiological and pathophysiological conditions is now critical for understanding the natural history of amyloidosis, its response to treatment and, crucially, the development of new and more effective therapies.

My PhD project has been designed to address the crucial question of the mechanism of globular to fibrillary conversion of a prototypic amyloidogenic protein in conditions that closely resemble the physiological environment and investigate the efficacy of putative anti-amyloid drugs in different systems of increased level of biological complexity. Indeed, the design of my experimental strategies were all constrained to the need to operate in conditions compatible with the biologic environment.

In fact, the elucidation of the pathophysiology of the disease and the preparation of models for drug discovery, can be only trusted if they are not too far from those visited in a biologic environment. Therefore, I have been trying to combine *in vitro* and *in vivo* methods in order to get a general and broadest comprehension of the process that leads toward the deposition of amyloid fibrils (see Figure 28, Chapter 1.5).

In particular, I mainly dedicated my work on the study of two amyloidogenic proteins: β_2-microglobulin and transthyretin.

The first protein is associated with the amyloidosis of patients under chronic haemodialytic treatment, known as dialysis-related amyloidosis, but in the presence of a specific mutation causes a familial form of systemic amyloidosis. The second protein is associated with senile systemic amyloidosis (SSA) and, in mutated forms, with familial amyloid cardiomyopathy (FAC), familial amyloid polyneuropathy (FAP) and leptomeningeal amyloidosis (LA).

For both β_2-microglobulin and transthyretin, many investigations have been conducted in order to understand the molecular basis of amyloid deposition and *in vitro* models have been developed describing the process of fibrillogensis and amyloid formation (Figure 44). Moreover, the development of predictive animal models able to completely mimic the disease is a major argument of interest in each case considered.

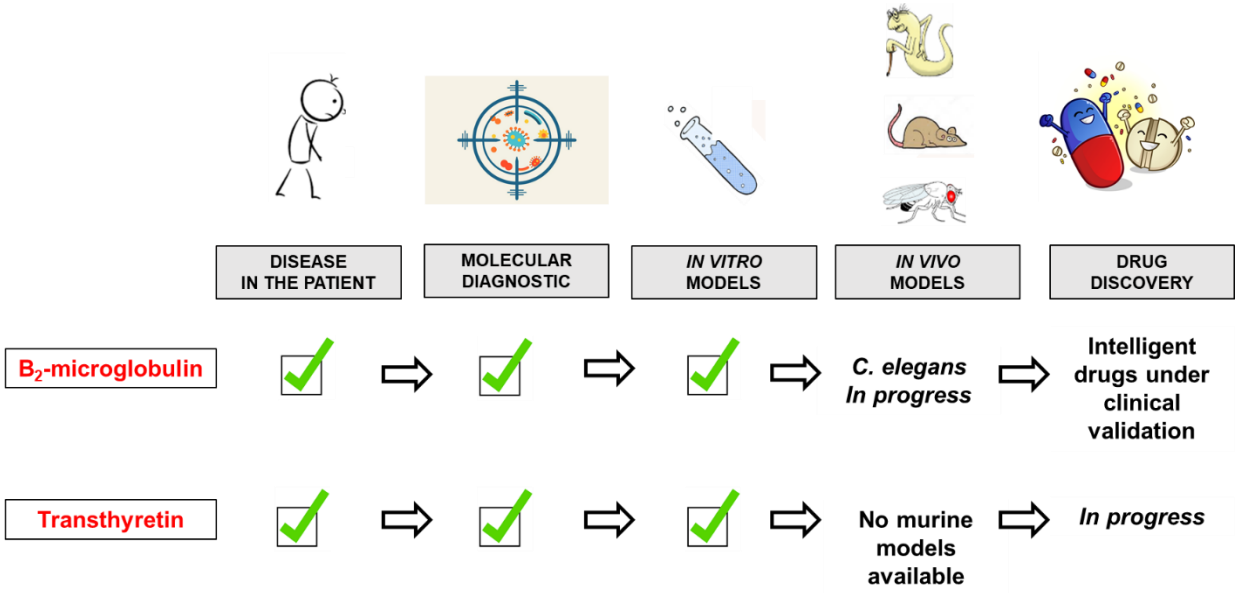

Figure 44. In the figure is depicted the state of art of the studies of two amyloidogenic proteins: β_2-microglobulin and transthyretin.

In particular, for what concerns TTR, in the absence of predictive animal models of the disease, the need of different animal or *in vitro* models has become urgent for the process of drug discovery. Recently, Madhivanan and co-workers have developed a new *C. elegans* model (Madhivanan et al. 2018) of TTR amyloidosis that exhibit aggregation and quantifiable cell nonautonomous neuronal phenotypes. However, in order to fully understand what is really happening *in vivo*, robust and reliable *in vitro* models are still essential for the identification of the process that leads towards the deposition of amyloid.

For those reasons, the first part of my thesis was addressed to the study of the *in vitro* mechanism of fibrillogenesis and aggregation of transthyretin and its isoforms.

For years, it has been widely accepted that tetramer dissociation and partial denaturation of released monomers at very low pH were the crucial and rate-limiting prerequisite for the formation of TTR amyloid fibrils (Colon and Kelly 1992). However,

there is no direct supportive evidence for this mechanism *in vivo*. Indeed, both Westermark's and Lundgren's groups have reported that the 49-127 TTR fragment is a major component of amyloid TTR fibrils (Westermark, Sletten and Johnson 1996, Thylén et al. 1993, Ihse et al. 2013), which reversely cannot be found in fibrils prepared according to Kelly's method. A key role for partial proteolysis of TTR has been proposed in the works of Mangione *et al*. 2014 and Marcoux *et al*. 2015. They demonstrated that the exposure of the highly amyloidogenic Ser52Pro variant TTR tetramer to very low-dose trypsin, under physiological conditions, rapidly generates the same residue 49-127 fragment that is found in the *ex vivo* TTR amyloid fibrils. Massive and rapid amyloid fibril formation proceeds as soon as the cleaved polypeptides are released. Later, it has been demonstrated that, by increasing the biomechanical forces generated by the combination between biological fluids flow and the connection with hydrophobic surfaces, is possible to boost the susceptibility to the proteolytic cleavage also of the more stable TTR variants, including the wild-type isoform (Marcoux et al. 2015). Therefore, in this new mechano-enzymatic mechanism, two physically different events affect the protein: partial unfolding and proteolysis. Local unfolding caused by biomechanical forces allows the action of specific proteases. Unfolding and proteolysis cannot therefore be considered as separate events, but have to be considered as integrated multiple steps at the origin of amyloid conversion of globular proteins.

The mechano-enzymatic mechanism offers a new challenge in terms of inhibition of aggregation by the mean of small ligands. Compounds able to stabilise TTR, such as tafamidis (Bulawa et al. 2012, Coelho et al. 2013), designed as drugs to treat and prevent systemic TTR amyloidosis, have been identified exclusively by their capacity to inhibit TTR dissociation and aggregation induced by low pH *in vitro*. However, even with apparently complete pharmacological stabilisation of circulating TTR, the clinical benefit observed so far is limited to modest slowing of the progression of peripheral neuropathy (Coelho et al. 2016). Considering the mechano-enzymatic pathway, we can assume that only ligands that occupy both binding sites in TTR can efficiently inhibit the process of amyloid formation. In chapter 2.1., I showed that Tolcapone, which is bound with similar high affinity in both TTR binding sites without the usual negative cooperativity, can more potently inhibits TTR fibrillogenesis than tafamidis, but neither, even in large molar excess, completely prevents amyloid fibril formation (Verona et al. 2017). Indeed, even when apparent complete inhibition of aggregation

is obtained, a careful analysis of the material obtained after aggregation highlights the presence of some amyloid aggregates that we can define as “minimal residual disease material”. The clinical significance of the presence of small residual materials not still clear but it could be relevant in the process of nucleation and propagation of amyloid. Indeed, we already demonstrated that the presence of seeds is able to notably trigger the formation of amyloid fibrils even starting from low concentrations of TTR.

However, bivalent ligands that are able to simultaneously occupy both T4 binding sites of transthyretin, such as Mds84 (Kolstoe et al. 2010), showed a superior efficacy over monovalent ligands (Verona et al. 2017). The superiority showed by bivalent ligands can be explained not only by the simultaneous occupancy of both binding sites, but also by the occupancy of the central cavity of the TTR molecule.

Even though trypsin effectively cleaves TTR and promotes its fibrillogenesis *in vitro*, one of the open questions about the mechano-enzymatic mechanism has always been the identity of the culprit protease responsible for proteolysis *in vivo*. In Chapter 2.2., I reported the bioinformatics approach that was used to identify a pool of possible candidate proteases by using MEROPS database (http://merops.sanger.ac.uk) which collects and catalogues peptidases based on their structures, function and tissue localization. The search was conducted in order to get informations about trypsin-like with tissue localization compatible with the pathofisiology of TTR related amyloidosis. Surprisingly, results have shown that plasmin, having an active site similar to the one of trypsin, displays those requirements (Mangione et al. 2018). Moreover, we demonstrated experimentally that plasmin can promote TTR fibrillogenesis in a similar fashion to trypsin, leading to the formation of genuine amyloid fibrils.

All the TTR isoforms were tested in the presence of plasmin and presented a different propensity to fibrillogenesis: as expected S52P variant rapidly aggregates in comparison to the others and to the wild-type protein. More importantly, the stable and not amyloidogenic T119M isoform was not susceptible to proteolytic cleavage in the conditions tested. Finally, the fibrillogenesis mediated by plasmin can be accelerated by the presence of fibrils *seeds*.

To conclude, it is interesting to note that plasmin is ubiquitously expressed and it is involved in the remodelling of the extracellular matrix as well as fibrinolysis. If we consider that these two events are constantly taking place in the body, it is highly

probable that plasmin represents the enzyme responsible for cleavage *in vivo*. Moreover, the discovery that the pathway of amyloidogenesis of TTR can be primed by activation of plasmin (in fibrinolysis or in extracellular matrix remodelling – see figure 5 reported in Mangione et al. 2018) shed completely new light on the natural history of the disease on the pathogenic role of cofactors. Those issues let us to consider how the genetic background can influence the individual susceptibility of the disease. This is a fundamental observation to be adressed, in particular for what concerns amyloidosis caused by wild type transthyretin. Moreover, the hypothesis of crucial role of plasmin in TTR amyloidogenesis has been strongly supported by recent data obtained at National Amyloidosis Center (Royal Free Hospital, London) in a mouse model of TTR amyloidosis. In this model, the deposition of amyloid is strongly accelerated when the α2-anti-plasmin is genetically knock-down.

Finally, the last part of Chapter 2 was focused on the comparative analysis of thermodynamic stability of fibrils derived from different procedures. A similarity, in terms of stability, was observed between the fibrils obtained with the method proposed by our research group that involves the use of trypsin and mechanical agitation, and the natural ones, thus supporting the hypothesis of the mechano-enzymatic mechanism for TTR fibrils formation in spite of Kelly's proposed mechanism.
Determination of the amyloid fibrils stability is an important tool for scrutinizing the similarities between materials prepared *in vitro* or extracted from natural sources. Thermodynamic stability of fibrils is determined by the specific intermolecular bonds and therefore its determination offers an important information complementary to the data on fibrils structure achievable through solid state NMR (Jaroniec 2019) and cryo-EM (Fitzpatrick et al. 2017). Recently several natural pathologic filaments (Fitzpatrick AWP 2017) and fibrils were analyzed through cryo-EM but a high-resolution structure of natural TTR fibrils is still missed. The ultrastructure polymorphism of amyloid fibrils emerge even from fibrils constituted by the same protein category. Different mutations, different sources of natural fibrils could influence significant structural differences. We can therefore hypothesize that specific sequences, truncations, and co-factors could influence the final structure of fibrils. The structural heterogeneity can certainly correlate with the thermodynamic stability of fibrils and subsequently with the kinetics of fibrils growth and resistance to solubilization.

The same comments made for transthyretin regarding the gap between experimetal models and the pathology in patients, may be translated to β_2-microglobulin. Also in this case, any attempt to develop murine models for the study of the disease have failed so far, although I'm aware of several attempts made in two laboratories in London and Osaka (personal communications).

However, the availability of a *C. elegans* model of dialysis-related amyloidosis (Diomede et al. 2012) and the generation of a new strain expressing its amyloidogenic variant (Faravelli and Raimondi et al. 2019, under revision by *Scientific Reports*) could contribute to reduce the gap and may be used in the search and validation of new molecules with potential therapeutic activity.

The discovery of the first mutation of β_2-m (Valleix et al. 2012), in which the disease develops without increase in its serum concentration, offered the unique opportunity to exploit the extensive knowledge on structure, misfolding propensity and amyloidogenesis of the wild type protein with emerging comparable data on the variant β_2-m (Stoppini and Bellotti 2015).

My group has previously described the phenotypes of transgenic *C. elegans* strains expressing wild type β_2-m (full length and truncated), and demonstrated that a correlation exists between the amyloidogenicity of each isoform and the biological abnormalities of the corresponding transgenic worms (Diomede et al. 2012). Based on our previous experience, we have now established a strain in which the mutated β_2-m cDNA is integrated in the *C. elegans* genome, CPV27 strain. The new strain expresses D76N β_2-m under a *myo-3* muscle promoter is controlled through a temperature-dependent transcriptional system. We are therefore able to express β_2-m in various stages of the worm's life just shifting the temperature from 16 to 23-25°C. To faithfully reproduce and study in *C. elegans* extracellular molecular dynamics that lead to β_2-m aggregation in humans, the temperature-inducible plasmid pPD118.60 was engineered with the *C. elegans* endogenous excretory *sel-1* signal peptide upstream of β_2-m sequence, to address β_2-m outside of nematodes muscle cells.

The second part of PhD project has regarded the characterization of this new transgenic *C. elegans* strain, which was called CPV27.

Despite the fact that it was not possible to detect any amyloid deposits in the worms expressing the D76N variant, we report the presence of soluble oligomers of the

protein. However, the abrogation of toxicity after silencing the β_2-m expression and the presence of high molecular species when β_2-m is normally synthesized suggests that β_2-m aggregation is the culprit event in pathologic phenotype of these strains.

The expression and accumulation of protein along the life of nematodes, as demonstrated by western blot analysis, correlate with the pathological phenotype. Indeed, thanks to our collaboration with Prof. Sattelle group (UCL, London) and by using the INVAPP/Paragon system, which was recently developed for high-throughput, plate-based chemical screening for compounds that have an effect on motility and development of parasitic worms, we were able to detect a larval growth defect in the CPV27 strain expressing the amyloidogenic protein. The reduction in the movement index given by the automated system is only partially due to the movement defect of CPV27 β_2-m expressing worms as showed by body bends assay. Moreover, it was observed that β_2-microglobulin expression increases the physiological embryonic lethality of nematodes and induces a reduction in worm's fertility.

Finally, the INVAPP/Paragon system has confirmed the efficacy of doxycycline, a drug able to inhibit β_2-m fibrillogenesis both *in vitro* (Giorgetti et al. 2011) and *in vivo* (Diomede et al. 2012), in rescuing the defective motility phenotype. More importantly, using doxycycline we successfully observed a reduction of the oligomeric β_2-m species in nematodes treated with this drug.

The mechanism of toxicity of β_2-m aggregates is still unclear. The demonstration that pre-amyloid aggregates are responsible for some pathologic features of this transgenic strain, further support the research of β_2-m oligomers in patients as early markers of the disease's activity.

Through this work (Faravelli & Raimondi et al. 2019, under a second revision by *Scientific Reports*), we can now offer to the scientific community the first model of an animal expressing the pathogenic variant of β_2-m and considering the failure, so far, to obtain a mouse model that recapitulates the features of β_2-m related amyloidosis. Our *C. elegans* system can be considered the best pre-clinical biologic model for drug discovery in this disease.

Considering our promising results obtained with the characterization of CPV27 *C. elegans* strain expressing D76N β_2-m, we are planning to continue the search of new molecules able to counteract β_2-m toxicity. In particular, my plan is to test a nanobody, which is called Nanobody24 (Nb24), for its efficacy in reverting the motility defect of

D76N β_2-m expressing worms. Nb24 has been shown to be effective in the inhibition of β_2-m fibrillogenesis *in vitro* (Raimondi et al. 2017).

Moreover, the availability of the new temperature-sensitive sterile worm strains, whose characterization has been discussed in Chapter 3.2., will help in performing drug screenings on a population of aged *C. elegans*. Furthermore, proteomic analysis would help to further characterize the pattern of protein expression of *C. elegans* transgenic strains expressing amyloidogenic proteins in comparison with not-pathological controls.

Since there is a growing interest in the scientific community on the development of high-throughput screening methods for both small molecules and macromolecules, the possibility to use an automated assay for *C. elegans* phenotyping proves to be crucial in the process of finding new drug candidates for the treatment of human diseases.

During my PhD, I have established a very successful and productive collaboration with Professor David Sattelle (UCL, London), and therefore I have had the possibility to use the automated system of *C. elegans* phenotyping available in his lab (Partridge et al. 2018). Through this system, I was able to test some molecules on well-characterized worm's models of Alzheimer's disease. First, by performing body bends assay, I demonstrated the efficacy *in vivo* in the rescuing of worms pathological phenotype of two curcumin related compounds, which were identified by Federica Betulli (University of Bologna) and whose efficacy *in vitro* was assessed by the group of Professor Ersilia De Lorenzi at University of Pavia (Bisceglia et al. 2019). Those data, which are reported in Chapter 4.1., were subsequently validated by using the INVAPP/Paragon system of phenotyping confirming the higher efficacy of the curcumin derivatives if compared to curcumin.

The second approach, which was followed and described in Chapter 4.2., has involved a large-scale screening of a library of protein-protein interactors' inhibitors (2P2I) which was designed by Dr. Graham Wynne in Oxford. The molecules used in this screen were designed starting from a structural database of protein-protein complexes and their Inhibitors that is available online (http://2p2idb.cnrs-mrs.fr/) (Basse et al. 2016). Surprisingly, starting from a library of about 1000 compounds, we were able to select 11 putative HITs compounds that are capable to revert the motility impairment of GMC101 *C. elegans* worms expressing Aβeta$_{1-42}$ peptide. The structural identities of

those molecules cannot be disclosed for potential patentability. However, some of the compounds identified are structural-related. Further experiments will be necessary in order to further dissect the mechanisms of action of the molecules selected and in order to perform dose-response curves.

Considering those promising results, my aim will be to test the same library of 2P2I also on the CPV27 worms expressing the amyloidogenic variant of β_2-m in order to evaluate if we can find any effective molecule able to act and improve their pathological phenotype.

Bibliography

Adams, D., A. Gonzalez-Duarte, W. D. O'Riordan, C. C. Yang, M. Ueda, A. V. Kristen, I. Tournev, H. H. Schmidt, T. Coelho, J. L. Berk, K. P. Lin, G. Vita, S. Attarian, V. Planté-Bordeneuve, M. M. Mezei, J. M. Campistol, J. Buades, T. H. Brannagan, B. J. Kim, J. Oh, Y. Parman, Y. Sekijima, P. N. Hawkins, S. D. Solomon, M. Polydefkis, P. J. Dyck, P. J. Gandhi, S. Goyal, J. Chen, A. L. Strahs, S. V. Nochur, M. T. Sweetser, P. P. Garg, A. K. Vaishnaw, J. A. Gollob & O. B. Suhr (2018) Patisiran, an RNAi Therapeutic, for Hereditary Transthyretin Amyloidosis. *N Engl J Med,* 379**,** 11-21.

Alavez, S., M. C. Vantipalli, D. J. Zucker, I. M. Klang & G. J. Lithgow (2011) Amyloid-binding compounds maintain protein homeostasis during ageing and extend lifespan. *Nature,* 472**,** 226-9.

Aprile, F. A., P. Sormanni, M. Perni, P. Arosio, S. Linse, T. P. J. Knowles, C. M. Dobson & M. Vendruscolo (2017) Selective targeting of primary and secondary nucleation pathways in Abeta42 aggregation using a rational antibody scanning method. *Sci Adv,* 3**,** e1700488.

Arosio, P., T. P. Knowles & S. Linse (2015) On the lag phase in amyloid fibril formation. *Phys Chem Chem Phys,* 17**,** 7606-18.

Avery, L. & B. B. Shtonda (2003) Food transport in the C. elegans pharynx. *J Exp Biol,* 206**,** 2441-57.

Barrière, A. & M. A. Félix (2014) Isolation of C. elegans and related nematodes. *WormBook***,** 1-19.

Basse, M. J., S. Betzi, R. Bourgeas, S. Bouzidi, B. Chetrit, V. Hamon, X. Morelli & P. Roche (2013) 2P2Idb: a structural database dedicated to orthosteric modulation of protein-protein interactions. *Nucleic Acids Res,* 41**,** D824-7.

Basse, M. J., S. Betzi, X. Morelli & P. Roche (2016) 2P2Idb v2: update of a structural database dedicated to orthosteric modulation of protein-protein interactions. *Database (Oxford),* 2016.

Bellotti, V., P. Mangione & M. Stoppini (1999) Biological activity and pathological implications of misfolded proteins. *Cell Mol Life Sci,* 55**,** 977-91.

Benilova, I., E. Karran & B. De Strooper (2012) The toxic Aβ oligomer and Alzheimer's disease: an emperor in need of clothes. *Nat Neurosci,* 15**,** 349-57.

Benkemoun, L., R. Sabaté, L. Malato, S. Dos Reis, H. Dalstra, S. J. Saupe & M. L. Maddelein (2006) Methods for the in vivo and in vitro analysis of [Het-s] prion infectivity. *Methods,* 39**,** 61-7.

Benson, M. D. & J. C. Kincaid (2007) The molecular biology and clinical features of amyloid neuropathy. *Muscle Nerve,* 36**,** 411-23.

Bisceglia, F., F. Seghetti, M. Serra, M. Zusso, S. Gervasoni, L. Verga, G. Vistoli, C. Lanni, M. Catanzaro, E. De Lorenzi & F. Belluti (2019) Prenylated Curcumin Analogues as Multipotent Tools To Tackle Alzheimer's Disease. *ACS Chem Neurosci,* 10**,** 1420-1433.

Blake, C. C., M. J. Geisow, S. J. Oatley, B. Rérat & C. Rérat (1978) Structure of prealbumin: secondary, tertiary and quaternary interactions determined by Fourier refinement at 1.8 A. *J Mol Biol,* 121**,** 339-56.

Blancas-Mejía, L. M. & M. Ramirez-Alvarado (2013) Systemic amyloidoses. *Annu Rev Biochem,* 82**,** 745-74.

Bleiholder, C., N. F. Dupuis, T. Wyttenbach & M. T. Bowers (2011) Ion mobility-mass spectrometry reveals a conformational conversion from random assembly to β-sheet in amyloid fibril formation. *Nat Chem,* 3**,** 172-7.

Bois, M. C., S. Dasari, J. R. Mills, J. Theis, W. E. Highsmith, J. A. Vrana, M. Grogan, A. Dispenzieri, P. J. Kurtin & J. J. Maleszewski (2017) Apolipoprotein A-IV-Associated Cardiac Amyloidosis. *J Am Coll Cardiol,* 69**,** 2248-2249.

Bolen, D. W. & M. M. Santoro (1988) Unfolding free energy changes determined by the linear extrapolation method. 2. Incorporation of delta G degrees N-U values in a thermodynamic cycle. *Biochemistry,* 27**,** 8069-74.

Brenner, S. (1973) The genetics of behaviour. *Br Med Bull,* 29**,** 269-71.

--- (2002) The worm's turn. *Curr Biol,* 12**,** R713.

Brunquell, J., P. Bowers & S. D. Westerheide (2014) Fluorodeoxyuridine enhances the heat shock response and decreases polyglutamine aggregation in an HSF-1-dependent manner in Caenorhabditis elegans. *Mech Ageing Dev,* 141-142**,** 1-4.

Bulawa, C. E., S. Connelly, M. Devit, L. Wang, C. Weigel, J. A. Fleming, J. Packman, E. T. Powers, R. L. Wiseman, T. R. Foss, I. A. Wilson, J. W. Kelly & R. Labaudinière (2012) Tafamidis, a potent and selective transthyretin kinetic stabilizer that inhibits the amyloid cascade. *Proc Natl Acad Sci U S A,* 109**,** 9629-34.

Burns, A. R., I. M. Wallace, J. Wildenhain, M. Tyers, G. Giaever, G. D. Bader, C. Nislow, S. R. Cutler & P. J. Roy (2010) A predictive model for drug bioaccumulation and bioactivity in Caenorhabditis elegans. *Nat Chem Biol,* 6**,** 549-57.

Carretero, M., G. M. Solis & M. Petrascheck (2017) C. elegans as Model for Drug Discovery. *Curr Top Med Chem,* 17**,** 2067-2076.

Cassada, R. C. & R. L. Russell (1975) The dauerlarva, a post-embryonic developmental variant of the nematode Caenorhabditis elegans. *Dev Biol,* 46**,** 326-42.

Chen, X. Q. & W. C. Mobley (2019) Alzheimer Disease Pathogenesis: Insights From Molecular and Cellular Biology Studies of Oligomeric Aβ and Tau Species. *Front Neurosci,* 13**,** 659.

Chiti, F. & C. M. Dobson (2006) Protein misfolding, functional amyloid, and human disease. *Annu Rev Biochem,* 75**,** 333-66.

--- (2017) Protein Misfolding, Amyloid Formation, and Human Disease: A Summary of Progress Over the Last Decade. *Annu Rev Biochem,* 86**,** 27-68.

Choi, H., W. Lee, G. Lee, D. S. Yoon & S. Na (2019) The formation mechanism of segmented ring-shaped Aβ oligomers and protofibrils. *ACS Chem Neurosci*.

Coelho, T., L. F. Maia, A. M. da Silva, M. W. Cruz, V. Planté-Bordeneuve, O. B. Suhr, I. Conceiçao, H. H. Schmidt, P. Trigo, J. W. Kelly, R. Labaudinière, J. Chan, J. Packman & D. R. Grogan (2013) Long-term effects of tafamidis for the treatment of transthyretin familial amyloid polyneuropathy. *J Neurol,* 260**,** 2802-14.

Coelho, T., G. Merlini, C. E. Bulawa, J. A. Fleming, D. P. Judge, J. W. Kelly, M. S. Maurer, V. Planté-Bordeneuve, R. Labaudinière, R. Mundayat, S. Riley, I. Lombardo & P. Huertas (2016) Mechanism of Action and Clinical Application of Tafamidis in Hereditary Transthyretin Amyloidosis. *Neurol Ther,* 5**,** 1-25.

Coker, A. R., A. Purvis, D. Baker, M. B. Pepys & S. P. Wood (2000) Molecular chaperone properties of serum amyloid P component. *FEBS Lett,* 473**,** 199-202.

Colon, W. & J. W. Kelly (1992) Partial denaturation of transthyretin is sufficient for amyloid fibril formation in vitro. *Biochemistry,* 31**,** 8654-60.

Corsi, A. K., B. Wightman & M. Chalfie (2015) A Transparent Window into Biology: A Primer on Caenorhabditis elegans. *Genetics,* 200**,** 387-407.

Culetto, E. & D. B. Sattelle (2000) A role for Caenorhabditis elegans in understanding the function and interactions of human disease genes. *Hum Mol Genet,* 9**,** 869-77.

Diomede, L., G. Cassata, F. Fiordaliso, M. Salio, D. Ami, A. Natalello, S. M. Doglia, A. De Luigi & M. Salmona (2010) Tetracycline and its analogues protect Caenorhabditis elegans from β amyloid-induced toxicity by targeting oligomers. *Neurobiol Dis,* 40**,** 424-31.

Diomede, L., C. Soria, M. Romeo, S. Giorgetti, L. Marchese, P. P. Mangione, R. Porcari, I. Zorzoli, M. Salmona, V. Bellotti & M. Stoppini (2012) C. elegans expressing human beta2-microglobulin: a novel model for studying the relationship between the molecular assembly and the toxic phenotype. *PLoS One,* 7**,** e52314.

Dungu, J. N., L. J. Anderson, C. J. Whelan & P. N. Hawkins (2012) Cardiac transthyretin amyloidosis. *Heart,* 98**,** 1546-54.

Dwulet, F. E. & M. D. Benson (1984) Primary structure of an amyloid prealbumin and its plasma precursor in a heredofamilial polyneuropathy of Swedish origin. *Proc Natl Acad Sci U S A,* 81**,** 694-8.

-- (1987) Primary structure of amyloid fibril protein AA in azocasein-induced amyloidosis of CBA/J mice. *J Lab Clin Med,* 110**,** 322-9.

Eichner, T. & S. E. Radford (2011) Understanding the complex mechanisms of β2-microglobulin amyloid assembly. *FEBS J,* 278**,** 3868-83.

Esposito, G., R. Michelutti, G. Verdone, P. Viglino, H. Hernandez, C. V. Robinson, A. Amoresano, F. Dal Piaz, M. Monti, P. Pucci, P. Mangione, M. Stoppini, G. Merlini, G. Ferri & V. Bellotti (2000) Removal of the N-terminal hexapeptide from human beta2-microglobulin facilitates protein aggregation and fibril formation. *Protein Sci,* 9**,** 831-45.

Fay, D. S., A. Fluet, C. J. Johnson & C. D. Link (1998) In vivo aggregation of beta-amyloid peptide variants. *J Neurochem,* 71**,** 1616-25.

Fielenbach, N. & A. Antebi (2008) C. elegans dauer formation and the molecular basis of plasticity. *Genes Dev,* 22**,** 2149-65.

Fire, A., S. Xu, M. K. Montgomery, S. A. Kostas, S. E. Driver & C. C. Mello (1998) Potent and specific genetic interference by double-stranded RNA in Caenorhabditis elegans. *Nature,* 391**,** 806-11.

Fitzpatrick, A. W. P., B. Falcon, S. He, A. G. Murzin, G. Murshudov, H. J. Garringer, R. A. Crowther, B. Ghetti, M. Goedert & S. H. W. Scheres (2017) Cryo-EM structures of tau filaments from Alzheimer's disease. *Nature,* 547**,** 185-190.

Félix, M. A. (2008) RNA interference in nematodes and the chance that favored Sydney Brenner. *J Biol,* 7**,** 34.

Gejyo, F., T. Yamada, S. Odani, Y. Nakagawa, M. Arakawa, T. Kunitomo, H. Kataoka, M. Suzuki, Y. Hirasawa & T. Shirahama (1985) A new form of amyloid protein associated with chronic hemodialysis was identified as beta 2-microglobulin. *Biochem Biophys Res Commun,* 129**,** 701-6.

Giacomotto, J. & L. Ségalat (2010) High-throughput screening and small animal models, where are we? *Br J Pharmacol,* 160**,** 204-16.

Gillmore, J. D. & P. N. Hawkins (2013) Pathophysiology and treatment of systemic amyloidosis. *Nat Rev Nephrol,* 9**,** 574-86.

Gillmore, J. D., P. N. Hawkins & M. B. Pepys (1997) Amyloidosis: a review of recent diagnostic and therapeutic developments. *Br J Haematol,* 99**,** 245-56.

Giorgetti, S., S. Raimondi, K. Pagano, A. Relini, M. Bucciantini, A. Corazza, F. Fogolari, L. Codutti, M. Salmona, P. Mangione, L. Colombo, A. De Luigi, R. Porcari, A.

Gliozzi, M. Stefani, G. Esposito, V. Bellotti & M. Stoppini (2011) Effect of tetracyclines on the dynamics of formation and destructuration of beta2-microglobulin amyloid fibrils. *J Biol Chem,* 286**,** 2121-31.

Giorgetti, S., A. Rossi, P. Mangione, S. Raimondi, S. Marini, M. Stoppini, A. Corazza, P. Viglino, G. Esposito, G. Cetta, G. Merlini & V. Bellotti (2005) Beta2-microglobulin isoforms display an heterogeneous affinity for type I collagen. *Protein Sci,* 14**,** 696-702.

Gosai, S. J., J. H. Kwak, C. J. Luke, O. S. Long, D. E. King, K. J. Kovatch, P. A. Johnston, T. Y. Shun, J. S. Lazo, D. H. Perlmutter, G. A. Silverman & S. C. Pak (2010) Automated high-content live animal drug screening using C. elegans expressing the aggregation prone serpin α1-antitrypsin Z. *PLoS One,* 5**,** e15460.

Grant, B. & I. Greenwald (1997) Structure, function, and expression of SEL-1, a negative regulator of LIN-12 and GLP-1 in C. elegans. *Development,* 124**,** 637-44.

Grant, B. D. & M. Sato (2006) Intracellular trafficking. *WormBook***,** 1-9.

Gravato-Nobre, M. J., H. R. Nicholas, R. Nijland, D. O'Rourke, D. E. Whittington, K. J. Yook & J. Hodgkin (2005) Multiple genes affect sensitivity of Caenorhabditis elegans to the bacterial pathogen Microbacterium nematophilum. *Genetics,* 171**,** 1033-45.

Griffin, E. F., K. A. Caldwell & G. A. Caldwell (2017) Genetic and Pharmacological Discovery for Alzheimer's Disease Using Caenorhabditis elegans. *ACS Chem Neurosci,* 8**,** 2596-2606.

Hardy, J. A. & G. A. Higgins (1992) Alzheimer's disease: the amyloid cascade hypothesis. *Science,* 256**,** 184-5.

Harper, J. D. & P. T. Lansbury (1997) Models of amyloid seeding in Alzheimer's disease and scrapie: mechanistic truths and physiological consequences of the time-dependent solubility of amyloid proteins. *Annu Rev Biochem,* 66**,** 385-407.

Hartl, F. U., A. Bracher & M. Hayer-Hartl (2011) Molecular chaperones in protein folding and proteostasis. *Nature,* 475**,** 324-32.

Hayden, E. Y. & D. B. Teplow (2013) Amyloid β-protein oligomers and Alzheimer's disease. *Alzheimers Res Ther,* 5**,** 60.

Hillier, L. W., A. Coulson, J. I. Murray, Z. Bao, J. E. Sulston & R. H. Waterston (2005) Genomics in C. elegans: so many genes, such a little worm. *Genome Res,* 15**,** 1651-60.

Hulme, S. E. & G. M. Whitesides (2011) Chemistry and the worm: Caenorhabditis elegans as a platform for integrating chemical and biological research. *Angew Chem Int Ed Engl,* 50**,** 4774-807.

Hurshman, A. R., J. T. White, E. T. Powers & J. W. Kelly (2004) Transthyretin aggregation under partially denaturing conditions is a downhill polymerization. *Biochemistry,* 43**,** 7365-81.

Ibrahim, R. B., Y. T. Liu, S. Y. Yeh & J. W. Tsai (2019) Contributions of Animal Models to the Mechanisms and Therapies of Transthyretin Amyloidosis. *Front Physiol,* 10**,** 338.

Ihse, E., C. Rapezzi, G. Merlini, M. D. Benson, Y. Ando, O. B. Suhr, S. Ikeda, F. Lavatelli, L. Obici, C. C. Quarta, O. Leone, H. Jono, M. Ueda, M. Lorenzini, J. Liepnieks, T. Ohshima, M. Tasaki, T. Yamashita & P. Westermark (2013) Amyloid fibrils containing fragmented ATTR may be the standard fibril composition in ATTR amyloidosis. *Amyloid,* 20**,** 142-50.

Jaroniec, C. P. (2019) Two decades of progress in structural and dynamic studies of amyloids by solid-state NMR. *J Magn Reson,* 306**,** 42-47.
Johnstone, I. L., Y. Shafi & J. D. Barry (1992) Molecular analysis of mutations in the Caenorhabditis elegans collagen gene dpy-7. *EMBO J,* 11**,** 3857-63.
Kabat, E. A., D. H. Moore & H. Landow (1942) AN ELECTROPHORETIC STUDY OF THE PROTEIN COMPONENTS IN CEREBROSPINAL FLUID AND THEIR RELATIONSHIP TO THE SERUM PROTEINS. *J Clin Invest,* 21**,** 571-7.
Kajava, A. V., U. Aebi & A. C. Steven (2005) The parallel superpleated beta-structure as a model for amyloid fibrils of human amylin. *J Mol Biol,* 348**,** 247-52.
Kajava, A. V., U. Baxa, R. B. Wickner & A. C. Steven (2004) A model for Ure2p prion filaments and other amyloids: the parallel superpleated beta-structure. *Proc Natl Acad Sci U S A,* 101**,** 7885-90.
Kaletta, T. & M. O. Hengartner (2006) Finding function in novel targets: C. elegans as a model organism. *Nat Rev Drug Discov,* 5**,** 387-98.
Kan, H. W., H. Chiang, W. M. Lin, I. S. Yu, S. W. Lin & S. T. Hsieh (2018) Sensory nerve degeneration in a mouse model mimicking early manifestations of familial amyloid polyneuropathy due to transthyretin Ala97Ser. *Neuropathol Appl Neurobiol,* 44**,** 673-686.
Kikis, E. A. (2016) The struggle by Caenorhabditis elegans to maintain proteostasis during aging and disease. *Biol Direct,* 11**,** 58.
Kikis, E. A., T. Gidalevitz & R. I. Morimoto (2010) Protein homeostasis in models of aging and age-related conformational disease. *Adv Exp Med Biol,* 694**,** 138-59.
Kim, J. S., S. H. Kim & S. K. Park (2017) Selenocysteine modulates resistance to environmental stress and confers anti-aging effects in C. elegans. *Clinics (Sao Paulo),* 72**,** 491-498.
Kisilevsky, R. (1992) Proteoglycans, glycosaminoglycans, amyloid-enhancing factor, and amyloid deposition. *J Intern Med,* 232**,** 515-6.
Klunk, W. E., J. W. Pettegrew & D. J. Abraham (1989) Quantitative evaluation of congo red binding to amyloid-like proteins with a beta-pleated sheet conformation. *J Histochem Cytochem,* 37**,** 1273-81.
Knowles, T. P., C. A. Waudby, G. L. Devlin, S. I. Cohen, A. Aguzzi, M. Vendruscolo, E. M. Terentjev, M. E. Welland & C. M. Dobson (2009) An analytical solution to the kinetics of breakable filament assembly. *Science,* 326**,** 1533-7.
Kolstoe, S. E., P. P. Mangione, V. Bellotti, G. W. Taylor, G. A. Tennent, S. Deroo, A. J. Morrison, A. J. Cobb, A. Coyne, M. G. McCammon, T. D. Warner, J. Mitchell, R. Gill, M. D. Smith, S. V. Ley, C. V. Robinson, S. P. Wood & M. B. Pepys (2010) Trapping of palindromic ligands within native transthyretin prevents amyloid formation. *Proc Natl Acad Sci U S A,* 107**,** 20483-8.
Kumar, A., H. Chetia, S. Sharma, D. Kabiraj, N. C. Talukdar & U. Bora (2015) Curcumin Resource Database. *Database (Oxford),* 2015**,** bav070.
Kwok, T. C., N. Ricker, R. Fraser, A. W. Chan, A. Burns, E. F. Stanley, P. McCourt, S. R. Cutler & P. J. Roy (2006) A small-molecule screen in C. elegans yields a new calcium channel antagonist. *Nature,* 441**,** 91-5.
Lamb, Y. N. & E. D. Deeks (2019) Tafamidis: A Review in Transthyretin Amyloidosis with Polyneuropathy. *Drugs,* 79**,** 863-874.
Lee, S. S., R. Y. Lee, A. G. Fraser, R. S. Kamath, J. Ahringer & G. Ruvkun (2003) A systematic RNAi screen identifies a critical role for mitochondria in C. elegans longevity. *Nat Genet,* 33**,** 40-8.

Lehner, B., J. Tischler & A. G. Fraser (2006) RNAi screens in Caenorhabditis elegans in a 96-well liquid format and their application to the systematic identification of genetic interactions. *Nat Protoc,* 1**,** 1617-20.

Li, X., Y. Lyu, J. Shen, Y. Mu, L. Qiang, L. Liu, K. Araki, B. P. Imbimbo, K. I. Yamamura, S. Jin & Z. Li (2018) Amyloid deposition in a mouse model humanized at the transthyretin and retinol-binding protein 4 loci. *Lab Invest,* 98**,** 512-524.

Link, C. D. (1995) Expression of human beta-amyloid peptide in transgenic Caenorhabditis elegans. *Proc Natl Acad Sci U S A,* 92**,** 9368-72.

Link, C. D., C. J. Johnson, V. Fonte, M. Paupard, D. H. Hall, S. Styren, C. A. Mathis & W. E. Klunk (2001) Visualization of fibrillar amyloid deposits in living, transgenic Caenorhabditis elegans animals using the sensitive amyloid dye, X-34. *Neurobiol Aging,* 22**,** 217-26.

López, L. C., S. Dos-Reis, A. Espargaró, J. A. Carrodeguas, M. L. Maddelein, S. Ventura & J. Sancho (2012) Discovery of novel inhibitors of amyloid β-peptide 1-42 aggregation. *J Med Chem,* 55**,** 9521-30.

Ma, L., Y. Zhao, Y. Chen, B. Cheng, A. Peng & K. Huang (2018) Caenorhabditis elegans as a model system for target identification and drug screening against neurodegenerative diseases. *Eur J Pharmacol,* 819**,** 169-180.

MacRaild, C. A., C. R. Stewart, Y. F. Mok, M. J. Gunzburg, M. A. Perugini, L. J. Lawrence, V. Tirtaatmadja, J. J. Cooper-White & G. J. Howlett (2004) Non-fibrillar components of amyloid deposits mediate the self-association and tangling of amyloid fibrils. *J Biol Chem,* 279**,** 21038-45.

Madhivanan, K., E. R. Greiner, M. Alves-Ferreira, D. Soriano-Castell, N. Rouzbeh, C. A. Aguirre, J. F. Paulsson, J. Chapman, X. Jiang, F. K. Ooi, C. Lemos, A. Dillin, V. Prahlad, J. W. Kelly & S. E. Encalada (2018) Cellular clearance of circulating transthyretin decreases cell-nonautonomous proteotoxicity in Caenorhabditis elegans. *Proc Natl Acad Sci U S A,* 115**,** E7710-e7719.

Mangione, P. P., G. Esposito, A. Relini, S. Raimondi, R. Porcari, S. Giorgetti, A. Corazza, F. Fogolari, A. Penco, Y. Goto, Y. H. Lee, H. Yagi, C. Cecconi, M. M. Naqvi, J. D. Gillmore, P. N. Hawkins, F. Chiti, R. Rolandi, G. W. Taylor, M. B. Pepys, M. Stoppini & V. Bellotti (2013) Structure, folding dynamics, and amyloidogenesis of D76N beta2-microglobulin: roles of shear flow, hydrophobic surfaces, and alpha-crystallin. *J Biol Chem,* 288**,** 30917-30.

Mangione, P. P., R. Porcari, J. D. Gillmore, P. Pucci, M. Monti, M. Porcari, S. Giorgetti, L. Marchese, S. Raimondi, L. C. Serpell, W. Chen, A. Relini, J. Marcoux, I. R. Clatworthy, G. W. Taylor, G. A. Tennent, C. V. Robinson, P. N. Hawkins, M. Stoppini, S. P. Wood, M. B. Pepys & V. Bellotti (2014) Proteolytic cleavage of Ser52Pro variant transthyretin triggers its amyloid fibrillogenesis. *Proc Natl Acad Sci U S A,* 111**,** 1539-44.

Mangione, P. P., G. Verona, A. Corazza, J. Marcoux, D. Canetti, S. Giorgetti, S. Raimondi, M. Stoppini, M. Esposito, A. Relini, C. Canale, M. Valli, L. Marchese, G. Faravelli, L. Obici, P. N. Hawkins, G. W. Taylor, J. D. Gillmore, M. B. Pepys & V. Bellotti (2018) Plasminogen activation triggers transthyretin amyloidogenesis in vitro. *J Biol Chem,* 293**,** 14192-14199.

Mango, S. E. (2001) Stop making nonSense: the C. elegans smg genes. *Trends Genet,* 17**,** 646-53.

Marcoux, J., P. P. Mangione, R. Porcari, M. T. Degiacomi, G. Verona, G. W. Taylor, S. Giorgetti, S. Raimondi, S. Sanglier-Cianferani, J. L. Benesch, C. Cecconi, M. M. Naqvi, J. D. Gillmore, P. N. Hawkins, M. Stoppini, C. V. Robinson, M. B. Pepys

& V. Bellotti (2015) A novel mechano-enzymatic cleavage mechanism underlies transthyretin amyloidogenesis. *EMBO Mol Med,* 7**,** 1337-49.
Mathew, M. D., N. D. Mathew & P. R. Ebert (2012) WormScan: a technique for high-throughput phenotypic analysis of Caenorhabditis elegans. *PLoS One,* 7**,** e33483.
McAdam, K. P. & J. D. Sipe (1976) Murine model for human secondary amyloidosis: genetic variability of the acute-phase serum protein SAA response to endotoxins and casein. *J Exp Med,* 144**,** 1121-7.
McColl, G., B. R. Roberts, A. P. Gunn, K. A. Perez, D. J. Tew, C. L. Masters, K. J. Barnham, R. A. Cherny & A. I. Bush (2009) The Caenorhabditis elegans A beta 1-42 model of Alzheimer disease predominantly expresses A beta 3-42. *J Biol Chem,* 284**,** 22697-702.
McColl, G., B. R. Roberts, T. L. Pukala, V. B. Kenche, C. M. Roberts, C. D. Link, T. M. Ryan, C. L. Masters, K. J. Barnham, A. I. Bush & R. A. Cherny (2012) Utility of an improved model of amyloid-beta (Abeta(1)(-)(4)(2)) toxicity in Caenorhabditis elegans for drug screening for Alzheimer's disease. *Mol Neurodegener,* 7**,** 57.
Mishra, S., S. Joshi, J. E. Ward, E. P. Buys, D. Mishra, I. Morgado, S. Fisch, F. Lavatelli, G. Merlini, S. Dorbala, C. A. MacRae & R. Liao (2019) Zebrafish model of amyloid light chain cardiotoxicity: regeneration versus degeneration. *Am J Physiol Heart Circ Physiol,* 316**,** H1158-H1166.
Mitchell, D. H., J. W. Stiles, J. Santelli & D. R. Sanadi (1979) Synchronous growth and aging of Caenorhabditis elegans in the presence of fluorodeoxyuridine. *J Gerontol,* 34**,** 28-36.
Morell, M., N. S. de Groot, J. Vendrell, F. X. Avilés & S. Ventura (2011) Linking amyloid protein aggregation and yeast survival. *Mol Biosyst,* 7**,** 1121-8.
Morelli, X., R. Bourgeas & P. Roche (2011) Chemical and structural lessons from recent successes in protein-protein interaction inhibition (2P2I). *Curr Opin Chem Biol,* 15**,** 475-81.
Morley, J. F., H. R. Brignull, J. J. Weyers & R. I. Morimoto (2002) The threshold for polyglutamine-expansion protein aggregation and cellular toxicity is dynamic and influenced by aging in Caenorhabditis elegans. *Proc Natl Acad Sci U S A,* 99**,** 10417-22.
Morris, A. M., M. A. Watzky & R. G. Finke (2009) Protein aggregation kinetics, mechanism, and curve-fitting: a review of the literature. *Biochim Biophys Acta,* 1794**,** 375-97.
Naiki, H., T. Okoshi, D. Ozawa, I. Yamaguchi & K. Hasegawa (2016) Molecular pathogenesis of human amyloidosis: Lessons from β2 -microglobulin-related amyloidosis. *Pathol Int,* 66**,** 193-201.
Natalello, A., P. P. Mangione, S. Giorgetti, R. Porcari, L. Marchese, I. Zorzoli, A. Relini, D. Ami, G. Faravelli, M. Valli, M. Stoppini, S. M. Doglia, V. Bellotti & S. Raimondi (2016) Co-fibrillogenesis of Wild-type and D76N β2-Microglobulin: THE CRUCIAL ROLE OF FIBRILLAR SEEDS. *J Biol Chem,* 291**,** 9678-89.
Nelson, K. M., J. L. Dahlin, J. Bisson, J. Graham, G. F. Pauli & M. A. Walters (2017) The Essential Medicinal Chemistry of Curcumin. *J Med Chem,* 60**,** 1620-1637.
Nencetti, S. & E. Orlandini (2012) TTR fibril formation inhibitors: is there a SAR? *Curr Med Chem,* 19**,** 2356-79.
O'Reilly, L. P., C. J. Luke, D. H. Perlmutter, G. A. Silverman & S. C. Pak (2014) C. elegans in high-throughput drug discovery. *Adv Drug Deliv Rev,* 69-70**,** 247-53.

Paravastu, A. K., R. D. Leapman, W. M. Yau & R. Tycko (2008) Molecular structural basis for polymorphism in Alzheimer's beta-amyloid fibrils. *Proc Natl Acad Sci U S A,* 105**,** 18349-54.

Partridge, F. A., A. E. Brown, S. D. Buckingham, N. J. Willis, G. M. Wynne, R. Forman, K. J. Else, A. A. Morrison, J. B. Matthews, A. J. Russell, D. A. Lomas & D. B. Sattelle (2018) An automated high-throughput system for phenotypic screening of chemical libraries on C. elegans and parasitic nematodes. *Int J Parasitol Drugs Drug Resist,* 8**,** 8-21.

Pepys, M. B. (2006) Amyloidosis. *Annu Rev Med,* 57**,** 223-41.

Porcari, R., C. Proukakis, C. A. Waudby, B. Bolognesi, P. P. Mangione, J. F. Paton, S. Mullin, L. D. Cabrita, A. Penco, A. Relini, G. Verona, M. Vendruscolo, M. Stoppini, G. G. Tartaglia, C. Camilloni, J. Christodoulou, A. H. Schapira & V. Bellotti (2015) The H50Q mutation induces a 10-fold decrease in the solubility of α-synuclein. *J Biol Chem,* 290**,** 2395-404.

Pras, M., M. Schubert, D. Zucker-Franklin, A. Rimon & E. C. Franklin (1968) The characterization of soluble amyloid prepared in water. *J Clin Invest,* 47**,** 924-33.

PUCHTLER, H. & F. SWEAT (1962) Amidoblack as a stain for hemoglobin. *Arch Pathol,* 73**,** 245-9.

Quarta, C. C., R. H. Falk & S. D. Solomon (2015) V122I transthyretin variant in elderly black Americans. *N Engl J Med,* 372**,** 1769.

Quintas, A., D. C. Vaz, I. Cardoso, M. J. Saraiva & R. M. Brito (2001) Tetramer dissociation and monomer partial unfolding precedes protofibril formation in amyloidogenic transthyretin variants. *J Biol Chem,* 276**,** 27207-13.

Raimondi, S., R. Porcari, P. P. Mangione, G. Verona, J. Marcoux, S. Giorgetti, G. W. Taylor, S. Ellmerich, M. Ballico, S. Zanini, E. Pardon, R. Al-Shawi, J. P. Simons, A. Corazza, F. Fogolari, M. Leri, M. Stefani, M. Bucciantini, J. D. Gillmore, P. N. Hawkins, M. Valli, M. Stoppini, C. V. Robinson, J. Steyaert, G. Esposito & V. Bellotti (2017) A specific nanobody prevents amyloidogenesis of D76N beta2-microglobulin in vitro and modifies its tissue distribution in vivo. *Sci Rep,* 7**,** 46711.

Rawlings, N. D., A. J. Barrett & R. Finn (2016) Twenty years of the MEROPS database of proteolytic enzymes, their substrates and inhibitors. *Nucleic Acids Res,* 44**,** D343-50.

Reinke, A. A. & J. E. Gestwicki (2011) Insight into amyloid structure using chemical probes. *Chem Biol Drug Des,* 77**,** 399-411.

Reinke, V., I. S. Gil, S. Ward & K. Kazmer (2004) Genome-wide germline-enriched and sex-biased expression profiles in Caenorhabditis elegans. *Development,* 131**,** 311-23.

Relini, A., C. Canale, S. De Stefano, R. Rolandi, S. Giorgetti, M. Stoppini, A. Rossi, F. Fogolari, A. Corazza, G. Esposito, A. Gliozzi & V. Bellotti (2006) Collagen plays an active role in the aggregation of beta2-microglobulin under physiopathological conditions of dialysis-related amyloidosis. *J Biol Chem,* 281**,** 16521-9.

Relini, A., S. De Stefano, S. Torrassa, O. Cavalleri, R. Rolandi, A. Gliozzi, S. Giorgetti, S. Raimondi, L. Marchese, L. Verga, A. Rossi, M. Stoppini & V. Bellotti (2008) Heparin strongly enhances the formation of beta2-microglobulin amyloid fibrils in the presence of type I collagen. *J Biol Chem,* 283**,** 4912-20.

Richardson, S. J. (2014) Tweaking the structure to radically change the function: the evolution of transthyretin from 5-hydroxyisourate hydrolase to triiodothyronine distributor to thyroxine distributor. *Front Endocrinol (Lausanne),* 5**,** 245.

ROBBINS, J., J. E. RALL & M. L. PETERMANN (1957) Thyroxine-binding by serum and urine proteins in nephrosis; qualitative aspects. *J Clin Invest,* 36**,** 1333-42.
Saraiva, M. J. (1995) Transthyretin mutations in health and disease. *Hum Mutat,* 5**,** 191-6.
Saraiva, M. J., S. Birken, P. P. Costa & D. S. Goodman (1984) Amyloid fibril protein in familial amyloidotic polyneuropathy, Portuguese type. Definition of molecular abnormality in transthyretin (prealbumin). *J Clin Invest,* 74**,** 104-19.
Sekijima, Y., P. Hammarström, M. Matsumura, Y. Shimizu, M. Iwata, T. Tokuda, S. Ikeda & J. W. Kelly (2003) Energetic characteristics of the new transthyretin variant A25T may explain its atypical central nervous system pathology. *Lab Invest,* 83**,** 409-17.
Shao, R. & J. Xiao (2013) Natural Products for Treatment of Alzheimer's Disease and Related Diseases: Understanding their Mechanism of Action. *Curr Neuropharmacol,* 11**,** 337.
Simmer, F., M. Tijsterman, S. Parrish, S. P. Koushika, M. L. Nonet, A. Fire, J. Ahringer & R. H. Plasterk (2002) Loss of the putative RNA-directed RNA polymerase RRF-3 makes C. elegans hypersensitive to RNAi. *Curr Biol,* 12**,** 1317-9.
Sipe, J. D. (1992) Amyloidosis. *Annu Rev Biochem,* 61**,** 947-75.
Sipe, J. D. & A. S. Cohen (2000) Review: history of the amyloid fibril. *J Struct Biol,* 130**,** 88-98.
Spring, D. R. (2005) Chemical genetics to chemical genomics: small molecules offer big insights. *Chem Soc Rev,* 34**,** 472-82.
Stoppini, M. & V. Bellotti (2015) Systemic amyloidosis: lessons from beta2-microglobulin. *J Biol Chem,* 290**,** 9951-8.
Stoppini, M. S., P. Arcidiaco, P. Mangione, S. Giorgetti, D. Brancaccio & V. Bellotti (2000) Detection of fragments of beta2-microglobulin in amyloid fibrils. *Kidney Int,* 57**,** 349-50.
Tawara, S., M. Nakazato, K. Kangawa, H. Matsuo & S. Araki (1983) Identification of amyloid prealbumin variant in familial amyloidotic polyneuropathy (Japanese type). *Biochem Biophys Res Commun,* 116**,** 880-8.
Tennent, G. A., L. B. Lovat & M. B. Pepys (1995) Serum amyloid P component prevents proteolysis of the amyloid fibrils of Alzheimer disease and systemic amyloidosis. *Proc Natl Acad Sci U S A,* 92**,** 4299-303.
Thylén, C., J. Wahlqvist, E. Haettner, O. Sandgren, G. Holmgren & E. Lundgren (1993) Modifications of transthyretin in amyloid fibrils: analysis of amyloid from homozygous and heterozygous individuals with the Met30 mutation. *EMBO J,* 12**,** 743-8.
Timmons, L., D. L. Court & A. Fire (2001) Ingestion of bacterially expressed dsRNAs can produce specific and potent genetic interference in Caenorhabditis elegans. *Gene,* 263**,** 103-12.
Valleix, S., J. D. Gillmore, F. Bridoux, P. P. Mangione, A. Dogan, B. Nedelec, M. Boimard, G. Touchard, J. M. Goujon, C. Lacombe, P. Lozeron, D. Adams, C. Lacroix, T. Maisonobe, V. Plante-Bordeneuve, J. A. Vrana, J. D. Theis, S. Giorgetti, R. Porcari, S. Ricagno, M. Bolognesi, M. Stoppini, M. Delpech, M. B. Pepys, P. N. Hawkins & V. Bellotti (2012) Hereditary systemic amyloidosis due to Asp76Asn variant beta2-microglobulin. *N Engl J Med,* 366**,** 2276-83.
van Ham, T. J., K. L. Thijssen, R. Breitling, R. M. Hofstra, R. H. Plasterk & E. A. Nollen (2008) C. elegans model identifies genetic modifiers of alpha-synuclein inclusion formation during aging. *PLoS Genet,* 4**,** e1000027.

Verona, G., P. P. Mangione, S. Raimondi, S. Giorgetti, G. Faravelli, R. Porcari, A. Corazza, J. D. Gillmore, P. N. Hawkins, M. B. Pepys, G. W. Taylor & V. Bellotti (2017) Inhibition of the mechano-enzymatic amyloidogenesis of transthyretin: role of ligand affinity, binding cooperativity and occupancy of the inner channel. *Sci Rep,* 7**,** 182.

Walsh, D. M. & D. J. Selkoe (2007) A beta oligomers - a decade of discovery. *J Neurochem,* 101**,** 1172-84.

Wasmer, C., A. Lange, H. Van Melckebeke, A. B. Siemer, R. Riek & B. H. Meier (2008) Amyloid fibrils of the HET-s(218-289) prion form a beta solenoid with a triangular hydrophobic core. *Science,* 319**,** 1523-6.

Westermark, P., K. Sletten, B. Johansson & G. G. Cornwell (1990) Fibril in senile systemic amyloidosis is derived from normal transthyretin. *Proc Natl Acad Sci U S A,* 87**,** 2843-5.

Westermark, P., K. Sletten & K. H. Johnson (1996) Ageing and amyloid fibrillogenesis: lessons from apolipoprotein AI, transthyretin and islet amyloid polypeptide. *Ciba Found Symp,* 199**,** 205-18; discussion 218-22.

Wiltzius, J. J., S. A. Sievers, M. R. Sawaya, D. Cascio, D. Popov, C. Riekel & D. Eisenberg (2008) Atomic structure of the cross-beta spine of islet amyloid polypeptide (amylin). *Protein Sci,* 17**,** 1467-74.

Winblad, B., P. Amouyel, S. Andrieu, C. Ballard, C. Brayne, H. Brodaty, A. Cedazo-Minguez, B. Dubois, D. Edvardsson, H. Feldman, L. Fratiglioni, G. B. Frisoni, S. Gauthier, J. Georges, C. Graff, K. Iqbal, F. Jessen, G. Johansson, L. Jönsson, M. Kivipelto, M. Knapp, F. Mangialasche, R. Melis, A. Nordberg, M. O. Rikkert, C. Qiu, T. P. Sakmar, P. Scheltens, L. S. Schneider, R. Sperling, L. O. Tjernberg, G. Waldemar, A. Wimo & H. Zetterberg (2016) Defeating Alzheimer's disease and other dementias: a priority for European science and society. *Lancet Neurol,* 15**,** 455-532.

www.wormatlas.org

Yakupova, E. I., L. G. Bobyleva, I. M. Vikhlyantsev & A. G. Bobylev (2019) Congo Red and amyloids: history and relationship. *Biosci Rep,* 39.

You, Y. J. & L. Avery (2012) Appetite Control: worm's-eye-view. *Anim Cells Syst (Seoul),* 16**,** 351-356.

Zaru, R., M. Magrane, C. O'Donovan & U. Consortium (2017) From the research laboratory to the database: the Caenorhabditis elegans kinome in UniProtKB. *Biochem J,* 474**,** 493-515.

Zhang, P., X. Fu, J. Sawashita, J. Yao, B. Zhang, J. Qian, H. Tomozawa, M. Mori, Y. Ando, H. Naiki & K. Higuchi (2010) Mouse model to study human A beta2M amyloidosis: generation of a transgenic mouse with excessive expression of human beta2-microglobulin. *Amyloid,* 17**,** 50-62.